

Performance of Jointed Concrete Pavements

Volume II Evaluation and Modification of Concrete Pavement Design and Analysis Models

Publication No. FHWA-RD-89-137

July 1990



NJ Route 130 10-in. JRCP 12-in. gravel base 36 Years 35 Million ESAL's PSR - 3.8



U.S. Department of Transportation
Federal Highway Administration

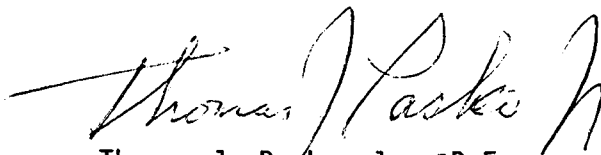
Research, Development, and Technology
Turner-Fairbank Highway Research Center
6300 Georgetown Pike
McLean, Virginia 22101-2296

FOREWORD

This report is one volume of a two-volume set of interim reports documenting a comprehensive evaluation of jointed concrete pavement design and analysis models. The capabilities and limitations and a sensitivity analysis of the various design and analysis models are given. New prediction models were developed for Present Serviceability Rating, longitudinal cracking, transverse joint faulting, transverse cracking (jointed plain concrete pavement only) and transverse joint spalling.

Volumes I, IV and V document the performance of 95 experimental or other in-service pavements in United States or Canada. These volumes have been previously distributed. Volume III (Summary of Research Findings) and the Technical Summary will be given widespread distribution in the near future. These reports will be of interest to those involved in the design, construction and maintenance of jointed concrete pavements.

Sufficient copies of this report are being distributed by FHWA memorandum to provide one copy to each FHWA Region and Division and two copies to each State highway agency. Direct distribution is being made to the Division offices. Additional copies for the public are available from the National Technical Information Service (NTIS), U. S. Department of Commerce, 5285 Port Royal Road, Springfield, Virginia 22161. A small charge will be imposed for each copy ordered from NTIS.



Thomas J. Pasko, Jr., P.E.
Director, Office of Engineering and
Highway Operations Research and Development

NOTICE

This document is disseminated under the sponsorship of the Department of Transportation in the interest of information exchange. The United States Government assumes no liability for its contents or use thereof. The contents of this report reflect the views of the contractor, who is responsible for the accuracy of the data presented herein. The contents do not necessarily reflect the official policy of the Department of Transportation. This report does not constitute a standard, specification, or regulation.

The United States Government does not endorse products or manufacturers. Trade or manufacturers' names appear herein only because they are considered essential to the object of this document.

1. Report No. FHWA-RD-89-137		2. Government Accession No.		3. Recipient's Catalog No.																			
4. Title and Subtitle PERFORMANCE OF JOINTED CONCRETE PAVEMENTS Volume II - Evaluation and Modification of Concrete Pavement Design and Analysis Models				5. Report Date July 1990																			
				6. Performing Organization Code																			
7. Author(s) K. D. Smith, A. L. Mueller, M. I. Darter, D. G. Peshkin				8. Performing Organization Report No.																			
9. Performing Organization Name and Address ERES Consultants, Inc. 1401 Regency Drive East Savoy, Illinois 61874				10. Work Unit No. 3C1A2012																			
				11. Contract or Grant No. DTFH61-86-C-00079																			
12. Sponsoring Agency Name and Address* Office of Engrg. and Highway Operations R & D Federal Highway Administration 6300 Georgetown Pike McLean, VA 22101-2296				13. Type of Report and Period Covered Interim Report Oct. 1986 - Feb. 1990																			
				14. Sponsoring Agency Code																			
15. Supplementary Notes FHWA Contract Manager (COTR): Roger M. Larson, HNR-20 Gratitude is expressed to Mr. Ricardo Salsilli and Mr. Ying-Haur Lee for their valuable assistance in Chapter 5.																							
16. Abstract <p>A major national field and analytical study has been conducted into the effect of various design features on the performance of jointed concrete pavements. Extensive design, construction, traffic, and performance data were obtained from ninety-five experimental and other concrete pavement sections throughout the country. Field data collected and analyzed included distress, drainage, roughness, present serviceability rating (PSR), deflections, destructive testing (coring and boring), and weigh-in-motion (WIM) on selected sites. This information was compiled into a comprehensive microcomputer database. Projects were evaluated on an individual basis and then compared at a national level to identify performance trends. The performance data was used to evaluate and modify several concrete pavement design procedures and analysis models.</p> <p>This volume investigates the accuracy of several concrete pavement performance models and shows the usefulness of several concrete design and analysis procedures. Performance models evaluated include AASHTO, PREDICT, PEARDARP and PFAULT; design and analysis models evaluated include PMARP, JSLAB, ILLISLAB, CMS, Liu-Lytton, JCP, JCS, and BERM. Based upon the data collected from this and other studies, new prediction models were developed for selected performance indicators.</p> <p>This volume is the second in a series. The other volumes are:</p> <table border="1" style="margin-left: auto; margin-right: auto;"> <thead> <tr> <th style="text-align: left;">FHWA No.</th> <th style="text-align: left;">Vol. No.</th> <th style="text-align: left;">Short Title</th> </tr> </thead> <tbody> <tr> <td>FHWA-RD-89-136</td> <td>I</td> <td>Evaluation of Concrete Pavement Performance and Design Features</td> </tr> <tr> <td>FHWA-RD-89-138</td> <td>III</td> <td>Summary of Research Findings</td> </tr> <tr> <td>FHWA-RD-89-139</td> <td>IV</td> <td>Appendix A Project Summary Reports & Summary Tables</td> </tr> <tr> <td>FHWA-RD-89-140</td> <td>V</td> <td>Appendix B Data Collection & Analysis Procedures</td> </tr> <tr> <td>FHWA-RD-89-141</td> <td>VI</td> <td>Appendix C Synthesis of Concrete Pavement Design Methods and Analysis Models Appendix D Summary of Analysis Data for the Evaluation of Predictive Models</td> </tr> </tbody> </table>						FHWA No.	Vol. No.	Short Title	FHWA-RD-89-136	I	Evaluation of Concrete Pavement Performance and Design Features	FHWA-RD-89-138	III	Summary of Research Findings	FHWA-RD-89-139	IV	Appendix A Project Summary Reports & Summary Tables	FHWA-RD-89-140	V	Appendix B Data Collection & Analysis Procedures	FHWA-RD-89-141	VI	Appendix C Synthesis of Concrete Pavement Design Methods and Analysis Models Appendix D Summary of Analysis Data for the Evaluation of Predictive Models
FHWA No.	Vol. No.	Short Title																					
FHWA-RD-89-136	I	Evaluation of Concrete Pavement Performance and Design Features																					
FHWA-RD-89-138	III	Summary of Research Findings																					
FHWA-RD-89-139	IV	Appendix A Project Summary Reports & Summary Tables																					
FHWA-RD-89-140	V	Appendix B Data Collection & Analysis Procedures																					
FHWA-RD-89-141	VI	Appendix C Synthesis of Concrete Pavement Design Methods and Analysis Models Appendix D Summary of Analysis Data for the Evaluation of Predictive Models																					
17. Key Words Concrete, concrete pavement, pavement performance, pavement evaluation, pavement design models, pavement analysis models, pavement performance models			18. Distribution Statement No restrictions. This document is available to the public through the National Technical Information Service, Springfield, Virginia 22161.																				
19. Security Classif. (of this report) Unclassified		20. Security Classif. (of this page) Unclassified		21. No. of Pages 301	22. Price																		

SI* (MODERN METRIC) CONVERSION FACTORS

APPROXIMATE CONVERSIONS TO SI UNITS

Symbol When You Know Multiply By To Find Symbol

LENGTH

in	inches	25.4	millimetres	mm
ft	feet	0.305	metres	m
yd	yards	0.914	metres	m
mi	miles	1.61	kilometres	km

AREA

in ²	square inches	645.2	millimetres squared	mm ²
ft ²	square feet	0.093	metres squared	m ²
yd ²	square yards	0.836	metres squared	m ²
ac	acres	0.405	hectares	ha
mi ²	square miles	2.59	kilometres squared	km ²

VOLUME

fl oz	fluid ounces	29.57	millilitres	mL
gal	gallons	3.785	litres	L
ft ³	cubic feet	0.028	metres cubed	m ³
yd ³	cubic yards	0.765	metres cubed	m ³

NOTE: Volumes greater than 1000 L shall be shown in m³.

MASS

oz	ounces	28.35	grams	g
lb	pounds	0.454	kilograms	kg
T	short tons (2000 lb)	0.907	megagrams	Mg

TEMPERATURE (exact)

°F	Fahrenheit temperature	5(F-32)/9	Celsius temperature	°C
----	------------------------	-----------	---------------------	----

APPROXIMATE CONVERSIONS FROM SI UNITS

Symbol When You Know Multiply By To Find Symbol

LENGTH

mm	millimetres	0.039	inches	in
m	metres	3.28	feet	ft
m	metres	1.09	yards	yd
km	kilometres	0.621	miles	mi

AREA

mm ²	millimetres squared	0.0016	square inches	in ²
m ²	metres squared	10.764	square feet	ft ²
ha	hectares	2.47	acres	ac
km ²	kilometres squared	0.386	square miles	mi ²

VOLUME

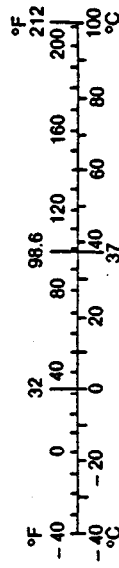
mL	millilitres	0.034	fluid ounces	fl oz
L	litres	0.264	gallons	gal
m ³	metres cubed	35.315	cubic feet	ft ³
m ³	metres cubed	1.308	cubic yards	yd ³

MASS

g	grams	0.035	ounces	oz
kg	kilograms	2.205	pounds	lb
Mg	megagrams	1.102	short tons (2000 lb)	T

TEMPERATURE (exact)

°C	Celsius temperature	1.8C + 32	Fahrenheit temperature	°F
----	---------------------	-----------	------------------------	----



* SI is the symbol for the International System of Measurement

(Revised April 1989)

TABLE OF CONTENTS

VOLUME I EVALUATION OF CONCRETE PAVEMENT PERFORMANCE AND DESIGN FEATURES

<u>Chapter</u>		<u>Page</u>
1	INTRODUCTION	1
	1. OBJECTIVES	1
	2. BACKGROUND AND RESEARCH APPROACH	2
	3. SEQUENCE OF REPORT	3
2	DESCRIPTION OF PROJECTS IN STUDY	4
	1. INTRODUCTION	4
	2. DESCRIPTION OF EXPERIMENTAL AND SINGLE PAVEMENT SECTIONS	6
	Dry-Freeze Environmental Region	6
	<u>Minnesota 1</u>	6
	<u>Minnesota 2</u>	6
	<u>Minnesota 3</u>	6
	<u>Minnesota 4</u>	6
	<u>Minnesota 6</u>	8
	Dry-Nonfreeze Environmental Region	8
	<u>Arizona 1</u>	8
	<u>Arizona 2</u>	8
	<u>California 1</u>	8
	<u>California 2</u>	8
	<u>California 6</u>	11
	<u>California 7</u>	11
	<u>California 8</u>	11
	Wet-Freeze Environmental Region	11
	<u>Michigan 1</u>	11
	<u>Michigan 3</u>	13
	<u>Michigan 4</u>	13
	<u>Michigan 5</u>	13
	<u>New York 1</u>	13
	<u>New York 2</u>	13
	<u>Ohio 1</u>	15
	<u>Ohio 2</u>	15
	<u>Ontario 1</u>	15
	<u>Ontario 2</u>	15
	<u>Pennsylvania 1</u>	15
	<u>New Jersey 2</u>	18
	<u>New Jersey 3</u>	18
	Wet-Nonfreeze Environmental Region	18
	<u>California 3</u>	18
	<u>North Carolina 1</u>	21
	<u>North Carolina 2</u>	21
	<u>Florida 2</u>	21
	<u>Florida 3</u>	21
3.	GENERAL DATA COLLECTION EFFORTS	21

TABLE OF CONTENTS (continued)

VOLUME I EVALUATION OF CONCRETE PAVEMENT PERFORMANCE AND DESIGN FEATURES (continued)

<u>Chapter</u>		<u>Page</u>
3	PERFORMANCE EVALUATION OF PROJECTS	25
1.	INTRODUCTION	25
2.	DRY-FREEZE ENVIRONMENTAL REGION	25
	Minnesota 1	27
	<u>Observations</u>	27
	<u>Conclusions</u>	27
	Minnesota 2	31
	<u>Observations</u>	31
	<u>Conclusions</u>	34
	Minnesota 3	35
	Minnesota 4	35
	Minnesota 6	37
3.	DRY-NONFREEZE ENVIRONMENTAL REGION	37
	Arizona 1	37
	<u>Observations</u>	40
	<u>Conclusions</u>	40
	Arizona 2	41
	California 1	41
	<u>Observations</u>	44
	<u>Conclusions</u>	44
	California 2	45
	<u>Observations</u>	45
	<u>Conclusions</u>	48
	California 6	48
	California 7	50
	<u>Observations</u>	50
	<u>Conclusions</u>	50
	California 8	51
4.	WET-FREEZE ENVIRONMENTAL REGION	51
	Michigan 1	51
	<u>Observations</u>	54
	<u>Conclusions</u>	55
	Michigan 3	56
	Michigan 4	56
	<u>Observations</u>	56
	<u>Conclusions</u>	60
	Michigan 5	61
	<u>Observations</u>	61
	<u>Conclusions</u>	61
	New York 1	63
	<u>Observations</u>	63
	<u>Conclusions</u>	63
	New York 2	65
	<u>Observations</u>	65
	<u>Conclusions</u>	68
	Ohio 1	69

TABLE OF CONTENTS (continued)

VOLUME I EVALUATION OF CONCRETE PAVEMENT PERFORMANCE AND DESIGN FEATURES (continued)

<u>Chapter</u>	<u>Page</u>
<u>Observations</u>	69
<u>Conclusions</u>	72
Ohio 2	72
<u>Observations</u>	73
<u>Conclusions</u>	75
Ontario 1	75
<u>Observations</u>	78
<u>Conclusions</u>	79
Ontario 2	79
<u>Observations</u>	80
<u>Conclusions</u>	80
Pennsylvania 1	80
<u>Observations</u>	80
<u>Conclusions</u>	84
New Jersey 2	85
<u>Observations</u>	85
<u>Conclusions</u>	85
New Jersey 3	85
<u>Observations</u>	88
<u>Conclusions</u>	89
5. WET-NONFREEZE ENVIRONMENTAL REGION	89
California 3	89
<u>Observations</u>	89
<u>Conclusions</u>	92
North Carolina 1	92
<u>Observations</u>	93
<u>Conclusions</u>	96
North Carolina 2	96
<u>Observations</u>	97
<u>Conclusions</u>	97
Florida 2	97
Florida 3	97
<u>Observations</u>	99
<u>Conclusions</u>	101
4 EFFECT OF DESIGN FEATURES ON PAVEMENT PERFORMANCE	102
1. INTRODUCTION	102
2. SLAB THICKNESS	102
Minnesota 1 and Minnesota 2	102
Arizona 1	102
California 1	104
Ohio 2	104
Ontario 1	104
North Carolina 2	104
Summary of the Effects of Slab Thickness	104
3. BASE TYPE	106

TABLE OF CONTENTS (continued)

VOLUME I EVALUATION OF CONCRETE PAVEMENT PERFORMANCE AND DESIGN FEATURES (continued)

<u>Chapter</u>	<u>Page</u>
Minnesota 1	106
Minnesota 6	107
Arizona 1	107
California 1	107
California 2	107
California 6	109
Michigan 1	109
Michigan 3	109
Michigan 5	109
New York 1	111
Ohio 1	111
Ontario 1	111
Pennsylvania 1	111
New Jersey 3	113
North Carolina 1	113
North Carolina 2	113
Florida 3	113
Summary of the Effects of Base Type	115
4. JOINT SPACING	117
Minnesota 1	117
Minnesota 2	121
California 1	121
Michigan 1	121
New York 1	121
New York 2	123
Ohio 1	123
New Jersey 2	123
North Carolina 1	123
Florida 3	123
Summary of the Effects of Joint Spacing	123
5. REINFORCEMENT DESIGN	133
Minnesota 1	133
Ohio 1	135
New Jersey 2 and New Jersey 3	135
Other Sections	135
Summary of the Effects of Reinforcement	135
6. JOINT ORIENTATION	135
New York 1	137
North Carolina 1	137
Summary of the Effects of Joint Orientation	137
7. TRANSVERSE JOINT LOAD TRANSFER	137
Doweled and Nondoweled Comparisons	139
<u>Minnesota 1</u>	139
<u>North Carolina 1</u>	139
Nondoweled Sections	141
Other Doweled Sections	141
Summary of the Effects of Load Transfer	144

TABLE OF CONTENTS (continued)

VOLUME I EVALUATION OF CONCRETE PAVEMENT PERFORMANCE AND DESIGN FEATURES (continued)

<u>Chapter</u>		<u>Page</u>
8.	DOWEL BAR COATINGS	144
	Michigan 1	144
	Michigan 5	144
	Ohio 1	145
	New York 2	145
	New Jersey 2	145
	Summary of the Effects of Dowel Coatings	145
9.	LONGITUDINAL JOINT DESIGN	145
	Summary of the Effects of Longitudinal Joint Design	148
10.	TRANSVERSE JOINT SEALANT	148
	Direct Sealant Comparisons	148
	California 3	148
	Minnesota 2	149
	Nonsealed Joints in California	149
	Preformed Compression Seals	149
	Other Sealant Types	150
	Summary of the Effects of Joint Sealing	150
11.	TIED PCC SHOULDERS/WIDENED LANES	150
	Minnesota 2	150
	Arizona 1	151
	Michigan 1	151
	Michigan 4	151
	New York 2	151
	Ohio 2	153
	Ontario 1	153
	California 3	153
	Widened Lanes	153
	Summary of the Effects of Tied PCC Shoulders/ Widened Lanes	153
12.	SUBDRAINAGE	154
	Michigan 1	154
	Michigan 5	156
	Arizona 1	156
	California 2	156
	Pennsylvania 1	156
	New Jersey 3	156
	Summary of the Effects of Subdrainage	156
5	SUMMARY AND CONCLUSIONS	159
	1. SUMMARY OF THE EFFECT OF DESIGN FEATURES	159
	2. FUTURE RESEARCH	164
	3. SUGGESTIONS FOR FUTURE DATA COLLECTION AND TESTING	165
6	BIBLIOGRAPHY	166

TABLE OF CONTENTS (continued)

VOLUME II EVALUATION AND MODIFICATION OF CONCRETE PAVEMENT DESIGN AND ANALYSIS MODELS

<u>Chapter</u>	<u>Page</u>
1 INTRODUCTION	1
1. INTRODUCTION	1
2. PROJECT BACKGROUND	2
Selection of Models	2
Research Approach	3
3. SEQUENCE OF REPORT	4
2 DESCRIPTION OF PAVEMENT SECTIONS	5
1. DRY-FREEZE ENVIRONMENTAL REGION	5
2. DRY-NONFREEZE ENVIRONMENTAL REGION	6
3. WET-FREEZE ENVIRONMENTAL REGION	6
4. WET-NONFREEZE ENVIRONMENTAL REGION	9
5. OVERALL DISTRIBUTION OF DESIGN FEATURES	9
Base Type	9
Slab Thickness	12
Joint Spacing/Pavement Type	12
Load Transfer	12
Shoulder Type/Widened Lanes	17
3 ANALYSIS OF THE ACCURACY OF SELECTED PREDICTION MODELS	19
1. INTRODUCTION	19
2. DESCRIPTION OF PREDICTION MODELS	19
AASHTO Design Model	20
PEARДАРP Prediction Models	25
Spalling Model	26
PSI Model	26
Roughness Model	26
Pumping Models	27
Cracking Model	29
Faulting Models	30
COPES Prediction Models	31
JPCP Pumping Model	31
JRCP Pumping Model	32
JPCP Joint Faulting Model	32
JRCP Joint Faulting Model	33
JPCP Joint Deterioration Model	33
JRCP Joint Deterioration Model	34
JPCP Slab Cracking Model	35
JRCP Slab Cracking Model	35
JPCP Present Serviceability Rating (PSR) Model	36
JRCP Present Serviceability Rating (PSR) Model	36
PFAULT Faulting Prediction Models	37
Doweled Jointed Concrete Pavements	37

TABLE OF CONTENTS (continued)

VOLUME II EVALUATION AND MODIFICATION OF CONCRETE PAVEMENT DESIGN AND ANALYSIS MODELS (continued)

<u>Chapter</u>	<u>Page</u>
Nondoweled Jointed Concrete Pavements	37
3. STATISTICAL ANALYSIS OF PREDICTION MODELS	39
4. ABILITY OF MODELS TO PREDICT THE PERFORMANCE OF INSERVICE PAVEMENTS	41
AASHTO	43
PEARДАРP	46
PSI Model	46
Roughness Model	46
Pumping Model	49
Spalling Model	49
Faulting Models	50
Cracking Model	51
COPEs	52
Pumping Models	52
Faulting Models	56
Joint Deterioration Models	57
Cracking Models	59
Present Serviceability Rating (PSR) Models	61
PFAULT Faulting Models	62
5. SUMMARY	65
4 CASE STUDIES	67
1. INTRODUCTION	67
Climatic Model	67
Drainage Model	68
Structural Analysis Models	68
Design Method	69
Shoulder Analysis and Design	69
2. PRESENTATION OF SECTIONS FOR CASE STUDIES	69
Minnesota 1	69
California 1	71
Michigan 1	71
North Carolina 1.	71
3. EVALUATION OF THE CMS PROGRAM	75
Introduction	75
Brief Technical Description	75
Analysis of Results	78
Rothsay, Minnesota	78
Tracy, California	85
Clare, Michigan	89
Rocky Mount, North Carolina	99
Conclusions and Recommendations	101
4. EVALUATION OF LIU-LYTON DRAINAGE MODELS	104
Introduction	104
Brief Technical Description	104
Analysis of Results	105

TABLE OF CONTENTS (continued)

VOLUME II EVALUATION AND MODIFICATION OF CONCRETE PAVEMENT DESIGN AND ANALYSIS MODELS (continued)

<u>Chapter</u>		<u>Page</u>
	Rothsay, Minnesota	107
	Tracy, California	114
	Clare, Michigan	119
	Rocky Mount, North Carolina	125
	Conclusions and Recommendations	128
5.	ANALYSIS OF JSLAB AND ILLISLAB	131
	Introduction	131
	Analysis of Results	132
	Analysis of the Edge Loading Condition	137
	Analysis of the Corner Loading Condition	137
	Analysis of a Temperature Gradient Through the Slab	138
	Conclusions	138
6.	EVALUATION OF THE ILLISLAB PROGRAM	139
	Introduction	139
	Brief Technical Description	140
	Analysis of Results	141
	Analysis of the Edge Loading Condition	141
	Analysis of the Corner Loading Condition	144
	Analysis of Voids Beneath the Slab	146
	Analysis of a Temperature Gradient Through a Slab	149
	Conclusions and Recommendations	153
7.	EVALUATION OF THE PMARP PROGRAM	153
	Introduction	153
	Brief Technical Description	154
	Analysis of Results	156
	Analysis of the Edge Loading Condition	158
	Analysis of the Corner Loading Condition	160
	Conclusions and Recommendations	161
8.	EVALUATION OF THE ZERO-MAINTENANCE DESIGN PROCEDURE	162
	Introduction	162
	Brief Technical Description	162
	Analysis of Results	165
	Conclusions and Recommendations	168
9.	EVALUATION OF JCS-1	168
	Brief Technical Description	168
	Analysis of Results	169
	Conclusions and Recommendations	170
10.	EVALUATION OF BERM	171
	Brief Technical Description	171
	Analysis of Results	172
	Conclusions and Recommendations	173
11.	SUMMARY AND CONCLUSIONS	173
5	DEVELOPMENT OF NEW PREDICTION MODELS	175
1.	INTRODUCTION	175

TABLE OF CONTENTS (continued)

VOLUME II EVALUATION AND MODIFICATION OF CONCRETE PAVEMENT DESIGN AND ANALYSIS MODELS (continued)

<u>Chapter</u>	<u>Page</u>
2. NEW PREDICTION MODELS	175
Present Serviceability Rating (PSR)	175
<u>Jointed Plain Concrete Pavements</u>	175
<u>Jointed Reinforced Concrete Pavements</u>	176
Longitudinal Cracking	177
Transverse Joint Faulting	178
<u>Doweled Concrete Pavements</u>	181
<u>Nondoweled Concrete Pavements</u>	183
Transverse Cracking	191
<u>Applied n</u>	191
<u>Allowable N</u>	192
<u>JPCP Cracking Model</u>	196
Transverse Joint Spalling	200
<u>JPCP Joint Spalling Model</u>	200
<u>JRCP Joint Spalling Model</u>	202
 6. EVALUATION OF THE COST-EFFECTIVENESS OF SELECTED PAVEMENT DESIGN FEATURES	 207
1. INTRODUCTION	207
2. ANALYSIS PROCEDURE	207
Cost Information	209
Life Prediction	209
Cost-Effectiveness	209
3. RESULTS	210
Arizona	210
<u>Comparative Design 1</u>	210
<u>Comparative Design 2</u>	210
<u>Comparative Design 3</u>	212
California	212
<u>Comparative Design 1</u>	212
<u>Comparative Design 2</u>	212
<u>Comparative Design 3</u>	215
<u>Comparative Design 4</u>	215
<u>Comparative Design 5</u>	215
<u>Comparative Design 6</u>	215
Michigan	216
<u>Comparative Design 1</u>	216
<u>Comparative Design 2</u>	216
<u>Comparative Design 3</u>	219
<u>Comparative Design 4</u>	219
<u>Comparative Design 5</u>	219
<u>Comparative Design 6</u>	219
Minnesota	220
<u>Comparative Design 1</u>	220
<u>Comparative Design 2</u>	220
<u>Comparative Design 3</u>	220

TABLE OF CONTENTS (continued)

VOLUME II EVALUATION AND MODIFICATION OF CONCRETE PAVEMENT DESIGN AND ANALYSIS MODELS (continued)

<u>Chapter</u>	<u>Page</u>
<u>Comparative Design 4</u>	223
<u>Comparative Design 5</u>	223
North Carolina	223
<u>Comparative Design 1</u>	223
<u>Comparative Design 2</u>	225
<u>Comparative Design 3</u>	225
4. SUMMARY	225
7. SUMMARY AND CONCLUSIONS	228
APPENDIX A — PAVEMENT DESIGNS FOR COST-EFFECTIVENESS EVALUATION	230
REFERENCES	239

VOLUME III SUMMARY OF RESEARCH FINDINGS

<u>Chapter</u>	<u>Page</u>
1. INTRODUCTION	1
STUDY OBJECTIVES	1
BACKGROUND AND RESEARCH SCOPE	2
DESCRIPTION OF REPORTS	2
2. STUDY SECTIONS AND DATA COLLECTION	3
STUDY SECTIONS	3
DRY-FREEZE ENVIRONMENTAL REGION	3
DRY-NONFREEZE ENVIRONMENTAL REGION	3
WET-FREEZE ENVIRONMENTAL REGION	8
WET-NONFREEZE ENVIRONMENTAL REGION	8
OVERALL DISTRIBUTION OF DESIGN FEATURES	8
BASE TYPE	8
SLAB THICKNESS	8
JOINT SPACING/PAVEMENT TYPE	12
LOAD TRANSFER	12
SHOULDER TYPE/WIDENED LANES	12
SINGLE PAVEMENT SECTIONS	12
FIELD DATA COLLECTION	12
PAVEMENT CONDITION SURVEY	17
DRAINAGE SURVEY	17
PHOTO SURVEY	18
FALLING WEIGHT DEFLECTOMETER (FWD)	18
PAVEMENT ROUGHNESS	18

TABLE OF CONTENTS (continued)

VOLUME III SUMMARY OF RESEARCH FINDINGS (continued)

<u>Chapter</u>		<u>Page</u>
	WEIGH-IN-MOTION (WIM)	18
	CORING AND BORING	18
	DATA BASE DESCRIPTION	19
3	SUMMARY OF THE EFFECTS OF DESIGN FEATURES	21
	PROJECT SUMMARIES	21
	EFFECTS OF PAVEMENT DESIGN FEATURES	21
	SLAB THICKNESS	21
	BASE TYPE	21
	SLAB LENGTH	23
	SLAB REINFORCEMENT	24
	JOINT ORIENTATION	26
	JOINT LOAD TRANSFER	26
	DOWEL BAR COATINGS	27
	LONGITUDINAL JOINT DESIGN	27
	JOINT SEALING	27
	TIED SHOULDERS	28
	WIDENED TRAFFIC LANES	28
	SUBDRAINAGE	29
	SUMMARY	29
4	CONCRETE PAVEMENT DESIGN AND ANALYSIS MODELS	30
	SYNTHESIS AND SELECTION OF INITIAL MODELS	30
	ANALYSIS OF THE ACCURACY OF SELECTED PREDICTION MODELS	30
	STATISTICAL ANALYSIS OF PREDICTION MODELS	31
	AASHTO PAVEMENT DESIGN MODEL	31
	PEARARP	32
	NCHRP 277 (COPEs)	35
	PFAULT FAULTING MODELS	35
	OVERALL EVALUATION OF THE PREDICTION MODELS	40
	CASE STUDIES FOR SELECTED ANALYSIS MODELS	40
	EVALUATION OF THE CMS PROGRAM	41
	EVALUATION OF THE LIU-LYTTON DRAINAGE MODELS	42
	EVALUATION OF THE ILLISLAB PROGRAM	43
	ANALYSIS OF JSLAB AND ILLISLAB	44
	<u>Analysis of the Edge Loading Condition</u>	45
	<u>Analysis of the Corner Loading Condition</u>	45
	<u>Analysis of a Temperature Gradient Through the Slab</u>	46
	Conclusions	47
	EVALUATION OF THE PMARP PROGRAM	47
	EVALUATION OF THE ZERO-MAINTENANCE DESIGN PROCEDURE	49
	EVALUATION OF JCS-1	49
	EVALUATION OF BERM	50
	SUMMARY AND CONCLUSIONS	51

TABLE OF CONTENTS (continued)

VOLUME III SUMMARY OF RESEARCH FINDINGS (continued)

<u>Chapter</u>		<u>Page</u>
5	DEVELOPMENT OF NEW PREDICTION MODELS	53
	INTRODUCTION	53
	PRESENT SERVICEABILITY RATING (PSR)	54
	LONGITUDINAL CRACKING	54
	TRANSVERSE JOINT FAULTING	55
	DOWELED CONCRETE PAVEMENTS	57
	NONDOWELED CONCRETE PAVEMENTS	57
	TRANSVERSE CRACKING	60
	TRANSVERSE JOINT SPALLING	62
	JPCP JOINT SPALLING MODEL	65
	JRCP JOINT SPALLING MODEL	65
	USE OF MODELS IN DESIGN	65
	ACCURACY OF MODELS	68
	SUMMARY	71
6	COST EFFECTIVENESS EVALUATION OF SELECTED PAVEMENT DESIGN FEATURES	73
	INTRODUCTION	73
	ANALYSIS PROCEDURE	73
	RESULTS	75
	SUMMARY OF COST EVALUATION	75
	APPENDIX A PARTIAL LISTING OF CANDIDATE SECTIONS	78
	APPENDIX B NEW PREDICTION MODELS	82
	PRESENT SERVICEABILITY RATING	82
	JOINTED PLAIN CONCRETE PAVEMENTS	82
	JOINTED REINFORCED CONCRETE PAVEMENTS	83
	TRANSVERSE JOINT FAULTING	84
	DOWELED CONCRETE PAVEMENTS	84
	NONDOWELED CONCRETE PAVEMENTS	87
	TRANSVERSE CRACKING - JOINTED PLAIN CONCRETE PAVEMENTS	90
	TRANSVERSE JOINT SPALLING	91
	JPCP JOINT SPALLING MODEL	91
	JRCP JOINT SPALLING MODEL	92
	REFERENCES	93

TABLE OF CONTENTS (continued)

VOLUME IV APPENDIX A - PROJECT SUMMARY REPORTS AND SUMMARY TABLES

<u>Chapter</u>		<u>Page</u>
1	INTERSTATE 94 -- ROTHSAY, MINNESOTA	1
	1. INTRODUCTION	1
	2. CLIMATE	1
	3. TRAFFIC	1
	4. MAINTENANCE AND REHABILITATION	2
	5. PHYSICAL TESTING RESULTS	2
	6. DRAINABILITY OF PAVEMENT SECTIONS	3
	7. DETERIORATION OF PAVEMENT SECTIONS	6
	Joint Spalling	6
	<u>Best Performance</u>	6
	<u>Worst Performance</u>	6
	Joint Faulting	6
	<u>Best Performance</u>	7
	<u>Worst Performance</u>	7
	Transverse Cracking	7
	<u>Best Performance</u>	8
	<u>Worst Performance</u>	8
	Longitudinal Cracking	8
	<u>Best Performance</u>	8
	<u>Worst Performance</u>	9
	Present Serviceability Rating (PSR) and Roughness	9
	Other Distress Types	9
	8. EFFECT OF DESIGN FEATURES ON PAVEMENT PERFORMANCE	9
	Base Type	9
	Joint Load Transfer	9
	Slab Thickness	10
	Joint Spacing	10
	9. COMPARISON OF OUTER LANE AND INNER LANE PERFORMANCE	10
	10. SUMMARY AND CONCLUSIONS	11
	11. ADDITIONAL READING	12
2	INTERSTATE 90 -- ALBERT LEA, MINNESOTA	13
	1. INTRODUCTION	13
	2. CLIMATE	13
	3. TRAFFIC	13
	4. MAINTENANCE AND REHABILITATION	13
	5. PHYSICAL TESTING RESULTS	14
	6. DRAINABILITY OF PAVEMENT SECTIONS	15
	7. DETERIORATION OF PAVEMENT SECTIONS	15
	Joint Spalling	15
	Joint Faulting	17
	Transverse Cracking	17
	Longitudinal Cracking	17
	Present Serviceability Rating (PSR) and Roughness	18
	Overall Shoulder Condition	18

TABLE OF CONTENTS (continued)

VOLUME IV APPENDIX A - PROJECT SUMMARY REPORTS AND SUMMARY TABLES (continued)

<u>Chapter</u>		<u>Page</u>
	8. EFFECT OF DESIGN FEATURES ON PAVEMENT PERFORMANCE	18
	Pavement Type	19
	Joint Spacing	19
	Slab Thickness	19
	Shoulder Type	19
	Widened Inside Lanes	20
	9. COMPARISON OF OUTER LANE AND INNER LANE PERFORMANCE ...	20
	10. SUMMARY AND CONCLUSIONS	20
	11. ADDITIONAL READING	22
3	INTERSTATE 90 -- AUSTIN, MINNESOTA	23
	1. INTRODUCTION	23
	2. DESIGN	23
	3. CLIMATE	23
	4. TRAFFIC	23
	5. DRAINABILITY AND OTHER PHYSICAL TESTING RESULTS	23
	6. MAINTENANCE AND REHABILITATION	24
	7. PAVEMENT PERFORMANCE	24
	8. CONCLUSIONS	24
4	TRUNK HIGHWAY 15 -- NEW ULM, MINNESOTA	25
	1. INTRODUCTION	25
	2. DESIGN	25
	3. CLIMATE	25
	4. TRAFFIC	25
	5. DRAINABILITY AND OTHER PHYSICAL TESTING RESULTS	25
	6. MAINTENANCE AND REHABILITATION	26
	7. PAVEMENT PERFORMANCE	26
	8. CONCLUSIONS	26
5	TRUNK HIGHWAY 15 -- TRUMAN, MINNESOTA	27
	1. INTRODUCTION	27
	2. DESIGN	27
	3. CLIMATE	27
	4. TRAFFIC	27
	5. DRAINABILITY AND OTHER PHYSICAL TESTING RESULTS	27
	6. MAINTENANCE AND REHABILITATION	28
	7. PAVEMENT PERFORMANCE	28
	8. CONCLUSIONS	28
6	STATE ROUTE 360 (SUPERSTITION FREEWAY) -- PHOENIX, ARIZONA	29
	1. INTRODUCTION	29

TABLE OF CONTENTS (continued)

VOLUME IV APPENDIX A - PROJECT SUMMARY REPORTS AND SUMMARY TABLES (continued)

<u>Chapter</u>	<u>Page</u>
2. CLIMATE	29
3. TRAFFIC	29
4. MAINTENANCE AND REHABILITATION	30
5. PHYSICAL TESTING RESULTS	30
6. DRAINABILITY OF PAVEMENT SECTIONS	31
7. DETERIORATION OF PAVEMENT SECTIONS	31
Joint Spalling	34
Joint Faulting	34
Transverse Cracking	34
Longitudinal Cracking	34
Present Serviceability Rating (PSR) and Roughness	35
8. EFFECT OF DESIGN FEATURES ON PAVEMENT PERFORMANCE	35
Base Type	35
Load Transfer Devices	35
Slab Thickness	36
Shoulder Type	36
Subdrainage	36
9. COMPARISON OF OUTER LANE AND MIDDLE LANE PERFORMANCE ..	36
10. SUMMARY AND CONCLUSIONS	37
11. ADDITIONAL READING	37
7 INTERSTATE 10 -- PHOENIX, ARIZONA	38
1. INTRODUCTION	38
2. DESIGN	38
3. CLIMATE	38
4. TRAFFIC	38
5. DRAINABILITY AND OTHER PHYSICAL TESTING RESULTS	38
6. MAINTENANCE AND REHABILITATION	39
7. PAVEMENT PERFORMANCE	39
8. CONCLUSIONS	39
8 INTERSTATE 5 -- TRACY, CALIFORNIA	41
1. INTRODUCTION	41
2. CLIMATE	41
3. TRAFFIC	41
4. MAINTENANCE AND REHABILITATION	42
5. PHYSICAL TESTING RESULTS	42
6. DRAINABILITY OF PAVEMENT SECTIONS	43
7. DETERIORATION OF PAVEMENT SECTIONS	44
Joint Spalling	44
Joint Faulting	44
<u>Best Performance</u>	47
<u>Worst Performance</u>	47
Transverse Cracking	47
<u>Best Performance</u>	47

TABLE OF CONTENTS (continued)

VOLUME IV APPENDIX A - PROJECT SUMMARY REPORTS AND SUMMARY TABLES (continued)

<u>Chapter</u>	<u>Page</u>
<u>Worst Performance</u>	48
Longitudinal Cracking	48
Present Serviceability Rating (PSR) and Roughness	48
8. EFFECT OF DESIGN FEATURES ON PAVEMENT PERFORMANCE	49
Base Type	49
Joint Spacing	49
High Strength Concrete	50
Slab Thickness	50
9. COMPARISON OF OUTER AND INNER LANE PERFORMANCE	50
10. SUMMARY AND CONCLUSIONS	51
11. ADDITIONAL READING	51
9 INTERSTATE 210 -- LOS ANGELES, CALIFORNIA	52
1. INTRODUCTION	52
2. CLIMATE	52
3. TRAFFIC	52
4. MAINTENANCE AND REHABILITATION	52
5. PHYSICAL TESTING RESULTS	53
6. DRAINABILITY OF PAVEMENT SECTIONS	53
7. DETERIORATION OF PAVEMENT SECTIONS	54
Joint Spalling	54
Joint Faulting	54
Transverse Cracking	56
Longitudinal Cracking	56
Present Serviceability Rating (PSR) and Roughness	56
Other Pavement Distress	56
8. EFFECT OF DESIGN FEATURES ON PAVEMENT PERFORMANCE	56
9. COMPARISON OF OUTER AND MIDDLE LANE PERFORMANCE	57
10. SUMMARY AND CONCLUSIONS	57
11. ADDITIONAL READING	58
10 ROUTE 14 -- SOLEMINT, CALIFORNIA	59
1. INTRODUCTION	59
2. DESIGN	59
3. CLIMATE	59
4. TRAFFIC	59
5. DRAINABILITY AND OTHER PHYSICAL TESTING RESULTS	59
6. MAINTENANCE AND REHABILITATION	60
7. PAVEMENT PERFORMANCE	60
8. CONCLUSIONS	60
11 INTERSTATE 5 -- SACRAMENTO, CALIFORNIA	61
1. INTRODUCTION	61
2. DESIGN	61

TABLE OF CONTENTS (continued)

VOLUME IV APPENDIX A - PROJECT SUMMARY REPORTS AND SUMMARY TABLES (continued)

<u>Chapter</u>	<u>Page</u>
3. CLIMATE	61
4. TRAFFIC	61
5. DRAINABILITY AND OTHER PHYSICAL TESTING RESULTS	62
6. MAINTENANCE AND REHABILITATION	62
7. PAVEMENT PERFORMANCE	62
8. CONCLUSIONS	63
12 U.S. 101 -- THOUSAND OAKS, CALIFORNIA	64
1. INTRODUCTION	64
2. DESIGN	64
3. CLIMATE	64
4. TRAFFIC	64
5. DRAINABILITY AND OTHER PHYSICAL TESTING RESULTS	64
6. MAINTENANCE AND REHABILITATION	65
7. PAVEMENT PERFORMANCE	65
8. CONCLUSIONS	65
13 U.S. 10 -- CLARE, MICHIGAN	66
1. INTRODUCTION	66
2. CLIMATE	66
3. TRAFFIC	66
4. MAINTENANCE AND REHABILITATION	67
5. PHYSICAL TESTING RESULTS	67
6. DRAINABILITY OF PAVEMENT SECTIONS	68
7. DETERIORATION OF PAVEMENT SECTIONS	69
Joint Spalling	69
<u>Best Performance</u>	72
<u>Worst Performance</u>	72
Joint Faulting	72
<u>Best Performance</u>	73
<u>Worst Performance</u>	73
Transverse Cracking	73
<u>Best Performance</u>	74
<u>Worst Performance</u>	74
Longitudinal Cracking	74
Present Serviceability Rating (PSR) and Roughness	74
8. EFFECT OF DESIGN FEATURES ON PAVEMENT PERFORMANCE	75
Base Type	75
Joint Load Transfer	75
Subdrainage	75
Joint Spacing	76
Concrete Acceleration Ramp	76
9. COMPARISON OF OUTER AND INNER LANE PERFORMANCE	76
10. SUMMARY AND CONCLUSIONS	77
11. ADDITIONAL READING	78

TABLE OF CONTENTS (continued)

VOLUME IV APPENDIX A - PROJECT SUMMARY REPORTS AND SUMMARY TABLES (continued)

<u>Chapter</u>		<u>Page</u>
14	INTERSTATE 94 -- MARSHALL, MICHIGAN	79
	1. INTRODUCTION	79
	2. DESIGN	79
	3. CLIMATE	79
	4. TRAFFIC	79
	5. DRAINABILITY AND OTHER PHYSICAL TESTING RESULTS	79
	6. MAINTENANCE AND REHABILITATION	80
	7. PAVEMENT PERFORMANCE	80
	8. CONCLUSIONS	80
15	INTERSTATE 69 -- CHARLOTTE, MICHIGAN	81
	1. INTRODUCTION	81
	2. CLIMATE	82
	3. TRAFFIC	82
	4. MAINTENANCE AND REHABILITATION	82
	5. PHYSICAL TESTING RESULTS	82
	6. DRAINABILITY OF PAVEMENT SECTIONS	83
	7. DETERIORATION OF PAVEMENT SECTIONS	84
	Joint Spalling	84
	Joint Faulting	84
	Transverse Cracking	84
	Transverse Crack Faulting	86
	Longitudinal Cracking	86
	Present Serviceability Rating and Roughness	86
	Shoulder Condition	87
	8. EFFECT OF DESIGN FEATURES ON PAVEMENT PERFORMANCE	87
	9. COMPARISON OF OUTER AND INNER LANE PERFORMANCE	88
	10. SUMMARY AND CONCLUSIONS	89
	11. ADDITIONAL READING	90
16	INTERSTATE 94 -- PAW PAW, MICHIGAN	91
	1. INTRODUCTION	91
	2. DESIGN	91
	3. CLIMATE	91
	4. TRAFFIC	91
	5. DRAINABILITY AND OTHER PHYSICAL TESTING RESULTS	91
	6. MAINTENANCE AND REHABILITATION	92
	7. PAVEMENT PERFORMANCE	92
	8. CONCLUSIONS	92
	9. ADDITIONAL READING	93
17	ROUTE 23 -- CATSKILL, NEW YORK	94
	1. INTRODUCTION	94
	2. CLIMATE	94

TABLE OF CONTENTS (continued)

VOLUME IV APPENDIX A - PROJECT SUMMARY REPORTS AND SUMMARY TABLES (continued)

<u>Chapter</u>	<u>Page</u>
3. TRAFFIC	95
4. MAINTENANCE AND REHABILITATION	95
5. PHYSICAL TESTING RESULTS	95
6. DRAINABILITY OF PAVEMENT SECTIONS	96
7. DETERIORATION OF PAVEMENT SECTIONS	99
Joint Spalling	99
<u>Best Performance</u>	99
<u>Worst Performance</u>	99
Joint Faulting	99
<u>Best Performance</u>	99
<u>Worst Performance</u>	100
Transverse Cracking	100
<u>Best Performance</u>	100
<u>Worst Performance</u>	100
Longitudinal Cracking	100
Present Serviceability Rating (PSR) and Roughness	101
8. EFFECT OF DESIGN FEATURES ON PAVEMENT PERFORMANCE	101
Base Type	101
Load Transfer Devices	101
Joint Spacing	102
Joint Orientation	102
9. COMPARISON OF OUTER LANE AND INNER LANE PERFORMANCE ...	102
10. SUMMARY AND CONCLUSIONS	103
11. ADDITIONAL READING	103
18 INTERSTATE 88 – OTEGO, NEW YORK	104
1. INTRODUCTION	104
2. CLIMATE	105
3. TRAFFIC	105
4. MAINTENANCE AND REHABILITATION	105
5. PHYSICAL TESTING RESULTS	105
6. DRAINABILITY OF PAVEMENT SECTIONS	107
7. DETERIORATION OF PAVEMENT SECTIONS	107
Joint Spalling	107
Joint Faulting	107
Transverse Cracking	107
Longitudinal Cracking	110
Present Serviceability Rating (PSR) and Roughness	111
Concrete Shoulder Distress Summary	111
8. EFFECT OF DESIGN FEATURES ON PAVEMENT PERFORMANCE	111
9. COMPARISON OF OUTER LANE AND INNER LANE PERFORMANCE ...	112
10. SUMMARY AND CONCLUSIONS	112
19 U.S. 23 – CHILlicoTHE, OHIO	114
1. INTRODUCTION	114

TABLE OF CONTENTS (continued)

VOLUME IV APPENDIX A - PROJECT SUMMARY REPORTS AND SUMMARY TABLES (continued)

<u>Chapter</u>	<u>Page</u>
2. CLIMATE	114
3. TRAFFIC	114
4. MAINTENANCE AND REHABILITATION	114
5. PHYSICAL TESTING RESULTS	115
6. DRAINABILITY OF PAVEMENT SECTIONS	116
7. DETERIORATION OF PAVEMENT SECTIONS	116
Joint Spalling	116
Joint Faulting	119
<u>Best Performance</u>	119
<u>Worst Performance</u>	119
Transverse Cracking	120
<u>Best Performance</u>	120
<u>Worst Performance</u>	120
Longitudinal Cracking	120
Present Serviceability Rating (PSR) and Roughness	120
8. EFFECT OF DESIGN FEATURES ON PAVEMENT PERFORMANCE	121
Base Type	121
Joint Spacing	121
Dowel Coating	121
9. COMPARISON OF OUTER AND INNER LANE PERFORMANCE	122
10. SUMMARY AND CONCLUSIONS	122
11. ADDITIONAL READING	123
20 STATE ROUTE 2 -- VERMILION, OHIO	124
1. INTRODUCTION	124
2. CLIMATE	124
3. TRAFFIC	124
4. MAINTENANCE AND REHABILITATION	124
5. PHYSICAL TESTING RESULTS	125
6. DRAINABILITY OF PAVEMENT SECTIONS	125
7. DETERIORATION OF PAVEMENT SECTIONS	125
Joint Spalling	125
Joint Faulting	127
Transverse Cracking	127
Longitudinal Cracking	127
Present Serviceability Rating (PSR) and Roughness	127
Other Pavement Distress	128
<u>"D" Cracking</u>	128
<u>Pumping</u>	128
<u>Longitudinal Joint Spalling</u>	128
8. EFFECT OF DESIGN FEATURES ON PAVEMENT PERFORMANCE	129
9. COMPARISON OF OUTER AND INNER LANE PERFORMANCE	129
10. SUMMARY AND CONCLUSIONS	130
11. ADDITIONAL READING	131
21 HIGHWAY 3N -- RUTHVEN, ONTARIO	132

TABLE OF CONTENTS (continued)

VOLUME IV APPENDIX A - PROJECT SUMMARY REPORTS AND SUMMARY TABLES (continued)

<u>Chapter</u>		<u>Page</u>
	1. INTRODUCTION	132
	2. CLIMATE	132
	3. TRAFFIC	133
	4. MAINTENANCE AND REHABILITATION	133
	5. PHYSICAL TESTING RESULTS	133
	6. DRAINABILITY OF PAVEMENT SECTIONS	134
	7. DETERIORATION OF PAVEMENT SECTIONS	135
	Joint Spalling	135
	Joint Faulting	135
	Transverse Cracking	137
	Longitudinal Cracking	137
	Present Serviceability Rating (PSR) and Roughness	137
	Shoulder Condition	138
	Other Distresses	138
	8. EFFECT OF DESIGN FEATURES ON PAVEMENT PERFORMANCE	138
	Base Type	138
	Shoulder Type	139
	Slab Thickness	139
	Base Drainability	139
	9. COMPARISON OF LANE PERFORMANCE BY DIRECTION	140
	10. SUMMARY AND CONCLUSIONS	140
22	HIGHWAY 27 -- TORONTO, ONTARIO	142
	1. INTRODUCTION	142
	2. DESIGN	142
	3. CLIMATE	142
	4. TRAFFIC	142
	5. DRAINABILITY AND OTHER PHYSICAL TESTING RESULTS	142
	6. MAINTENANCE AND REHABILITATION	142
	7. PAVEMENT PERFORMANCE	143
	8. CONCLUSIONS	143
23	ROUTES 66 AND 422 -- KITTANNING, PENNSYLVANIA	144
	1. INTRODUCTION	144
	2. CLIMATE	145
	3. TRAFFIC	145
	4. MAINTENANCE AND REHABILITATION	145
	5. PHYSICAL TESTING RESULTS	145
	6. DRAINABILITY OF PAVEMENT SECTIONS	147
	7. DETERIORATION OF PAVEMENT SECTIONS	147
	Joint Spalling	150
	Joint Faulting	150
	Transverse Cracking	150
	Longitudinal Cracking	150
	Present Serviceability Rating (PSR) and Roughness	150

TABLE OF CONTENTS (continued)

VOLUME IV APPENDIX A - PROJECT SUMMARY REPORTS AND SUMMARY TABLES (continued)

<u>Chapter</u>		<u>Page</u>
	8. EFFECT OF DESIGN FEATURES ON PAVEMENT PERFORMANCE	150
	9. COMPARISON OF OUTER AND INNER LANE PERFORMANCE	151
	10. SUMMARY AND CONCLUSIONS	151
	11. ADDITIONAL READING	152
24	ROUTE 130 -- YARDVILLE, NEW JERSEY	153
	1. INTRODUCTION	153
	2. DESIGN	153
	3. CLIMATE	153
	4. TRAFFIC	153
	5. DRAINABILITY AND OTHER PHYSICAL TESTING RESULTS	153
	6. MAINTENANCE AND REHABILITATION	154
	7. PAVEMENT PERFORMANCE	154
	8. CONCLUSIONS	154
	9. ADDITIONAL READING	154
25	INTERSTATE 676 -- CAMDEN, NEW JERSEY	155
	1. INTRODUCTION	155
	2. CLIMATE	155
	3. TRAFFIC	155
	4. MAINTENANCE AND REHABILITATION	156
	5. PHYSICAL TESTING RESULTS	156
	6. DRAINABILITY OF PAVEMENT SECTIONS	157
	7. DETERIORATION OF PAVEMENT SECTIONS	157
	Joint Spalling	157
	Joint Faulting	159
	Transverse Cracking	159
	Longitudinal Cracking	159
	Present Serviceability Rating (PSR) and Roughness	159
	8. EFFECT OF DESIGN FEATURES ON PAVEMENT PERFORMANCE	159
	9. COMPARISON OF OUTER AND MIDDLE LANE PERFORMANCE	160
	10. SUMMARY AND CONCLUSIONS	160
	11. ADDITIONAL READING	161
26	U.S. 101 -- GEYSERVILLE, CALIFORNIA	162
	1. INTRODUCTION	162
	2. CLIMATE	162
	3. TRAFFIC	162
	4. MAINTENANCE AND REHABILITATION	163
	5. PHYSICAL TESTING RESULTS	163
	6. DRAINABILITY OF PAVEMENT SECTIONS	164
	7. DETERIORATION OF PAVEMENT SECTIONS	164
	Joint Spalling	164
	Joint Faulting	167

TABLE OF CONTENTS (continued)

VOLUME IV APPENDIX A - PROJECT SUMMARY REPORTS AND SUMMARY TABLES (continued)

<u>Chapter</u>	<u>Page</u>
Transverse Cracking	167
Longitudinal Cracking	168
Present Serviceability Rating (PSR) and Roughness	168
Other Pavement Distress	168
8. EFFECT OF DESIGN FEATURES ON PAVEMENT PERFORMANCE	168
Tied Concrete Shoulders	168
Joint Sealant	169
9. COMPARISON OF OUTER AND INNER LANE PERFORMANCE	169
10. SUMMARY AND CONCLUSIONS	170
11. ADDITIONAL READING	171
27 INTERSTATE 95 -- ROCKY MOUNT, NORTH CAROLINA	172
1. INTRODUCTION	172
2. CLIMATE	172
3. TRAFFIC	172
4. MAINTENANCE AND REHABILITATION	172
5. PHYSICAL TESTING RESULTS	172
6. DRAINABILITY OF PAVEMENT SECTIONS	174
7. DETERIORATION OF PAVEMENT SECTIONS	174
Joint Spalling	174
Joint Faulting	174
<u>Best Performance</u>	177
<u>Worst Performance</u>	177
Transverse Cracking	177
Longitudinal Cracking	178
<u>Best Performance</u>	178
<u>Worst Performance</u>	178
Present Serviceability Rating (PSR) and Roughness	178
8. EFFECT OF DESIGN FEATURES ON PAVEMENT PERFORMANCE	179
Base Type	179
Joint Load Transfer	179
Pavement Type/Joint Spacing	179
Joint Orientation	180
9. COMPARISON OF OUTER LANE AND INNER LANE PERFORMANCE ...	180
10. SUMMARY AND CONCLUSIONS	181
11. ADDITIONAL READING	182
28 INTERSTATE 85 -- GREENSBORO, NORTH CAROLINA	183
1. INTRODUCTION	183
2. DESIGN	183
3. CLIMATE	183
4. TRAFFIC	183
5. DRAINABILITY AND OTHER PHYSICAL TESTING RESULTS	183
6. MAINTENANCE AND REHABILITATION	184
7. PAVEMENT PERFORMANCE	184

TABLE OF CONTENTS (continued)

VOLUME IV APPENDIX A - PROJECT SUMMARY REPORTS AND SUMMARY TABLES (continued)

<u>Chapter</u>	<u>Page</u>
8. CONCLUSIONS	184
9. ADDITIONAL READING	185
29 I-75 -- TAMPA, FLORIDA (HILLSBOROUGH COUNTY)	186
1. INTRODUCTION	186
2. DESIGN	186
3. CLIMATE	186
4. TRAFFIC	186
5. DRAINABILITY AND OTHER PHYSICAL TESTING RESULTS	186
6. MAINTENANCE AND REHABILITATION	187
7. PAVEMENT PERFORMANCE	187
8. CONCLUSIONS	187
30 INTERSTATE 75 -- TAMPA, FLORIDA (MANATEE COUNTY)	188
1. INTRODUCTION	188
2. DESIGN	188
3. CLIMATE	188
4. TRAFFIC	188
5. DRAINABILITY AND OTHER PHYSICAL TESTING RESULTS	188
6. MAINTENANCE AND REHABILITATION	189
7. PAVEMENT PERFORMANCE	189
8. CONCLUSIONS	191
9. ADDITIONAL READING	191
31 KEY TO PROJECT SUMMARY TABLES	192
1. GENERAL AND ENVIRONMENTAL DATA	192
2. DESIGN DATA	193
3. MONITORING DATA	199
4. PERFORMANCE DATA	203
32 SUMMARY OF PROJECT DATA	205
33 REFERENCES	246

VOLUME V APPENDIX B - DATA COLLECTION AND ANALYSIS PROCEDURES

<u>Chapter</u>	<u>Page</u>
1 FIELD DATA COLLECTION PROCEDURES	1
1. INTRODUCTION	1

TABLE OF CONTENTS (continued)

VOLUME V APPENDIX B - DATA COLLECTION AND ANALYSIS PROCEDURES (continued)

<u>Chapter</u>		<u>Page</u>
	2. CONDITION SURVEY	1
	Measurements	1
	Mapped Distresses	5
	Evaluated Conditions	6
	Noted Conditions	6
	3. PHOTO SURVEY	6
	4. DRAINAGE SURVEY	8
	5. FIELD TESTING	9
	Falling Weight Deflectometer (FWD)	9
	Coring and boring	9
	Roughness/PSR	14
	Traffic Control	14
	6. WEIGH-IN-MOTION DATA COLLECTION	14
	7. SUGGESTIONS FOR FUTURE DATA COLLECTION AND TESTING	16
2	WEIGH-IN-MOTION DATA COLLECTION PROCEDURES	17
	1. INTRODUCTION	17
	2. SITE SETUP AND CALIBRATION	17
	3. ACCURACY OF WIM DATA	19
3	TRAFFIC ANALYSIS	23
	1. INTRODUCTION	23
	2. INPUTS FOR PROCEDURE	23
	Average Daily Traffic, ADT	23
	Percentage of Heavy Trucks, TKS	23
	Directional Distribution, DD	24
	Lane Distribution, LD	24
	Average Truck Factor, TF	24
	3. CALCULATION PROCEDURE	25
	4. SUMMARY	25
4	DRAINAGE ANALYSIS AND DETERMINATION OF DRAINAGE COEFFICIENTS	26
	1. INTRODUCTION	26
	2. AASHTO DRAINAGE CRITERIA	27
	Roadbed Soils	27
	Cross Section	27
	3. MAD INDEX	28
	Base Drainability	29
	Climatic Moisture	29
	Subgrade	29
	MAD Index Categories	29
	<u>Base Drainage</u>	29
	<u>Subgrade Drainage</u>	30

TABLE OF CONTENTS (continued)

VOLUME V APPENDIX B - DATA COLLECTION AND ANALYSIS PROCEDURES (continued)

<u>Chapter</u>		<u>Page</u>
	<u>Climatic Moisture Availability</u>	30
4.	DEVELOPING A DRAINAGE COEFFICIENT	32
	Time of Saturation	32
	Base Drainability	35
	Subgrade Drainability	37
	Combining Base and Subgrade	37
	Cross Section	37
5.	DRAINAGE COEFFICIENTS FOR SECTIONS	39
	Arizona 1	40
	Arizona 2	40
	California 1	41
	California 2	41
	California 3	42
	California 6	43
	California 7	43
	California 8	44
	Florida 2	44
	Florida 3	44
	Michigan 1	44
	Michigan 3	45
	Michigan 4	46
	Michigan 5	46
	Minnesota 1	47
	Minnesota 2	48
	Minnesota 3	49
	Minnesota 4	49
	Minnesota 5	49
	Minnesota 6	50
	New Jersey 2	50
	New Jersey 3	51
	New York 1	51
	New York 2	52
	North Carolina 1	53
	North Carolina 2	54
	Ohio 1	54
	Ohio 2	55
	Ontario 1	55
	Ontario 2	56
	Pennsylvania 1	56
5	BACKCALCULATION METHODOLOGY	58
	1. INTRODUCTION	58
	2. FUNDAMENTAL CONCEPTS	58
	3. OUTLINE OF BACKCALCULATION PROCEDURE	63
	4. APPLICATION OF CLOSED-FORM BACKCALCULATION PROCEDURE ..	64
	5. VARIABILITY AND RELIABILITY OF TESTING AND	

TABLE OF CONTENTS (continued)

VOLUME V APPENDIX B - DATA COLLECTION AND ANALYSIS PROCEDURES (continued)

<u>Chapter</u>		<u>Page</u>
	BACKCALCULATED VALUES	65
	Plate Theory	66
	Deflection Measurement	69
	Finite Element Analysis	70
6.	ADVANTAGES OF CLOSED-FORM BACKCALCULATION PROCEDURE ..	75
6	DATABASE DESCRIPTION	77
7	REFERENCES	82
8	ANNOTATED BIBLIOGRAPHY	85
	1. EXPERIMENTAL PROJECTS AND PAVEMENT PERFORMANCE	85
	2. SUBDRAINAGE	102
	3. LOAD TRANSFER	109
	4. JOINTS AND JOINT SEALING	111
	5. CONCRETE SHOULDERS	116
	6. PAVEMENT DESIGN	119
	7. PAVEMENT ANALYSIS	123
	8. LIFE CYCLE COSTS	125
	9. WEIGH-IN-MOTION	126

VOLUME VI APPENDIX C AND APPENDIX D

APPENDIX C - SYNTHESIS OF CONCRETE PAVEMENT DESIGN METHODS AND ANALYSIS MODELS

<u>Chapter</u>		<u>Page</u>
PART I.	REVIEW OF SELECTED DESIGN AND ANALYSIS MODELS	1
1.	INTRODUCTION	1
2.	EVALUATION OF THE ANALYSIS AND DESIGN MODELS	1
3.	CAPABILITIES AND LIMITATIONS OF ANALYSIS MODELS	2
	ILLISLAB	2
	<u>Capabilities</u>	2
	<u>Limitations</u>	3
	JSLAB	4
	<u>Capabilities</u>	4
	<u>Limitations</u>	4
	WESLIQID	5
	<u>Capabilities</u>	5
	<u>Limitations</u>	5
	WESLAYER	6
	<u>Capabilities</u>	6
	<u>Limitations</u>	6

TABLE OF CONTENTS (continued)

VOLUME VI APPENDIX C AND APPENDIX D

APPENDIX C - SYNTHESIS OF CONCRETE PAVEMENT DESIGN METHODS AND ANALYSIS MODELS (continued)

<u>Chapter</u>	<u>Page</u>
PMARP	7
<u>Capabilities</u>	7
<u>Limitations</u>	7
RISC	9
<u>Capabilities</u>	9
<u>Limitations</u>	10
H51	10
<u>Capabilities</u>	10
<u>Limitations</u>	11
CMS	11
<u>Capabilities</u>	11
<u>Limitations</u>	12
Liu-Lytton Drainage Models	12
<u>Capabilities</u>	13
<u>Limitations</u>	13
JRCP4	14
<u>Capabilities</u>	14
<u>Limitations</u>	14
4. CAPABILITIES AND LIMITATIONS OF DESIGN AND PREDICTION MODELS	15
PREDICT	15
<u>Capabilities</u>	15
<u>Limitations</u>	16
PEARLARP	16
<u>Capabilities</u>	16
<u>Limitations</u>	17
JCP-1	17
<u>Capabilities</u>	17
<u>Limitations</u>	18
DNPS86	19
<u>Capabilities</u>	19
<u>Limitations</u>	19
RPS-3	20
<u>Capabilities</u>	20
<u>Limitations</u>	21
PCA Design Procedure	22
<u>Capabilities</u>	22
<u>Limitations</u>	22
California Rigid Pavement Design Procedure	23
<u>Capabilities</u>	23
<u>Limitations</u>	23
BERM	24
<u>Capabilities</u>	24
<u>Limitations</u>	25
JCS-1	25

TABLE OF CONTENTS (continued)

VOLUME VI APPENDIX C AND APPENDIX D

APPENDIX C - SYNTHESIS OF CONCRETE PAVEMENT DESIGN METHODS AND ANALYSIS MODELS (continued)

<u>Chapter</u>		<u>Page</u>
	<u>Capabilities</u>	25
	<u>Limitations</u>	26
5.	OVERALL PROGRAM EVALUATION	26
	Structural Analysis Models	27
	Drainage/Climatic Analysis Models	27
	Pavement Design Methods	28
6.	RECOMMENDATIONS	28
	Structural Analysis Model	28
	Prediction Models	30
	Drainage/Climatic Model	30
	Design Method	30
PART II.	STANDARD PAVEMENT SECTION AND VARIABLES UNDER CONSIDERATION	32
PART III.	SUMMARY OF INPUT AND OUTPUT VARIABLES	51
PART IV.	RESULTS OF SENSITIVITY ANALYSIS	79

APPENDIX D - SUMMARY OF ANALYSIS DATA FOR THE EVALUATION OF PREDICTIVE MODELS

<u>Chapter</u>		<u>Page</u>
1.	INTRODUCTION	115
2.	DESCRIPTION OF TABLES AND FIGURES	115
REFERENCES	329

LIST OF FIGURES

VOLUME I EVALUATION OF CONCRETE PAVEMENT PERFORMANCE AND DESIGN FEATURES

<u>Figure</u>	<u>Title</u>	<u>Page</u>
1.	States and Provinces participating in study	5
2.	Experimental design matrix for Minnesota 1	7
3.	Experimental design matrix for Minnesota 2	7
4.	Experimental design matrix for Arizona 1	9
5.	Experimental design matrix for California 1	10
6.	Experimental design matrix for California 2	10
7.	Experimental design matrix for Michigan 1	12
8.	Experimental design matrix for Michigan 4	12
9.	Experimental design matrix for New York 1	14
10.	Experimental design matrix for New York 2	14
11.	Experimental design matrix for Ohio 1	16
12.	Experimental design matrix for Ohio 2	16
13.	Experimental design matrix for Ontario 1	17
14.	Experimental design matrix for Pennsylvania 1	19
15.	Experimental design matrix for New Jersey 3	20
16.	Experimental design matrix for California 3	20
17.	Experimental design matrix for North Carolina 1	22
18.	Outer lane performance data for Minnesota 1 (Age = 17 years, ESAL's = 5.5 million)	29
19.	Outer lane performance data for Minnesota 2 (Age = 10 years, ESAL's = 2.8 million)	33
20.	Outer lane performance data for Arizona 1	39
21.	Outer lane performance data for California 1 (Age = 16 years, ESAL's = 7.6 million)	43
22.	Outer lane performance data for California 2 (Age = 7 years, ESAL's = 4.4 million)	47
23.	Outer lane performance data for Michigan 1 (Age = 12 years, ESAL's = 0.89 million)	53
24.	Outer lane performance data for Michigan 4 (Age = 17 years, ESAL's = 4.4 million)	58
25.	Outer lane performance data for New York 1 (Age = 19 years, ESAL's = 3.1 million)	64
26.	Outer lane performance data for New York 2 (Age = 12 years, ESAL's = 1.4 million)	67
27.	Outer lane performance data for Ohio 1 (Age = 14 years, ESAL's = 3.4 million)	71
28.	Outer lane performance data for Ohio 2 (Age = 13 years, ESAL's = 3.3 million)	74
29.	Performance data by direction for Ontario 1 (Age = 5 years, ESAL's = 1.0 million)	77
30.	Outer lane performance data for Pennsylvania 1	83
31.	Outer lane performance data for New Jersey 3 (Age = 8 years, ESAL's = 4.2 million)	87
32.	Outer lane performance data for California 3 (Age = 12 years, ESAL's = 3.6 million)	91
33.	Outer lane performance data for North Carolina 1 (Age = 20 years, ESAL's 9.1 million)	95

LIST OF FIGURES (continued)

VOLUME I EVALUATION OF CONCRETE PAVEMENT PERFORMANCE AND DESIGN FEATURES (continued)

<u>Figure</u>	<u>Title</u>	<u>Page</u>
34.	Percent cracked slabs vs. L/1 for California 1 (Tracy) sections	131
35.	Percent cracked slabs vs. L/1 for all sections with cement-treated and lean concrete bases	132
36.	Percent cracked slabs vs. L/1 for all sections with aggregate bases	134

VOLUME II EVALUATION AND MODIFICATION OF CONCRETE PAVEMENT DESIGN AND ANALYSIS MODELS

<u>Figure</u>	<u>Title</u>	<u>Page</u>
1.	Distribution of base type by environmental region	13
2.	Distribution of slab thickness by environmental region	14
3.	Distribution of joint spacing and pavement type by environmental region (P=JPCP, R=JRCP)	15
4.	Distribution of load transfer method by environmental region	16
5.	Distribution of shoulder type by environmental region	18
6.	Scattergram of actual field-measured faulting versus faulting as predicted using the COPES faulting models for the dry-freeze region	42
7.	Experimental design matrix for Minnesota 1	70
8.	Experimental design matrix for California 1	72
9.	Experimental design matrix for Michigan 1	73
10.	Experimental design matrix for North Carolina 1	74
11.	Use of CMS in the design process	77
12.	Temperature profile versus depth through the slab on July 15, 1987, Rothsay, Minnesota	81
13.	Change in 6 a.m. thermal gradient in June 1987, Rothsay, Minnesota	82
14.	Change in 3 p.m. thermal gradient in June 1987, Rothsay, Minnesota	82
15.	Temperature profile versus depth through the slab on July 15, 1987, Tracy, California	86
16.	Change in 6 a.m. thermal gradient from January through June 1987, Tracy, California	88
17.	Change in 6 a.m. thermal gradient from July through December 1987, Tracy, California	88
18.	Change in 3 p.m. thermal gradient from January through June 1987, Tracy, California	90
19.	Change in 3 p.m. thermal gradient from July through December 1987, Tracy, California	90
20.	Temperature profile versus depth through the slab on July 15, 1987, Clare, Michigan	91
21.	Change in 6 a.m. thermal gradient in April 1987, Clare, Michigan	92
22.	Change in 3 p.m. thermal gradient in April 1987, Clare, Michigan	92
23.	Change in 6 a.m. thermal gradient in June 1987, Clare, Michigan	93
24.	Change in 3 p.m. thermal gradient in June 1987, Clare, Michigan	93

LIST OF FIGURES (continued)

VOLUME II EVALUATION AND MODIFICATION OF CONCRETE PAVEMENT DESIGN AND ANALYSIS MODELS (continued)

<u>Figure</u>	<u>Title</u>	<u>Page</u>
25.	Change in 6 a.m. thermal gradient in August 1987, Clare, Michigan	94
26.	Change in 3 p.m. thermal gradient in August 1987, Clare, Michigan	94
27.	Change in 6 a.m. thermal gradient in December 1987, Clare Michigan	95
28.	Change in 3 p.m. thermal gradient in December 1987, Clare Michigan	95
29.	Frostline versus depth in January, 1987, Clare, Michigan	96
30.	Temperature profile versus depth through the slab on July 15, 1987, Rocky Mount, North Carolina	100
31.	Change in 6 a.m. thermal gradient in July 1987, Rocky Mount, North Carolina	102
32.	Change in 3 p.m. thermal gradient in April 1987, Clare, Michigan	102
33.	Percent drainage versus time for MN 1-1, MN 1-5, and MN 1-9	108
34.	Percent saturation versus base course modulus for MN 1-1, MN 1-2, MN 1-3, and MN 1-4	111
35.	Percent saturation versus subgrade modulus for MN 1-1, MN 1-2, MN 1-3, and MN 1-4	113
36.	Percent drainage versus time for CA 1-1, CA 1-7, and CA 1-9	115
37.	Percent saturation versus subbase modulus for CA 1-1, CA 1-7, and CA 1-9	117
38.	Percent saturation versus subgrade modulus for CA 1-1, CA 1-7, and CA 1-9	118
39.	Percent drainage versus time for MI 1-1a, MI 1-4a, and MI 1-10b	120
40.	Percent saturation versus base or subbase modulus for MI 1-1a, MI 1-10a, and MI 1-10b	122
41.	Percent saturation versus subgrade modulus for MI 1-1a, MI 1-4a, and MI 1-10b	123
42.	Percent drainage versus time for NC 1-1, NC 1-2, and NC 1-7	126
43.	Percent saturation versus base modulus for NC 1-1, NC 1-7, and NC 1-8	127
44.	Percent saturation versus subgrade modulus for NC 1-1, NC 1-7, and NC 1-8	129
45.	Example finite element mesh for the edge loading condition	136
46.	FWD sensor location at the approach joint	148
47.	Measured deflection basin and calculated deflection basin from void analysis	150
48.	Finite element mesh for a 15-ft (4.6 m) slab used in the PMARP evaluation of the corner loading condition	157
49.	Original zero-maintenance fatigue damage curve supplemented with projects from current study	167
50.	Predicted versus actual faulting for doweled joint faulting model	184
51.	Sensitivity of doweled joint faulting model to dowel diameter	185
52.	Sensitivity of doweled joint faulting model to drainage and shoulder type	186
53.	Predicted versus actual faulting for nondoweled joint faulting model	189
54.	Sensitivity of doweled and nondoweled faulting models to drainage and shoulder type	190
55.	Relation between deflection load transfer efficiency and stress load transfer efficiency	195
56.	Percent slabs cracked versus accumulated fatigue damage	197
57.	Sensitivity of cracking model to shoulder type	198
58.	Sensitivity of cracking model to joint spacing	199
59.	Sensitivity of cracking model to slab thickness	201
60.	Sensitivity of JPCP joint spalling model to sealant type	203

LIST OF FIGURES (continued)

VOLUME II EVALUATION AND MODIFICATION OF CONCRETE PAVEMENT DESIGN AND ANALYSIS MODELS (continued)

<u>Figure</u>	<u>Title</u>	<u>Page</u>
61.	Sensitivity of JRCF joint spalling model to climate	204
62.	Sensitivity of JRCF joint spalling model to sealant type	206

VOLUME III SUMMARY OF RESEARCH FINDINGS

<u>Figure</u>	<u>Title</u>	<u>Page</u>
1.	States participating in study	4
2.	Distribution of base type by climatic region	11
3.	Distribution of slab thickness by climatic region	13
4.	Distribution of joint spacing/pavement type by climatic region	14
5.	Distribution of load transfer mechanism by climatic region	15
6.	Distribution of shoulder type (and widened lanes) by climatic region	16
7.	Percent slab cracking as a function of L/l for sections with aggregate bases	25
8.	Percent slab cracking as a function of L/l for sections with LCB and CTB bases	25
9.	Sensitivity of doweled faulting model to dowel diameter	58
10.	Sensitivity of doweled faulting model to drainage and shoulder type	58
11.	Sensitivity of faulting models to dowels, drainage, and shoulder type	59
12.	Percent slab cracking as a function of accumulated fatigue damage	59
13.	Sensitivity of JPCP cracking model to shoulder type	63
14.	Sensitivity of JPCP cracking model to joint spacing	63
15.	Sensitivity of JPCP cracking model to slab thickness	64
16.	Sensitivity of JPCP spalling model to joint sealant type	64
17.	Sensitivity of JPCP spalling model to climate	66
18.	Sensitivity of JRCF spalling model to joint sealant type	66

VOLUME IV APPENDIX A - PROJECT SUMMARY REPORTS AND SUMMARY TABLES

<u>Figure</u>	<u>Title</u>	<u>Page</u>
1.	Outer lane performance data for Minnesota 1	4
2.	Inner lane performance data for Minnesota 1	5
3.	Outer and inner lane performance data for Minnesota 2	16
4.	Outer lane performance data for Arizona 1	32
5.	Inner lane performance data for Arizona 1	33
6.	Outer lane performance data for California 1	45
7.	Inner lane performance data for California 1	46
8.	Outer and middle lane performance data for California 2	55
9.	Outer lane performance data for Michigan 1	70
10.	Inner lane performance data for Michigan 1	71
11.	Outer and inner lane performance data for Michigan 4	85
12.	Outer lane performance data for New York 1	97

LIST OF FIGURES (continued)

VOLUME IV APPENDIX A - PROJECT SUMMARY REPORTS AND SUMMARY TABLES (continued)

<u>Figure</u>	<u>Title</u>	<u>Page</u>
13.	Inner lane performance data for New York 1	98
14.	Outer lane performance data for New York 2	108
15.	Inner lane performance data for New York 2	109
16.	Outer lane performance data for Ohio 1	117
17.	Inner lane performance data for Ohio 1	118
18.	Outer and inner lane performance data for Ohio 2	126
19.	Performance data by direction for Ontario 1	136
20.	Outer lane performance data for Pennsylvania 1	148
21.	Inner lane performance data for Pennsylvania 1	149
22.	Outer and middle lane performance data for New Jersey 3	158
23.	Outer lane performance data for California 3	165
24.	Inner lane performance data for California 3	166
25.	Outer lane performance data for North Carolina 1	175
26.	Inner lane performance data for North Carolina 1	176

VOLUME V APPENDIX B - DATA COLLECTION AND ANALYSIS PROCEDURES

<u>Figure</u>	<u>Title</u>	<u>Page</u>
1.	General field survey sheet	2
2.	Drainage field survey sheet	3
3.	Field data collection form	4
4.	Project photographic record	7
5.	Layout for FWD testing of projects with AC shoulders	10
6.	Layout for FWD testing of projects with PCC shoulders	11
7.	Layout for FWD testing of projects with widened lanes	12
8.	Raw data file from the Dynatest model 8000	13
9.	Sample raw output from Mays Roughness Meter	15
10.	Climatic zones for AASHTO and FHWA procedures	31
11.	Plot of monthly rainfall and potential evapotranspiration for Clare, Michigan	34
12.	Procedure to combine drainabilities of base and subgrade	38
13.	Variation in deflection basin AREA with radius of relative stiffness	60
14.	Variation in dimensionless deflections with radius of relative stiffness for the dense liquid foundation	61
15.	Variation in dimensionless deflections with radius of relative stiffness for the elastic solid foundation	62
16.	Deflection basin as measured by the FWD and as calculated using the closed-form procedure	71
17.	Deflection basin as measured by the FWD and as calculated using the closed-form procedure	72
18.	Deflection basin as measured by the FWD and as calculated using the closed-form procedure	73
19.	Eh**3 versus kl**4 for all Phase I sections	74
20.	Main UNIFY database menu	79
21.	Inventory database menu	80
22.	Monitoring database menu	81

LIST OF FIGURES (continued)

VOLUME VI APPENDIX C AND APPENDIX D

APPENDIX C - SYNTHESIS OF CONCRETE PAVEMENT DESIGN METHODS AND ANALYSIS MODELS

<u>Figure</u>	<u>Title</u>	<u>Page</u>
1.	Assumed standard pavement section	33
2.	ILLISLAB and JSLAB finite element mesh for standard pavement section analysis	38
3.	ILLISLAB and JSLAB finite element mesh for 10-ft joint spacing analysis	39
4.	ILLISLAB and JSLAB finite element mesh for 20-ft joint spacing analysis	40
5.	ILLISLAB and JSLAB finite element mesh for widened lane analysis	41
6.	WESLIQID and WESLAYER finite element mesh for standard pavement analysis using a four-slab system	42
7.	WESLIQID and WESLAYER finite element mesh for standard pavement analysis using a two-slab system	43
8.	WESLIQID and WESLAYER finite element mesh for 10-ft joint spacing analysis	44
9.	WESLIQID and WESLAYER finite element mesh for 20-ft joint spacing analysis	45
10.	WESLIQID and WESLAYER finite element mesh for widened lane analysis	46
11.	PMARP finite element mesh for standard pavement section	47
12.	PMARP finite element mesh for widened lane analysis	48
13.	PMARP finite element mesh for 20-ft joint spacing analysis	49
14.	Wheel configuration used for H-51 analysis	50
15.	Temperature gradient as measured by CMS	93
16.	Climatic zones based on Thornthwaite potential evapotranspiration and moisture index and their interaction with performance, with similar performance expected in similar climatic regions (5)	98

APPENDIX D - SUMMARY OF ANALYSIS DATA FOR THE EVALUATION OF PREDICTIVE MODELS

<u>Figure</u>	<u>Title</u>	<u>Page</u>
17.	Actual ESAL's (based on ADT) versus ESAL's as predicted using the AASHTO design equation for all Phase I sections	119
18.	Actual ESAL's (based on ADT) versus ESAL's as predicted using the AASHTO design equation for the dry-freeze region	122
19.	Actual ESAL's (based on ADT) versus ESAL's as predicted using the AASHTO design equation for the dry-nonfreeze region	122
20.	Actual ESAL's (based on ADT) versus ESAL's as predicted using the AASHTO design equation for the wet-freeze region	126
21.	Actual ESAL's (based on ADT) versus ESAL's as predicted using the AASHTO design equation for the wet-nonfreeze region	126

LIST OF FIGURES (continued)

VOLUME VI APPENDIX C AND APPENDIX D

APPENDIX D - SUMMARY OF ANALYSIS DATA FOR THE EVALUATION OF PREDICTIVE MODELS (continued)

<u>Figure</u>	<u>Title</u>	<u>Page</u>
22.	Actual PSR as determined by a panel of users versus PSI as predicted by the PEARDARP PSI model for all Phase I sections	130
23.	Actual PSR as determined by a panel of users versus PSI as predicted by the PEARDARP PSI model for the dry-freeze region	133
24.	Actual PSR as determined by a panel of users versus PSI as predicted by the PEARDARP PSI model for the dry-nonfreeze region	133
25.	Actual PSR as determined by a panel of users versus PSI as predicted by the PEARDARP PSI model for the wet-freeze region	137
26.	Actual PSR as determined by a panel of users versus PSI as predicted by the PEARDARP PSI model for the wet-nonfreeze region	137
27.	Actual field measured roughness versus roughness as predicted using the PEARDARP roughness model for all Phase I sections	141
28.	Actual field measured roughness versus roughness as predicted using the PEARDARP roughness model for the dry-freeze region	144
29.	Actual field measured roughness versus roughness as predicted using the PEARDARP roughness model for the dry-nonfreeze region	144
30.	Actual field measured roughness versus roughness as predicted using the PEARDARP roughness model for the wet-freeze region	148
31.	Actual field measured roughness versus roughness as predicted using the PEARDARP roughness model for the wet-nonfreeze region	148
32.	Actual field measured spalling versus spalling as predicted using the PEARDARP spalling model for all Phase I sections	155
33.	Actual field measured spalling versus spalling as predicted using the PEARDARP spalling model for the dry-freeze region	158
34.	Actual field measured spalling versus spalling as predicted using the PEARDARP spalling model for the dry-nonfreeze region	158
35.	Actual field measured spalling versus spalling as predicted using the PEARDARP spalling model for the wet-freeze region	162
36.	Actual field measured spalling versus spalling as predicted using the PEARDARP spalling model for the wet-nonfreeze region	162
37.	Actual field measured faulting versus faulting as predicted using the PEARDARP faulting models for all Phase I sections	166
38.	Actual field measured faulting versus faulting as predicted using the PEARDARP faulting models for the dry-freeze region	168
39.	Actual field measured faulting versus faulting as predicted using the PEARDARP faulting models for doweled pavements for the dry-freeze region	171
40.	Actual field measured faulting versus faulting as predicted using the PEARDARP faulting models for nondoweled pavements for the dry-freeze region	171
41.	Actual field measured faulting versus faulting as predicted using the PEARDARP faulting models for the dry-nonfreeze region	173

LIST OF FIGURES (continued)

VOLUME VI APPENDIX C AND APPENDIX D

APPENDIX D - SUMMARY OF ANALYSIS DATA FOR THE EVALUATION OF PREDICTIVE MODELS (continued)

<u>Figure</u>	<u>Title</u>	<u>Page</u>
42.	Actual field measured faulting versus faulting as predicted using the PEARDARP faulting models for the wet-freeze region	176
43.	Actual field measured faulting versus faulting as predicted using the PEARDARP faulting models for doweled pavements for the wet-freeze region	179
44.	Actual field measured faulting versus faulting as predicted using the PEARDARP faulting models for nondoweled pavements for the wet-freeze region	179
45.	Actual field measured faulting versus faulting as predicted using the PEARDARP faulting models for the wet-nonfreeze region	181
46.	Actual field measured faulting versus faulting as predicted using the PEARDARP faulting models for doweled pavements for the wet-nonfreeze region	184
47.	Actual field measured faulting versus faulting as predicted using the PEARDARP faulting models for nondoweled pavements for the wet-nonfreeze region	184
48.	Actual field measured cracking versus cracking as predicted using the PEARDARP cracking models for all Phase I sections	188
49.	Actual field measured cracking versus cracking as predicted using the PEARDARP cracking model for the dry-freeze region	191
50.	Actual field measured cracking versus cracking as predicted using the PEARDARP cracking model for the dry-nonfreeze region	191
51.	Actual field measured cracking versus cracking as predicted using the PEARDARP cracking model for the wet-freeze region	195
52.	Actual field measured cracking versus cracking as predicted using the PEARDARP cracking model for the wet-nonfreeze region	195
53.	Actual field observed pumping versus pumping as predicted using COPES pumping models for all Phase I sections	199
54.	Actual field observed pumping versus pumping as predicted using COPES pumping models for the dry-freeze region	201
55.	Actual field observed pumping versus pumping as predicted using COPES JPCP pumping model for the dry-freeze region	204
56.	Actual field observed pumping versus pumping as predicted using COPES JRCP pumping model for the dry-freeze region	204
57.	Actual field observed pumping versus pumping as predicted using COPES pumping model for the dry-nonfreeze region	206
58.	Actual field observed pumping versus pumping as predicted using COPES pumping model for the wet-freeze region	209
59.	Actual field observed pumping versus pumping as predicted using COPES JPCP pumping model for the wet-freeze region	212
60.	Actual field observed pumping versus pumping as predicted using COPES JRCP pumping model for the wet-freeze region	212
61.	Actual field observed pumping versus pumping as predicted using COPES pumping model for the wet-nonfreeze region	214

LIST OF FIGURES (continued)

VOLUME VI APPENDIX C AND APPENDIX D

APPENDIX D - SUMMARY OF ANALYSIS DATA FOR THE EVALUATION OF PREDICTIVE MODELS (continued)

<u>Figure</u>	<u>Title</u>	<u>Page</u>
62.	Actual field measured faulting versus faulting as predicted using the COPES faulting models for all Phase I sections	218
63.	Actual field measured faulting versus faulting as predicted using the COPES faulting models for the dry-freeze region	220
64.	Actual field measured faulting versus faulting as predicted using the COPES JPCP faulting model for the dry-freeze region	223
65.	Actual field measured faulting versus faulting as predicted using the COPES JRCP faulting model for the dry-freeze region	223
66.	Actual field measured faulting versus faulting as predicted using the COPES faulting models for the dry-nonfreeze region	225
67.	Actual field measured faulting versus faulting as predicted using the COPES faulting models for the wet-freeze region	228
68.	Actual field measured faulting versus faulting as predicted using the COPES JPCP faulting model for the wet-freeze region	231
69.	Actual field measured faulting versus faulting as predicted using the COPES JRCP faulting model for the wet-freeze region	231
70.	Actual field measured faulting versus faulting as predicted using the COPES faulting models for the wet-nonfreeze region	233
71.	Actual field measured spalling versus joint deterioration (spalling) as predicted using the COPES spalling models for all Phase I sections	237
72.	Actual field measured spalling versus joint deterioration (spalling) as predicted using the COPES spalling models for the dry-freeze region	239
73.	Actual field measured spalling versus joint deterioration (spalling) as predicted using the COPES JPCP joint deterioration model for the dry-freeze region	242
74.	Actual field measured spalling versus joint deterioration (spalling) as predicted using the COPES JRCP joint deterioration model for the dry-freeze region	242
75.	Actual field measured spalling versus joint deterioration (spalling) as predicted using the COPES spalling models for the dry-nonfreeze region	244
76.	Actual field measured spalling versus joint deterioration (spalling) as predicted using the COPES spalling models for the wet-freeze region	247
77.	Actual field measured spalling versus joint deterioration (spalling) as predicted using the COPES JPCP joint deterioration model for the wet-freeze region	250
78.	Actual field measured spalling versus joint deterioration (spalling) as predicted using the COPES JRCP joint deterioration model for the wet-freeze region	250

LIST OF FIGURES (continued)

VOLUME VI APPENDIX C AND APPENDIX D

APPENDIX D - SUMMARY OF ANALYSIS DATA FOR THE EVALUATION OF PREDICTIVE MODELS (continued)

<u>Figure</u>	<u>Title</u>	<u>Page</u>
79.	Actual field measured spalling versus joint deterioration (spalling) as predicted using the COPEs spalling models for the wet-nonfreeze region	252
80.	Actual field measured cracking versus cracking as predicted by the COPEs cracking models for all Phase I sections	256
81.	Actual field measured cracking versus cracking as predicted by the COPEs cracking models for the dry-freeze region	258
82.	Actual field measured cracking versus cracking as predicted by the COPEs JPCP cracking model for the dry-freeze region	261
83.	Actual field measured cracking versus cracking as predicted by the COPEs JRCP cracking model for the dry-freeze region	261
84.	Actual field measured cracking versus cracking as predicted by the COPEs cracking models for the dry-nonfreeze region	263
85.	Actual field measured cracking versus cracking as predicted by the COPEs cracking models for the wet-freeze region	266
86.	Actual field measured cracking versus cracking as predicted by the COPEs JPCP cracking models for the wet-freeze region	269
87.	Actual field measured cracking versus cracking as predicted by the COPEs JRCP cracking models for the wet-freeze region	269
88.	Actual field measured cracking versus cracking as predicted by the COPEs cracking models for the wet-nonfreeze region	271
89.	Actual PSR as determined by a panel of users versus PSR as predicted by the COPEs PSR models for all Phase I sections	275
90.	Actual PSR as determined by a panel of users versus PSR as predicted by the COPEs PSR models for the dry-freeze region	277
91.	Actual PSR as determined by a panel of users versus PSR as predicted by the COPEs JPCP PSR model for the dry-freeze region	280
92.	Actual PSR as determined by a panel of users versus PSR as predicted by the COPEs JRCP PSR model for the dry-freeze region	280
93.	Actual PSR as determined by a panel of users versus PSR as predicted by the COPEs PSR models for the dry-nonfreeze region	282
94.	Actual PSR as determined by a panel of users versus PSR as predicted by the COPEs PSR models for the wet-freeze region	285
95.	Actual PSR as determined by a panel of users versus PSR as predicted by the COPEs JPCP PSR model for the wet-freeze region	288
96.	Actual PSR as determined by a panel of users versus PSR as predicted by the COPEs JRCP PSR model for the wet-freeze region	288
97.	Actual PSR as determined by a panel of users versus PSR as predicted by the COPEs PSR models for the wet-nonfreeze region	290
98.	Actual field measured faulting versus faulting as predicted using the PFAULT models for all Phase I sections	294
99.	Actual field measured faulting versus faulting as predicted using the PFAULT models for the dry-freeze region	296

LIST OF FIGURES (continued)

VOLUME VI APPENDIX C AND APPENDIX D

APPENDIX D - SUMMARY OF ANALYSIS DATA FOR THE EVALUATION OF PREDICTIVE MODELS (continued)

<u>Figure</u>	<u>Title</u>	<u>Page</u>
100.	Actual field measured faulting versus faulting as predicted using the PFAULT models for doweled pavements for the dry-freeze region	299
101.	Actual field measured faulting versus faulting as predicted using the PFAULT models for nondoweled pavements for the dry-freeze region	299
102.	Actual field measured faulting versus faulting as predicted using the PFAULT models for the dry-nonfreeze region	301
103.	Actual field measured faulting versus faulting as predicted using the PFAULT models for the wet-freeze region	304
104.	Actual field measured faulting versus faulting as predicted using the PFAULT models for doweled pavements for the wet-freeze region	307
105.	Actual field measured faulting versus faulting as predicted using the PFAULT models for nondoweled pavements for the wet-freeze region	307
106.	Actual field measured faulting versus faulting as predicted using the PFAULT models for the wet-nonfreeze region	309
107.	Actual field measured faulting versus faulting as predicted using the PFAULT models for doweled pavements for the wet-nonfreeze region	312
108.	Actual field measured faulting versus faulting as predicted using the PFAULT models for nondoweled pavements for the wet-nonfreeze region	312

LIST OF TABLES

VOLUME I EVALUATION OF CONCRETE PAVEMENT PERFORMANCE AND DESIGN FEATURES

<u>Table</u>	<u>Title</u>	<u>Page</u>
1.	Listing of critical distress values by pavement type	26
2.	Slab modulus and composite k-values for Minnesota 1	28
3.	Deflection testing results and drainage coefficients for Minnesota 1	28
4.	Slab modulus and composite k-values for Minnesota 2	32
5.	Deflection testing results and drainage coefficients for Minnesota 2	32
6.	Longitudinal lane-shoulder joint load transfer efficiency for Minnesota 2	32
7.	Design and performance data for the outer lane of Minnesota 3 (Age = 1 year, ESAL's = 1.5 million)	36
8.	Design and performance data for the outer lane of Minnesota 4 (Age = 1 year, ESAL's = 0.22 million)	36
9.	Design and performance data for the outer lane of Minnesota 6 (Age = 4 years, ESAL's = 0.85 million)	36
10.	Traffic information for Arizona 1	38
11.	Slab modulus and composite k-values for Arizona 1	38
12.	Deflection testing results and drainage coefficients for Arizona 1	38
13.	Longitudinal lane-shoulder joint load transfer efficiency for Arizona 1	38
14.	Design and performance data for the outer lane of Arizona 2 (Age = 4 years, ESAL's = 1.6 million)	42
15.	Slab modulus and composite k-values for California 1	42
16.	Deflection testing results and drainage coefficients for California 1	42
17.	Slab modulus and composite k-values for California 2	46
18.	Deflection testing results and drainage coefficients for California 2	46
19.	Design and performance data for the outer lane of California 6 (Age = 7 years, ESAL's = 4.4 million)	49
20.	Design and performance data for the outer lane of California 7 (Age = 8 years, ESAL's = 10.5 million)	49
21.	Design and performance data for the outer lane of California 8 (Age = 4 years, ESAL's = 5.3 million)	49
22.	Slab modulus and composite k-values for Michigan 1	52
23.	Deflection testing results and drainage coefficients for Michigan 1	52
24.	Design and performance data for the outer lane of Michigan 3 (Age = 1 year, ESAL's = 2.8 million)	57
25.	Slab modulus and composite k-values for Michigan 4	57
26.	Deflection testing results and drainage coefficients for Michigan 4	57
27.	Longitudinal lane-shoulder joint load transfer efficiency for Michigan 4	57
28.	Design and performance data for the outer lane of Michigan 5 (Age = 3 years, ESAL's = 3.1 million)	62
29.	Slab modulus and composite k-values for New York 1	62
30.	Deflection testing results and drainage coefficients for New York 1	62
31.	Slab modulus and composite k-values for New York 2	66
32.	Deflection testing results and drainage coefficients for New York 2	66
33.	Longitudinal lane-shoulder joint load transfer efficiency for New York 2	66
34.	Slab modulus and composite k-values for Ohio 1	67
35.	Deflection testing results and drainage coefficients for Ohio 1	75
36.	Deflection testing results and drainage coefficients for Ontario 1	76
37.	Design and performance data for the outer lane of Ontario 2 (Age = 16 years, ESAL's = 36 million)	81

LIST OF TABLES (continued)

VOLUME I EVALUATION OF CONCRETE PAVEMENT PERFORMANCE AND DESIGN FEATURES (continued)

<u>Table</u>	<u>Title</u>	<u>Page</u>
38.	Traffic information for Pennsylvania 1	82
39.	Slab modulus and composite k-values for Pennsylvania 1	82
40.	Deflection testing results and drainage coefficients for Pennsylvania 1	82
41.	Design and performance data for the outer lane of New Jersey 2 (Age = 36 years, ESAL's = 35 million)	86
42.	Slab modulus and composite k-values for New Jersey 3	86
43.	Deflection testing results and drainage coefficients for New Jersey 3	86
44.	Slab modulus and composite k-values for California 3	90
45.	Deflection testing results and drainage coefficients for California 3	90
46.	Longitudinal lane-shoulder joint load transfer efficiency for California 3	90
47.	Slab modulus and composite k-values for North Carolina 1	94
48.	Deflection testing results and drainage coefficients for North Carolina 1	94
49.	Design and performance data for the outer lane of North Carolina 2 (Age = 5 years, ESAL's = 5.8 million)	98
50.	Design and performance data for the outer lane of Florida 2 (Age = 1 year, ESAL's = 2.0 million)	98
51.	Design and performance data for the outer lane of Florida 3 (Age = 5 years, ESAL's = 4.1 million)	100
52.	Transverse cracking by lane for Florida 3	100
53.	Effect of slab length on cracking for Florida 3	100
54.	Outer lane performance data relative to slab thickness for Minnesota 1 (Age = 17 years, ESAL's = 5.5 million)	103
55.	Outer lane performance data relative to slab thickness for Minnesota 2 (Age = 10 years, ESAL's = 2.8 million)	103
56.	Outer lane performance data relative to slab thickness for Arizona 1	103
57.	Outer lane performance data relative to slab thickness for California 1 (Age = 16 years, ESAL's = 7.6 million)	105
58.	Outer lane performance data relative to slab thickness for Ontario 1 (Age = 5 years, ESAL's = 0.84 million)	105
59.	Outer lane performance data relative to base type for Minnesota 1 (Age = 17 years, ESAL's = 5.5 million)	108
60.	Outer lane performance data relative to base type for Arizona 1	108
61.	Outer lane performance data relative to base type for California 1 (Age = 16 years, ESAL's = 7.6 million)	108
62.	Outer lane performance data relative to base type for California 2 (Age = 7 years, ESAL's = 4.4 million)	108
63.	Outer lane performance data relative to base type for Michigan 1 (Age = 12 years, ESAL's = 0.9 million)	110
64.	Outer lane performance data relative to base type for New York 1 (Age = 22 years, ESAL's = 2.0 million)	112
65.	Outer lane performance data relative to base type for Ohio 1 (Age = 14 years, ESAL's = 3.4 million)	112
66.	Average performance data relative to base type for Ontario 1 (Age = 5 years, ESAL's = 0.84 million)	112
67.	Outer lane performance data relative to base type for North Carolina 1 (Age = 20 years, ESAL's = 9.1 million)	114
68.	Overall relative summary of the performance of base types	116

LIST OF TABLES (continued)

VOLUME I EVALUATION OF CONCRETE PAVEMENT PERFORMANCE AND DESIGN FEATURES (continued)

<u>Table</u>	<u>Title</u>	<u>Page</u>
69.	Gradation information for permeable bases required for filter criteria evaluation	118
70.	Evaluation of filter criteria	119
71.	Outer lane performance data relative to joint spacing for Minnesota 1 (Age = 17 years, ESAL's = 5.5 million)	120
72.	Outer lane performance data relative to joint spacing for Minnesota 2 (Age = 10 years, ESAL's = 2.8 million)	120
73.	Outer lane performance data relative to joint spacing for California 1 (Age = 16 years, ESAL's = 7.6 million)	122
74.	Outer lane performance data relative to joint spacing for Michigan 1 (Age = 12 years, ESAL's = 0.9 million)	122
75.	Outer lane performance data relative to joint spacing for New York 1 (Age = 22 years, ESAL's = 2.0 million)	122
76.	Outer lane performance data relative to joint spacing for New York 2 (Age = 12 years, ESAL's = 1.43 million)	122
77.	Outer lane performance data relative to joint spacing for Ohio 1 (Age = 14 years, ESAL's = 3.4 million)	124
78.	Summary of cracking by slab length for sections with random joint spacing	126
79.	Ratio of slab length to the radius of relative stiffness (L/l)	127
80.	Effect of joint spacing, slab thickness, and base type on transverse cracking for California 1	130
81.	Summary of performance data related to reinforcement design	136
82.	Outer lane performance data relative to joint orientation for New York 1 (Age = 22 years, ESAL's = 2.0 million)	138
83.	Outer lane performance data relative to joint orientation for North Carolina 1 (Age = 20 years, ESAL's = 9.1 million)	138
84.	Outer lane performance data relative to joint load transfer for Minnesota 1 (Age = 17 years, ESAL's = 5.5 million)	140
85.	Outer lane performance data relative to joint load transfer for North Carolina 1 (Age = 20 years, ESAL's = 9.1 million)	140
86.	Load transfer performance data for nondoweled pavement sections	142
87.	Load transfer performance data for doweled sections	143
88.	Outer lane performance data relative to dowel coating for Ohio 1 (Age = 14 years, ESAL's = 3.4 million)	146
89.	Summary of longitudinal cracking and related design data	147
90.	Influence of shoulder on performance of mainline pavement for Michigan 4 (Age = 15 years, ESAL's = 4.4 million)	152
91.	Performance data relative to drainage for Michigan 1 (Age = 12 years, ESAL's = 0.9 million)	155
92.	Summary of selected performance data related to C _d	158

LIST OF TABLES (continued)

VOLUME II EVALUATION AND MODIFICATION OF CONCRETE PAVEMENT DESIGN AND ANALYSIS MODELS

<u>Table</u>	<u>Title</u>	<u>Page</u>
1.	Listing of pavement sections in dry-freeze environmental region	7
2.	Listing of pavement sections in dry-nonfreeze environmental region	8
3.	Listing of pavement sections in wet-freeze environmental region	10
4.	Listing of pavement sections in wet-nonfreeze environmental region	11
5.	Recommended levels of reliability for various functional classifications (1)	22
6.	Values of the drainage coefficient for the design of rigid pavements as presented in the AASHTO Guide (1)	24
7.	Load transfer coefficients for various pavement types and design conditions as presented in the AASHTO Guide (1)	24
8.	Actual field-measured faulting versus faulting as predicted using the COPEs faulting models for the dry-freeze region	40
9.	Summary of the statistical analysis of the AASHTO design model	44
10.	Summary of the statistical analyses of the PEARDARP prediction models	47
11.	Summary of the statistical analyses of the COPEs prediction models	53
12.	Summary of the statistical analyses of the PFAULT faulting prediction models	63
13.	CMS inputs for use with concrete pavements	76
14.	Specific sections and analyses performed using the CMS program	79
15.	Summary of thermal gradients at specified times for MN 1-1 for July 15 through July 21, 1987	80
16.	Analysis of stiffness of the paving layers in the deep frost, thaw-recovery, and nonfrost periods for MN 1-1	84
17.	Summary of thermal gradients at specified times for CA 1-1 for July 15 through July 21, 1987	87
18.	Summary of thermal gradients at specified times for MI 1-10a for July 15 through July 21, 1987	97
19.	Summary of thermal gradients at specified times for NC 1-1 for July 15 through July 21, 1987	101
20.	Summary of the results of the Liu-Lytton percent drainage versus time analyses for MN 1	107
21.	Relationships used in the Liu-Lytton drainage program to determine the base strength based on the level of saturation	112
22.	Summary of the results of the Liu-Lytton percent drainage versus time analysis for CA 1	114
23.	Permeabilities and porosities of subbase and subgrade for CA 1	114
24.	Time required to reach an 85 percent saturation level for CA 1 sections	116
25.	Probability of a wet subbase course for the CA 1 sections	119
26.	Summary of the results of the Liu-Lytton percent drainage versus time analyses for MI 1	119
27.	Permeabilities and porosities of subbase and subgrade for MI 1	121
28.	Time required to reach an 85 percent saturation level for MI 1 sections	124
29.	Probability of a wet subbase course for the MI 1 sections	124
30.	Summary of the results of the Liu-Lytton percent drainage versus time analyses for NC 1	125
31.	Time required to reach an 85 percent saturation level for NC 1 sections	128
32.	Summary of maximum surface deflection as calculated by ILLISLAB and JSLAB for a 14.4 kip (64 kN) dual wheel load with a tire pressure of 120 psi (83 kPa) placed at the slab's edge	133

LIST OF TABLES (continued)

VOLUME II EVALUATION AND MODIFICATION OF CONCRETE PAVEMENT DESIGN AND ANALYSIS MODELS (continued)

<u>Table</u>	<u>Title</u>	<u>Page</u>
33.	Summary of maximum tensile stress as calculated by ILLISLAB and JSLAB for a 14.4 kip (64 kN) dual wheel load with a tire pressure of 120 psi (83 kPa) placed at the slab's edge	133
34.	Summary of maximum surface deflection as calculated by ILLISLAB and JSLAB for a 14.4 kip (64 kN) dual wheel load with a tire pressure of 120 psi (83 kPa) placed at the slab's corner	134
35.	Summary of maximum tensile stress as calculated by ILLISLAB and JSLAB for a 14.4 kip (64 kN) dual wheel load with a tire pressure of 120 psi (83 kPa) placed at the slab's corner	134
36.	Summary of maximum thermal stresses as calculated by ILLISLAB and JSLAB	135
37.	Summary of maximum surface deflection, maximum edge stress, and maximum subgrade distress as calculated by ILLISLAB for a 14.4 kip (64 kN) dual wheel load with a tire pressure of 120 psi (83 kPa) placed at the slab's edge	142
38.	Summary of deflection and stress load transfer efficiencies as calculated by ILLISLAB for a 14.4 kip (64 kN) dual wheel load with a tire pressure of 120 psi (83 kPa) placed at the slab corner	145
39.	Measured deflection basin under 13,000 lb (58 kN) load at STA 3+73 approach joint, MI 1-10a	147
40.	Finite element analysis for the void analysis performed for STA 3+73, MI 1-10a	147
41.	Maximum positive and minimum negative thermal gradient calculated by the CMS program for MN 1, CA 1, MI 1, and NC 1	151
42.	Stresses developing due to thermal gradients through the slab	152
43.	Summary of PMARP results for the edge loading condition employing a 9 kip (40 kN) dual wheel load with a tire pressure of 80 psi (55 kPa)	159
44.	Summary of PMARP results for the corner loading condition employing a 9 kip (40 kN) dual wheel load with a tire pressure of 80 psi (55 kPa)	160
45.	Summary of Miner's fatigue damage and transverse cracking for MN 2, CA 2, MI 1, and NC 1	166
46.	Shoulder fatigue damage analysis for AZ 1 and MI 4-1 using the JCS-1 program	170
47.	Shoulder fatigue analysis for NC 1 using the BERM program	172
48.	Mean longitudinal cracking for all sections included in COPES and RIPPER databases	179
49.	Distribution of pavement sections and designs used in development of faulting models	180
50.	Yearly average daytime thermal gradients used in curling computations(2)	193
51.	Critical distress levels, by pavement type (46)	208
52.	Cost-effectiveness evaluation for Arizona	211
53.	Cost-effectiveness evaluation for California	213
54.	Cost-effectiveness evaluation for Michigan	217
55.	Cost-effectiveness evaluation for Minnesota	221
56.	Cost-effectiveness evaluation for North Carolina	224
57.	Arizona designs for cost-effectiveness evaluation	231
58.	California designs for cost-effectiveness evaluation	232
59.	Michigan designs for cost-effectiveness evaluation	234
60.	Minnesota designs for cost-effectiveness evaluation	236
61.	North Carolina designs for cost-effectiveness evaluation	238

LIST OF TABLES (continued)

VOLUME III SUMMARY OF RESEARCH FINDINGS

<u>Table</u>	<u>Title</u>	<u>Page</u>
1.	General information for pavements included in study	5
2.	Listing of pavement sections in dry-freeze environmental region	6
3.	Listing of pavement sections in dry-nonfreeze environmental regions	7
4.	Listing of pavement sections in wet-freeze environmental region	9
5.	Listing of pavement sections in wet-nonfreeze environmental region	10
6.	Listing of major data items contained in the data base	20
7.	Analysis and design models evaluated in this study	30
8.	Summary of the statistical analysis of the AASHTO design model	32
9.	Summary of the statistical analyses of the PEARDARP prediction models	33
10.	Summary of the statistical analyses of the COPES prediction models	36
11.	Summary of the statistical analyses of the PFAULT faulting prediction models	39
12.	Summary of maximum edge deflection as calculated by ILLISLAB and JSLAB	45
13.	Summary of maximum thermal stress as calculated by ILLISLAB and JSLAB	46
14.	Mean longitudinal cracking for all sections included in COPES and RIPPER data bases	56
15.	Suggested design limits for use with prediction models	67
16.	Performance results for 12 "replicate" inservice pavement sections in Illinois ⁽⁴¹⁾	69
17.	Computed coefficients of variation for replicate pavement sections ⁽⁴¹⁾	70
18.	Critical distress levels by pavement type ⁽³⁹⁾	74
19.	Example of the cost-effectiveness evaluation for Arizona projects	76

VOLUME IV APPENDIX A - PROJECT SUMMARY REPORTS AND SUMMARY TABLES

<u>Table</u>	<u>Title</u>	<u>Page</u>
1.	Corner voids on MN 1 sections at Rothsay	3
2.	Drainage summary for MN 1 and MN 5 sections	3
3.	Transverse joint spalling, by design variable	6
4.	Transverse joint faulting, by design variable	7
5.	Transverse cracking, by design variable	7
6.	Longitudinal cracking, by design variable	8
7.	Comparison of performance by lane	10
8.	Composite k-values	14
9.	Load transfer efficiency and corners with voids	14
10.	Drainage summary for MN 2 sections	15
11.	Transverse joint spalling on MN 2 sections	15
12.	Longitudinal cracking at MN 2, by design variable	17
13.	Shoulder performance at MN 2 sections	18
14.	Comparison of performance by lane at MN 2	21
15.	Traffic summary of AZ 1 sections	30
16.	Summary of k-value by base type	30
17.	Drainage summary for AZ 1 sections	31
18.	Comparison of performance by lane at AZ 1	36

LIST OF TABLES (continued)

VOLUME IV APPENDIX A - PROJECT SUMMARY REPORTS AND SUMMARY TABLES (continued)

<u>Table</u>	<u>Title</u>	<u>Page</u>
19.	Comparison of performance by lane at AZ 2	39
20.	Backcalculated E-value by concrete type	42
21.	Composite k-value by base type	43
22.	Corners with voids and pumping severity by base type	43
23.	Drainage summary for CA 1 sections	43
24.	Transverse joint faulting	44
25.	Transverse cracking on CA 1 sections	47
26.	Longitudinal cracking on CA 1 sections	48
27.	Roughness and present serviceability on CA 1 sections	48
28.	Performance summarized by base type	49
29.	Performance summarized by joint spacing	49
30.	Performance summarized by slab thickness	50
31.	Comparison of performance by lane at CA 1	50
32.	Summary of composite k-values of CA 2	53
33.	Load transfer efficiencies and corners with voids at CA 2	53
34.	Drainage summary for CA 2 sections	54
35.	Transverse joint faulting at CA 2	54
36.	Roughness and present serviceability at CA 2	56
37.	Comparison of performance by lane at CA 2	57
38.	Comparison of performance by lane at CA 6	60
39.	Summary of performance by lane at CA 7	62
40.	Comparison of performance by lane at CA 8	65
41.	Summary of composite k-value by base type	67
42.	Corners with voids at MI 1	68
43.	Drainage summary for MI 1 sections	69
44.	Transverse joint spalling on MI 1 sections	69
45.	Transverse joint faulting on MI 1 sections	72
46.	Transverse joint faulting summarized by subdrainage	73
47.	Roughness and present serviceability at MI 1	74
48.	Faulting as a function of load transfer and drainage	75
49.	Comparison of performance by transverse joint spacing	76
50.	Comparison of performance by lane at MI 1	77
51.	Corner void detection on MI 4 sections	83
52.	Drainage summary for MI 4 sections	83
53.	Composite k-value by base type	95
54.	Load transfer efficiencies and corners with voids at NY 1	96
55.	Drainage summary for NY 1 sections	96
56.	Roughness and present serviceability on NY 1 sections	101
57.	Comparison of performance by lane at NY 1	102
58.	Composite k-values and average mid-slab deflections at NY 2	106
59.	Load transfer efficiencies and corners with voids at NY 2	106
60.	Drainage summary for NY 2 sections	107
61.	Transverse cracking summarized by lane and transverse joint spacing	110
62.	Longitudinal cracking summarized by lane and transverse joint spacing	110
63.	Roughness and present serviceability at NY 2	111
64.	Summary of slab cracking on sections with concrete shoulders	111
65.	Performance comparison of sections with 20-ft transverse joint spacing	112

LIST OF TABLES (continued)

VOLUME IV APPENDIX A - PROJECT SUMMARY REPORTS AND SUMMARY TABLES (continued)

<u>Table</u>	<u>Title</u>	<u>Page</u>
66.	Comparison of performance by lane and pavement type at NY 2	112
67.	Composite k-values at OH 1	115
68.	Load transfer efficiencies and corners with voids at OH 1	115
69.	Drainage summary for OH 1 sections	116
70.	Transverse joint faulting at OH 1	119
71.	Roughness and present serviceability at OH 1	120
72.	Comparison of performance by lane and base type of OH 1	122
73.	Drainage summary for OH 2 Sections	125
74.	Transverse joint spalling at OH 2	125
75.	Transverse joint performance at OH 2	127
76.	Roughness and present serviceability on OH 2 sections	128
77.	Summary of longitudinal joint spalling at OH 2	129
78.	Outer shoulder performance at OH 2	129
79.	Comparison of performance by lane at OH 2	130
80.	Load transfer efficiency and corners with voids at ONT 1	134
81.	Summary of drainage characteristics at ONT 1	134
82.	Summary of transverse joint faulting by direction of traffic	135
83.	Roughness and present serviceability at ONT 1	137
84.	Shoulder performance at ONT 1	138
85.	Comparison of performance by lane at ONT 1	140
86.	Summary of performance variables at ONT 2	143
87.	Traffic summary of PA 1 sections	145
88.	Summary of composite k-value by base type	146
89.	FWD deflection testing results at PA 1	146
90.	Drainage summary for PA 1 sections	147
91.	Roughness and present serviceability at PA 1	150
92.	Comparison of performance by lane at PA 1	151
93.	Comparison of performance by lane at NJ 2	154
94.	Summary of composite k-values at NJ 3	156
95.	Drainage summary for NJ 3	157
96.	Transverse joint faulting at NJ 3	159
97.	Roughness and present serviceability at NJ 3	159
98.	Comparison of performance by lane at NJ 3	160
99.	Composite k-values at CA 3	163
100.	FWD deflection testing results at CA 3	164
101.	Drainage summary for CA 3	164
102.	Transverse joint spalling at CA 3	167
103.	Transverse joint faulting at CA 3	167
104.	Transverse cracking at CA 3	167
105.	Roughness and present serviceability at CA 3	168
106.	Outer shoulder performance at CA 3	169
107.	Comparison of performance by lane at CA 3	169
108.	Composite k-values and load transfer efficiency at NC 1	173
109.	Percent corners with voids at NC 1	173
110.	Drainage summary for NC 1 sections	174
111.	Transverse joint faulting by load transfer type	177
112.	Longitudinal cracking at NC 1	178

LIST OF TABLES (continued)

VOLUME IV APPENDIX A - PROJECT SUMMARY REPORTS AND SUMMARY TABLES (continued)

<u>Table</u>	<u>Title</u>	<u>Page</u>
113.	Comparison of performance by transverse joint orientation	180
114.	Comparison of performance by lane and base type at NC 1	180
115.	Comparison of performance by lane for NC 2	184
116.	Pavement performance at FL 2	187
117.	Comparison of performance by lane for FL 3	189
118.	Transverse cracking at FL 3	189
119.	Slab cracking as a function of slab length at FL 3	190
120.	General information and design data for projects included in study	205
121.	Slab design data for projects in dry-freeze environmental zone	206
122.	Base, subbase, subgrade, and outer shoulder design data for projects in dry-freeze environmental zone	207
123.	Pavement joint data for projects in dry-freeze environmental zone	208
124.	Outer lane deflection data of projects in dry-freeze environmental zone	209
125.	Outer shoulder and drainage information for projects in dry-freeze environmental zone	210
126.	Traffic information for projects in dry-freeze environmental zone	211
127.	Outer lane performance data for projects in dry-freeze environmental zone	212
128.	Lane 2 performance data for projects in dry-freeze environmental zone	213
129.	Slab design for projects in dry-nonfreeze environmental zone	214
130.	Base, subbase, subgrade, and outer shoulder design data for projects in dry-nonfreeze environmental zone	215
131.	Pavement joint data for projects in dry-nonfreeze environmental zone	216
132.	Outer lane deflection data of projects in dry-nonfreeze environmental zone	217
133.	Outer shoulder and drainage information for projects in dry-nonfreeze environmental zone	218
134.	Traffic information for projects in dry-nonfreeze environmental zone	219
135.	Outer lane performance data for projects in dry-nonfreeze environmental zone	220
136.	Lane 2 performance data for projects in dry-nonfreeze environmental zone	221
137.	Slab design for projects in wet-freeze environmental zone	222
138.	Base, subbase, subgrade, and outer shoulder design data for projects in wet-freeze environmental zone	224
139.	Pavement joint data for projects in wet-freeze environmental zone	226
140.	Outer lane deflection data of projects in wet-freeze environmental zone	228
141.	Outer shoulder and drainage information for projects in wet-freeze environmental zone	230
142.	Traffic information for projects in wet-freeze environmental zone	232
143.	Outer lane performance data for projects in wet-freeze environmental zone	234
144.	Lane 2 performance data for projects in wet-freeze environmental zone	236
145.	Slab design for projects in wet-nonfreeze environmental zone	238
146.	Base, subbase, subgrade, and outer shoulder design data for projects in wet-nonfreeze environmental zone	239
147.	Pavement joint data for projects in wet-nonfreeze environmental zone	240
148.	Outer lane deflection data of projects in wet-nonfreeze environmental zone	241
149.	Outer shoulder and drainage information for projects in wet-nonfreeze environmental zone	242
150.	Traffic information for projects in wet-nonfreeze environmental zone	243

LIST OF TABLES (continued)

VOLUME IV APPENDIX A - PROJECT SUMMARY REPORTS AND SUMMARY TABLES (continued)

<u>Table</u>	<u>Title</u>	<u>Page</u>
151.	Outer lane performance data for projects in wet-nonfreeze environmental zone	244
152.	Lane 2 performance data for projects in wet-nonfreeze environmental zone	245

VOLUME V APPENDIX B - DATA COLLECTION AND ANALYSIS PROCEDURES

<u>Table</u>	<u>Title</u>	<u>Page</u>
1.	WIM project locations	18
2.	FHWA vehicle classification types (5)	18
3.	Field procedures for collection of WIM data	20
4.	Chart to calculate saturation time curve	36
5.	Eh ³ values for all Phase I sections	67
6.	Effect of deflection error on backcalculated E and k	69
7.	Listing of major data items contained in the database	78

VOLUME VI APPENDIX C AND APPENDIX D

APPENDIX C - SYNTHESIS OF CONCRETE PAVEMENT DESIGN METHODS AND ANALYSIS MODELS

<u>Table</u>	<u>Title</u>	<u>Page</u>
1.	Evaluation of analysis models and design methods	29
2.	Levels of design variables	34
3.	Parameters assumed for use in the analysis models and design methods (5)	35
4.	Traffic data assumed in design models (5)	36
5.	Loadometer data assumed in design models (5)	37
6.	ILLISLAB input and output variables	52
7.	JSLAB input and output variables	53
8.	WESLIQID input and output variables	54
9.	WESLAYER input and output variables	55
10.	RISC input and output variables	56
11.	PMARP input and output variables	57

LIST OF TABLES (continued)

VOLUME VI APPENDIX C AND APPENDIX D

APPENDIX C - SYNTHESIS OF CONCRETE PAVEMENT DESIGN METHODS AND ANALYSIS MODELS (continued)

<u>Table</u>	<u>Title</u>	<u>Page</u>
12.	H-51 input and output variables	58
13.	CMS input and output variables	59
14.	Liu-Lytton drainage models input and output variables	60
15.	PREDICT input and output variables	61
16.	PEARL input and output variables	62
17.	JCP-1 input and output variables	63
18.	DNPS86 input and output variables	64
19.	RPS-3 input and output variables	65
20.	PCA and California Rigid Pavement Design Procedure input and output variables .	67
21.	JCS-1 and BERM input and output variables	68
22.	Method of obtaining input variables for ILLISLAB	69
23.	Methods of obtaining input variables for JSLAB	70
24.	Methods of obtaining input variables for CMS	71
25.	Methods of obtaining input variables for Liu-Lytton Drainage Models	72
26.	Method of obtaining input variables for PMARP	73
27.	Method of obtaining input variables for PEARL	74
28.	Method of obtaining input variables for PREDICT	75
29.	Method of obtaining input variables for BERM	76
30.	Method of obtaining input variables for JCS-1	77
31.	Method of obtaining input variables for JCP-1	78
32.	Effect of slab thickness on pavement responses as measured by ILLISLAB, JSLAB, WESLIQID, and WESLAYER	80
33.	Effect of shoulder parameters on pavement responses as measured by ILLISLAB, JSLAB, WESLIQID, and WESLAYER	81
34.	Effect of subgrade strength on pavement responses as measured by ILLISLAB, JSLAB, WESLIQID, and WESLAYER	82
35.	Effect of joint width and slab length on pavement responses as measured by ILLISLAB, JSLAB, WESLIQID, and WESLAYER	83
36.	Effect of load transfer on pavement responses as measured by ILLISLAB and JSLAB	84
37.	Effect of base type on pavement responses as measured by ILLISLAB and JSLAB	85
38.	Effect of slab length/joint width, slab thickness, and shoulder parameters on pavement responses as measured by PMARP	86
39.	Effect of void depth, drainage factor, rainfall factor, and subbase treatment factor on pavement responses as measured by PMARP	87
40.	ILLISLAB and JSLAB curling analysis	88
41.	WESLIQID and WESLAYER curling analysis	89
42.	Analysis of RISC	90
43.	Effect of subgrade strength and pavement thickness on pavement response as measured by H-51	91
44.	CMS capabilities	92
45.	Effect of subgrade strength and slab thickness on cracking and PSR of JPCP as measured by PREDICT	94

LIST OF TABLES (continued)

VOLUME VI APPENDIX C AND APPENDIX D

APPENDIX C - SYNTHESIS OF CONCRETE PAVEMENT DESIGN METHODS AND ANALYSIS MODELS (continued)

<u>Table</u>	<u>Title</u>	<u>Page</u>
46.	Effect of subgrade strength and slab thickness on pumping of JPCP as measured by PREDICT	95
47.	Effect of climatic region on distresses of JPCP as measured by PREDICT	96
48.	Specific variables for the nine climatic zones (5)	97
49.	Effect of climatic region on distresses of JRCP as measured by PREDICT	99
50.	Effect of climatic region on distress of JRCP as measured by PREDICT	100
51.	Effect of subdrainage on JRCP distress as measured by PREDICT	101
52.	Effect of subgrade strength on JPCP distress as measured by PEARDARP	102
53.	Effect of pavement thickness on JPCP distress as measured by PEARDARP	103
54.	Effect of various inputs on fatigue damage as measured by JCP-1	104
55.	Effect of various inputs on serviceability as measured by JCP-1	105
56.	Effect of various inputs on DNPS86 design outputs	106
57.	Effect of loss of support, drainage factor, and ESAL's on design using DNPS86	107
58.	Effect of various inputs on RPS-3 outputs	108
59.	Effect of subgrade strength and load transfer on PCA design outputs	109
60.	Effect of subgrade strength on California rigid pavement design outputs	110
61.	Effect of shoulder type and thickness on BERM shoulder design outputs	111
62.	Effect of various inputs on JCS-1 design outputs	112
63.	Effect of various inputs on the Liu-Lytton drainage models outputs	113
64.	Effect of various inputs on JRCP4 outputs	114

VOLUME VI APPENDIX C AND APPENDIX D

APPENDIX D - SUMMARY OF ANALYSIS DATA FOR THE EVALUATION OF PREDICTIVE MODELS

<u>Table</u>	<u>Title</u>	<u>Page</u>
65.	Actual ESAL's (based on ADT) versus ESAL's as predicted using the AASHTO design equation for all Phase I sections	116
66.	Actual ESAL's (based on ADT) versus ESAL's as predicted using the AASHTO design equation for the dry-freeze region	120
67.	Actual ESAL's (based on ADT) versus ESAL's as predicted using the AASHTO design equation for the dry-nonfreeze region	121
68.	Actual ESAL's (based on ADT) versus ESAL's as predicted using the AASHTO design equation for the wet-freeze region	123
69.	Actual ESAL's (based on ADT) versus ESAL's as predicted using the AASHTO design equation for the wet-nonfreeze region	125
70.	Actual PSR as determined by a panel of users versus PSI as predicted by the PEARDARP PSI model for all Phase I sections	127
71.	Actual PSR as determined by a panel of users versus PSI as predicted by the PEARDARP PSI model for the dry-freeze region	131
72.	Actual PSR as determined by a panel of users versus PSI as predicted by the PEARDARP PSI model for the dry-nonfreeze region	132

LIST OF TABLES (continued)

VOLUME VI APPENDIX C AND APPENDIX D

APPENDIX D - SUMMARY OF ANALYSIS DATA FOR THE EVALUATION OF PREDICTIVE MODELS (continued)

<u>Table</u>	<u>Title</u>	<u>Page</u>
73.	Actual PSR as determined by a panel of users versus PSI as predicted by the PEARDARP PSI model for the wet-freeze region	134
74.	Actual PSR as determined by a panel of users versus PSI as predicted by the PEARDARP PSI model for the wet-nonfreeze region	136
75.	Actual field measured roughness versus roughness as predicted using the PEARDARP roughness model for all Phase I sections	138
76.	Actual field measured roughness versus roughness as predicted using the PEARDARP roughness model for the dry-freeze region	142
77.	Actual field measured roughness versus roughness as predicted using the PEARDARP roughness model for the dry-nonfreeze region	143
78.	Actual field measured roughness versus roughness as predicted using the PEARDARP roughness model for the wet-freeze region	145
79.	Actual field measured roughness versus roughness as predicted using the PEARDARP roughness model for the wet-nonfreeze region	147
80.	Comparison of actual field observed pumping with the normalized pumping index, volume of pumping, number of joints pumping, and volume of undersealing material required as predicted by the PEARDARP pumping model for all Phase I sections	149
81.	Actual field measured spalling versus spalling as predicted using the PEARDARP spalling model for all Phase I sections	152
82.	Actual field measured spalling versus spalling as predicted using the PEARDARP spalling model for the dry-freeze region	156
83.	Actual field measured spalling versus spalling as predicted using the PEARDARP spalling model for the dry-nonfreeze region	157
84.	Actual field measured spalling versus spalling as predicted using the PEARDARP spalling model for the wet-freeze region	159
85.	Actual field measured spalling versus spalling as predicted using the PEARDARP spalling model for the wet-nonfreeze region	161
86.	Actual field measured faulting versus faulting as predicted using the PEARDARP faulting models for all Phase I sections	163
87.	Actual field measured faulting versus faulting as predicted using the PEARDARP faulting models for the dry-freeze region	167
88.	Actual field measured faulting versus faulting as predicted using the PEARDARP faulting models for doweled pavements for the dry-freeze region	169
89.	Actual field measured faulting versus faulting as predicted using the PEARDARP faulting models for nondoweled pavements for the dry-freeze region	170
90.	Actual field measured faulting versus faulting as predicted using the PEARDARP faulting models for the dry-nonfreeze region	172
91.	Actual field measured faulting versus faulting as predicted using the PEARDARP faulting models for the wet-freeze region	174
92.	Actual field measured faulting versus faulting as predicted using the PEARDARP faulting models for doweled pavements for the wet-freeze region	177

LIST OF TABLES (continued)

VOLUME VI APPENDIX C AND APPENDIX D

APPENDIX D - SUMMARY OF ANALYSIS DATA FOR THE EVALUATION OF PREDICTIVE MODELS (continued)

<u>Table</u>	<u>Title</u>	<u>Page</u>
93.	Actual field measured faulting versus faulting as predicted using the PEARDARP faulting models for nondoweled pavements for the wet-freeze region	178
94.	Actual field measured faulting versus faulting as predicted using the PEARDARP faulting models for the wet-nonfreeze region	180
95.	Actual field measured faulting versus faulting as predicted using the PEARDARP faulting models for doweled pavements for the wet-nonfreeze region	182
96.	Actual field measured faulting versus faulting as predicted using the PEARDARP faulting models for nondoweled pavements for the wet-nonfreeze region	183
97.	Actual field measured cracking versus cracking as predicted using the PEARDARP cracking models for all Phase I sections	185
98.	Actual field measured cracking versus cracking as predicted using the PEARDARP cracking model for the dry-freeze region	189
99.	Actual field measured cracking versus cracking as predicted using the PEARDARP cracking model for the dry-nonfreeze region	190
100.	Actual field measured cracking versus cracking as predicted using the PEARDARP cracking model for the wet-freeze region	192
101.	Actual field measured cracking versus cracking as predicted using the PEARDARP cracking model for the wet-nonfreeze region	194
102.	Actual field observed pumping versus pumping as predicted using COPES pumping models for all Phase I sections	196
103.	Actual field observed pumping versus pumping as predicted using COPES pumping models for the dry-freeze region	200
104.	Actual field observed pumping versus pumping as predicted using COPES JPCP pumping model for the dry-freeze region	202
105.	Actual field observed pumping versus pumping as predicted using COPES JRCP pumping model for the dry-freeze region	203
106.	Actual field observed pumping versus pumping as predicted using COPES pumping model for the dry-nonfreeze region	205
107.	Actual field observed pumping versus pumping as predicted using COPES pumping model for the wet-freeze region	207
108.	Actual field observed pumping versus pumping as predicted using COPES JPCP pumping model for the wet-freeze region	210
109.	Actual field observed pumping versus pumping as predicted using COPES JRCP pumping model for the wet-freeze region	211
110.	Actual field observed pumping versus pumping as predicted using COPES pumping model for the wet-nonfreeze region	213
111.	Actual field measured faulting versus faulting as predicted using the COPES faulting models for all Phase I sections	215
112.	Actual field measured faulting versus faulting as predicted using the COPES faulting models for the dry-freeze region	219
113.	Actual field measured faulting versus faulting as predicted using the COPES JPCP faulting model for the dry-freeze region	221

LIST OF TABLES (continued)

VOLUME VI APPENDIX C AND APPENDIX D

APPENDIX D - SUMMARY OF ANALYSIS DATA FOR THE EVALUATION OF PREDICTIVE MODELS (continued)

<u>Table</u>	<u>Title</u>	<u>Page</u>
114.	Actual field measured faulting versus faulting as predicted using the COPES JRCP faulting model for the dry-freeze region	222
115.	Actual field measured faulting versus faulting as predicted using the COPES faulting models for the dry-nonfreeze region	224
116.	Actual field measured faulting versus faulting as predicted using the COPES faulting models for the wet-freeze region	226
117.	Actual field measured faulting versus faulting as predicted using the COPES JPCP faulting model for the wet-freeze region	229
118.	Actual field measured faulting versus faulting as predicted using the COPES JRCP faulting model for the wet-freeze region	230
119.	Actual field measured faulting versus faulting as predicted using the COPES faulting models for the wet-nonfreeze region	232
120.	Actual field measured spalling versus joint deterioration (spalling) as predicted using the COPES spalling models for all Phase I sections	234
121.	Actual field measured spalling versus joint deterioration (spalling) as predicted using the COPES spalling models for the dry-freeze region	238
122.	Actual field measured spalling versus joint deterioration (spalling) as predicted using the COPES JPCP joint deterioration model for the dry-freeze region	240
123.	Actual field measured spalling versus joint deterioration (spalling) as predicted using the COPES JRCP joint deterioration model for the dry-freeze region	241
124.	Actual field measured spalling versus joint deterioration (spalling) as predicted using the COPES spalling models for the dry-nonfreeze region	243
125.	Actual field measured spalling versus joint deterioration (spalling) as predicted using the COPES spalling models for the wet-freeze region	245
126.	Actual field measured spalling versus joint deterioration (spalling) as predicted using the COPES JPCP joint deterioration model for the wet-freeze region	248
127.	Actual field measured spalling versus joint deterioration (spalling) as predicted using the COPES JRCP joint deterioration model for the wet-freeze region	249
128.	Actual field measured spalling versus joint deterioration (spalling) as predicted using the COPES spalling models for the wet-nonfreeze region	251
129.	Actual field measured cracking versus cracking as predicted by the COPES cracking models for all Phase I sections	253
130.	Actual field measured cracking versus cracking as predicted by the COPES cracking models for the dry-freeze region	257
131.	Actual field measured cracking versus cracking as predicted by the COPES JPCP cracking model for the dry-freeze region	259

LIST OF TABLES (continued)

VOLUME VI APPENDIX C AND APPENDIX D

APPENDIX D - SUMMARY OF ANALYSIS DATA FOR THE EVALUATION OF PREDICTIVE MODELS (continued)

<u>Table</u>	<u>Title</u>	<u>Page</u>
132.	Actual field measured cracking versus cracking as predicted by the COPEs JRCP cracking model for the dry-freeze region	260
133.	Actual field measured cracking versus cracking as predicted by the COPEs cracking models for the dry-nonfreeze region	262
134.	Actual field measured cracking versus cracking as predicted by the COPEs cracking models for the wet-freeze region	264
135.	Actual field measured cracking versus cracking as predicted by the COPEs JPCP cracking models for the wet-freeze region	267
136.	Actual field measured cracking versus cracking as predicted by the COPEs JRCP cracking model for the wet-freeze region	268
137.	Actual field measured cracking versus cracking as predicted by the COPEs cracking models for the wet-nonfreeze region	270
138.	Actual PSR as determined by a panel of users versus PSR as predicted by the COPEs PSR models for all Phase I sections	272
139.	Actual PSR as determined by a panel of users versus PSR as predicted by the COPEs PSR models for the dry-freeze region	276
140.	Actual PSR as determined by a panel of users versus PSR as predicted by the COPEs JPCP PSR model for the dry-freeze region	278
141.	Actual PSR as determined by a panel of users versus PSR as predicted by the COPEs JRCP PSR model for the dry-freeze region	279
142.	Actual PSR as determined by a panel of users versus PSR as predicted by the COPEs PSR models for the dry-nonfreeze region	281
143.	Actual PSR as determined by a panel of users versus PSR as predicted by the COPEs PSR models for the wet-freeze region	283
144.	Actual PSR as determined by a panel of users versus PSR as predicted by the COPEs JPCP PSR model for the wet-freeze region	286
145.	Actual PSR as determined by a panel of users versus PSR as predicted by the COPEs JRCP PSR model for the wet-freeze region	287
146.	Actual PSR as determined by a panel of users versus PSR as predicted by the COPEs PSR models for the wet-nonfreeze region	289
147.	Actual field measured faulting versus faulting as predicted using the PFAULT models for all Phase I sections	291
148.	Actual field measured faulting versus faulting as predicted using the PFAULT models for the dry-freeze region	295
149.	Actual field measured faulting versus faulting as predicted using the PFAULT models for doweled pavements for the dry-freeze region	297
150.	Actual field measured faulting versus faulting as predicted using the PFAULT models for nondoweled pavements for the dry-freeze region	298
151.	Actual field measured faulting versus faulting as predicted using the PFAULT models for the dry-nonfreeze region	300
152.	Actual field measured faulting versus faulting as predicted using the PFAULT models for the wet-freeze region	302
153.	Actual field measured faulting versus faulting as predicted using the PFAULT models for doweled pavements for the wet-freeze region	305

LIST OF TABLES (continued)

VOLUME VI APPENDIX C AND APPENDIX D

APPENDIX D - SUMMARY OF ANALYSIS DATA FOR THE EVALUATION OF PREDICTIVE MODELS (continued)

<u>Table</u>	<u>Title</u>	<u>Page</u>
154.	Actual field measured faulting versus faulting as predicted using the PFAULT models for nondoweled pavements for the wet-freeze region	306
155.	Actual field measured faulting versus faulting as predicted using the PFAULT models for the wet-nonfreeze region	308
156.	Actual field measured faulting versus faulting as predicted using the PFAULT models for doweled pavements for the wet-nonfreeze region	310
157.	Actual field measured faulting versus faulting as predicted using the PFAULT models for nondoweled pavements for the wet-nonfreeze region	311
158.	Data used for the analysis of the PEARDARP, COPES, AND PFAULT predictive models	313

CHAPTER 1 INTRODUCTION

1. INTRODUCTION

Models are important tools available to the pavement engineer to assist in the design and analysis of pavements and extend the understanding of pavement performance. They can be based on theory (mechanistic), on observed performance (empirical) or a combination of the two.

Models can be broadly grouped into two categories for use in the pavement field: design and analysis. Pavement design models may be classified as empirical, in which the design equation for pavement thickness is derived from field data, and mechanistic-empirical, in which pavement responses such as stresses and strains are related to the number of allowable loads until failure of the pavement. The major empirical method in use in the United States today for the design of concrete pavements is the AASHTO Design Guide, whose design equations are based on data collected during the 1958-1960 AASHTO Road Test.⁽¹⁾ An example of a mechanistic-empirical pavement design method is the Zero-Maintenance Design Procedure.⁽²⁾

A subset of the design models are prediction models. Prediction models attempt to predict the condition of a pavement after it has been subjected to a given number of environmental and traffic loads. This prediction is usually based on models for performance that are developed from actual inservice pavements. Prediction models can incorporate mechanistic variables which are based on the properties of the pavement materials and their response to loading. It is believed that mechanistic-empirical models provide a more accurate characterization of the pavement structure, and provide more flexibility in design and analysis than strictly empirical models.

Pavement analysis models have been developed to provide behavioral information about pavement structures. The interaction of the different layers in a pavement system, the different designs that are used, the range of environmental conditions to which a pavement is exposed, and the variation in location and magnitude of applied loads define a very complex structure. The available analysis models attempt to explain one or several of these factors through computer modeling techniques. The goal in the development and use of an analysis model is to improve the understanding of pavement responses to loading and the environment, and through that understanding, improve pavement design.

Pavement analysis models vary in their completeness and complexity by the number of variables that they are able to incorporate. Models exist that can consider loading variables (e.g., Westergaard edge stress model), loading and environmental variables (e.g., ILLISLAB finite element model), or primarily environmental variables (e.g., CMS). Ideally, an analysis model would accommodate the maximum number of factors that are believed to affect the performance or behavior of pavements.

2. PROJECT BACKGROUND

This report details a portion of the work conducted for a major national study on the effect of various design features on the performance of jointed concrete pavements and selected structural rehabilitation techniques of jointed concrete pavements. The first phase of the project deals with the performance of jointed concrete pavements. The findings of this phase are found in a six-volume report, "Performance of Jointed Concrete Pavements." Observations and preliminary conclusions regarding the effects of design features on concrete performance are presented in volumes I, IV, and V, which document the data collection activities, data analysis procedures, and the establishment of the database used in the study. This volume covers the second part of the phase I research; the evaluation of design and analysis models, the determination of the accuracy of predictive models, the development of improved models, and an analysis of the cost-effectiveness of design features.

Selection of Models

One of the major goals of the project is to determine the adequacy of the available design procedures and analysis models, based on the performance of in-service concrete pavements. A number of available analysis models and design procedures were thoroughly reviewed and evaluated during the initial stages of the project. This was accomplished by obtaining the computer program and procedure documentation, performing analyses of the sensitivity of the models to changes in their variables, and documenting the capabilities and limitations of each model. The following models were considered:

<u>Design</u>	<u>Structural Analysis</u>	<u>Prediction</u>	<u>Drainage/ Climatic</u>
AASHTO (DNPS 86)*	ILLISLAB*	PEARDARP*	CMS*
CALTRANS	JSLAB*	PREDICT*	Liu/Lytton*
JCS-1*	JRCP-4		
BERM*	H51		
RPS-3	RISC		
PCA	WESLAYER		
JCP-1*	WESLIQID		
PMARP*			

The results of that evaluation are reported in volume VI of this report. Those models that were selected for use in this project are marked with a (*). In addition to those models evaluated and selected, one predictive model that was not initially evaluated, PFAULT, was also subsequently selected for evaluation.

Research Approach

The 95 different pavement sections incorporating design features of interest were selected to be included in Phase I of this study. The selection process, described in volume I, was based on the ability of the sections to satisfy a number of criteria, including a range of environmental and traffic conditions, inclusion of the design variables of interest, and the ability to contribute to the desired design matrix. Those sections that were selected were subjected to a complete condition survey and evaluation.

Of the 95 sections, 84 were sections that were part of experimental projects or were selected to serve as a "control" section to the experimental project. The other 11 sections were included because they incorporated new or innovative design features whose effect on pavement performance was of interest.

The evaluation of the models and design procedures is composed of four discrete tasks. The first task is an analysis of the predictive models. In this analysis, the distresses as predicted by the models are compared to the actual field-measured distresses. The comparison, performed with the use of a statistical software package, demonstrates the ability of the models to predict the performance of inservice pavements.

The second task involves case studies of pavement sections in four States. Experimental projects which included a range of variables were chosen in each of the four climatic regions. The States selected were Minnesota (MN 1), Michigan (MI 1), North Carolina (NC 1), and California (CA 1). These sections are evaluated using design, drainage, and structural analysis programs to determine the applicability and usefulness of selected available models in the design and evaluation process. The complexity of the models and their exhaustive input requirements necessitated the limiting of this evaluation to only these projects. New or improved predictive models will be developed based on the results of the previous two tasks.

The third task consists of estimating the expected performance periods of recently constructed projects that incorporated design features to improve drainage and reduce slab deflections. There were 15 sections included in this study that were constructed during the past 7 years and incorporated new or innovative design features. The performance period of these sections was estimated based on the available predictive models. The projections take into account their performance at the time that they were surveyed.

The fourth and final part of the analysis is an examination of the cost-effectiveness of several new design features that were included in this study. These include features such as widened lanes and drainable bases. Incorporating these new or innovative features results in increased initial construction costs, but constructing pavements with these features may result in pavements with a longer life. Through the use of a life cycle cost analysis, these assumptions are tested.

3. SEQUENCE OF REPORT

This report constitutes the second of six volumes covering the Phase I research. Supplemental information central to the analysis and development of conclusions is presented in the other volumes. Of particular interest to readers of this volume will be volume IV, which presents project summary reports and summary tables, and volume VI, which contains the project analysis summary tables and a comprehensive review of numerous design models and analysis procedures.

In this volume, chapter 2 provides a brief description of the pavement sections included in the database, presented by environmental region. Also included is a discussion of the design features that were evaluated. Chapter 3 presents the results of the comparison between predicted results and actual observed results, by environmental region and model for each of the sections.

The individual analysis models are evaluated and discussed in chapter 4. Based on that evaluation, modifications and improvements are made to the models and are presented in chapter 5. In chapter 6, an assessment of the cost-effectiveness of several design features is presented. Finally, in chapter 7 the results from this study are summarized and conclusions are presented.

CHAPTER 2 DESCRIPTION OF PAVEMENT SECTIONS

This chapter presents a broad overview of the projects included and evaluated in the study. The description provided here is only intended to provide a foundation for the evaluations performed in chapters 3 and 4. By introducing the project identifications, their location, the range of variables, and the number of sections in each project, a more complete understanding and appreciation of the evaluations presented in chapters 3 and 4 is achieved.

More detailed descriptions of the pavement sections discussed here are included in volume I and in volume IV. Volume IV in particular provides detailed summaries of the design, construction, and performance of each pavement section.

A total of 95 jointed concrete pavement sections representing the four major climatic regions were evaluated. These pavement sections ranged from 1 year to 36 years of age. Design features evaluated include slab thickness, pavement type, base type, joint spacing, method of load transfer, and shoulder type.

The projects can be broadly categorized into two groups: experimental and older projects, and recently-constructed projects. The main thrust of the study was to analyze experimental projects which were constructed to evaluate one or more pavement design feature. Sixteen experimental projects totaling 80 pavement sections were included in the study. Additionally, four older, single-section projects representing "control" designs were also included.

Recently-constructed projects (1980 or newer) were included to consider the impact and cost-effectiveness of new design features, such as permeable bases and widened lanes, on concrete pavement performance. Eleven single-section projects were included from this category.

A brief introduction to all of the projects follows. This introduction is presented by environmental region to facilitate the presentations of the model analyses in chapters 3 and 4. Projects were selected from each of the four primary environmental regions.

1. DRY-FREEZE ENVIRONMENTAL REGION

A total of 20 pavement sections were evaluated in the dry-freeze environmental region. This includes 17 experimental or older sections and 3 recently-constructed sections. All of these sections were located in Minnesota.

Environmental data for the projects in the region include a Corps of Engineers Freezing Index range of 1688 to 2188, a Thornthwaite Moisture Index range of 0 to 10, and a range in annual precipitation of 23 to 30 in (584 to 762 mm). In addition, the highest average monthly maximum temperature for the

projects in the region averaged 84 °F (29 °C), while the lowest average monthly minimum temperatures ranged from -3 °F (-19 °C) to 6 °F (-14 °C).

Minnesota is actually located in a transition area between the wet-freeze and the dry-freeze environmental regions, but was included in the dry-freeze zone for purposes of categorization. However, an examination of the Thornthwaite Moisture Index, which represents the potential amount of annual free moisture available in an area, shows that Minnesota has values ranging from 0 to 10. This is certainly much drier than such States in the wet-freeze environmental zone as Michigan or New York, which have Thornthwaite Moisture Indices of 30 or more. It should be noted that in the evaluation of the models, actual climatic indices for each section were used.

Table 1 provides a listing of the projects included from the dry-freeze environmental region. It is observed from the table that the pavements ranged in age from 1 to 17 years at the time of survey (1987). Such design features as slab thickness, pavement type, load transfer, shoulder type, and base type were included from this region.

2. DRY-NONFREEZE ENVIRONMENTAL REGION

A total of 17 pavement sections were evaluated in the dry-nonfreeze environmental region. Of those 17 sections, 14 sections were experimental or older and 3 sections were recently-constructed. All projects were located in either Arizona or California.

Climatic indices for the projects in the region include a Corps of Engineers Freezing Index of 0, a Thornthwaite Moisture Index range of -10 to -30, and an annual precipitation range of 8 to 17 in (203 to 432 mm). The highest average monthly maximum temperature for the projects in the region ranges from 89 °F (32 °C) to 105 °F (41 °C), while the lowest average monthly minimum temperature ranges from 36 °F (2 °C) to 41 °F (5 °C).

A listing of the projects included in the dry-nonfreeze environmental region is presented in table 2. The oldest sections were 16 years old and the youngest 4 years old at the time of the survey. Design features from this environmental zone include base type, slab thickness, joint spacing, drainage, and widened lanes.

3. WET-FREEZE ENVIRONMENTAL REGION

The wet-freeze environmental region contributed by far the largest number of sections to the study. A total of 44 pavement sections, consisting of 42 experimental or older sections and 2 recently-constructed sections, were included for evaluation in this region. States in the wet-freeze environmental region contributing sections include Michigan, New York, Ohio, Ontario, Pennsylvania, and New Jersey.

Table 1. Listing of pavement sections in dry-freeze environmental region.

Project ID	Location	Year Built	Number of Sections	Design Feature(s)
MN 1	I-94 Rothsay	1970	12	Base Type Slab Thickness Load Transfer Joint Spacing Shoulder Type
MN 2	I-90 Albert Lea	1977	4	Pavement Type Joint Spacing Slab Thickness Shoulder Type
MN 3	I-90 Austin	1984	1	Widened Lanes
MN 4	T.H. 15 New Ulm	1986	1	Widened Lanes
MN 5	I-94 Rothsay	1969	1	Joint Spacing
MN 6	T.H. 15 Truman	1983	1	Widened Lanes Permeable Base
TOTAL			20	

Table 2. Listing of pavement sections in dry-nonfreeze environmental region.

Project ID	Location	Year Built	Number of Sections	Design Feature(s)
AZ 1	S.R. 360 Phoenix	1972- 1981	6	Base Type Slab Thickness Shoulder Type Drainage
AZ 2	I-10 Phoenix	1983	1	Load Transfer PCC Shoulder
CA 1	I-5 Tracy	1971	5	Base Type Slab Thickness Joint Spacing Concrete Strength
CA 2	I-210 Los Angeles	1980	2	Base Type
CA 6	Route 14 Solemint	1980	1	Base Type
CA 7	I-5 Sacramento	1979	1	Drainage
CA 8	U.S. 101 Thousand Oaks	1983	1	Widened Lanes
TOTAL			17	

Climatic indices for projects located in the wet-freeze environmental region include a Corps of Engineers Freezing Index range of 25 to 1000, a Thornthwaite Moisture Index range of 30 to 60, and an annual precipitation range of 30 to 43 in (763 to 1092 mm). The highest average monthly maximum temperature for projects in the region ranges from 80 °F (27 °C) to 86 °F (30 °C), while the lowest average monthly minimum temperature ranges from 10 °F (-12 °C) to 25 °F (-4 °C).

Table 3 provides a listing of the projects included in the study from the wet-freeze environmental region. A range of 1 year to 36 years in project age is noted from the table. Pavement design features in this environmental region include base type, slab thickness, joint spacing, pavement type, shoulder type, load transfer, drainage, joint orientation (skewed or perpendicular), and joint design.

4. WET-NONFREEZE ENVIRONMENTAL REGION

A total of 14 pavement sections, consisting of 11 experimental and older sections and 3 recently-constructed sections, were included from the wet-nonfreeze environmental region. California, North Carolina, and Florida contributed projects to the study.

Climatic indices for projects in the region include a Corps of Engineers Freezing Index of 0, a Thornthwaite Moisture Index range of 20 to 40, and an annual precipitation range of 44 to 59 in (1118 to 1499 mm). The highest average monthly maximum temperature for projects in the region averages 90 °F (32 °C), while the lowest average monthly minimum temperature ranges from 29 °F (-2 °C) to 50 °F (10 °C).

Table 4 provides a listing of the sections included in this environmental region. Projects range in age from 1 year to 20 years. Design features in this region include base type, slab thickness, pavement type, load transfer, joint orientation, and shoulder type.

5. OVERALL DISTRIBUTION OF DESIGN FEATURES

As discussed, a total of 95 pavement sections representing a wide range of concrete pavement design features were included in the study. In order to more fully present the overall distribution of design features, a brief discussion of selected design features is described below.

Base Type

There were six general types of base courses that were included in the study: aggregate (AGG), cement-treated (CTB), asphalt-treated (ATB), permeable stabilized or permeable nonstabilized (PERM), lean concrete (LCB), and soil cement (SC). In addition, some sections were constructed directly on subgrade without benefit of a base course (NONE).

Table 3. Listing of pavement sections in wet-freeze environmental region.

Project ID	Location	Year Built	Number of Sections	Design Feature(s)
MI 1	U.S. 10 Clare	1975	8	Base Type Pavement Type Load Transfer Shoulder Type Drainage
MI 3	I-94 Marshall	1986	1	Permeable Base Shoulder Type
MI 4	I-69 Charlotte	1970	2	Shoulder Type
MI 5	I-94 Paw Paw	1984	1	Permeable Base Shoulder Type
NY 1	Route 23 Catskill	1968	6	Base Type Pavement Type Load Transfer Joint Orientation
NY 2	I-88 Otego	1975	4	Joint Spacing Pavement Type Shoulder Type
OH 1	U.S. 23 Chillicothe	1973	7	Base Type Joint Spacing Dowel Coating
OH 2	S.R. 2 Vermilion	1974	2	Shoulder Type Thick Slab on Grade
ONT 1	Highway 3N Ruthven	1982	4	Base Type Slab Thickness Shoulder Type
ONT 2	Highway 427 Toronto	1971	1	Load Transfer
PA 1	Rte. 422 & 66 Kittanning	1980	5	Base Type
NJ 2	Route 130 Yardville	1951	1	Joint Spacing Joint Design
NJ 3	I-676 Camden	1979	2	Base Type Joint Design
TOTAL			44	

Table 4. Listing of pavement sections in wet-nonfreeze environmental region.

Project ID	Location	Year Built	Number of Sections	Design Feature(s)
CA 3	U.S. 101 Geyserville	1975	3	Shoulder Type Joint Sealing
NC 1	I-95 Rocky Mount	1967	8	Base Type Slab Thickness Pavement Type Joint Orientation Load Transfer
NC 2	I-85 Greensboro	1982	1	Load Transfer Shoulder Type
FL 2	I-75 Tampa (Hillsborough)	1986	1	Slab Thickness
FL 3	I-75 Tampa (Manatee)	1982	1	Base Type
TOTAL			14	

The distribution of base type by environmental region is depicted in figure 1. By far the most common base type were the aggregate base courses. These were well-represented in all but the dry-nonfreeze environmental zone. There was also a fair distribution of stabilized bases (cement-treated, asphalt-treated, soil-cement). Permeable base sections were primarily located in the wet-freeze environmental zone.

Slab Thickness

Slab thickness ranged from a minimum of 7.5 in (191 mm) to a maximum of 15 in (381 mm). Thicker slabs in excess of 11 in (279 mm) were most often constructed without a base course. The distribution of projects with slab thickness less than 10 in (254 mm) and greater than or equal to 10 in (254 mm) is shown in figure 2. The most common slab thickness encountered was 9 in (229 mm), which was found on a majority of the Interstate projects.

Joint Spacing/Pavement Type

Both jointed plain concrete pavements (JPCP) and jointed reinforced concrete pavements (JRCP) were included in the study. By nature of the design characteristics inherent in each pavement type, a wide range of joint spacings were encountered. However, very rarely could direct comparisons of joint spacings be made within a pavement type, although relative comparisons of slab lengths could be made for sections with random joint spacing.

The distribution of joint spacings by pavement type is illustrated in figure 3. It is observed that there were no JRCP in the dry-nonfreeze zone, and only 1 JRCP in the wet-nonfreeze zone. The joint spacings for JPCP ranged from a low of 7.75 ft (2.4 m) in California to a maximum of 30 ft (9.1 m) in North Carolina. The joint spacings for JRCP ranged from a minimum of 21 ft (6.4 m) in Ohio to a maximum of 78 ft (23.8 m) in New Jersey.

Load Transfer

Transverse joint load transfer is typically accomplished through either aggregate interlock or mechanical load transfer devices. This study included a fair sampling of each type. The mechanical load transfer devices most commonly used in this study were dowel bars, although sections from New York utilized other devices, namely ACME two-part malleable iron load transfer devices and epoxy-coated I-beams.

The distribution of load transfer is shown in figure 4. Not surprising, projects in the wet-freeze and dry-freeze environmental regions contained mechanical load transfer devices more often than those projects in the wet-nonfreeze and dry-nonfreeze environmental regions. In fact, only 1 dowelled section was included in the study from the dry-nonfreeze environmental region.

BASE TYPE

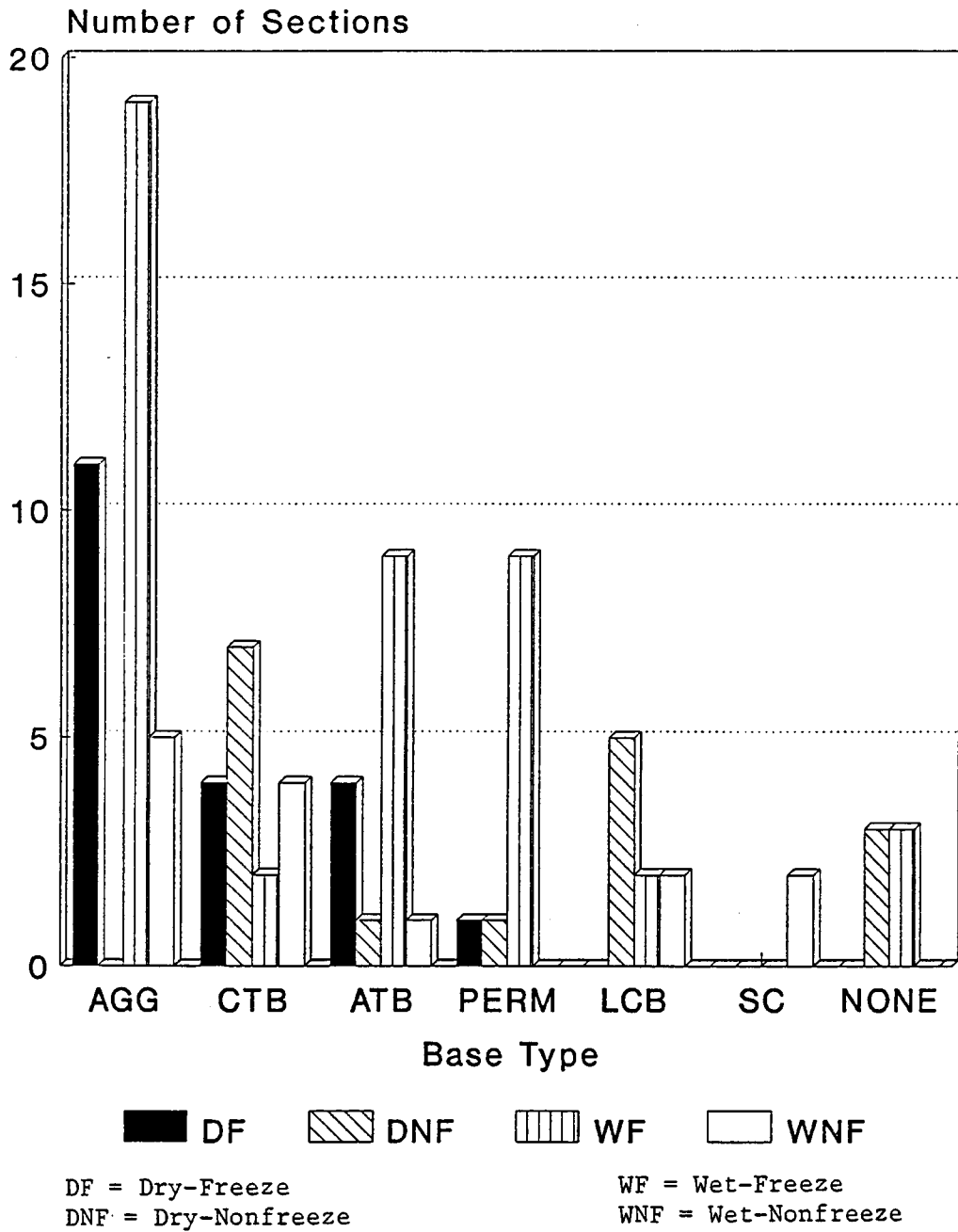


Figure 1. Distribution of base type by environmental region.

SLAB THICKNESS

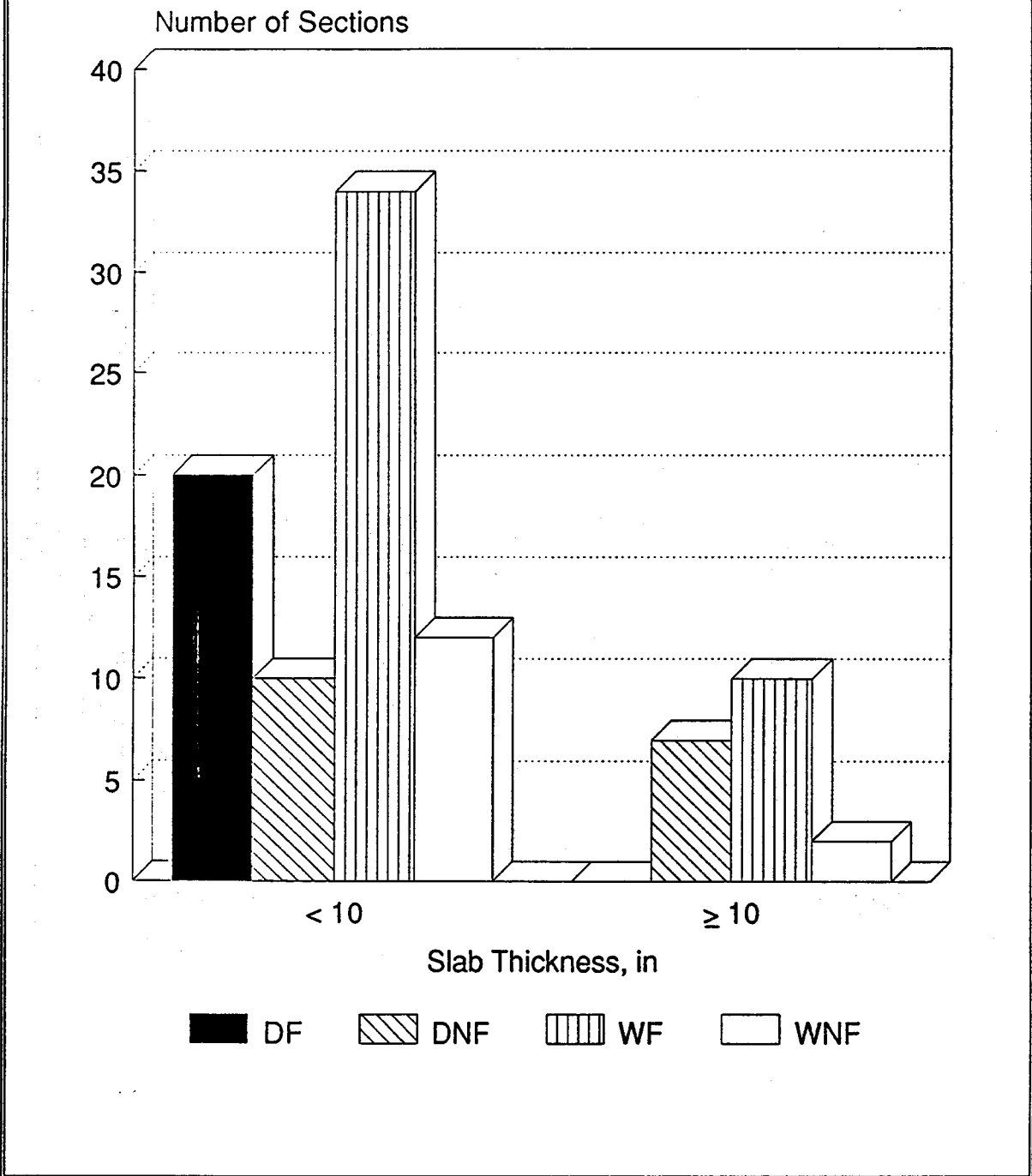


Figure 2. Distribution of slab thickness by environmental region.

JOINT SPACING/PAVEMENT TYPE

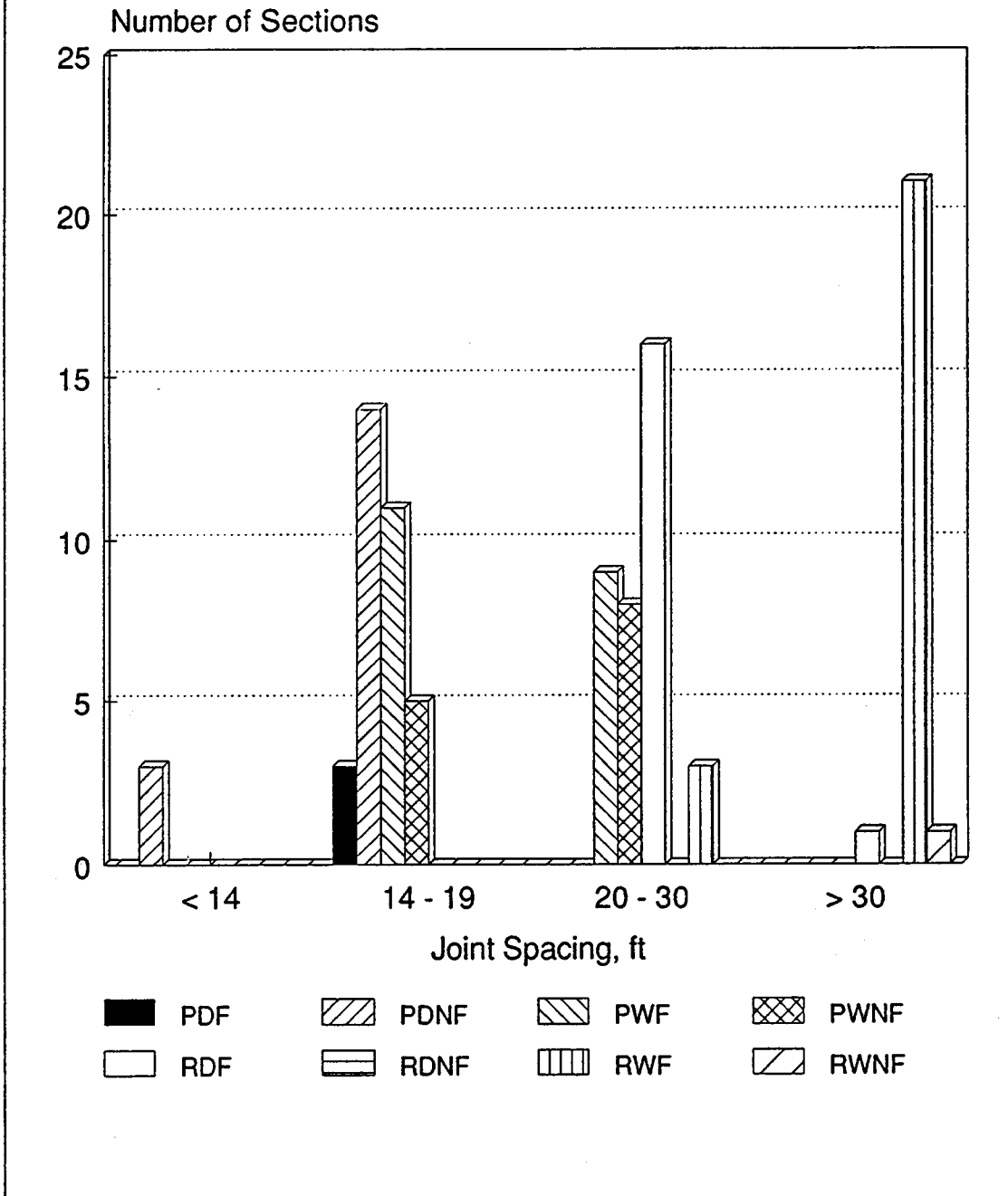


Figure 3. Distribution of joint spacing and pavement type by environmental region (P=JPCP, R=JRCP).

METHOD OF LOAD TRANSFER

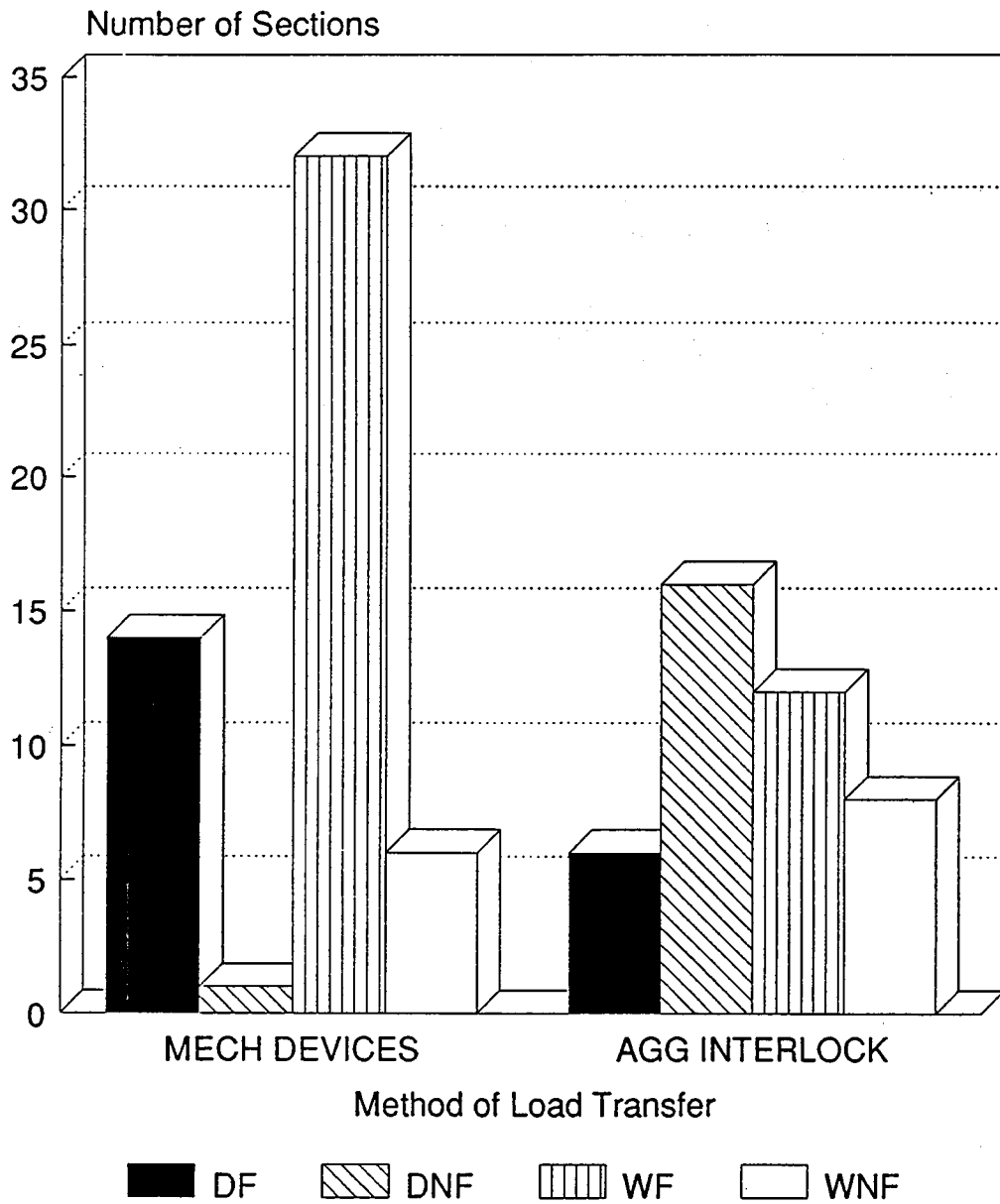


Figure 4. Distribution of load transfer method by environmental region.

Shoulder Type/Widened Lanes

Shoulder type was of interest in the study to compare the structural benefits of portland cement concrete (PCC) shoulders with traditional asphalt concrete (AC) shoulders. By providing additional support to the mainline pavement, tied PCC shoulders are believed to increase concrete pavement life.

Along similar lines, the use of widened lanes was also investigated. Since this design allows for an interior-loading condition, critical edge stresses are reduced and concrete pavement life should be increased. However, there were very few sections with widened lanes and these were relatively new.

The distribution of shoulder type is shown in figure 5. It is observed that there were many more sections with AC shoulders, particularly in the wet-freeze environmental region. It should be noted that the four projects with widened lanes were grouped with the PCC shoulders for purposes of presentation.

SHOULDER TYPE

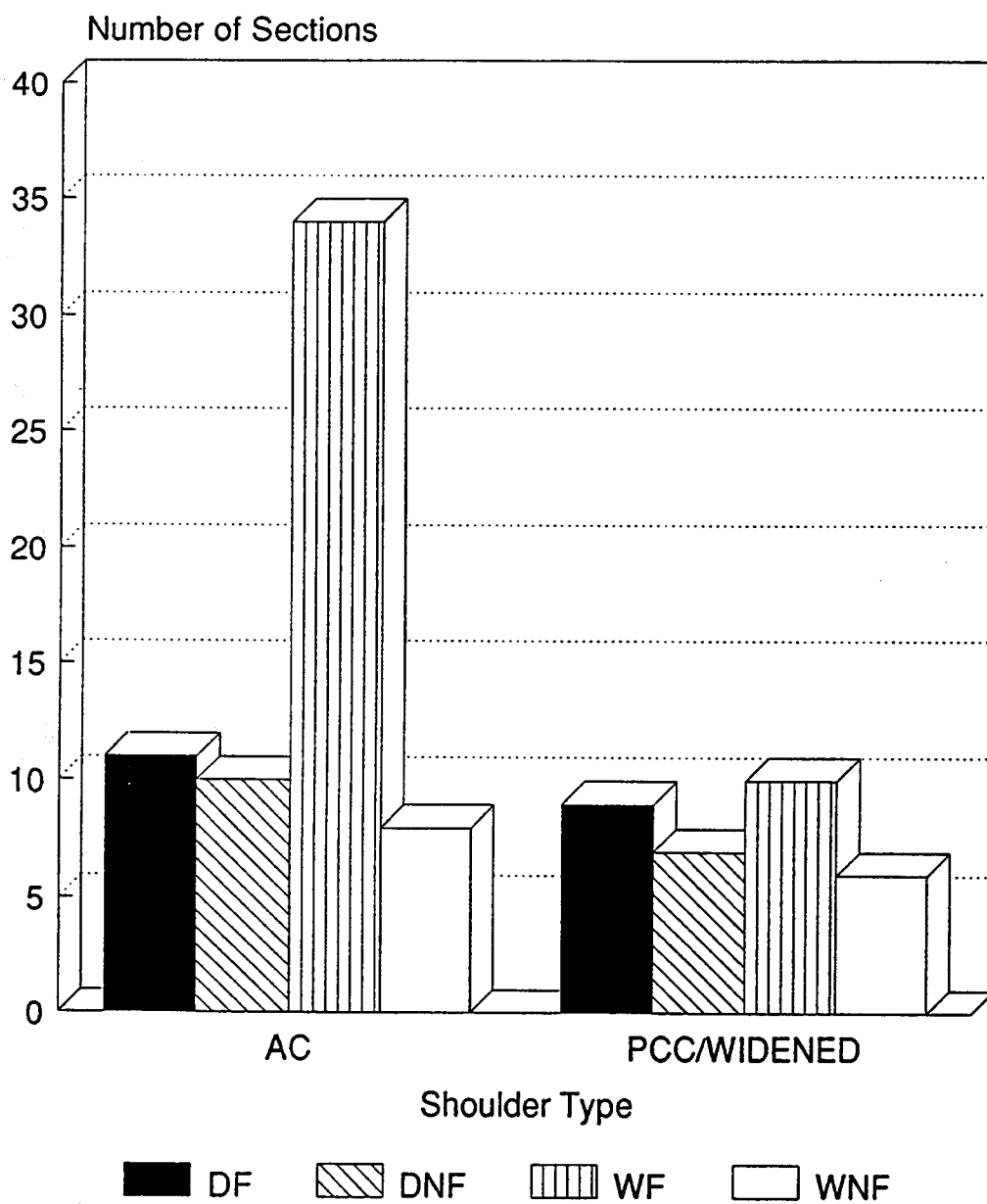


Figure 5. Distribution of shoulder type by environmental region.

CHAPTER 3 ANALYSIS OF THE ACCURACY OF SELECTED PREDICTION MODELS

1. INTRODUCTION

Over the past several years, various researchers have developed models to predict the performance of inservice concrete pavements. However, to date the accuracy of these models has not been extensively tested. Since accurate models can be very useful tools for pavement design and performance prediction, it is of great interest to know if these models are applicable to pavements other than those from which they were developed. With the database of pavements collected under this study (called the RIPPER study), an evaluation of the ability of the existing models to accurately predict pavement performance can be accomplished.

The models selected for evaluation include the AASHTO design equation (see reference 1) the PEARDARP models (see references 3 through 5) the NCHRP 1-19 COPES models (see reference 6) and the PFAULT models (see reference 7). A brief description and the functional form of each of the models is presented in section 2 of this chapter. The models were analyzed through a combination of the use of statistical procedures and a graphical examination of the results. The statistical procedure used in this analysis is presented in section 3. The accuracy of the models in terms of predicting the performance of the Phase I sections is discussed in section 4.

It is important to realize that the accuracy of the existing models to predict performance of inservice pavements cannot be determined conclusively with the available data. It is only possible to determine whether the models are able to predict the actual performance of the sections that are included in this database. Until a more comprehensive database is developed which is considered representative of the entire population of pavements in the four environmental regions, it is not possible to determine the overall accuracy of the models or to develop models which accurately reflect the total population of pavements since it is not always possible to identify nondesign (construction) related distresses.

2. DESCRIPTION OF PREDICTION MODELS

Each prediction model requires a unique set of inputs. The inputs for each individual section were obtained from the design and construction information, distress surveys, physical testing, and nondestructive testing. In addition, many of the models require the user to calculate or select inputs, based on a set of recommendations which accompany the model. A data set was created, using the Statistical Analysis System (SASTM), which includes all of the required inputs for each model.⁽⁸⁾ The data set, containing all Phase I sections, is illustrated in table 158 of volume VI.

A brief discussion of the various models evaluated follows. This includes a presentation of the form of the model and a listing of required inputs.

AASHTO Design Model

The 1986 AASHTO Design Guide represents a revision of the original AASHTO design procedure.⁽¹⁾ The basic design equation was developed from the results of the AASHTO Road Test, conducted in Northern Illinois in the late 1950's. The Road Test included both jointed plain concrete pavements (JPCP) and jointed reinforced concrete pavements (JRCP). The JPCP pavements were doweled, with 15 ft (4.6 m) joint spacing and the JRCP pavements were doweled and had 40 ft (12.2 m) joint spacing. These pavements were subjected to a fixed number of axle loads and types over a 2-year period. Their serviceability under this loading was monitored very closely over this 2-year period and the basic empirical design model was developed using regression techniques for the jointed plain and jointed reinforced pavements.

In recognition of several limitations of the basic model, several modifications were made in 1986. New inputs were added, reflecting variables that the developers determined were important in the design of rigid pavements. The modified equation is presented below:

$$\log_{10}(\text{ESAL}) = z_R \cdot s_o + 7.35 \log_{10}(\text{THICK} + 1) - 0.06 + \frac{\log_{10} [(\Delta\text{PSI}/(4.5-1.5))]}{[1 + (1.624 \cdot 10^7 / (\text{THICK} + 1)^{8.46})]} + (4.22 - 0.32 \cdot p_i) \cdot \log_{10} \left[\frac{[M_R \cdot C_d \cdot (\text{THICK}^{0.75} - 1.132)]}{\{215.63 \cdot J \cdot [\text{THICK}^{0.75} - (18.42 / (E_{\text{pcc}}/k)^{0.25})]\}} \right] \quad (1)$$

where:

- ESAL = Cumulative 18-kip (80 kN) equivalent axle loads expected during the design period
- z_R^* = Standard normal deviate based on level of reliability
- s_o^* = Overall standard deviation
- D = THICK = slab thickness, in
- p_i = Initial serviceability directly after construction
- p_t = Terminal serviceability at the end of the design period
- ΔPSI = Change in serviceability over the design period, = $p_i - p_t$
- M_R = Mean modulus of rupture, psi
- C_d = Drainage coefficient
- J = J-factor
- E_{pcc} = Concrete slab modulus of elasticity, psi
- k = Effective modulus of subgrade reaction, pci

* indicates new variables added in 1986 revision

In order to use the AASHTO design equation in the analysis presented here, the number of 18-kip (80 kN) Equivalent Single-Axle Load (ESAL) applications required to bring the pavement to the serviceability at the time of survey will be predicted. This concept is explained in more detail in section 4.

The AASHTO Design Guide provides some direction on the selection of input variables. However, the allowable ranges are typically quite broad. The criteria for the selection of input values and a brief explanation of the input variables are presented below.

ESAL The Guide recommends that the design traffic be calculated by using the AASHTO equivalency factors to convert mixed traffic to the equivalent number of 18-kip (80 kN) ESAL applications. The traffic calculations performed under this study are documented in volume V. In a design process, the traffic would be calculated and the thickness would be determined through use of the nomographs. However, for this analysis, the ESAL's are predicted based on the actual design thickness and inservice performance of the Phase I sections.

z_R The standard normal deviate is the value on the normal distribution curve corresponding to the level of reliability chosen. According to the Guide, the level of reliability is based on the functional classification of the roadway. Table 5 shows the recommended level of reliability required for various functional classifications. However, for this analysis, a reliability of 50 percent was used since that was the level of reliability used in the development of the original AASHO models.

s_o The standard deviation in the model is an attempt to account for variability in the overall design and construction process. For rigid pavements, the guide recommends an overall standard deviation of 0.25 to 0.35. While the standard deviation coefficient tries to account for the weighted variation of all factors, the Guide recommends 0.25 if traffic data is considered accurate. The higher end of the scale is to be used when traffic data is believed to contain some error. Given the method of traffic calculation, a value of 0.30 was chosen for all sections for this analysis.

D Typically, the thickness is the output of the design procedure. The design thickness of each section was used for this study.

p_i The initial serviceability for all sections was assumed to be 4.5. This is the value recommended by the Guide for new concrete pavements.

p_t The terminal serviceabilities were set to the serviceability of the section at the time of survey. This was necessary in order to use the AASHTO equation to predict the cumulative ESAL's that the pavement had experienced at the time of survey.

Table 5. Recommended levels of reliability for various functional classifications.⁽¹⁾

Functional Classification	Recommended Level of Reliability	
	Urban	Rural
Interstate and other freeways	85 - 99.9	80 - 99.9
Principal Arterials	80 - 99	75 - 95
Collectors	80 - 95	75 - 95
Local	50 - 80	50 - 80

- Δ PSI The change in serviceability is the initial serviceability (4.5) minus the serviceability at the time of survey. Therefore, the ESAL's to reach the serviceability at the time of survey will be predicted from the AASHTO equation.
- M_R The Guide recommends testing of concrete beams at 28-days using third-point loading (AASHTO T97, ASTM C78). Adjustment of this value based on the variability of the material and the percentage of strength gain is also recommended. For this study, the modulus of rupture was determined based on correlation with the split tensile strength of the material. These values were used because very little information was available on the strength of the portland cement concrete (PCC) at the time of construction. Since PCC gains strength as it ages, the M_R from the split tensile correlations will be somewhat larger than the 28-day M_R . Also, since only one core was retrieved from each section, the ability to accurately determine the M_R is questionable.
- C_d The drainage coefficient is determined based on the quality of drainage and the percent of the time the pavement structure is exposed to moisture levels approaching saturation. The recommendations presented in the Guide are shown in table 6. The method followed for the selection of C_d values is presented in volume V.
- J The J-factor accounts for the amount of transverse load transfer and edge support that is present on a pavement section. The primary factors it considers are the use of dowel bars and the use of tied concrete shoulders. The recommendations from the Guide for the J-factor is presented in table 7.
- E_{pcc} The Guide recommends determination of the stiffness of the material according to ASTM C469. Relationships between the modulus of elasticity and the compressive strength of the material are given, also. The E_{pcc} used for this analysis was determined through the backcalculation of deflection data.
- k The effective k -value (on top of the base) is determined by correlating the seasonal resilient modulus values to an equivalent k -value. The yearly composite k -value is determined from the equivalent k -values and the yearly value is then adjusted for loss of support potential and depth to bedrock. For this analysis, the static k -value determined from backcalculation of deflection data collected under this study was used.¹

The analysis and evaluation of the AASHTO design procedure is presented in section 4 of this chapter.

¹ The static k -value is one-half of the dynamic backcalculated k -value.

Table 6. Values of the drainage coefficient for the design of rigid pavements as presented in the AASHTO Guide.(1)

Quality of Drainage	Percent of Time Pavement Structure is Exposed to Moisture Levels Approaching Saturation			
	Less Than 1%	1 - 5%	5 - 25%	Greater Than 25%
Excellent	1.25 - 1.20	1.20 - 1.15	1.15 - 1.10	1.10
Good	1.20 - 1.15	1.15 - 1.10	1.10 - 1.00	1.00
Fair	1.15 - 1.10	1.10 - 1.00	1.00 - 0.90	0.90
Poor	1.10 - 1.00	1.00 - 0.90	0.90 - 0.80	0.80
Very Poor	1.00 - 0.90	0.90 - 0.80	0.80 - 0.70	0.70

Table 7. Load transfer coefficients for various pavement types and design conditions as presented in the AASHTO Guide.(1)

Shoulder	Asphalt		Tied P.C.C.	
	Yes	No	Yes	No
Load Transfer Devices				
Pavement Type				
1. Plain Jointed and Jointed Reinforced	3.2	3.8 - 4.4	2.5 - 3.1	3.6 - 4.2
2. CRCP	2.9 - 3.2	N/A	2.3 - 2.9	N/A

PEARDARP Prediction Models

As part of a comprehensive analysis on pumping of rigid pavements which was conducted for the FHWA, prediction models were developed for pumping and other rigid pavement distresses. A computer program entitled PEARDARP was developed which includes these models as well as economic analysis models. Performance prediction models which are incorporated into the PEARDARP program include models to predict pumping, faulting, cracking, spalling, roughness, and serviceability. The models were developed from various sources of data and the exact database used is a function of the particular model in question. A brief discussion of the origins of each model follows.

1. The spalling model was developed from data from the Michigan Road Test.
2. The serviceability model included in PEARDARP are those developed at the AASHO Road Test for the Present Serviceability Index.
3. The roughness model was developed from the serviceability model developed in the Zero-Maintenance study, which was based on AASHO Road Test data.⁽²⁾ The serviceability model was modified using roughness measurements from AASHO Road Test data.
4. The pumping model is mechanistic-empirical in form. It is based on AASHO Road Test data and the mechanistic analysis of slab properties. The model was modified to correct some of the inherent problems with the AASHO Road Test data. Correction factors were developed to consider the effects of climate, subbase type, subgrade type, dowels, and subdrainage. These correction factors were developed based on equations developed by Rauhut.⁽⁹⁾ A large experimental matrix considering all factors in the Rauhut equations was developed and the matrix was filled by using these equations. Regression analysis, employing the experimental matrix data, was used to develop the models. A detailed discussion on the development of this model is presented in reference 3.
5. The cracking model included in PEARDARP is a modified version of a model developed under the Zero-Maintenance study.⁽²⁾ The Zero-Maintenance cracking model was developed from a database of inservice pavements supplemented by mechanistic analysis of edges stresses developing in rigid pavement slabs. This model was modified to include the effects of base type on fatigue cracking of rigid slabs.
6. The faulting model was developed by Packard.⁽¹⁰⁾ A normal distribution function was added to the model to generate the number of faulted joints beyond specified tolerance levels for rehabilitation estimation purposes.

The actual models for each distress type are presented below.

Spalling Model

The PEARDARP spalling model is shown below:

$$F_s = 1 - e^{-\alpha(J^3)} \quad (2)$$

where:

- F_s = fraction of joints spalled
- α = 0.0000162 $A^{3.0806}$
- J = transverse joint spacing, ft
- A = pavement age, years

The inputs to this model are all readily available from the field and office data collection activities, as summarized in volume IV. In the case of a pavement with variable joint spacing, the average joint spacing was used as the input.

PSI Model

The model for present serviceability (PSI) is the same model as was developed at the AASHO Road Test. It is shown below:

$$PSI = 5.41 - 1.80 \log (SV + 1) - 0.09 (C + P)^{0.5} \quad (3)$$

where:

- PSI = Present Serviceability Index
- SV = slope variance (radians² X 10⁶)
= SVR + SVF
- C = linear cracks, lin ft/1000 ft²
- P = patched area, sq ft/1000 ft²

and

- SVR = 0.000145 $R^{2.255}$
- SVF = (0.00159/J) * $F^{1.7229}$
- F = average faulting, in
- R = roughness, in/mi

In the original equation for the PSI, slope variance was a roughness term that was obtained from measurements made with a CHLOE profilometer. This input has been estimated from measurements of average faulting and roughness (measured by the Mays Ride Meter), as shown above. It should be noted that this equation is very sensitive to changes in the roughness term, and fairly insensitive to changes in the cracking and patching terms.

Roughness Model

The PEARDARP model for roughness is:

$$R = 360 - 216 \left[1.5 - (1 + e^{-\beta/\rho X})^{-1} + (1 + e^{\Sigma\text{ESAL} - \beta/\rho X})^{-1} \right] \quad (4)$$

where:

$$\begin{aligned} R &= \text{roughness, in/mi} \\ \beta &= -50.088 - 3.775*D + 30.644*D^{0.5} \\ \rho &= -6.697 + 0.139*D^2 \\ X &= 10^{1.774Y} \end{aligned}$$

$$Y = \log \left[\left(M_R/690 \right) \frac{4*\log(8.789 D^{0.75}/F) + 0.359}{4*\log(Z^{0.25} (0.54 D^{0.75}/F)) + 0.359} \right]$$

$$\begin{aligned} F &= (30.56 + D^2)^{0.5} - 0.675D \\ Z &= E/k \\ D &= \text{slab thickness, in} \\ E &= \text{modulus of the slab, psi} \\ k &= \text{effective modulus of subgrade reaction, pci} \\ M_R &= \text{mean 28-day modulus of rupture, psi} \\ \Sigma\text{ESAL} &= \text{cumulative 18-kip (80 kN) equivalent single axle loads, millions} \end{aligned}$$

An examination of the inputs for this roughness model shows that it is a function of the slab thickness, slab strength, and support values, and the cumulative ESAL's. These values were obtained during the data collection activities and through backcalculation procedures described elsewhere.

Pumping Models

There are several models developed under PEARDARP for pumping. They were all developed from data collected at the AASHO Road Test, supplemented with data generated from equations developed by Rauhut.⁽⁹⁾ The first model calculates a "normalized" pumping index. It has been normalized to handle conditions that were not present at the AASHO Road Test, including different traffic loadings, subbase materials, drainage conditions, load transfer, moisture, and subgrade types. The second model uses the normalized pumping index to calculate a volume of pumped material per mile. The third model incorporates the previous two models and combines them with an average volume of the void space to estimate the amount of material required to underseal the void. These models and a description of the variables follows.

$$\text{NPI} = F * e^{-2.884 + 1.652 \log(\Sigma\text{ESAL} * DE/10,000)} \quad (5)$$

$$P = 36.67 * \text{NPI} \quad (6)$$

$$\text{PU} = P + (I * nP) \quad (7)$$

where:

- NPI = normalized pumping index, in³
DE = deformation energy per application, in-lb
log(DE) = $3.5754 - 0.3323 \cdot D$
P = volume of pumped material, ft³/mi
PU = volume of underseal material required, ft³/mi
nP = number of pumping joints per mile
nP = P/v_{void}
vvoid = average void volume per joint, ft³
D = slab thickness, in
ΣESAL = cumulative 18-kip (80 kN) equivalent single axle loads, millions
F = f_{JPCP} , if nonreinforced PCC
= f_{JRCP} , if reinforced PCC
 f_{JPCP} = $f_{\text{sbl}} \cdot f_{\text{d}} \cdot f_{\text{lt}} \cdot f_{\text{prec}} \cdot f_{\text{sg}}$
 f_{sbl} = subbase adjustment factor
= 1.0, for granular material
= $0.65 + 0.18 \log(\Sigma\text{ESAL})$, for stabilized material
 f_{d} = drainage adjustment factor
= 1.0, for poor drainage
= $0.91 + 0.12 \log(\Sigma\text{ESAL}) - 0.03 \cdot D$, for fair drainage
= $0.68 + 0.15 \log(\Sigma\text{ESAL}) - 0.04 \cdot D$, for good drainage
= 0.01, for excellent drainage
 f_{lt} = load transfer adequacy adjustment factor
= 1.0, with dowels
= $1.17 + 0.68 \log(\Sigma\text{ESAL}) - 0.078 \cdot D$, without dowels
 f_{prec} = rainfall adjustment factor
= $0.89 + 0.26 \log(\Sigma\text{ESAL}) - 0.07 \cdot D$, for dry climates
= $0.96 - 0.06 \log(\Sigma\text{ESAL}) + 0.02 \cdot D$, for wet climates
 f_{sg} = subgrade adjustment factor
= 1.0, for coarse subgrades
= $0.57 + 0.21 \log(\Sigma\text{ESAL})$, for fine subgrades
 f_{JRCP} = $f_{\text{sb2}} \cdot f_{\text{e}}$
 f_{sb2} = subbase adjustment factor
= 1.0, for nonstabilized subbase
= $0.91 - 0.02 \cdot D$, for stabilized subbase
 f_{e} = adjustment for climate
= $0.011 + 0.003 \log(\Sigma\text{ESAL}) - 0.001 \cdot D$, for a dry, warm climate
= $1.44 - 0.03 \log(\Sigma\text{ESAL}) - 0.06 \cdot D$, for a wet, warm climate
= $1.04 - 0.32 \log(\Sigma\text{ESAL}) - 0.08 \cdot D$, for a dry, cold climate
= $0.54 - 0.85 \log(\Sigma\text{ESAL}) + 0.19 \cdot D$, for a wet, cold climate

An examination of the pumping models shows them to be a function of accumulated ESAL's, thickness, subbase type, drainage conditions, climatic conditions, load transfer, and pavement type. Joint spacing, and therefore the number of joints per mile, is not included, although outputs include the volume of pumped material per mile and the volume of underseal material required per mile.

It is not known how this relationship between the number of pumping joints per mile is related to the actual number of joints in a mile.

These pumping models cannot be used to make a direct comparison between the predicted values from the models and the actual, measured values. In this project, pumping was evaluated in the field by severity, not volume, ranging from "NONE" to "HIGH." Low severity pumping is defined as there being evidence of water pumping, but no fines visible on the shoulder. Medium and high severity pumping are differentiated by the presence of fines on fewer than or more than 20 percent of the joints. These ratings do not readily correspond to cubic volumes of pumped material.

Cracking Model

The PEARDARP model for slab cracking is:

$$CR = (DA/4000) * 2 * 5280/63.35 \quad (8)$$

where:

$$DA = e^{(a_1 + a_2 \log(\Sigma ESAL) + a_3 D + a_4 k_R)^6}$$

$$a_1 = 39.006$$

$$a_2 = 3.941$$

$$a_3 = -4.387$$

$$a_4 = -0.0036$$

for *stabilized* materials,

$$\log(k_c) = 0.7405 \log(D) + 0.7256 \log(k) + 0.5559, \text{ and}$$

$$k_R = k_c$$

for *nonstabilized* materials,

$$\log(k_c) = 0.3483 \log(D) + 0.8163 \log(k) + 0.8163, \text{ and}$$

$$k_R = 1.7 * k_c$$

and where:

DA = damage area per joint, in²

CR = length of crack, lin ft/1000 ft²

(ΣESAL) = cumulative equivalent 18-kip (80 kN) single axle loads, millions

D = slab thickness, in

k = modulus of subgrade reaction, pci

k_c = composite modulus of slab support (on top of the base), pci

The amount of linear transverse cracking, expressed in terms of lin ft/1000 ft², is modeled as a function of cumulative ESAL's, slab thickness, and the composite

modulus of slab support. The subgrade reaction is shown to differ for stabilized and nonstabilized base materials. These inputs were all collected during either the data collection or field surveys. The modulus values were backcalculated from deflections measured with the Falling Weight Deflectometer (FWD).

Faulting Models

There are two PEARDARP models to predict transverse joint faulting. These models predict faulting for nondoweled and doweled pavements respectively.

$$F_{n-avg} = (1.29 + (K_1 * (T * A^2)) * f_{SD})/32.0 \quad (9)$$

$$F_{d-avg} = f_d * F_{n-avg} \quad (10)$$

where:

- F_{n-avg} = average faulting for nondoweled pavements, in
- F_{d-avg} = average faulting for doweled pavements, in
- K_1 = $[48.95 * S^{0.610} (J - 13.5)^b]/D^{3.9}$
- T = $(\Sigma Vol * p_t)/n$
- f_d = $(1 + A)^{-0.5}$
- A = age, years = n
- f_{SD} = subdrainage factor
 - = 0.1, if subdrainage is excellent
 - = 0.6, if subdrainage is good
 - = 1.0, if subdrainage is fair
 - = 1.4, if subdrainage is poor
- S = subgrade drainage
 - = 1, if subgrade drainage is good
 - = 2, if subgrade drainage is poor
- J = slab length, ft
- b = 0.241 for granular subbase
= 0.037 for stabilized subbase
- D = slab thickness, in
- ΣVol = cumulative traffic volume in one direction, millions
- p_t = proportion of trucks in the design lane

In these models, faulting is a function of many variables, including subgrade drainage, joint spacing, slab thickness, pavement age, pavement subdrainage, and traffic volume and the proportion of that volume that is trucks. Subgrade drainage and pavement subdrainage are both subjective inputs. The subgrade drainage was determined as a function of subgrade type; AASHTO soils A-1 through A-3 were determined to have good drainage properties and A-4 to A-7 were determined to have poor drainage properties. The subdrainage factor was determined by coordination with the AASHTO C_d drainage values and

permeabilities of the drainable layers. The remainder of the inputs were obtained from the field surveys and data collection activities.

COPES Prediction Models

Under NCHRP Project 1-19, termed the COPES study, a large amount of design and performance data was collected from rigid pavement sections in seven States.⁽⁶⁾ The collected information included inventory data and monitoring data for JPCP, JRCP, and CRCP, totalling 410 individual sections and 1297 lane miles. The data was stored in a database and used to develop models predicting the performance of concrete pavements. The steps involved in the development of the prediction models are described below.

Nationwide regression models were developed for JPCP and JRCP based on the data from the seven States. These models were developed for transverse joint faulting, transverse joint deterioration (spalling), slab cracking, pumping, and the Present Serviceability Rating (PSR). A combination of multiple linear regression and nonlinear regression techniques were used to develop the models. Multiple linear regression was used to determine which independent variables significantly affected the dependent variables.

The pavement designs that are included in the database are typical of pavements constructed during the 1960's and 1970's. These models are only legitimately extendable to pavements with similar designs. The database did not include pavements with such features as open-graded drainage layers, widened lanes, corrosion-resistant dowel bars, or thickened slabs.

The models for both pavement types, as well as the model statistics, are presented below by distress type. In order to avoid duplication, only previously undefined variables are defined for each equation.

IPCP Pumping Model

$$\text{PUMP} = \text{ESAL}^{0.443} [-1.479 + 0.255*(1-\text{SOILCRS}) + 0.0605*\text{SUMPREC}^{0.5} + 52.65/(\text{THICK})^{1.747} + 0.0002269*\text{FI}^{1.205}] \quad (11)$$

where:

- PUMP = pumping
- = 0, no pumping
- = 1, low severity pumping
- = 2, medium severity pumping
- = 3, high severity pumping
- ESAL = accumulated 18 kip (80 kN) equivalent single axle loads, millions
- SOILCRS = 0, fine-grained subgrade soil
- = 1, coarse-grained subgrade soil
- SUMPREC = Average annual precipitation, cm

THICK = Slab thickness, in
 FI = freezing index

$$R^2 = 0.68$$

$$SEE = 0.42$$

$$n = 289$$

Pumping severity is measured as the average amount of pumping occurring throughout the pavement section. The statistical information indicates that the model accounts for 68 percent of the variability in the development and prediction of pumping. The standard error of the estimate (SEE) indicates that the model will predict pumping within ± 0.42 for the specified confidence level (typically 95 percent). For this model, there were 289 observations which were used in the development of the model.

Each of the inputs required for this model are very straightforward and easily obtained from the office and field data collection.

JRCP Pumping Model

$$\begin{aligned} \text{PUMP} = & \text{ESAL}^{0.670} [-22.82 + 26102.2/(\text{THICK})^{5.0} - 0.129*\text{DRAIN} \\ & - 0.118*\text{SOILCRS} + 13.224*\text{SUMPREC}^{0.0395} \\ & + 6.834(\text{FI}+1)^{0.00805}] \end{aligned} \quad (12)$$

where:

DRAIN = 0, if no subdrainage exists
 = 1, if subdrainage exists

$$R^2 = 0.57$$

$$SEE = 0.52$$

$$n = 481$$

With the exception of the subdrainage, the other inputs for the JRCP model are the same as described for the JPCP model. It is observed that the pumping model for JRCP has more variability associated with it then does the pumping model for JPCP.

JPCP Joint Faulting Model

$$\begin{aligned} \text{FAULT} = & \text{ESAL}^{0.144} [-0.2980 + 0.2671*\text{THICK}^{-0.3184} - 0.0285*\text{BASETYP} + \\ & 0.00406*(\text{FI} + 1)^{0.3598} - 0.0462*\text{EDGESUP} + 0.2384*(\text{PUMP} + 1)^{0.0109} - \\ & 0.0340*\text{DOW}^{2.0587}] \end{aligned} \quad (13)$$

where:

FAULT = mean transverse joint faulting, in
 BASETYP = 0, if granular base
 = 1, if stabilized base
 EDGESUP = 0, if AC shoulder
 = 1, if tied PCC shoulder
 PUMP = 0, if no pumping
 = 1, if low severity pumping
 = 2, if medium severity pumping
 = 3, if high severity pumping
 DOW = diameter of dowel bar, in

$R^2 = 0.79$
 $SEE = 0.02$
 $n = 259$

The inputs for this model are all straightforward and are easily obtained from the field surveys and data collection.

JRCP Joint Faulting Model

$$\begin{aligned}
 \text{FAULT} = \text{ESAL}^{0.4731} &[-3.8536 - 1.5355 \cdot \text{SOILCRS} + 197.124 \cdot (\text{THICK} \cdot \text{DOW}^{2.0})^{-1.7842} \\
 &+ 0.00024 \cdot \text{FI} + 0.09858 \cdot \text{JSPACE} + 0.24115 \cdot \text{PUMP}^{2.0}] / 100 \quad (14)
 \end{aligned}$$

where:

JSPACE = transverse joint spacing, ft

$R^2 = 0.69$
 $SEE = 0.06$
 $n = 384$

The inputs for this model are also readily obtained from the data collected during the field surveys and office data collection. As the R^2 shows, this model does not account for as much of the variability in the prediction of faulting of JRCP pavements as does the JPCP model.

JPCP Joint Deterioration Model

The joint deterioration models predict spalling of the transverse joints. The joint deterioration model for JPCP is shown below.

$$\begin{aligned}
 \text{DETJT} = \text{AGE}^{1.695} & (0.9754 \cdot \text{DCRACK}) + \text{AGE}^{2.841} (0.01247 \cdot \text{UNITUBE}) + \\
 & \text{AGE}^{3.038} (0.001346 \cdot \text{INCOMP}) \quad (15)
 \end{aligned}$$

where:

DETJT = number of deteriorated (medium and high severity) joints/mile
 AGE = time since construction
 UNITUBE = 0, if no unitube inserts used
 = 1, if unitube inserts used
 INCOMP = 0, if no incompressibles are visible in the joints
 = 1, if incompressibles are visible in the joints

$R^2 = 0.59$
 SEE = 16 joints/mi
 n = 252

JRCP Joint Deterioration Model

The joint deterioration model for JRCP is shown below.

$$\begin{aligned}
 \text{DETJT} = & \text{AGE}^{0.756}(2.4367*\text{DCRACK} + 2.744*\text{REACTAG}) + \\
 & \text{AGE}^{2.1521}*\text{ESAL}^{0.1419}(0.05202 + 0.0000254*\text{FI} + 0.01109*\text{TJSD} - \\
 & 0.003384*\text{K1}*\text{JTSPACE} - 0.0006446*\text{K2}*\text{JTSPACE}) \quad (16)
 \end{aligned}$$

where:

DCRACK = 0, if no "D" cracking exists
 = 1, if "D" cracking exists
 REACTAG = 0, if no reactive aggregate exists
 = 1, if reactive aggregate exists
 TJSD = transverse joint seal damage
 = 0, if none or low severity
 = 1, if medium or high severity
 K1 = 1, if JTSPACE is 27 ft
 = 0, if JTSPACE is not 27 ft
 K2 = 1, if JTSPACE is from 39 to 100 ft
 = 0, if JTSPACE is less than 39 ft

$R^2 = 0.61$
 SEE = 15 joints/mi
 n = 319

These models show the enormous impact that "D" cracking or reactive aggregate has on the probability of the pavement exhibiting spalling. Other factors which influence the predicted joint deterioration are the age and traffic loadings, the joint spacing for JRCP, and the climate for JRCP. However, the statistics show that a little over one-half of the variability in the development and prediction of joint deterioration is accounted for by the models' variables and interactions between the variables. All of the inputs were readily available from the data

collected. There were not any sections included in this study whose transverse joints were formed by unitubes.

JPCP Slab Cracking Model

The slab cracking models provide the total amount (both longitudinal and transverse) of cracking in ft/mi. Traffic is a major factor in the JPCP slab cracking model. In addition, the ratio of the calculated Westergaard's edge stress to the modulus of rupture is also a key term. This term does not appear in the cracking model for JRCP. Other variables in the JPCP model are subgrade type and climatic inputs.

$$\begin{aligned} \text{CRACKS} = & \text{ESAL}^{2.755}[3092.4(1 - \text{SOILCRS})*\text{RATIO}^{10.0}] + \\ & \text{ESAL}^{0.5}(1.233*\text{TRANGE}^{2.0}\text{RATIO}^{2.868}) + \\ & \text{ESAL}^{2.416}(0.2296*\text{FI}^{1.53}\text{RATIO}^{7.31}) \end{aligned} \quad (17)$$

where:

- CRACKS = total length of cracking of all severities (ft/lane mi)
- RATIO = Westergaard's edge stress/mean 28-day modulus of rupture
- TRANGE = difference between average maximum temperature in July and average minimum temperature in January

$$\begin{aligned} R^2 &= 0.69 \\ \text{SEE} &= 176 \text{ ft/mi} \\ n &= 303 \end{aligned}$$

JRCP Slab Cracking Model

The JRCP slab cracking model includes several variables that are not in the JPCP model. These are the transverse joint spacing, the area of the reinforcing steel, the slab thickness, the base type, and the presence of pumping.

$$\begin{aligned} \text{CRACKS} = & \text{ESAL}^{0.897}[7130.0*\text{JTSPACE}/(\text{ASTEEL}*\text{THICK}^{5.0})] + \\ & \text{ESAL}^{0.10}(2.281*\text{PUMP}^{5.0}) + \text{ESAL}^{2.16}[1.81/(\text{BASETYP} + 1)] + \\ & \text{AGE}^{1.3}[0.0036(\text{FI} + 1)^{0.36}] \end{aligned} \quad (18)$$

where:

- CRACKS = length of deteriorated (medium and high-severity) cracks, ft/lane mile
- ASTEEL = area of reinforcing steel, in²/ft width

$$\begin{aligned} R^2 &= 0.41 \\ \text{SEE} &= 280 \text{ ft/mi} \\ n &= 313 \end{aligned}$$

The statistics show that about 70 percent of the variability involved in the development and prediction of cracking on JPCP is accounted for in the variables and interaction between the variables within the equation. The JRCP equation accounts for only 40 percent of this variability.

All of the inputs for both cracking models were easily obtained from the field surveys or from the office data collection activities.

JPCP Present Serviceability Rating (PSR) Model

The PSR is a subjective rating of the serviceability of a pavement. This concept was originally developed at the AASHO Road Test, and was based on the philosophy that roads should provide acceptable service to the users. Panels of users were asked to rate the pavements at the AASHO Road Test for ride comfort. The PSR is the mean rating of a panel of users and provides an indication of the overall rideability of a roadway on a scale of 1 to 5.

The JPCP model for PSR is based on traffic, the ratio of Westergaard's edge stress to the modulus of rupture, the pavement's age, and climatic inputs. None of the inputs to this serviceability model were obtained from the field surveys; they were all provided from the office data collection.

$$\text{PSR} = 4.5 - 1.486 \cdot \text{ESAL}^{0.1467} + 0.4963 \cdot \text{ESAL}^{0.265} \cdot \text{RATIO}^{-0.5} - 0.01082 \cdot \text{ESAL}^{0.644} \cdot (\text{SUMPREC}^{0.91} / \text{AVGMT}^{1.07}) \cdot \text{AGE}^{0.525} \quad (19)$$

where:

PSR = present serviceability rating
 SUMPREC = average annual precipitation, cm
 AVGMT = average monthly temperature, °C

$R^2 = 0.69$
 $\text{SEE} = 0.25$
 $n = 316$

JRCP Present Serviceability Rating (PSR) Model

The JRCP model for the PSR is very similar to that for JPCP. It does include some additional factors such as the presence of materials distress and pumping. These inputs were provided from the field surveys. The other inputs to this model are obtained from the office data collection.

$$\text{PSR} = 4.5 - \text{ESAL}^{0.424} \cdot (-1.88 \cdot 10^{-3} + 14.417 \cdot \text{RATIO}^{3.58} + 0.0399 \cdot \text{PUMP} + 0.0021528 \cdot \text{JTSPACE} + 0.1146 \cdot \text{DCRACK} + 0.05903 \cdot \text{REACTAG} + 4.156 \cdot 10^{-5.0} \cdot \text{FI} + 0.00163 \cdot \text{SUMPREC} - 0.070535 \cdot \text{BASETYP}) \quad (20)$$

$$R^2 = 0.78$$

$$SEE = 0.30$$

$$n = 377$$

The statistics indicate that 70 to 80 percent of the variability involved in the prediction of PSR is accounted for by the variables and the interaction of the variables included in the model.

PFAULT Faulting Prediction Models

In an effort to improve the faulting models developed under the COPES project, the COPES database was expanded to include additional data from California (24 sections), New Jersey (1 section), and Michigan (1 section). The resulting faulting model was termed PFAULT.⁽⁷⁾ The PFAULT model also reflects additional data collected from the I-94 experimental sections at Rothsay, Minnesota (MN 1). Whereas the original models developed from the COPES data were divided into JPCP and JRCP pavements, the PFAULT models are divided by doweled and nondoweled pavements. The PFAULT prediction models for faulting are as follows:

Doweled Jointed Concrete Pavements

$$PFAULT = ESAL^{0.5377} [2.2073 + 0.002171 * BSTRESS^{0.4918} + 0.0003292 * JTSPACE^{1.0793} - 2.1397 * KVALUE^{0.01305}] \quad (21)$$

$$R^2 = 0.53$$

$$SEE = 0.05 \text{ in}$$

$$n = 280$$

Nondoweled Jointed Concrete Pavements

$$PFAULT = ESAL^{0.3157} [0.4531 + 0.3367 * OPENING^{0.3322} - 0.5376 * (100 DEFL)^{-0.008437} + 0.0009092 * FI^{0.5998} + 0.004654 * ERODF - 0.03608 * EDGESUP - 0.01087 * SOILCRS - 0.009467 * DRAIN] \quad (22)$$

$$R^2 = 0.55$$

$$SEE = 0.03 \text{ in}$$

$$n = 186$$

where:

PFAULT = mean faulting of transverse joints, in
 ESAL = accumulated equivalent 18-kip (80 kN) single axle loads in traffic lane, millions

- BSTRESS** = dowel/concrete bearing stress, psi, calculated using Friberg's procedure with an effective length of l instead of $1.8l$ (where l is the radius of relative stiffness)
JSPACE = transverse joint spacing, ft
KVALUE = effective k-value on top of the base layer, psi/in
OPENING = calculated joint opening for input temperature range, in
= $CON \cdot JSPACE \cdot 12 [a \cdot TRANGE + e]$
CON = adjustment factor due to subbase/slab frictional restraint (0.65 for stabilized base and 0.80 for granular base)
a = thermal coefficient of contraction of PCC, per °C
TRANGE = temperature range, °C (maximum mean daily air temperature in July minus minimum mean daily air temperature in January)
e = drying shrinkage coefficient of PCC ($0.5\text{--}2.5 \times 10^{-4}$ strain)
DEFL = unprotected corner deflection from Westergaard's equation, in
FI = Freezing Index, degree days below freezing
ERODF = erodibility factor for base materials
= 0.5, if lean concrete base
= 1.0, if cement-treated base with granular subbase
= 1.5, if cement-treated base without granular subbase
= 2.0, if asphalt-treated base
= 2.5, if granular base
EDGESUP = 0, if no tied concrete shoulder exists
= 1, if tied concrete shoulder exists
SOILCRS = AASHTO subgrade soil classification
= 0, if A-4 to A-7
= 1, if A-1 to A-3
DRAIN = 0, if no longitudinal edge subdrains exist
= 1, if longitudinal edge subdrains exist

As is shown above, there are a number of factors that were found to have an effect on faulting in these models. The nondoweled model includes eight variables. The values for these variables were all obtained from data collected during the field and office data collection procedures. The doweled model consists of four variables, also obtained from the field and office data collection procedures.

While these models were developed to improve the faulting prediction capabilities based on the COPEs data, the statistics show that these models actually account for less variability than do the original COPEs models. However, the PFAULT equation does attempt to introduce mechanistic variables believed to be important for the development of faulting. Nevertheless, the PFAULT models are still heavily empirical and should not be used beyond the ranges and the combination of inputs for which they were developed. For example, they can not be used to predict faulting for pavements with an open-graded drainage layer directly beneath the slab or which contain corrosion-resistant dowel bars.

3. STATISTICAL ANALYSIS OF PREDICTION MODELS

In order to analytically determine the ability of the models to predict the actual performance of the pavements contained in the RIPPER database, a statistical procedure is followed which determines whether the two data sets, the actual (observed) values and the values predicted from the models, are statistically the same data set. The paired-difference method, using a student *t*-distribution, is used to determine if the performance indicator (visible distress, faulting, roughness, and PSR) as predicted by the predictive models is statistically the same population (data set) as the *actual, measured* performance indicator.

The SASTM statistical software was used to compare the actual, field-measured performance indicator to the performance indicators as predicted by the various predictive models.⁽⁸⁾ The paired *t*-test was conducted to examine the statistical similarity of the data sets. The paired *t*-test assumes the following methodology:

1. For each section, the absolute value of the difference between the measured performance indicator (field data = PI) and the predicted performance indicator (predictive model = PMPI) is calculated as shown below:

$$DIF_{PI} = \text{abs} [PI - PMPI] \quad (23)$$

Note that if the predictive models *exactly* predict the measured performance indicator (PI = PMPI), then DIF_{PI} will equal 0.0 for every section.

This concept is illustrated in table 8 using the COPES faulting models with sections in the dry-freeze region.

2. The mean of the DIF_{PI} ($d_{PI} = \sum[DIF_{PI}]/\text{Number of observations}$) values for all sections is calculated. The null hypothesis to be tested is:

$$d_{PI} = 0.0.$$

This hypothesis assumes that the mean difference of the measured and predicted performance indicator values is 0.0 or, in other words, that the sample of field-collected performance indicator data comes from the same population as the sample of data generated by the predictive models.

3. The one-sample *t*-statistic is calculated using the following:

$$t_{calc} = d/SE_d \quad (24)$$

Table 8. Actual field-measured faulting versus faulting as predicted using the COPES faulting models for the dry-freeze region.

ID	Measured Faulting	Predicted Faulting	Difference
MN 1-1	0.31	0.11013	0.19987
MN 1-2	0.06	0.03139	0.02861
MN 1-3	0.31	0.11624	0.19376
MN 1-4	0.06	0.04819	0.01181
MN 1-5	0.37	0.13754	0.23246
MN 1-6	0.00	0.04819	0.04819
MN 1-7	0.31	0.13144	0.17856
MN 1-8	0.06	0.03139	0.02861
MN 1-9	0.37	0.07583	0.29417
MN 1-10	0.13	0.03139	0.09861
MN 1-11	0.50	0.08194	0.41806
MN 1-12	0.06	0.04819	0.01181
MN 2-1	0.06	0.06382	0.00382
MN 2-2	0.06	0.07003	0.01003
MN 2-3	0.05	0.02578	0.02422
MN 2-4	0.06	0.02578	0.03422
MN 3	0.02	0.01794	0.00206
MN 4b	0.01	0.08775	0.07775
MN 5	0.09	0.03831	0.05169
MN 6a	0.01	0.02335	0.01335

Analysis Variable : DIFCFLT

No. Obs	Mean Difference	Standard Error	t_{calc}	Prob> t_{table}
20	0.0980837	0.0260088	3.7711794	0.0013

Where:

- t_{calc} = t -statistic calculated from data
- d_{PI} = Mean of DIF_{PI} values
- SE_d = Standard error of the mean = $s_d/(n)^{0.5}$
- n = Number of observations
- s_d = Standard deviation of DIF_{PI} values
= $[\sum(DIF_{PI} - d_{PI})/(n - 1)]^{0.5}$

4. The calculated t -statistic (t_{calc}) is compared to a tabulated t -statistic (t_{table}) for a specified confidence level. If $t_{calc} > t_{table}$, then the null hypothesis is rejected with a 10 percent chance of error since the confidence level selected for this analysis is 90 percent. If the null hypothesis is rejected, then *it can be inferred with 90 percent confidence that the sample of predicted performance indicators (from the models) is not statistically from the same population as the sample of measured performance indicators.*
5. The data are plotted on scattergrams to visually examine the scatter of the data. The actual, measured value of the performance indicator is plotted against the predicted value. If all the models predict the measured performance indicator *exactly*, then all of the data will fall on a straight line with a slope of 1.000 (which is shown in each figure). An example of a scattergram using the COPES faulting models with sections in the dry-freeze region is shown in figure 6.

4. ABILITY OF MODELS TO PREDICT THE PERFORMANCE OF INSERVICE PAVEMENTS

The accuracy of the predictive capabilities of each of the models was compared for each of the four climatic zones as well as for all of the Phase I sections. This distinction by climatic zone was made to assess the effect that climate had on the models' capabilities. While there were 95 different sections, the separation of sections by direction for the Ontario 1 project increased the total number of sections to 99.

The evaluation of the models' abilities to predict the performance of the concrete pavement sections included in this study required the generation of many tables and figures which depict actual versus predicted performance trends for each model. In addition, further breakdowns for each model, such as by climatic region, by pavement type, or by load transfer method, had to be performed. In order to maintain continuity, only summary tables reporting the ability of each model to predict performance are provided in this report. The supporting tables and figures, along with the SAS™ data set used in the analysis, are provided in volume VI. Also included there is a summary table listing all inputs used for the analysis of each pavement section.

COPES Faulting Models Dry-Freeze Region

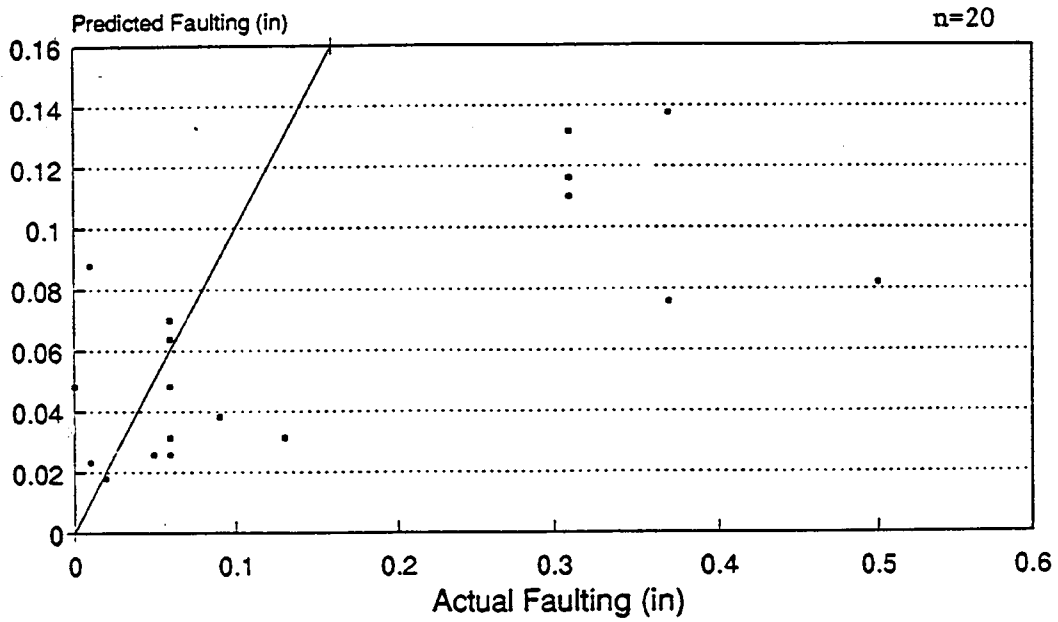


Figure 6. Scattergram of actual field measured faulting versus faulting as predicted using the COPES faulting models for the dry-freeze region.

AASHTO

The AASHTO design equation is used differently for this analysis than it would typically be used in design. In design, the engineer determines the design thickness based on the forecasted traffic over the design life. The design life is based on a specific change in serviceability (Δ PSI). In this analysis, the thickness of a specific section is known and the cumulative ESAL's are calculated. The Δ PSI is calculated as the difference between the initial serviceability (assumed to be 4.5) and the serviceability at the time of survey (PSR_{survey}). Therefore, the design equation will predict the amount of ESAL's that the pavement *should have* sustained (if the equation predicts accurately) to reach a Δ PSI of $4.5 - PSR_{survey}$.

Five sets of analyses were performed to examine the ability of the model to predict the amount of traffic actually sustained by each section. An analysis containing all Phase I sections was performed to determine the predictive ability of the model for the entire data set. Additional analyses were performed for each of the four environmental regions.

The summary of the statistical analysis is presented in table 9. It is observed that t_{calc} is greater than t_{table} for every data set, which indicates that the AASHTO model does not adequately predict the ESAL's actually sustained by the pavement sections included in the study. This holds true when considering any environmental region.

The basis for the results shown in table 9 is provided in tables 65 through 69 of volume VI. These tables make the comparison of actual ESAL's and predicted ESAL's for each data set. Figures 17 through 21 of volume VI provide graphical interpretations of the data provided in the tables.

Examining table 65 and figure 17 of volume VI for the analysis performed on all Phase I sections, it is observed that, in general, the AASHTO design equation overpredicts the number of loads for the pavement to reach its present PSR. Tables 66 through 69 and figures 18 through 21 of volume VI show the predicted ESAL's versus the actual ESAL's for each of the four climatic zones. It is clear from these figures that the model generally overpredicts traffic. This is most obvious in the wet-freeze region, where the predicted ESAL's are almost uniformly higher than the actual ESAL's. This suggests that the combination of available moisture and freeze-thaw cycling are not adequately considered in the AASHTO design process. However, this is not surprising given the fact that the model is based on only two years of performance results. This short period of time was inadequate to sufficiently account for environmental effects on pavement performance.

An examination of these results highlights the fact that one of the key terms in the AASHTO model is serviceability loss. This change in serviceability can occur prematurely due to materials problems, design problems, construction problems, and unexpectedly harsh climatic conditions. These factors are typically

Table 9. Summary of the statistical analysis of the AASHTO design model.

Data Set	Number of Observations	t_{calc}	t_{table}^*	$t_{calc} > t_{table}$	Adequately Predict Performance?
All Phase I	99	5.288	1.670	YES	NO
Dry-Freeze	20	4.871	1.729	YES	NO
Dry-Nonfreeze	17	2.915	1.746	YES	NO
Wet-Freeze	48	3.596	1.680	YES	NO
Wet-Nonfreeze	14	2.660	1.771	YES	NO

* t_{table} based on 90 percent confidence level.

not considered in design. In addition, while an average initial PSI of 4.5 was assumed, many of these projects may have had a much lower initial PSI.

Pavements included in this project have, with few exceptions, carried a lower traffic level. An examination of the traffic loadings sustained by these pavement sections indicates that two sections had over 35 million ESAL's, eight sections had over 9 million ESAL's, and the rest averaged about 3 million ESAL's.

Another factor to consider is that many of the projects included in the database were experimental projects intended to test the effect on performance of different design variables. It is inevitable that some of the experimental designs did not work. Since the database is oriented much more toward experimental designs than toward standard designs, it is not unexpected that there are differences between predicted traffic and actual traffic. For example, consider specific experimental variables, such as thicker slabs on grade. An examination of the AASHTO equation shows that thicker slabs dramatically increase the number of predicted ESAL's. However, the actual performance of the thicker slabs in the database showed that other factors were important, including drainage, the depth of longitudinal sawcut, and joint spacing.

This same principle can be applied to the sections which include widened lanes. It is believed that the inclusion of widened lanes or tied shoulders will increase the fatigue life of a jointed concrete pavement. However, this study showed that in order to reap the full benefits of this additional support, other factors were important, including spacing of tie bars, and method and timing of longitudinal joint formation. It is not sufficient to account for a variable in the design equation, such as the additional support from tied shoulders or widened lanes which is incorporated in the J-factor, if that variable is not properly designed or constructed. A final example of this concept is the use of dowel bars at transverse joints; if the dowels are not corrosion-resistant or of insufficient diameter, then the full benefits of the dowel bars will not be realized.

Another factor that is not considered in the AASHTO equation but was found to affect performance is the transverse joint spacing. It was shown that longer plain concrete slabs tended to experience more cracking than shorter slabs. This results in a drop in PSI.

Base type is considered indirectly in the AASHTO equation two ways. First, the k -value incorporates the relative stiffness of the base, allowing differentiation between aggregate and lean concrete bases, for example. The drainage coefficient incorporates the drainability of the base layer, which allows for differentiation between a dense, impermeable base layer and an open-graded, permeable base layer. However, the equation does not take into account the additional slab cracking that was observed on some of the stiff bases, or the suspected clogging or other design problems associated with some of the permeable layers.

PEARDARP

Each of the models for PSI, roughness, spalling, faulting, and cracking was used to predict performance for all sections and by climatic zone. The results of the comparisons of the predicted and the actual performance are summarized below for each model.

PSI Model

Table 10 provides the summary of the statistical analysis of the PEARDARP predictive models, including the model for PSI. This table shows that the PEARDARP PSI model does not adequately predict the actual PSI for any of the pavement sections included in the study from the various environmental regions.

The comparison of predicted PSI versus actual PSR for all of the sections is illustrated in table 70 and figure 22 of volume VI. It is observed that the PEARDARP PSI model overpredicted PSI for almost 90 percent of the sections included in the study. The actual PSR's ranged from 2.5 to 4.8 while the predicted PSI's ranged from 3.3 to greater than 5.0. Since the maximum PSR achievable is 5.0, and since the PSR of new concrete construction rarely approaches a value of 5.0, the fact that the model yields unattainable results is certainly a deficiency of the model. The model predicted a PSI of 4.8 or higher on almost 15 percent of the sections. An examination of the model shows that if there is very little faulting or roughness, as might be found in a new pavement, than the PSI will tend to be very high.

When the comparison between predicted PSI and actual PSR is made by climatic zone (tables 71 through 74 and figures 23 through 26 of volume VI), the model again consistently overpredicts the results. Overall, the predicted values were closer to the actual values in the zones without freezing.

Roughness Model

The statistical analysis of the PEARDARP roughness model is summarized in table 10. The results indicate that the roughness model is not able to satisfactorily predict the measured pavement roughness for the pavement sections included in this study.

Supporting documentation for this table is shown in tables 75 through 79 and figures 27 through 31 in volume VI. The model was least capable of predicting actual roughness for all of the Phase I sections considered together, where most of the error was in the overprediction of roughness (table 75 and figure 27 of volume VI). Examining the data by climatic zone, (tables 76 through 79 and figures 28 through 31 of volume VI), the model always overpredicted in the nonfreeze zones, while no clear trends were observed for the freeze zones.

Table 10. Summary of the statistical analyses of the PEARDARP prediction models.

Data Set	Number of Observations	t_{calc}	t_{table}^*	$t_{calc} > t_{table}$	Adequately Predict Performance?
PSI					
All Phase I	99	17.276	1.670	YES	NO
Dry-Freeze	20	7.995	1.729	YES	NO
Dry-Nonfreeze	17	6.509	1.746	YES	NO
Wet-Freeze	48	12.047	1.680	YES	NO
Wet-Nonfreeze	14	7.120	1.771	YES	NO
ROUGHNESS					
All Phase I	99	16.882	1.670	YES	NO
Dry-Freeze	20	8.162	1.729	YES	NO
Dry-Nonfreeze	17	9.233	1.746	YES	NO
Wet-Freeze	48	10.828	1.680	YES	NO
Wet-Nonfreeze	14	13.429	1.771	YES	NO
SPALLING					
All Phase I	99	11.474	1.670	YES	NO
Dry-Freeze	20	6.924	1.729	YES	NO
Dry-Nonfreeze	17	3.413	1.746	YES	NO
Wet-Freeze	48	8.357	1.680	YES	NO
Wet-Nonfreeze	14	4.994	1.771	YES	NO

Table 10. Summary of the statistical analyses of the PEARDARP prediction models (continued).

Data Set	Number of Observations	t_{calc}	t_{table}^*	$t_{calc} > t_{table}$	Adequately Predict Performance?
FAULTING					
All Phase I	99	7.825	1.670	YES	NO
Dry-Freeze					
All Sections	20	4.083	1.729	YES	NO
Doweled	14	5.465	1.771	YES	NO
Nondoweled	6	9.521	2.015	YES	NO
Dry-Nonfreeze	17	4.606	1.746	YES	NO
Wet-Freeze					
All Sections	48	8.598	1.680	YES	NO
Doweled	28	5.544	1.703	YES	NO
Nondoweled	20	7.109	1.729	YES	NO
Wet-Nonfreeze					
All Sections	14	5.325	1.771	YES	NO
Doweled	6	3.217	2.015	YES	NO
Nondoweled	8	5.942	1.895	YES	NO
CRACKING					
All Phase I	99	16.728	1.670	YES	NO
Dry-Freeze	20	11.855	1.729	YES	NO
Dry-Nonfreeze	17	6.958	1.746	YES	NO
Wet-Freeze	48	10.805	1.680	YES	NO
Wet-Nonfreeze	14	5.288	1.771	YES	NO

* t_{table} based on 90 percent confidence level.

It should be noted that the actual roughness values were obtained from a Mays Ride Meter driven over the pavement sections at a standard speed. The pavement sections were approximately 0.2 mi (0.32 km) long. There are many different proprietary devices available which measure roughness in inches per mile. Most devices are typically calibrated over a set of standard sections, to permit inter-agency comparisons and to promote consistency. However, the different devices will not give the same reading over the same section of pavement for many reasons, including calibration differences and measurement differences. To better test the effectiveness of this roughness model, it would be necessary to develop relationships between roughness as measured by the CHLOE profilograph (which was used at the AASHO Road Test) and by the Mays Ride Meter.

Pumping Model

The PEARDARP pumping model could not be directly compared to field pumping measurements. This is because the PEARDARP pumping model calculates the volume of pumped material, the number of joints pumping, and the volume of undersealing necessary to fill the voids. In the field surveys of the projects in this study, the presence of pumping was noted and assigned severity levels based on how much pumping was observed throughout the section. Table 80 of volume VI provides a general comparison of field observed pumping severities and the various outputs of the PEARDARP pumping model. It is not known exactly what pumping volumes correspond with the various severity levels, but an examination of table 80 shows that different pumping volumes are quite often predicted for pavement sections that actually had no visible signs of pumping. However, this can partially be explained by the fact that visible evidence of pumping is related to the occurrence of the last rainfall. If a section is dry and not received any recent precipitation, the section may not exhibit signs of pumping, although it may be occurring. In other words, a pavement section can be experiencing pumping without visible indications of the distress.

Spalling Model

The results of the statistical analysis for the joint spalling model are shown in table 10 for all of the Phase I sections and for each environmental region. Again, the results of the statistical analysis indicate that the model is not able to satisfactorily predict the spalling for the sections included in this study.

The measured versus actual results for transverse joint spalling are presented in tables 81 through 85 of volume VI; these results are portrayed graphically in figures 32 through 36 of that volume. Typically, the model overpredicted transverse joint spalling for the analysis incorporating all Phase I sections. Further, it is noted that there were quite a few sections for which there was no measured spalling, but the predicted spalling ranged from 0 to 100 percent.

None of the data from any of the four climatic zones was particularly better than the others. Again, the model tended to overpredict transverse joint spalling for every environmental region.

A possible explanation for this large discrepancy in predicted versus actual spalling lies in an examination of the variables in the spalling model. The percent of spalled joints is shown to be a function of age and joint spacing. The occurrence of joint spalling in the actual sections seemed to be more closely related to a combination of nondurable aggregates and harsh climates. Transverse joints that were locked-up due to corrosion of the dowel bars also increased joint spalling. Spalling was found on pavements of all ages and joint spacing where material problems existed or the dowel bars had corroded and locked-up the joint. Similarly, the absence of the locked joints and materials problems, combined with good joint forming, sealing, and maintenance techniques, would help to provide much longer trouble-free performance at the joints than this model would predict.

Faulting Models

The PEARDARP faulting models predict faulting for both doweled and nondoweled pavements. Thus, in addition to considering faulting for all Phase I sections and for each environmental region, faulting was also evaluated for doweled and nondoweled pavement sections within each environmental region. However, it should be noted that the lack of doweled pavement sections in the dry-nonnfreeze environmental region prevented the evaluation of doweled and nondoweled sections in that region.

The results of the statistical analysis of the PEARDARP faulting model are given in table 10 for various data set combinations. The analysis indicates that the model does not adequately predict joint faulting for all of the Phase I sections considered together. Furthermore, the model is unable to adequately predict faulting in any environmental region for any type of load transfer method.

Table 86 in volume VI provides the comparison of measured versus predicted faulting for all Phase I sections considered together; figure 37 presents the results graphically. Generally speaking, the model appears to underpredict faulting, although there is a large range of scatter. The model predicted faulting in a range from approximately 0.02 in to 0.18 in (0.51 to 4.6 mm). The measured average faulting ranged from 0 in to 0.5 in (0 to 13 mm). With the exception of six sections at MN 1 with faulting over 0.3 in (7.6 mm), all of the measured faulting was under 0.22 in (5.6 mm). The MN 1 faulting values are 1984 pre-grinding data provided by the Minnesota Department of Transportation, and it is not certain that their measurement methods were similar to those used in this study.

A review of the predicted faulting by environmental region (tables 87, 90, 91, and 94 and figures 38, 41, 42 and 45 of volume VI) generally indicate that the

model is underpredicting joint faulting. The trends were slightly more balanced for the wet regions than for the dry regions.

An examination of the model pertaining to load transfer provides some interesting results (tables 88, 89, 92, 93, 95 and 96 and figures 39, 40, 43, 44, 46 and 47 of volume VI). It is observed that the faulting model severely underpredicts faulting for doweled pavement sections. The predicted faulting for nondoweled sections is more balanced, with the exception of the dry-freeze environmental region. A review of the functional form of the model reveals that the presence of dowels is not directly considered. Rather, for doweled pavements, the model runs the standard nondoweled equation and then multiplies this by a fudge factor to provide doweled pavement faulting. This fudge factor is a function *only* of age. Thus, the equation does not consider the diameter of the dowel bars, or any dowel characteristics for that matter. Therefore, a pavement section with an insufficient dowel bar diameter would have the same amount of faulting predicted as a similar section with an adequate dowel bar diameter.

Cracking Model

The PEARDARP cracking model was used to predict the quantity of transverse cracking on each of the pavement sections and this was compared to the actual measured cracking. Table 10 provides the summary of the statistical analysis of the PEARDARP cracking model. These results indicate that the model does not adequately predict slab cracking for the pavement sections included in this study. This finding holds true for each environmental region.

Table 97 of volume VI provides the comparison of measured versus predicted values for all of the Phase I sections, and figure 48 provides a graphical representation of that table. The majority of the *predicted* cracking fell into a very narrow band of between 320 and 420 lin ft/1000 ft², when there was actual cracking measured, and between 0 and 320 lin ft/1000 ft², when there was no actual cracking measured. This trend becomes more accentuated when the individual regions are considered (tables 98 through 101 and figures 49 through 52 of volume VI). In the dry-freeze region, all of the predicted cracking was between 380 and 420 lin ft/1000 ft², for actual cracking from 0 to almost 900 lin ft/1000 ft². This is about the same range of predicted values for the dry-nonfreeze and wet-nonfreeze regions. However, in the dry-nonfreeze regions there were sections with predicted cracking of up to 400 lin ft/1000 ft² that actually had none.

It is clear from the results that the cracking model is fairly insensitive to the inputs. The PEARDARP cracking model was based on a mechanistic analysis of concrete pavement slabs. The model predicts cracking as a damaged area per joint. The damaged area is a function of the number of nodes where strains in the slab would induce cracks and the area of influence of each node. The area of influence of each node was held constant at 4000 in² (2,580,640 mm²). An average crack length of 24 in (610 mm) in each influence area was assumed in order to obtain the total length of linear cracking. This is converted to linear cracks per

1000 ft². The functional form of the regression model dilutes the effect of the factors by taking the arctangent or logarithm of the values. These mathematical functions transform a wide range of values into a very narrow range of values. This may be the reason for the insensitivity of the model to the various inputs.

COPES

The COPES predictive models, for pumping, faulting, spalling, cracking, and PSR, includes a different model for each jointed pavement type. This allows for further breakdown of the data set within each environmental region. However, given the pavement sections within the study, this was not always possible. Specifically, there were no JRCP sections in the dry-nonfreeze environmental region and only one JRCP section in the wet-nonfreeze region, so that a breakout of the evaluation in those regions was not possible or practical.

Pumping Models

Unlike the PEARDARP pumping model, the COPES pumping model predicts the severity of pumping expected to occur within a pavement section, instead of the volume of pumping. This allows for a direct comparison of the actual pumping observed on the pavement sections included in this study. It should be noted that the actual pumping and the predicted pumping from the COPES pumping model are both based on visible signs of pumping. Therefore, sections that are experiencing pumping but do not display any visible evidence could not be appraised in the field surveys or in the development of the model.

The results of the statistical analysis for the COPES pumping model are displayed in table 11. The results generally indicate that the model is not able to adequately predict pumping for the sections included in the study. However, the analysis in the wet-nonfreeze environmental region shows that the model does adequately predict pumping for the pavement sections included in the study from this environmental region.

Summary tables and scattergrams for the different data sets are displayed in tables 102 through 110 and figures 53 through 61 of volume VI. An examination of the scattergram for the consideration of all Phase I sections shows predicted values both above and below the line of equality; this observation is also true for the analysis of the dry-freeze and wet-freeze environmental regions. However, when the dry-freeze and wet-freeze data sets were broken out by pavement type, it is observed that the model consistently *underpredicts* pumping for JRCP sections, whereas there is more scatter associated with the JPCP analysis.

In the wet-nonfreeze environmental zone, the model predicted that none of the sections would exhibit pumping. In actuality, only 2 sections exhibited pumping while the remaining 12 sections did not. Thus, as the results of the statistical analysis show, the model is able to predict pumping in the wet-nonfreeze climatic zone.

Table 11. Summary of the statistical analyses of the COPES prediction models.

Data Set	Number of Observations	t_{calc}	t_{table}^*	$t_{calc} > t_{table}$	Adequately Predict Performance?
PUMPING					
All Phase I	99	6.154	1.670	YES	NO
Dry-Freeze					
All Sections	20	4.498	1.729	YES	NO
JPCP	3	3.500	2.920	YES	NO
JRCP	17	4.243	1.746	YES	NO
Dry-Nonfreeze	17	1.951	1.746	YES	NO
Wet-Freeze					
All Sections	48	4.090	1.680	YES	NO
JPCP	22	4.125	1.721	YES	NO
JRCP	26	1.729	1.708	YES	NO
Wet-Nonfreeze	14	1.439	1.771	NO	YES
FAULTING					
All Phase I	99	4.181	1.670	YES	NO
Dry-Freeze					
All Sections	20	3.771	1.729	YES	NO
JPCP	3	2.910	2.920	NO	YES
JRCP	17	3.722	1.746	YES	NO
Dry-Nonfreeze	17	4.280	1.746	YES	NO
Wet-Freeze					
All Sections	48	8.532	1.680	YES	NO
JPCP	22	6.809	1.721	YES	NO
JRCP	26	5.459	1.708	YES	NO
Wet-Nonfreeze	14	5.421	1.771	YES	NO

Table 11. Summary of the statistical analyses of the COPES prediction models (continued).

Data Set	Number of Observations	t_{calc}	t_{table}^*	$t_{calc} > t_{table}$	Adequately Predict Performance?
JOINT DETERIORATION					
All Phase I	99	6.633	1.670	YES	NO
Dry-Freeze					
All Sections	20	4.521	1.729	YES	NO
JPCP	3	1.220	2.920	NO	YES
JRCP	17	4.654	1.746	YES	NO
Dry-Nonfreeze	17	2.219	1.746	YES	NO
Wet-Freeze					
All Sections	48	4.938	1.680	YES	NO
JPCP	22	2.741	1.721	YES	NO
JRCP	26	4.806	1.708	YES	NO
Wet-Nonfreeze	14	1.558	1.771	NO	YES
CRACKING					
All Phase I	99	7.307	1.670	YES	NO
Dry-Freeze					
All Sections	20	2.925	1.729	YES	NO
JPCP	3	3.792	2.920	YES	NO
JRCP	17	7.110	1.746	YES	NO
Dry-Nonfreeze	17	1.899	1.746	YES	NO
Wet-Freeze					
All Sections	48	3.691	1.680	YES	NO
JPCP	22	3.898	1.721	YES	NO
JRCP	26	3.651	1.708	YES	NO
Wet-Nonfreeze	14	5.080	1.771	YES	NO

Table 11. Summary of the statistical analyses of the COPES prediction models (continued).

Data Set	Number of Observations	t_{calc}	t_{table}^*	$t_{calc} > t_{table}$	Adequately Predict Performance?
PSR					
All Phase I	99	10.567	1.670	YES	NO
Dry-Freeze					
All Sections	20	4.782	1.729	YES	NO
JPCP	3	4.426	2.920	YES	NO
JRCP	17	4.534	1.746	YES	NO
Dry-Nonfreeze	17	5.833	1.746	YES	NO
Wet-Freeze					
All Sections	48	7.068	1.680	YES	NO
JPCP	22	3.514	1.721	YES	NO
JRCP	26	6.637	1.708	YES	NO
Wet-Nonfreeze	14	4.057	1.771	YES	NO

* t_{table} based on 90 percent confidence level.

An examination of the COPES model indicates that the model appears to include all important parameters with the exception of base and subbase type. It is believed that base type and depth of subbase are important factors in the development of pumping and should be included. In addition, the amount of thermal curling may influence pumping as it can create a void that accelerates pumping and subsequent faulting. Thermal curling is related to the temperature difference between the top and bottom of the slab and also the concrete thermal coefficient of expansion.

Faulting Models

The results of the statistical analysis performed on the COPES faulting models are provided in table 11. For the consideration of all of the Phase I sections and for the general analysis in each environmental region, the model is unable to adequately predict the actual faulting. However, within the dry-freeze zone, it is observed that the model can adequately predict the faulting of the JPCP sections included in the study. Tables 111 through 119 and figures 62 through 70 of volume VI provide comparisons of the actual and predicted faulting for various data sets. The following discussion pertains to the scattergrams for the given data set.

All Phase I Sections

Figure 62 shows a wide range of scatter about the line of equality. The outliers that were underpredicted are the nondoweled JRCP sections from Minnesota 1, whose faulting measurements were supplied by the Minnesota DOT; thus, their accuracy and consistency relative to the faulting measurements of the other data points is not known.

It is theorized by some researchers that transverse joint faulting on a new pavement begins immediately after construction and continues to develop quite rapidly for the first several years. Thereafter, the faulting rate levels off and faulting develops much more slowly. Many of the newer pavement sections may be in the "rapid faulting" stage and therefore, it is expected that the faulting of these sections would be difficult to predict.

Dry-Freeze Environmental Region

Figure 63 shows the overall graph of predicted versus actual results for the dry-freeze region, while figures 64 and 65 provide the scattergrams for the JPCP and JRCP sections, respectively. Again, the outliers in figure 63 and 65 are the nondoweled sections of Minnesota 1. It is not surprising that the COPES model did not predict these sections since the original model did not include nondoweled JRCP sections. Figure 64 shows a fairly good correlation for the JPCP model and this is confirmed by the results of the statistical analysis. However, it should be noted that there were only 3 JPCP sections included from the region which are too few to provide a true indication of the model's ability to predict faulting.

Dry-Nonfreeze Environmental Region

The overall graph of predicted versus actual results for the dry-nonfreeze region is shown in figure 66. The largest faulting predicted by the model is 0.07 in (1.8 mm), although the actual faulting was as high as 0.15 in (3.8 mm). The model appeared to do reasonably well on the sections from Arizona, but had problems with the California sections. This is an interesting phenomenon since the original COPES database did not include any sections from Arizona while containing many sections from California with designs similar to those included in this study.

Wet-Freeze Environmental Region

Figure 67 shows the overall graph of predicted versus actual results for the wet-freeze region. A large amount of scatter is observed, but the predicted values generally range between 0 and 0.14 in (3.6 mm), although there is one predicted value of 0.29 in (7.4 mm). This particular section was NJ 2, which contained stainless steel clad dowel bars and had sustained over 35 million 18-kip (80 kN) ESAL applications and was only exhibiting 0.06 in (1.5 mm) of faulting.

Figures 68 and 69 provide the scattergrams for the JPCP and JRCP sections, respectively. The model generally overpredicted faulting for the JPCP sections, although it severely underpredicted faulting for 2 JPCP sections on Michigan 1 which were constructed on ATB in a bathtub section. No clear trend emerges for the JRCP model.

Wet-Nonfreeze Environmental Region

The scattergram for the wet-nonfreeze region is shown in figure 70. It is observed that the model underpredicts faulting in this region. Faulting less than 0.02 in (0.05 mm) was predicted for nearly half of the sections, whereas the actual faulting ranged from 0.01 to 0.16 in (0.03 to 4.1 mm). Due to the zero freezing index for the nonfreeze regions, it is expected that the model would predict less faulting for the nonfreeze regions than for the freeze regions.

Joint Deterioration Models

Recall that joint deterioration was defined as the percentage of the transverse joints that were spalled. Since the output of the COPES joint deterioration models is number of spalled joints per mile, this was converted to percent of joints spalled for each section.

The summary of the statistical analysis for joint deterioration is shown in table 12. It is observed that there the model adequately predicts joint deterioration for sections in the study from two environmental regions: dry-freeze JPCP and wet-nonfreeze. However, for the other data sets, the model is unable to adequately predict joint deterioration for the sections included in the study.

Tables 120 through 128 and figures 71 through 79 of volume VI provide comparisons of the actual and predicted joint deterioration for various data sets. The following discussion pertains to the scattergrams for the given data set.

All Phase I Sections

Figure 71 shows a wide range of scatter about the line of equality. There appears to be a slight tendency to overpredict joint deterioration. Age, materials durability problems, and joint spacing (JRCP), all contribute greatly to the value of predicted joint deterioration. Since many of the pavement sections included in the study are relatively new, it would be expected that the model would underpredict joint deterioration rather than overpredict.

Dry-Freeze Environmental Region

Figure 72 shows the overall graph of predicted versus actual results for the dry-freeze region, while figures 73 and 74 provide the scattergrams for the JPCP and JRCP sections, respectively. Again, it appears that the model overpredicts joint deterioration. The reason for this may be due to the fact that low-severity "D" cracking was present on the Minnesota 1 sections. The model evidently predicts a significant amount of spalling because of the presence of "D" cracking, although in actuality it has not translated into a substantial amount of spalling. As was previously mentioned, the JPCP model adequately predicts spalling for the three pavement sections in this region.

Dry-Nonfreeze Environmental Region

The overall graph of predicted versus actual results for the dry-nonfreeze region is shown in figure 75. It appears from the figure that the model predicts fairly well, although the statistical analysis indicates that the model does not adequately predict joint deterioration. With the exception of the oldest section in Arizona, it is interesting that the range of predicted values falls nicely in line with the range of actual values.

Wet-Freeze Environmental Region

Figure 76 shows the overall graph of predicted versus actual results for the wet-freeze region. The model again tends to overpredict joint deterioration. As was the case for some of the Minnesota sections, several sections from Michigan exhibited "D" cracking which had not yet resulted in much joint spalling. However, because of the presence of "D" cracking, the model predicts a significant amount of spalling for those sections. The scattergrams for the JPCP and the JRCP models (figures 77 and 78) confirm that the model overpredicts values within this environmental region.

Wet-Nonfreeze Environmental Region

The scattergram for the wet-nonfreeze region is shown in figure 79. From an examination of the scattergram and from the *t*-test results, the model is observed to adequately predict spalling very well for the pavement sections included in the study from this region. In all but two cases, the model predicted the actual value or very close to it.

Cracking Models

The COPES cracking models predict total linear feet of cracking, including both transverse and longitudinal. This required the conversion and addition of the transverse and longitudinal cracking obtained in this study since it was grouped separately. The fact that the COPES cracking models do not distinguish between transverse and longitudinal cracking is a shortcoming of the model, since different mechanisms are responsible for the development of each type of cracking.

The COPES cracking model for JPCP includes cracking of all severity levels; the COPES cracking model for JRCP includes only deteriorated (medium- and high-severity) cracks. These guidelines were followed for the evaluation of the model. However, it is believed that for JRCP, *all* severity levels of longitudinal cracking should be included.

Because of the scale required to include the data from all of the sections, the comparison of predicted cracking to actual cracking may be difficult to interpret. The actual relationship is somewhat muted in these graphs, as the scales of the x-axis and y-axis are different on each graph in order to include all of the data points.

Table 11 provides the summary of the statistical analysis for the COPES cracking models. These results show that the models were unable to adequately predict cracking for any data set. Tables 129 through 137 and figures 80 through 88 of volume VI provide comparisons of the actual and predicted cracking for various data sets. The following discussion pertains to the scattergrams for the given data set.

All Phase I Sections

Figure 80 shows that the model overpredicted the total cracking occurring within the section; only 11 of the 99 sections were underpredicted. Please note that ONT 2 was not included on the graph, as it would have resulted in a distorted scale. This section, which had been subjected to over 35 million 18-kip (80 kN) ESAL applications, only exhibited 12 linear feet of cracking per mile, whereas the model predicted over 19,000 linear feet of cracking per mile. While other unsurveyed segments of this section displayed more cracking than 12 linear feet, the pavement design is providing outstanding performance for the heavy traffic loadings that it sustains.

Dry-Freeze Environmental Region

Figure 81 shows the overall graph of predicted versus actual results for the dry-freeze region. The model is observed to overpredict in all but one case. Figures 82 and 83 provide the scattergrams for the JPCP and JRCP sections, respectively. Again, the model is shown to consistently overpredict.

Dry-Nonfreeze Environmental Region

The overall graph of predicted versus actual results for the dry-nonfreeze region is shown in figure 84. In this region, the models are observed to underpredict the actual cracking. It is interesting to note from the figure that, for small amounts of cracking (say, less than 300 ft/mile), the model predicts the cracking with extraordinary accuracy. However, above the 300 ft/mile level, the accuracy of the model decreases.

Wet-Freeze Environmental Region

Figure 85 shows the overall graph of predicted versus actual results for the wet-freeze region. The model again predicts much more cracking than was actually observed. The scattergrams for the JPCP and the JRCP models (figures 86 and 87) show the same results. A partial explanation for the disparity in the JRCP analysis of this region is the good performance of several of the long-jointed JRCP sections. Most notably, New York and Michigan had long-jointed pavements constructed with epoxy-coated dowels and granular base courses which exhibited very little deteriorated transverse cracks. However, overall, the JRCP model appears to be more accurate than the JPCP model.

Wet-Nonfreeze Environmental Region

The scattergram for the wet-nonfreeze region is shown in figure 88. No clear trend emerges from an examination of this data. It is interesting to note that the model overpredicts cracking for the thicker slabs (11 and 13 in [279 and 330 mm]) in the region.

The data suggests that the factors contributing to cracking on the pavements in these sections are not well taken into account in the COPES models. These pavements were typically younger and less heavily trafficked than the COPES database pavements, which is probably a very important factor in explaining the difference.

The conclusions in volume I indicate that thicker slabs reduce cracking and the COPES cracking models follow that trend. However, the cracking is still overpredicted for the thicker slabs. The exception to this is the 15 in (381 mm) slabs in Ohio, for which COPES predicted no cracking.

Present Serviceability Rating (PSR) Models

The COPES models for PSR are based on a panel rating of serviceability of the pavement sections included in that study's database. It is a measure of the effects of distress and other factors, such as joint spacing, on pavement rideability. These results are directly comparable to the PSR values obtained from the actual field surveys in this project.

Table 11 provides the summary of the statistical analysis for the COPES PSR models. It is observed that the models are unable to adequately predict PSR for the sections included in the study. Tables 138 through 146 and figures 89 through 97 of volume VI provide comparisons of the actual and predicted PSR for various data sets. The following discussion pertains to the scattergrams for the given data set.

All Phase I Sections

Figure 89 shows a wide range of scatter for the predicted versus actual results. It should be noted that the model provides reasonable results at the higher end of the scale; that is, unlike the PEARDARP equation, there were no PSR values greater than 4.6. However, there were three sections with predicted PSR values less than 2, although their actual PSR was much higher: MN 1-4, MN 1-6, and NC 1-7. These sections all shared a common element: they were all 8-in (203 mm) slabs under relatively heavy traffic. Thus, the model is evidently sensitive to the combination of slab thickness and high traffic levels. Unfortunately, the Minnesota sections had been diamond ground which distorts the relative comparisons.

On the other hand, the highest PSR predicted was for the thicker slab section at California 1 under relatively high traffic levels. In that case, the combination of slab thickness and mild climate contributed to a high rating. There were several sections with very high actual PSR values that the models did not predict. These were found on new sections less than 3 years old and with light traffic.

Dry-Freeze Environmental Region

Figure 90 shows the overall graph of predicted versus actual results for the dry-freeze region. In this region, the model is observed to underpredict for most cases. The predicted PSR was in a relatively small range of 3.8 to 4.5, while the actual PSR's ranged from 2.5 to 4.2. Figures 91 and 92 provide the scattergrams for the JPCP and JRCP sections, respectively. As discussed above, the low predicted PSR values were for the 8-in (203 mm) slabs at Minnesota, which, to further complicate matters, had also been diamond ground. From the form of the model, it is observed that freezing index is an input. The high freezing indices for the Minnesota sections may have contributed to the model underpredicting in this region by extrapolating the model out of its inference space.

Dry-Nonfreeze Environmental Region

The overall graph of predicted versus actual results for the dry-nonfreeze region is shown in figure 93. It is observed that, in this region, the model typically overpredicts the actual PSR values. The model overestimated PSR values for the thick slab designs and mild climates of Arizona and California. This may be due to the model assuming that a thicker slab results in a smoother-riding pavement; often there are problems associated with the construction of thick slabs which could result in roughness problems.

Wet-Freeze Environmental Region

Figure 94 shows the overall graph of predicted versus actual results for the wet-freeze region. Similar to the trends in the dry-nonfreeze climatic region, the model again predicts higher PSR values than were actually measured. The scattergrams for the JPCP and the JRCP models (figures 95 and 96) show the same results. It is believed that this may be partially attributed to the freezing index for the sections in this region. However, with the exception of two JPCP over ATB sections at Michigan, the JPCP PSR model appears to provide reasonable results. The JRCP model has difficulty in predicting the PSR of several of the older sections, particularly the NJ 2 section and the MI 4 sections. One interesting feature of the PSR models in this region is that it appears to predict a PSR of about $4.0, \pm 0.5$ for almost all of the pavement sections. This effect is most pronounced for the JPCP model.

Wet-Nonfreeze Environmental Region

The scattergram for the wet-nonfreeze region is shown in figure 97. With the exception of NC 1-7, the model consistently overpredicts. Again, the NC 1-7 section contained an 8-in (203 mm) slab. For the thicker slabs in this region, the model appears to do reasonably well. In this region, similar to the wet-freeze region, the PSR models appears to predict a PSR of about $4.0, \pm 0.5$ for almost all of the pavement sections.

PFAULT Faulting Models

There were two PFAULT models developed for faulting prediction, one for doweled transverse joints and the other for nondoweled transverse joints. There are some mechanistic terms included in the model. Each of the models was considered by climatic zone.

Table 12 provides the summary of the statistical analysis for the PFAULT faulting model. The data shows that the model was unable to adequately predict faulting for all data sets but one (doweled wet-nonfreeze). Tables 147 through 157 and figures 98 through 108 of volume VI provide comparisons of the actual and predicted faulting for various data sets. The following discussion pertains to the scattergrams for the given data set.

Table 12. Summary of the statistical analyses of the PFAULT faulting prediction models.

Data Set	Number of Observations	t_{calc}	t_{table}^*	$t_{calc} > t_{table}$	Adequately Predict Performance?
All Phase I	99	9.327	1.670	YES	NO
Dry-Freeze					
All Sections	20	4.986	1.729	YES	NO
Doweled	14	9.885	1.771	YES	NO
Nondoweled	6	3.836	2.015	YES	NO
Dry-Nonfreeze	17	3.569	1.746	YES	NO
Wet-Freeze					
All Sections	48	6.523	1.680	YES	NO
Doweled	28	3.997	1.703	YES	NO
Nondoweled	20	6.312	1.729	YES	NO
Wet-Nonfreeze					
All Sections	14	3.775	1.771	YES	NO
Doweled	6	1.281	2.015	NO	YES
Nondoweled	8	4.631	1.895	YES	NO

* t_{table} based on 90 percent confidence level.

All Phase I Sections

Figure 98 provides the scattergram considering all Phase I sections. There does not appear to be any clear trend in the way that the model predicts. As noted in the faulting analyses of PEARDARP and COPEs, the nondoweled sections in Minnesota had very large faulting values which may not be representative. These are several of the outliers that the model does not predict very well. It is observed that there are several projects for which PFAULT predicts little faulting. These projects were typically newer sections with very little traffic constructed on stabilized base courses and containing dowel bars. The COPEs database may not have included several of the designs that were included in the current study. For example, there were not any nondoweled JPCP sections in the wet-freeze zone in the COPEs study, so the model would not be expected to adequately predict faulting for this design.

Dry-Freeze Environmental Region

Figure 99 shows the overall graph of predicted versus actual results for the dry-freeze region. Again, there is no clear trend in the way that the model predicts. At lower faulting values, the model overpredicts whereas at higher faulting values, the model underpredicts.

The results of the comparison in the dry-freeze zone made for the doweled transverse joints model are shown in figure 100. It is observed that the model generally overpredicts the faulting occurring on these sections. All of the sections in this analysis are part of the MN 1 sections at Rothsay.

In every case, the model for nondoweled transverse joints underpredicted faulting in the dry-freeze region, as seen in figure 101. However, there were only six sections in the dry-freeze region which did not contain dowels; these were the located on I-94 near Rothsay. These sections experienced a substantial amount of faulting and required diamond grinding after 14 years of service. Pre-grinding fault measurements were provided by the Minnesota Department of Transportation.

Dry-Nonfreeze Environmental Region

The overall graph of predicted versus actual results for the dry-nonfreeze region is shown in figure 102. On the whole, the model appeared to underpredict faulting more in this region, although there is a wide amount of scatter. This model was fairly good, however, if a certain amount of measured faulting is considered to be insignificant. For example, if 0.02 in (0.5 mm) is considered a trivial amount and a band of ± 0.02 in (0.5 mm) is drawn on either side of the line of equality shown in figure 102, almost 60 percent of the data falls within this zone.

Wet-Freeze Environmental Region

Figure 103 shows the overall graph of predicted versus actual results for the wet-freeze region; figures 104 and 105 provide the predicted versus actual results by doweled and nondoweled sections. Again, there is a wide range of scatter about the line of equality. An examination of table 152 indicates that, even within a project, the predicted faulting can vary tremendously depending upon design conditions. Dowel bars, stabilized bases, and tied shoulders all appear to influence the amount of predicted faulting. The model is evidently able to account for the changes in the experimental design that were part of these sections.

As with the overall scattergram for the wet-freeze region (figure 103), the doweled and nondoweled scattergrams for the wet-freeze region (figures 104 and 105) show a lot of scatter about the line of equality. No clear trends emerge as to how the model is able to predict.

Wet-Nonfreeze Environmental Region

The scattergram for the wet-nonfreeze region is shown in figure 106. As was with the predicted faulting in the other regions, there is a lot of scatter about the line of equality. The breakdown by load transfer method within this region is given in figure 107 and 108. For the doweled sections, the model is observed to predict faulting extremely well. In fact, the model passes the *t*-test for faulting of doweled pavements in this area. However, it should be noted that the data set is fairly small ($n = 6$). The faulting for the nondoweled sections ranged from 0.05 in to 0.22 in (1.3 to 5.6 mm). The nondoweled predicted faulting ranged from about 0.13 in to 0.16 in.

5. SUMMARY

This chapter has documented an evaluation of the adequacy of several concrete pavement prediction models. In general, these models do not adequately predict the distress (faulting, cracking, joint deterioration, pumping), serviceability or roughness measured on the pavements included in the study. Therefore, it is clear that improved prediction models are needed for a variety of pavement analysis, design, and management purposes.

Throughout the chapter, potential reasons were offered in an effort to explain why specific models were not able to adequately predict performance. However, there are several *general* reasons which may have influenced the models' ability to predict performance that should also be mentioned.

- The COPES traffic data was based on W-4 truck factors which have been determined to be as much as 45 percent low for Interstate-type highways. Thus, in general, the results show an overprediction of the pavement performance for the sections in the current study (which were supplemented by WIM data).

- There were many combinations of design variables in the current database which did not exist at the AASHTO Road Test or in the COPES database. Since all of the models are empirical to some extent, the models were not able to adequately predict these different conditions (e.g., permeable bases, widened lanes, tied shoulders, etc.).
- Several of the projects in the current database exhibited distresses that were the result of construction-related problems (late or inadequate depth of sawing, omission of "whitewashing" of ATB, poor consolidation of concrete at the joints, etc.). Where the distress was known to be a construction-related problem, these were excluded from the database for model development. Prediction models can never be expected to account for distress resulting from poor construction practices.

CHAPTER 4 CASE STUDIES

1. INTRODUCTION

There are a number of different design methods and analysis programs available for the design and evaluation of concrete pavements. These programs assist in the determination of concrete pavement responses to environmental and traffic loading, which ultimately can be used in design. A thorough description of some of the more prominent models, including a discussion of their capabilities and limitations and a sensitivity analysis, is presented in volume VI, "*Synthesis of Concrete Pavement Design Methods and Analysis Models.*"

Based on the results of the analysis presented in volume VI, five specific types of models were selected:

1. A climatic model.
2. A drainage characteristics model.
3. Structural analysis models.
4. A design method.
5. Shoulder analysis and design models.

One model was chosen from each category for further investigation. This chapter summarizes the results of that investigation.

The models were evaluated using data from the major experimental project located in each of the four climatic zones. The experimental projects are MN 1, I-94 Rothsay (dry-freeze), CA 1, I-5 Tracy (dry-nonfreeze), MI 1, US 10 Clare (wet-freeze), and NC 1, I-95 Rocky Mount (wet-nonfreeze). More information on these projects is provided in section 2.

Several structural analysis programs were evaluated for use in the case studies, with the ILLISLAB structural analysis program initially recommended. However, the relative merits of the ILLISLAB program and the JSLAB program are compared for the sections in Clare, MI and the results of this analysis are presented in section 5. The selected structural analysis model was evaluated using all of the sections in Minnesota, California, Michigan, and North Carolina.

A brief description of the capabilities of the specific analysis models and design procedures selected for detailed evaluation is given below.

Climatic Model

The CMS (Climatic-Materials-Structural Model) was initially developed for the determination of the effect of climate and moisture on the structural properties on multilayered flexible pavement systems.^(11,12) Because the model is based on fundamental principles of heat transfer, moisture movement, and material response to repeated loading, the theories can be applied to rigid pavements as well.

Several of the input variables were modified based on the recommendations of the developer of the CMS model. These are discussed in section 3.

This program fully models the effect of the environment on the pavement structure in terms of:

1. Temperature changes in the slab.
2. The effect of moisture (and temperature) on the paving layers in terms of stiffness of the layers.
3. Frost penetration within the paving layers.

The thermal gradient capabilities of this program were used extensively to determine the seasonal variation in thermal gradient. The thermal gradient, in turn, was used for the determination of stresses induced by temperature differences between the top and bottom of the slab.

Drainage Model

The Liu-Lytton drainage analysis model, calculates the drainage capabilities of the pavement system, the average stiffness of the paving layers (both wet and dry), and the probabilities of wet and dry conditions.^(13,14) The program accomplishes this with inputs on the drainability of the paving layers, the condition of the joints and cracks in terms of moisture infiltration, information on the design cross section, and climatic information about the area.

Structural Analysis Models

ILLISLAB is a finite element, structural analysis program for rigid pavements which was developed at the University of Illinois in 1977.^(15,16,17) Since that time the program has gone through numerous technical changes, revisions, and refinements. Finite element analysis methods are used to model the pavement system and analyze the system's responses to loads. Under this study, ILLISLAB was used to calculate the stresses and deflections of the pavement system. This program also models the development of thermal stresses due to thermal gradients within the slab. Thermal stresses and stresses induced by wheel loading play a major role in the structural deterioration of concrete slabs.

JSLAB is a structural analysis program that was based on an early version of ILLISLAB.^(18,19) It was selected for comparison with ILLISLAB because of its widespread use and since the relative merits of either program have not been clearly illustrated to date. As discussed in section 4, JSLAB was not chosen for the future analyses.

The PMARP program is a finite element program which was also based on an early version of ILLISLAB.^(20,21,22,23) PMARP and its sister program PEARDARP (which, in combination, are frequently referred to as the Purdue pumping models), model the pumping action of jointed concrete pavements. PMARP can be used to

calculate the stresses and deflections in jointed pavements, to provide an indication of the pumping potential of various pavement designs, and to model the fatigue-related cracking in rigid slabs.^(3,4,5) The PEARDARP program contains a number of prediction models that have already been discussed in detail in chapter 3.

Design Method

A program which can be used to evaluate rigid pavement designs or to design a rigid pavement structure is ICP-1.^(2,24) This program performs a detailed analysis of the fatigue characteristics associated with a particular design. The fatigue characteristics are evaluated in this program in terms of load, load placement, and the effect of thermal stresses. A separate analysis is also performed considering serviceability as a failure mode.

Shoulder Analysis and Design

The JCS-1 program can be used to design or to evaluate the design of a tied concrete shoulder.⁽²⁵⁾ Using the mainline pavement axle load distribution, a fatigue analysis is performed for the shoulder considering encroaching and parked traffic.

The BERM program can be used to design or to evaluate the design of an asphalt concrete or tied concrete shoulders.⁽²⁶⁾ The materials properties of the shoulder layers are used to determine the shoulder's fatigue properties and the expected life, in terms of encroaching or parked equivalent axle loads, of the shoulder. Under this study, the use of the BERM program is limited to the analysis of asphalt concrete shoulders.

2. PRESENTATION OF SECTIONS FOR CASE STUDIES

The various design methods and analysis procedures were evaluated using performance data from four experimental projects totaling 33 pavement sections. A brief description of these sections is given below.

Minnesota 1

The experimental project at I-94 near Rothsay, Minnesota was constructed in 1970 to evaluate the effect of base type, slab thickness and load transfer on concrete pavement performance. The variables included three different base types, 8- and 9-in (203 and 229 mm) slabs, and doweled and nondoweled joints. This is shown in the full factorial design matrix in the upper part of figure 7. Another section, MN 5, representing Minnesota's concrete pavement design of the 1960's, is also included in the study. This pavement section, located on I-94 in close proximity to the experimental sections and of similar design and age, is included to evaluate the effect of joint spacing.

		8 in Slab		9 in Slab	
		No Load Transfer	Load Transfer	No Load Transfer	Load Transfer
JRCP	6 in AGG Base	MN 1-3	MN 1-4	MN 1-1	MN 1-2
27 ft Skewed Joints	5 in ATB Base	MN 1-5	MN 1-6	MN 1-7	MN 1-8
	5 in CTB Base	MN 1-11	MN 1-12	MN 1-9	MN 1-10
JRCP 40 ft Joints	6 in AGG Base				MN 5

Dowel diameter = 1 in
Shoulder Type = AC
Subgrade = AASHTO A-6

Figure 7. Experimental design matrix for Minnesota 1.

Common to all of the designs is a JRCPC slab and an A-6 subgrade. Sections 1-1, 1-3, 1-9 and 1-11 had tied and doweled concrete shoulders added in 1984, while the outer lane of the nondoweled sections was diamond ground. The two-way ADT was estimated to be 5000 vehicles per day, including 21 percent trucks in 1987. Through 1987, it is estimated that the outer lanes of these sections have accumulated approximately 5.5 million 18-kip (80 kN) Equivalent Single-Axle Load (ESAL) applications.

California 1

This set of experimental sections was constructed on I-5 near Tracy, California, in 1971. Four different designs were constructed to study the effect of slab thickness, joint spacing, and base type (see figure 8). Additionally, one section was constructed with high-strength concrete.

All of the sections had JPCPC slabs and nondoweled, skewed and nonsealed transverse joints. The longitudinal joint was not tied and both lanes sloped toward the outer shoulder. The subgrade soils ranged from an AASHTO A-1-a to an A-2-4. The ADT in 1987 was 12,000 vehicles per day, including 19 percent trucks. Through 1987, the accumulated 18-kip (80 kN) ESAL applications for the outer lanes was estimated to be 7.6 million.

Michigan 1

An experimental project was constructed on U.S. 10 at Clare, MI in 1975. It includes the following variables: jointed plain and jointed reinforced concrete pavements 9 in (229 mm) thick; random joint spacing and long joint spacing; three different base types; skewed and non-skewed joints; doweled and nondoweled sections; and drained and non-drained sections. The drains were actually French drains retrofitted in 1981, but they still allow for an evaluation of drainage.

The subgrade for all sections was A-2-4. The average daily traffic on this section in 1987 was 5100 vehicles per day, with 8 percent trucks. The accumulated 18-kip (80 kN) load applications for the outer lanes of these sections was estimated to be 0.9 million (through 1987). All of the sections had full-depth AC shoulders, resulting in bathtub conditions.

Twenty-five sections were constructed, representing triplicate sections of 8 different designs. The selected sections are shown in the design matrix in figure 9. This design matrix represents an unbalanced experimental layout, in which only the effect of drainage is isolated. However, comparisons can be made between different design types.

North Carolina 1

Experimental pavement sections were constructed on I-95 near Rocky Mount, North Carolina, in 1967. The design matrix is shown in figure 10. Eight sections

		J P C P Skewed, Nondoweled		
		12-13-19-18 ft Jts	11.4 in PCC	5-8-11-7 ft Jts 8.4 in PCC
Normal Strength Concrete	CTB 5.4 in	CA 1-3	CA 1-5	CA 1-1
Concrete	LCB 5.4 in	CA 1-7		
High Strength Concrete	LCB 5.4 in	CA 1-9		

Subbase = 24 in gravel
Shoulder Type = AC
Subgrade Type = A-1-a to A-2-4
Nonsealed Joints

Figure 8. Experimental design matrix for California 1.

		Drained		Nondrained	
		Skewed Joints	Nonskewed Joints	Skewed Joints	Nonskewed Joints
		No Load Transfer	Load Transfer	No Load Transfer	Load Transfer
12-13-17-16 ft Joints 9 in JPCP	AGG 4 in		MI 1-7a		MI 1-7b
12-13-19-18 ft Joints 9 in JPCP	PATB 4 in	MI 1-4a			
12-13-19-18 ft Joints 9 in JPCP	ATB 4 in	MI 1-10a		MI 1-10b MI 1-25	
71.2 ft Joints 9 in JRCP	AGG		MI 1-1a		MI 1-1b

Subbase = 10 in sand
Shoulder Type = Full-depth AC
Dowel Bars = 1.25 in epoxy-coated

Edgedrains constructed initially. All other sections retrofitted with French (vertical drains) in 1981.

Figure 9. Experimental design matrix for Michigan 1.

		JPCP 30 ft Joints			JRCP 60 ft Joints
		Skewed Joints	Perpendicular Joints		Perpendicular Joints
		No Load Transfer	Load Transfer	No Load Transfer	Load Transfer
8 in	AGG 4 in				NC 1-7
9 in Slab	AGG 4 in	NC 1-1	NC 1-4	NC 1-8	
	Soil Cement 6 in		NC 1-2	NC 1-3	
	CTB 4 in			NC 1-5	
	ATB 4 in			NC 1-6	

Subgrade = AASHTO A-2-4 to A-4
Shoulder = AC

Figure 10. Experimental design matrix for North Carolina 1.

were constructed and design variables in the project include base type, jointed reinforced and jointed plain concrete pavements, joint spacing, slab thickness, skewed and nonskewed joints, and doweled and nondoweled joints.

The subgrade for the sections ranged from an A-2-4 to an A-4. The average daily traffic on this section in 1987 was 19,100 vehicles per day, with 9 percent trucks. The accumulated 18-kip (80 kN) load applications for the outer lanes of these sections was estimated to be 9.1 million (through 1987).

3. EVALUATION OF THE CMS PROGRAM

Introduction

The Climatic-Materials-Structural (CMS) program was developed to model the influence of climate on the behavior of pavement systems. Using the climatic and materials information from the region of a given pavement section, time-dependent temperature profiles, moisture profiles, and structural parameters of the pavement system are calculated. The program was originally developed to model flexible pavements, although the basic theoretical principles also apply to rigid pavements. The input variables pertaining to the portland cement concrete material were determined by the developer to enable the program to be used on rigid pavement systems; these are listed in table 13. The other required input variables are a function of the specific materials used for the base and subbase, subgrade conditions, and environmental factors.

The accurate modeling of the effects of moisture and temperature on paving layers is important in the design of a pavement system. The program was developed to be used as an integral step in the design process as shown in figure 11. Using site-specific climatic data and detailed information about the paving materials, the program generates materials properties and temperature and moisture profiles over time. These outputs are, in turn, used as inputs to structural analysis models, fatigue analysis models, and predictive models which aid the engineer in the design of the pavement system. Through accurate modeling of effect of moisture and temperature on the paving layers, a more realistic pavement design can be achieved.

Brief Technical Description

The CMS program contains three discrete models: a temperature model, a moisture model, and a material stiffness model. A detailed examination of each of these models is presented in reference 11. A brief summary of the three models is presented below:

1. The effect of temperature on the pavement system is modeled through the use of a one-dimensional, forward-finite difference heat transfer model. This heat transfer model was developed to evaluate the frost action and temperature distribution in multilayered pavement systems.

Table 13. CMS inputs for use with concrete pavements.

<u>Variable</u>	<u>Concrete Input</u>
Thermal conductivity, btu/hr-ft-°F	
dry	0.54
10 % moisture	0.70
wet	1.0
Heat capacity, BTU/lb-°F	0.23 (0.20-0.25)
Air content of surface, %	4.0
Short-wave absorptivity	0.65
Emissivity factor	0.65
Material Code	1
Penetration value	60.0
Poisson's ratio	0.15
Ring and Ball value	170.0
Stiffness value, kg/cm ²	PCC stiffness
Gravimetric Water Content (percent of weight of solids)	3.0

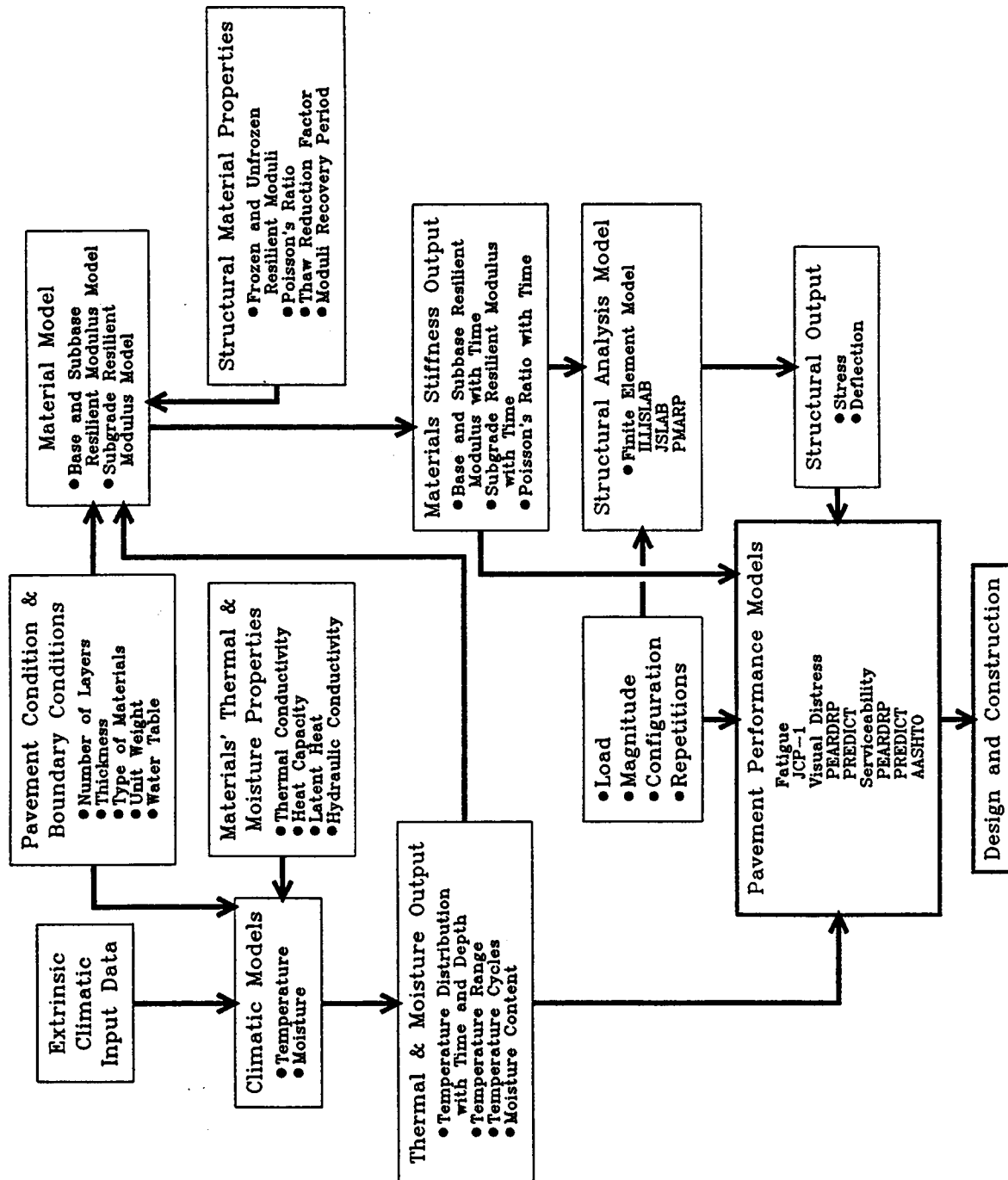


Figure 11. Use of CMS in the design process.

2. The moisture model, used to predict moisture movements through soils subject to isothermal conditions, is based on a finite-difference solution to the cases of 1- and 2-dimensional moisture movements. The model is capable of characterizing the transient moisture conditions in subgrade soil for a wide range of boundary conditions.
3. The properties of the granular materials are modeled through the use of the resilient modulus. The resilient modulus of the granular materials will change with varying moisture and temperature (frozen, unfrozen, or thaw-recovery) conditions. Based on work by many researchers, regression equations were developed to determine the material's properties as a function of temperature and moisture conditions.^(27,28,29)

The accuracy of the CMS program output is highly dependent on the quality of the input data. It is extremely important that the boundary conditions, climatic conditions, and materials properties accurately represent the system to be analyzed. The theoretical validity of the individual models comprising the CMS model have been demonstrated, although the validity of the interaction of the models has not been proven.⁽¹¹⁾ This validation would require the instrumentation and long-term monitoring of pavement sections to compare the outputs from the CMS program to the actual field-measured values.

Analysis of Results

The CMS program was executed for one experimental project in each of the four environmental zones. Due to the voluminous program outputs and the proximity of the sections within the experimental projects, specific sections were chosen for analysis within each project. The sections were selected based on the base and subbase types. The results of each analysis will be presented on a project by project basis. The sections which were chosen and the specific analyses performed on each are shown in table 14.

Rothsay, Minnesota

The CMS program was executed twice using site-specific climatic data to analyze the temperature differential through the portland cement concrete slab. First, a rigorous analysis was performed for the week of July 15 through July 21, 1987. In this analysis, the temperature profiles through the depth of the 9 in (229 mm) slab were calculated (via the CMS program) at 12 a.m., 4 a.m., 8 a.m., 12 p.m., 4 p.m., and 8 p.m.. Secondly, the program was executed for the entire month of June to examine the fluctuation in thermal gradient at 6 a.m. and 3 p.m.

The average thermal gradient is defined as shown in equation 25 below.

$$g = [\text{TEMP}_{\text{top}} - \text{TEMP}_{\text{bottom}}] / \text{THICK} \quad (25)$$

where:

g = average thermal gradient, °F/in
 $TEMP_{top}$ = temperature at the top of the slab, °F
 $TEMP_{bottom}$ = temperature at the bottom of the slab, °F
 $THICK$ = thickness of the slab, in

Table 14. Specific sections and analyses performed using the CMS program.

Section ID	Environmental Region	Base Type	Subbase Type	Specific Analysis
MN 1-1	Dry-Freeze	AGG	NONE	<u>Thermal analysis</u> for June 1987. <u>Materials stiffness analysis</u> for the frozen, thaw-recovery, and unfrozen periods.
CA 1-1	Dry-Nonfreeze	CTB	24 in AGG	<u>Thermal analysis</u> for the entire year 1987.
MI 1-10a	Wet-Freeze	ATB	10 in SAND	<u>Thermal analysis</u> for the months of January, April, June, August, and December, 1987. <u>Moisture analysis</u> for April 1987.
NC 1-1	Wet-Nonfreeze	AGG	NONE	<u>Thermal analysis</u> for July 1987.

A positive gradient indicates the top of the slab is warmer than the bottom which normally occurs during the daytime. A negative gradient indicates that the bottom of the slab is warmer than the top of the slab. The negative gradient condition typically occurs during the cooler hours of the evening. The effect of the thermal gradient on the development of stresses in concrete pavements is discussed in section 5.

Figure 12 shows typical results for July 15, 1987 using the first analysis approach. The temperature profile through the depth of the 9 in (229 mm) slab is plotted for the specified times of the day. For July 15, 1987 the largest thermal gradient ($g = [74.5 - 51]/9 = 2.61$ °F/in [1.45 °C/mm]) occurred at 4 p.m. and the smallest thermal gradient ($g = 0.37$ °F/in [0.21 °C/mm]) at 4 a.m. The top of the slab was never cooler than the bottom of the slab during entire day of July 15, 1987; therefore, a negative thermal gradient was not present that day. This may be due to the high intensity of the solar radiation during this period of the year in conjunction with the minimal cooling during the nighttime. The difference between the maximum and minimum ambient temperature for July 15 was 14 °F (7.8 °C) which is a relatively small change in temperature. This will also have an effect on the thermal gradient through the slab. Table 15 presents a summary of the thermal gradients for all of the times under analysis. For the chosen analysis period, the maximum positive thermal gradient always occurs at 4 p.m. and, if the climatic conditions are appropriate for the development of a negative thermal gradient, the maximum negative gradient occurs at 4 a.m.

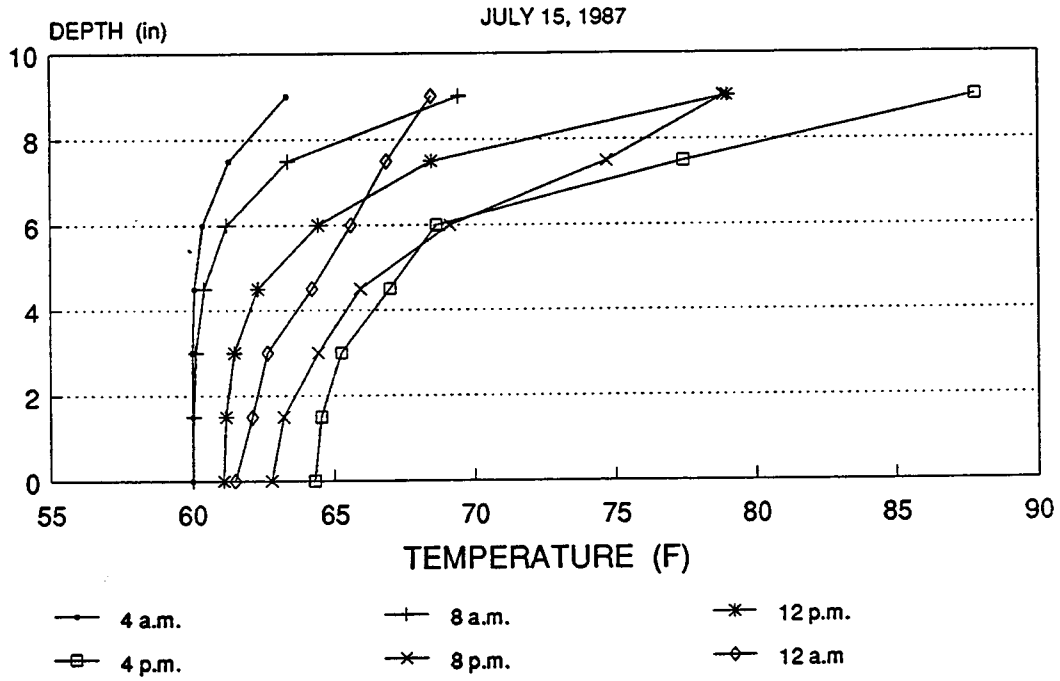
Table 15. Summary of thermal gradients at specified times for MN 1-1 for July 15 through July 21, 1987.

T H E R M A L G R A D I E N T, ° F / i n

Date	12 a.m.	4 a.m.	8 a.m.	12 p.m.	4 p.m.	8 p.m.
7/15/87	0.56	0.37	1.05	2.10	2.61	2.01
7/16/87	0.45	1.08	1.44	2.29	3.67	1.89
7/17/87	0.13	0.95	1.29	2.12	2.48	1.78
7/18/87	-0.23	-0.76	0.30	1.93	2.30	1.65
7/19/87	-0.31	-0.79	0.13	2.09	2.51	1.82
7/20/87	-0.22	-0.82	0.25	2.00	2.39	1.69
7/21/87	-0.29	-0.87	0.70	1.85	2.25	1.72

Figure 13 shows the thermal gradient at 6 a.m. as it varies throughout the month of June for MN 1-1. The thermal gradient at 6 a.m. is positive for the first part of the month which may be due to high intensity solar radiation during this period. The change in temperature between the daytime and nighttime hours was relatively small (14 °F [7.8 °C]) for the period of positive thermal gradient (as compared to about 25 °F [13.9 °C] for the period of negative thermal gradient). Therefore, since the air temperature does not decrease as much, the temperature of the surface of the pavement will not decrease either; that is, the pavement surface does not cool as quickly because the air temperature is warmer. The 6 a.m. gradient is negative during the last weeks of the month, as expected in the early morning hours. Since the bottom of the slab retains heat from the previous day, the slab surface is expected to be cooler during the morning hours, thus causing a negative thermal gradient.

ROTHSAY, MINNESOTA TEMPERATURE VS. DEPTH



Temperature Change = 14°F

Figure 12. Temperature profile versus depth through the slab on July 15, 1987, Rothsay, Minnesota.

ROTHSAY, MINNESOTA
GRADIENT VS. DAY

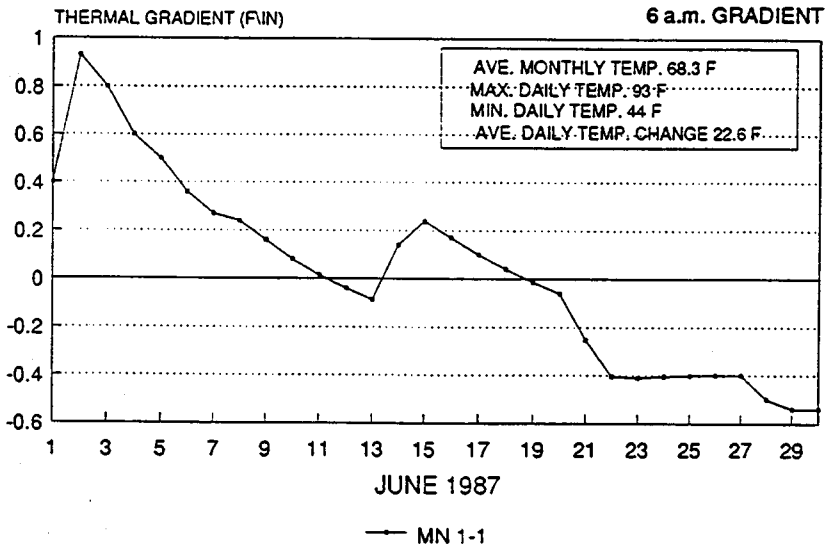


Figure 13. Change in 6 a.m. thermal gradient in June 1987, Rothsay, Minnesota.

ROTHSAY, MINNESOTA
GRADIENT VS. DAY

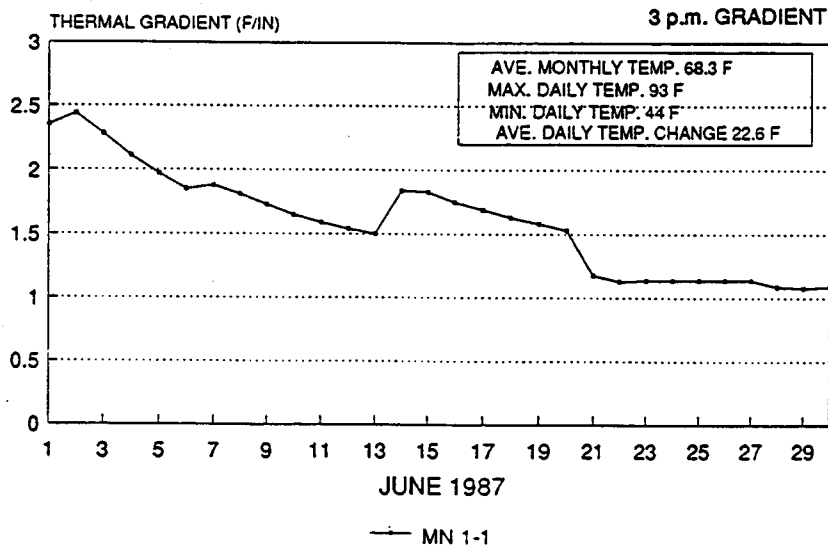


Figure 14. Change in 3 p.m. thermal gradient in June 1987, Rothsay, Minnesota.

The gradient at 3 p.m. for month of June is shown in figure 14. The thermal gradient is positive as is expected during the hot hours of the day. The sun warms the surface of the pavement rapidly while the bottom of the slab is still cool. Higher thermal gradients are calculated for the early portion of the month which may be due to the intensity of the solar radiation at the time due to lack of cloud cover. The period of positive morning thermal gradient corresponds with this same period of high negative daytime thermal gradient, supporting the theory that the higher temperatures and intense solar radiation contribute to the development of a positive thermal gradient.

In executing the CMS program and specifying the materials stiffness model, the program was terminated prematurely due to an execution error. The file that was used was identical to a file which executed for the analysis of the heat-transfer model with the exception of the specification of the stiffness routine in lieu of the heat-transfer routine. However, the equations for the analysis of the materials stiffness are straightforward and an approximation of the frozen, unfrozen, and thaw-recovery can be estimated manually as described on page 84. It is important to note that the specific conditions present at a given depth of the system cannot be evaluated manually. An estimate of the stiffness of the material in the three temperature conditions is estimated, however, whether these conditions are present at a given day of the year cannot be estimated without use of the program. The program assumes that the granular base and subbase materials are not influenced by the effects of frost in the same way that fine-grained soils are affected. The base and subbase courses are treated in the program as explained in reference 11:

The resilient modulus of the base and subbase materials do not vary throughout the year to the extent that the fine-grained soils do. For prediction of the resilient modulus the CMS program categorizes the course grained materials in one of two states; frozen or unfrozen [standard]. Therefore, for the base and subbase materials, including the stabilized materials, the user must input the values for the frozen and unfrozen resilient modulus. The CMS program will then select the appropriate value for the material depending on the location of the layer (which node in the system) in the pavement structure and the climatic conditions.

The stiffness of fine-grained soils is greatly increased when the soil is in the frozen state. However, during the thaw-recovery period, the stiffness of the material is drastically reduced from its unfrozen (standard) state. The CMS program uses the following equations to estimate the *unfrozen* resilient modulus based on volumetric moisture content.

For $\gamma_d \leq 100$ pcf (1602 kg/m³):

$$E_{Ri} = 27.06 - 0.526 * \Theta \quad (26)$$

For $\gamma_d > 100$ pcf (1602 kg/m³):

$$E_{Ri} = 18.18 - 0.404 * \Theta \quad (27)$$

where:

- E_{Ri} = resilient modulus at a repeated deviator stress of 6 psi (41.4 kPa), ksi
- γ_d = density of the soil, pcf
- Θ = volumetric moisture content

The *frozen* and *unfrozen (standard)* resilient modulus values are calculated as shown in equations 28 and 29 below:

$$E_{Ri}(f) = E_{Ri} * 100 \quad (28)$$

$$E_{Ri}(t) = \{ [E_{Ri} * (100 - REDUCT) / 100] / RECPER \} + E_{Ri} * REDUCT \quad (29)$$

where:

- $E_{Ri}(f)$ = frozen resilient modulus, ksi
- $E_{Ri}(t)$ = thaw-recovery resilient modulus, ksi
- REDUCT = percentage reduction in E_{Ri} (default value = 10%)
- RECPER = recovery period, days (default value = 60 days)

The results of the manual analysis are presented in table 16.

Table 16. Analysis of stiffness of the paving layers in the deep frost, thaw-recovery, and nonfrost periods for MN 1-1.

Variable	Input
γ_d	> 100 pcf
Θ	14.1%
REDUCT	10%
RECPER	60 days
E_{Ri}	12.5 ksi
$E_{Ri}(f)$	1250 ksi
$E_{Ri}(t)$	1.44 ksi

It is important to note that if the CMS materials stiffness routine were executable, the results would be far more in-depth. The analysis would evaluate the pavement system based on the actual temperature conditions existing at Rothsay for a given analysis period. The actual presence of the frozen, unfrozen, and thaw-recovery period would be established based on those climatic conditions.

The results of the analysis show that at the onset of the spring thaw, the subgrade is substantially weakened. This weakening may be attributed to the dissolving of ice lenses in the subgrade layers and to the presence of excess moisture. However, when the subgrade is frozen, the stiffness of the material increases dramatically. This is supported by the decreased deflections measured during periods of deep frost.

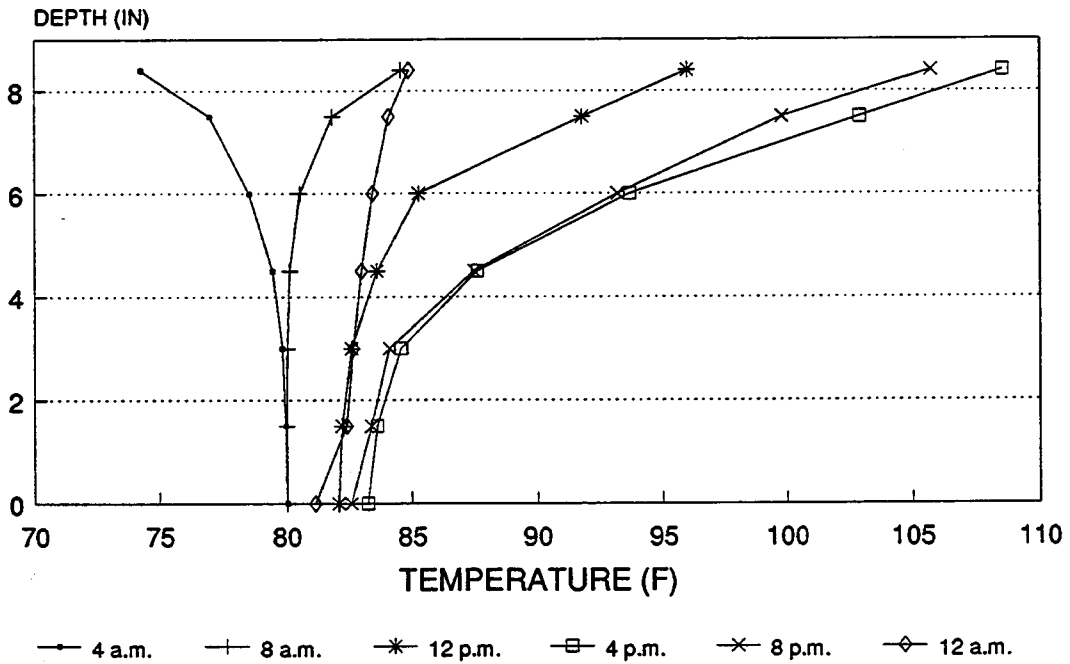
The developers state that the thaw-recovery period is critical in terms of the strength of the subgrade layers. It can be seen from the model that a large reduction in strength is probable at that time. If fine-grained subgrade soil is subjected to many wheel loads during the thaw-weakened period, the subgrade could experience permanent deformation which could potentially cause settlement problems.

Tracy, California

The CMS program was executed twice using site-specific climatic data to analyze the temperature differential through the portland cement concrete slab. First, a rigorous analysis was performed for the week of July 15 through July 21, 1987. In this analysis, the temperature profiles through the depth of the 8.4 in (213 mm) slab were calculated (via the CMS program) at 12 a.m., 4 a.m., 8 a.m., 12 p.m., 4 p.m., and 8 p.m. Secondly, the program was executed for the entire year of 1987 to examine the fluctuation in thermal gradient at 6 a.m. and 3 p.m.

Figure 15 shows typical results for July 15, 1987 using the first analysis approach. The temperature profile through the depth of the 8.4 in slab is plotted for the specified times of the day. For July 15, 1987 the largest thermal gradient ($g = [109.0 - 82.5/8.4 = 3.16 \text{ }^\circ\text{F/in} [1.76 \text{ }^\circ\text{C/mm}]$) occurred at 4 p.m. and the smallest (most negative) thermal gradient ($g = -0.66 \text{ }^\circ\text{F/in} [-0.37 \text{ }^\circ\text{C/mm}]$) at 4 a.m. As expected, the maximum positive thermal gradient occurred during the afternoon and the minimum thermal gradient occurred during the early morning. Table 17 presents a summary of the thermal gradients for all of the times under analysis.

TRACY, CALIFORNIA
 TEMPERATURE VS. DEPTH
 JULY 15, 1987



Temperature Change = 26° F

Figure 15. Temperature profile versus depth through the slab on July 15, 1987, Tracy, California.

Table 17. Summary of thermal gradients at specified times for CA 1-1 for July 15 through July 21, 1987.

T H E R M A L G R A D I E N T, °F / in						
Date	12 a.m.	4 a.m.	8 a.m.	12 p.m.	4 p.m.	8 p.m.
7/15/87	0.14	-0.66	0.38	1.48	3.16	2.35
7/16/87	0.17	-0.47	0.64	1.86	3.91	3.00
7/17/87	0.10	-0.77	0.41	2.22	3.85	2.71
7/18/87	0.15	-0.58	0.59	2.08	3.70	2.73
7/19/87	0.12	-0.81	0.33	1.69	3.22	2.26
7/20/87	0.09	-0.55	0.43	1.46	3.01	2.06
7/21/87	0.13	-0.49	0.62	1.31	3.88	2.17

For the chosen analysis period, the maximum positive thermal gradient always occurs at 4 p.m. and the maximum negative gradient occurs at 4 a.m. The gradient at 12 a.m. is positive and very close to zero. Sometime between 12 a.m. and 4 a.m. the gradient changes from positive to negative and since the 12 a.m. gradient is very near zero the change probably occurs closer to 12 a.m. Between 4 a.m. and 8 a.m. the gradient shifts once again, this time from negative to positive. The time of the transition from negative to positive gradient changes from day to day. The time is most likely a function of the amount (and intensity) of sunshine in the early morning hours. Due the high levels of solar radiation during the daytime hours, the gradient increases rapidly to its maximum sometime the late afternoon (near 4 p.m.). Between 4 p.m. and 12 a.m. the gradient gradually decrease and the cycle repeats itself.

Figures 16 and 17 show the thermal gradient at 6 a.m. varies throughout the year (1987) for CA 1-1. The thermal gradient at 6 a.m. is negative for the majority of the year, as expected. The 6 a.m. gradient is highly variable throughout the year. There are two periods where the thermal gradient is positive during the morning hours. The first period of positive thermal gradient occurs in early February and the second occurs in late February and early March. The daily temperature change during those periods was relatively small compared to the average temperature change for the month. For example, the average temperature

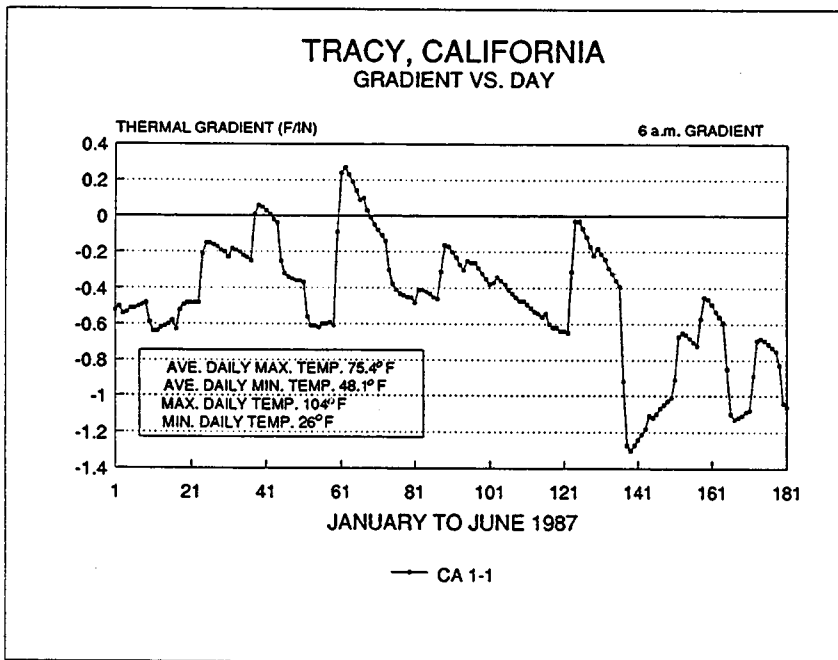


Figure 16. Change in 6 a.m. thermal gradient from January through June 1987, Tracy, California.

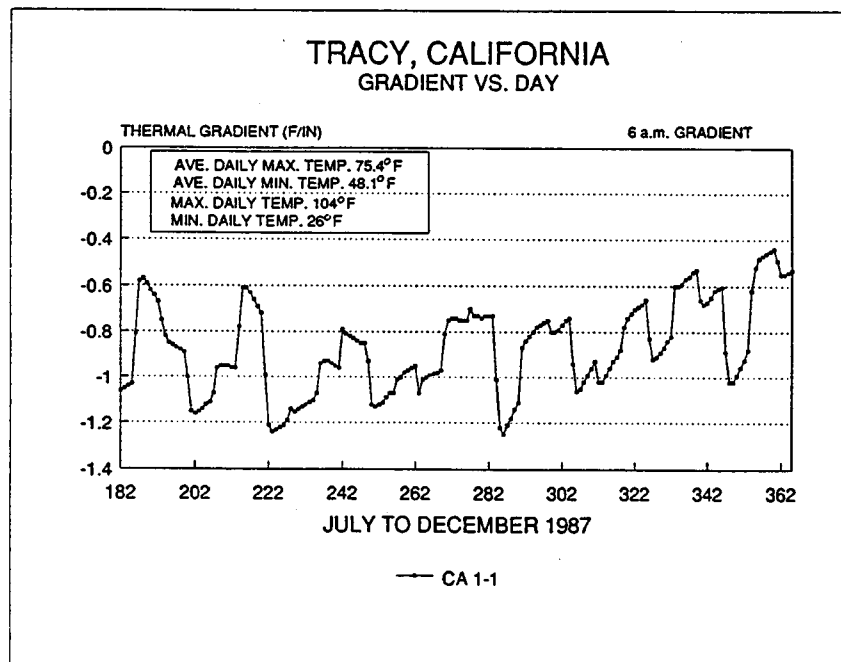


Figure 17. Change in 6 a.m. thermal gradient from July through December 1987, Tracy, California.

drop between daytime and nighttime for February, 1987 was 22 °F (12.2 °C), whereas, during the period of positive thermal gradient, the average temperature drop was 15 °F (8.3 °C). A similar trend was observed at Rothsay.

Periods where the thermal gradient is highly negative typically correspond to days when the maximum daytime temperature is much higher than the minimum nighttime temperature. This change causes the slab surface to heat up during the hot day and cool down quickly at night. On the other hand, the temperature at the bottom of the slab is not affected by the solar radiation and temperature nearly as much due to its greater depth.

The gradient at 3 p.m. for 1987 is shown in figures 18 and 19. The thermal gradient is positive throughout most of the year, as expected, during the hot hours of the day. The sun warms the surface of the pavement rapidly while the bottom of the slab is still cool. As a general trend, the 3 p.m. thermal gradient peaks during the summer months when the solar radiation is at a maximum and the number of hours of sunshine are also at a maximum. During the cooler months of the year, the 3 p.m. gradient is much closer to 0. This may be due to less intense solar radiation, more frequent cloud cover, lower temperatures, and less severe temperature variation between day and night during the cooler months. In fact, there is a small period in December of 1987 when the 3 p.m. gradient is negative. This could be caused by a rapidly decreasing air temperatures which cools the top of the slab quickly. The bottom of the slab may stay warmer for a longer period (due to its depth) and therefore a negative thermal gradient exists.

The relationship between the 6 a.m. and 3 p.m. thermal gradient is interesting. It appears that the days when the 6 a.m. gradient is higher (more positive), then the 3 p.m. gradient is higher also. The opposite is also true; on days when the 6 a.m. gradient is lower (more negative), the 3 p.m. gradient is lower. This phenomenon may be due to the fact that the cyclic air temperature fluctuations affect both the top and bottom of the slab. The top of the slab and the bottom of the slab respond to the changes in ambient temperature. As the air temperature increases, the temperature at the top and bottom of the slab also increase. However, they do so at different *rates*. The top of the slab is significantly affected by exposure to solar radiation.

Clare, Michigan

The CMS program was executed to examine the changes in thermal gradient with time of day and year, the temperature with depth in the slab, and the determination of the frost penetration into the pavement system. The results of these analysis are presented in figures 20 through 29.

The program was executed to determine temperatures at 12 a.m., 4 a.m., 8 a.m., 12 p.m., 4 p.m., and 8 p.m. for July 15 though July 21, 1987. Figure 20

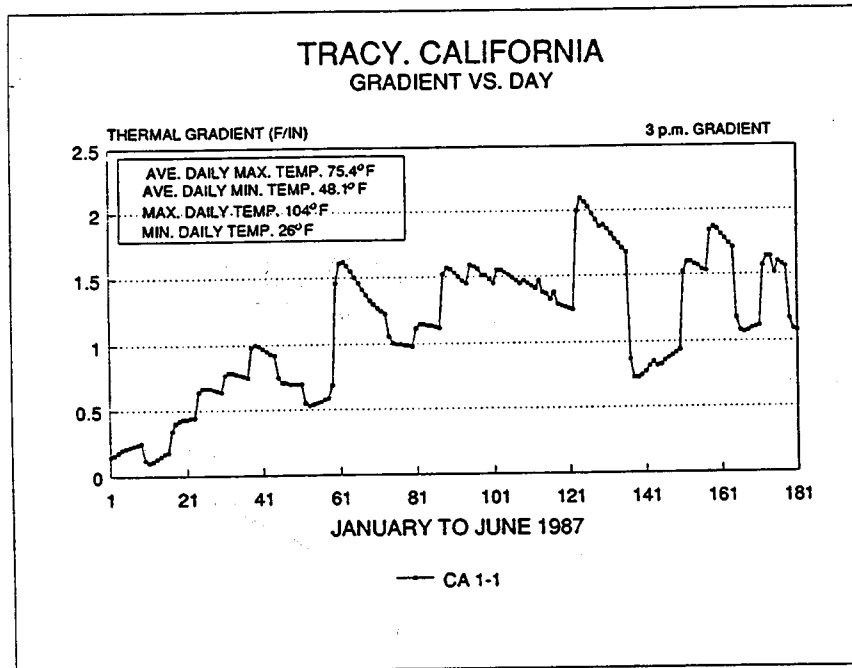


Figure 18. Change in 3 p.m. thermal gradient from January through June 1987, Tracy, California.

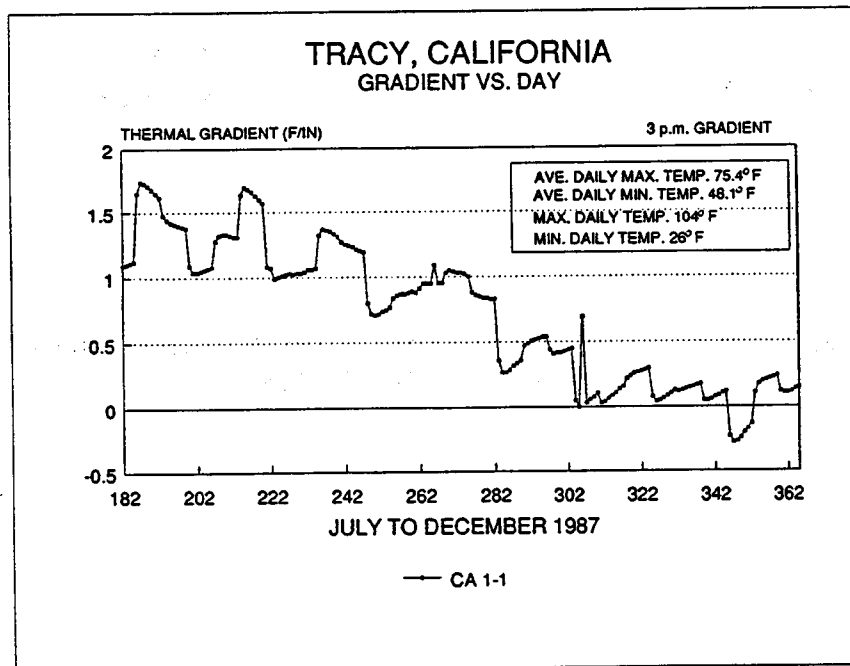
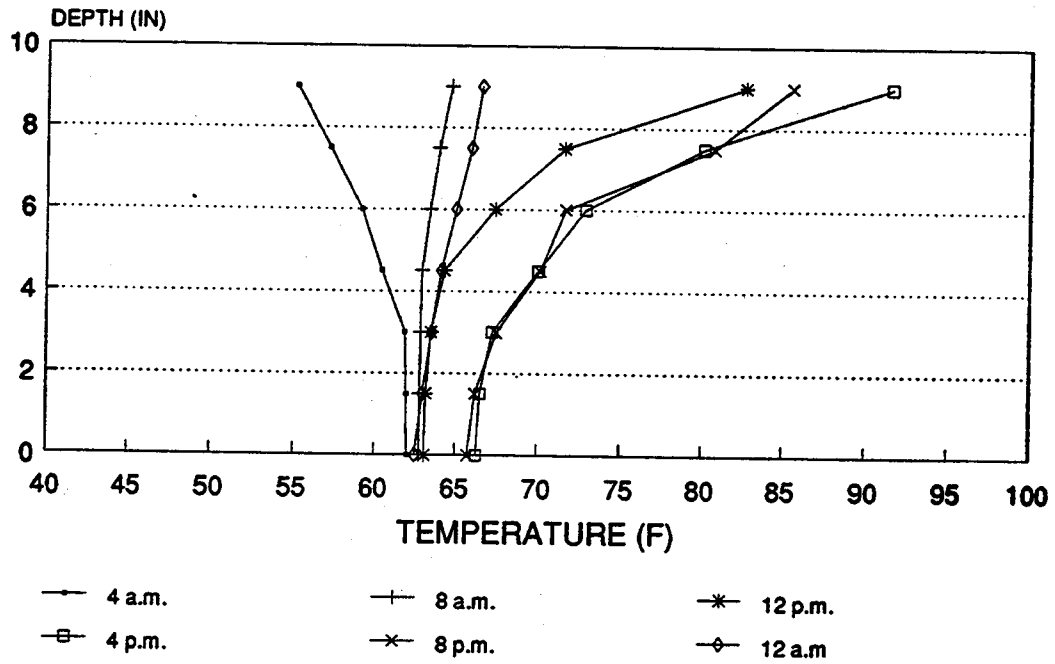


Figure 19. Change in 3 p.m. thermal gradient from July through December 1987, Tracy, California.

CLARE, MICHIGAN
TEMPERATURE VS. DEPTH
 JULY 15, 1987



Temperature Change = 24°F

Figure 20. Temperature profile versus depth through the slab on July 15, 1987, Clare, Michigan.

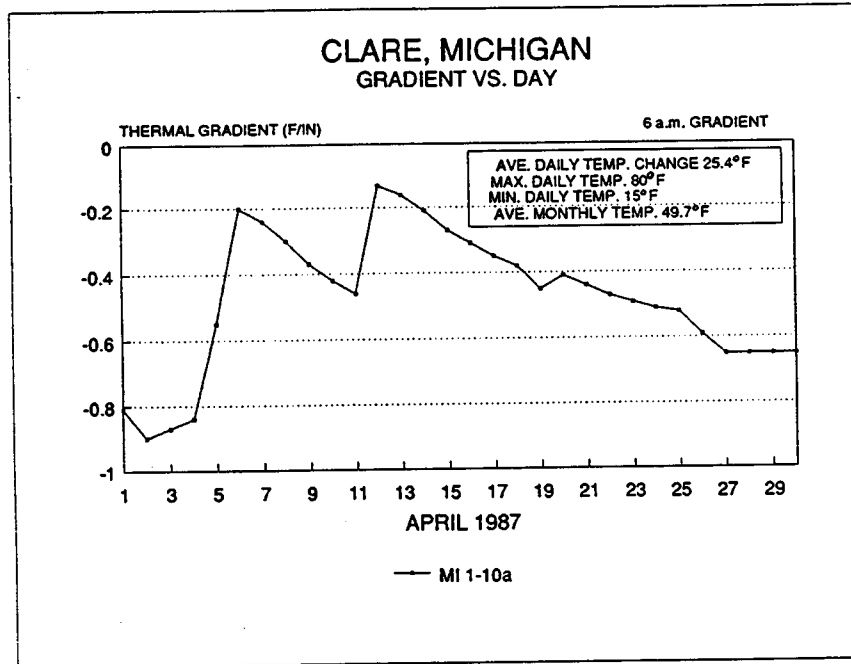


Figure 21. Change in 6 a.m. thermal gradient in April 1987, Clare, Michigan.

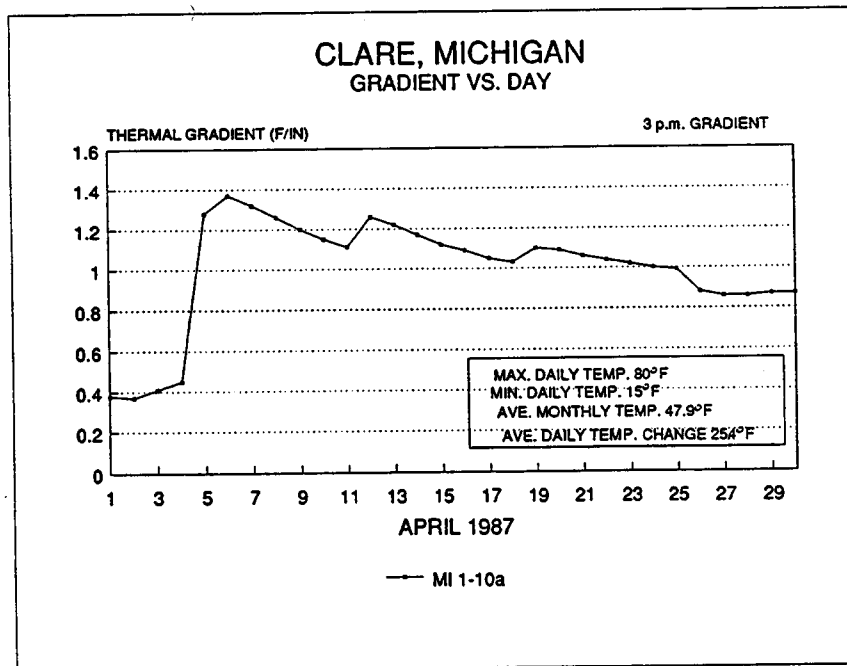


Figure 22. Change in 3 p.m. thermal gradient in April 1987, Clare, Michigan.

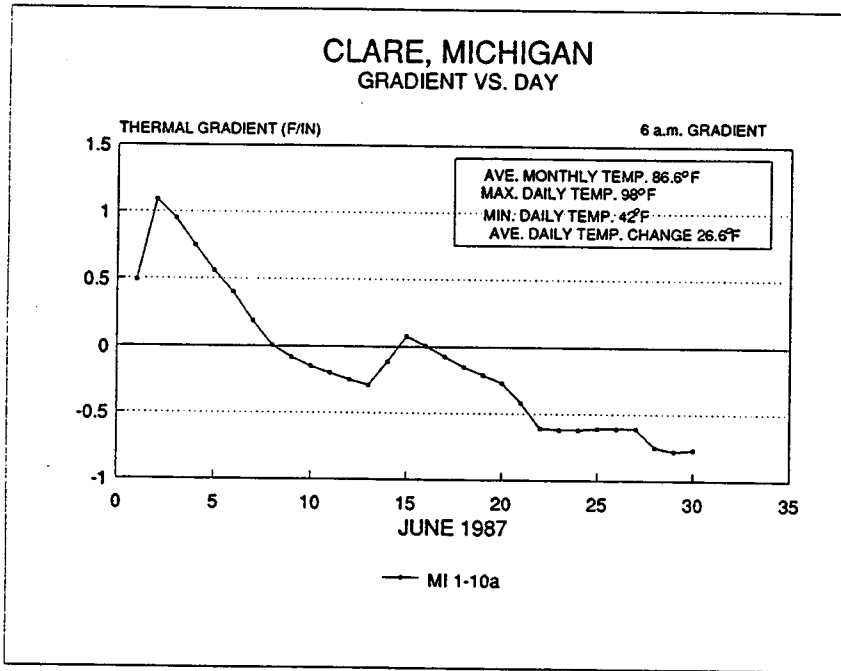


Figure 23. Change in 6 a.m. thermal gradient in June, 1987
Clare, Michigan.

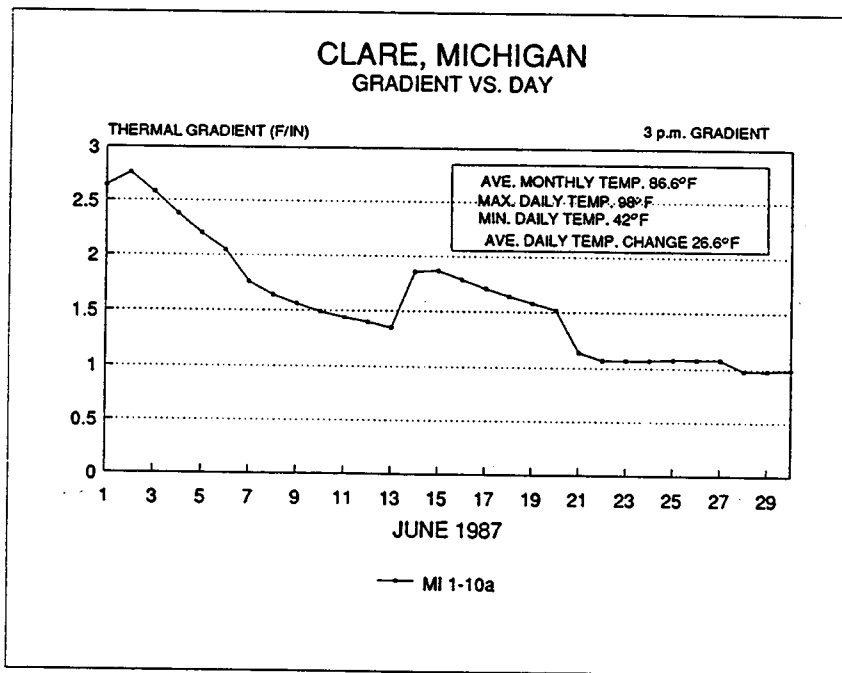


Figure 24. Change in 3 p.m. thermal gradient in June 1987
Clare, Michigan.

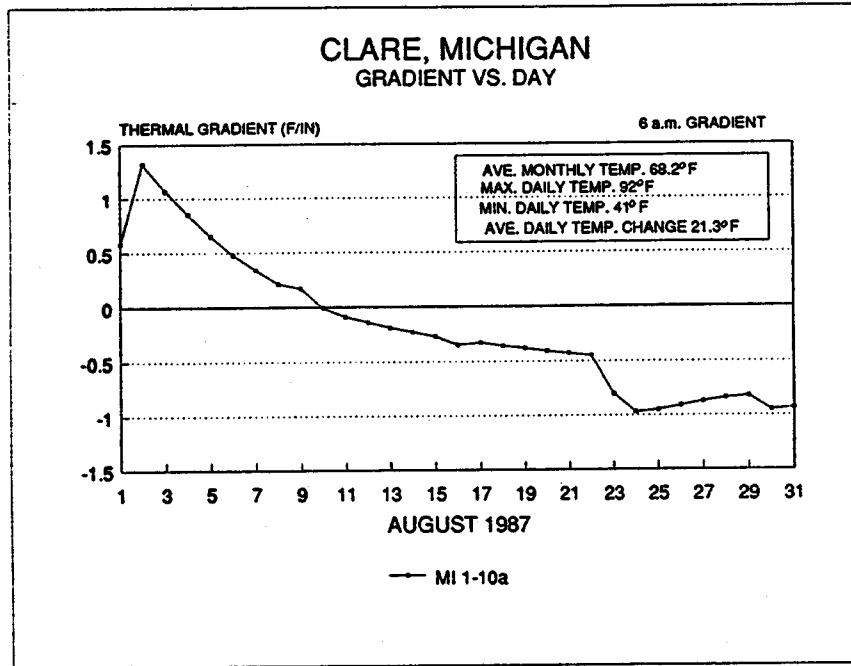


Figure 25. Change in 6 a.m. thermal gradient in August 1987, Clare, Michigan.

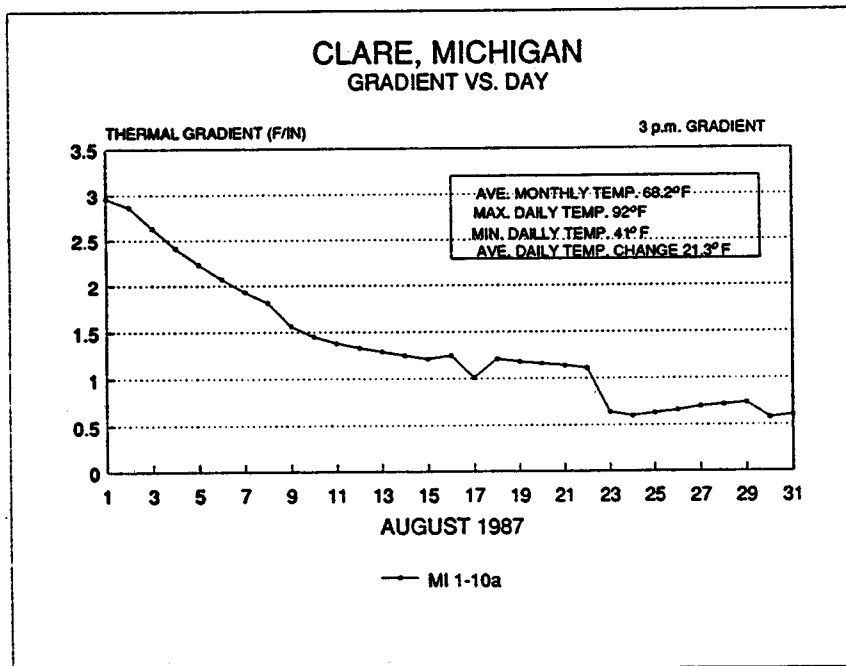


Figure 26. Change in 3 p.m. thermal gradient in August 1987, Clare, Michigan.

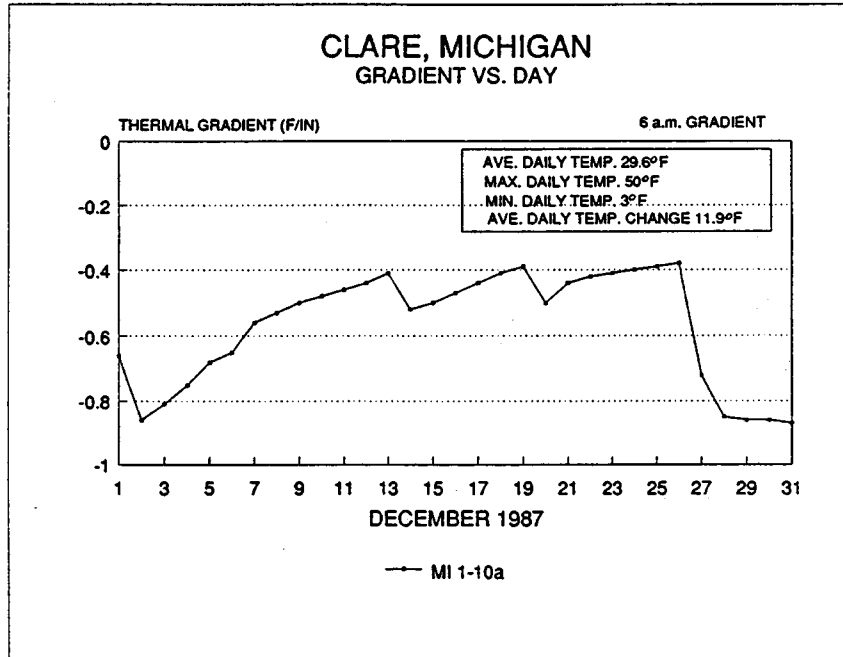


Figure 27. Change in 6 a.m. thermal gradient in December 1987, Clare, Michigan.

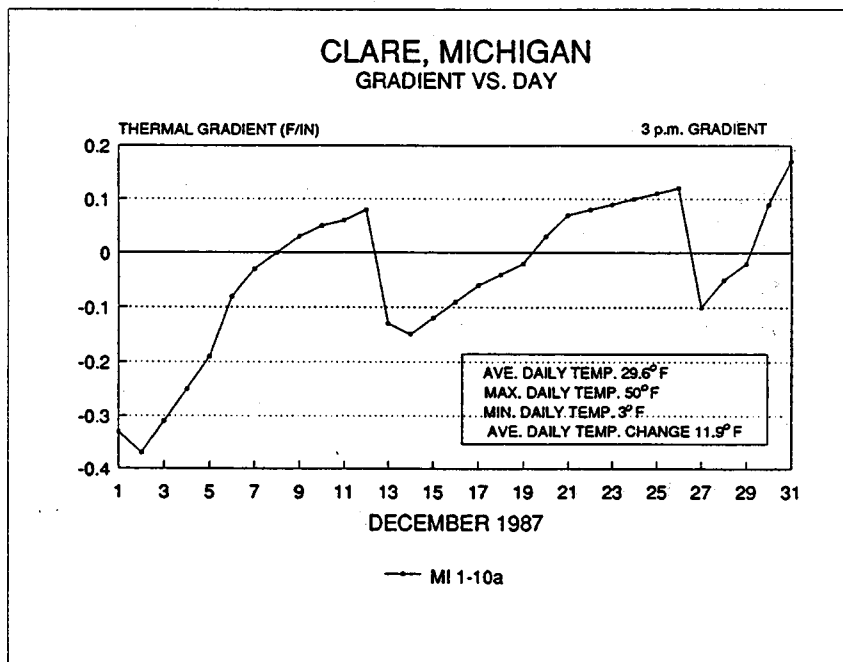
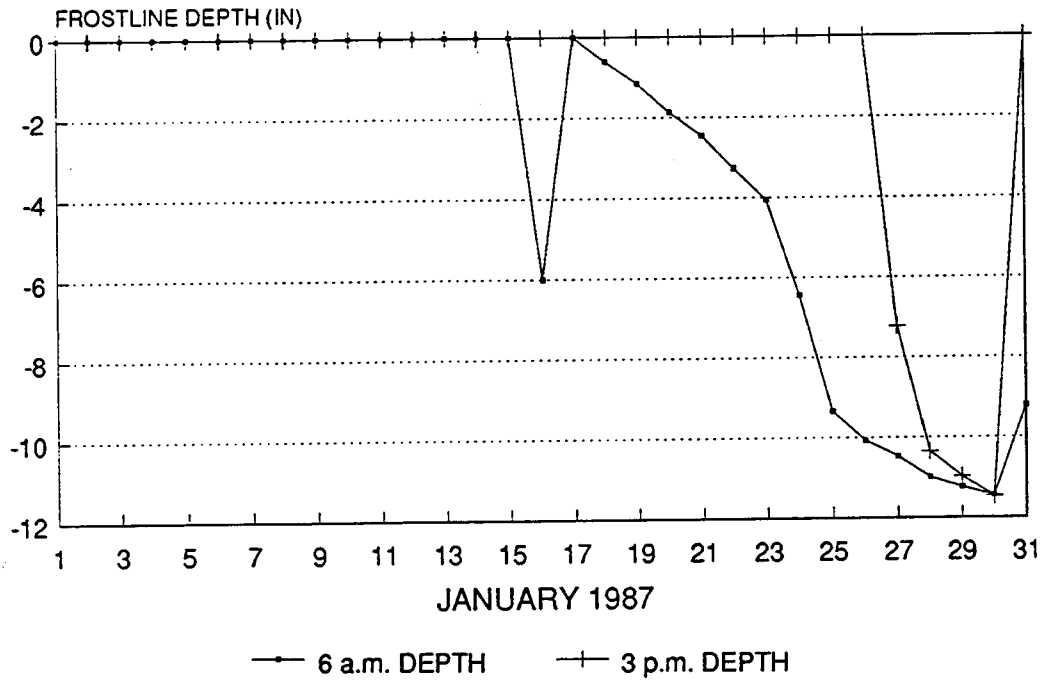


Figure 28. Change in 3 p.m. thermal gradient in December 1987, Clare, Michigan.

CLARE, MICHIGAN FROSTLINE DEPTH VS. TIME



MI 1-10a

Figure 29. Frostline versus depth in January, 1987, Clare, Michigan.

shows the change in temperature with depth into the concrete slab for MI 1-10a for July 15, 1987. For July 15, 1987 the largest thermal gradient ($g = 2.90$ °F/in [-1.61 °C/mm]) occurred at 4 p.m. and the smallest (most negative) thermal gradient ($g = -0.91$ °F/in [-0.51 °C/mm]) at 4 a.m. As expected, the maximum positive thermal gradient occurred during the afternoon and the minimum thermal gradient occurred during the early morning. Table 18 presents a summary of the thermal gradients for all of the times under analysis.

Table 18. Summary of thermal gradients at specified times for MI 1-10a for July 15 through July 21, 1987.

T H E R M A L G R A D I E N T , ° F / i n						
Date	12 a.m.	4 a.m.	8 a.m.	12 p.m.	4 p.m.	8 p.m.
7/15/87	0.13	-0.91	0.05	1.83	2.90	2.07
7/16/87	0.21	-0.73	0.05	1.95	2.91	2.01
7/17/87	0.19	-0.66	0.01	1.77	2.72	1.99
7/18/87	0.19	-0.62	0.04	2.04	2.51	2.10
7/19/87	0.14	-0.88	0.05	2.09	2.72	2.33
7/20/87	0.10	-0.80	0.06	2.00	2.62	2.21
7/21/87	0.15	-0.81	0.07	1.87	2.47	2.07

The observed trends are very similar to those observed at Tracy, California, although at lower temperature levels. For the chosen analysis period, the maximum positive thermal gradient always occurs at 4 p.m. and the maximum negative gradient occurs at 4 a.m. Sometime between 12 a.m. and 4 a.m. the gradient changes from positive to negative and since the 12 a.m. gradient is very near zero the change probably occurs closer to 12 a.m. Between 4 a.m. and 8 a.m. the gradient shifts once again, this time from negative to positive. The time of the transition from negative to positive seems to occur very near 8 a.m. since the gradient is very near zero at 8 a.m. Due the high levels of solar radiation during the daytime hours, the gradient increases rapidly to its maximum sometime the late afternoon (near 4 p.m.). Between 4 p.m. and 12 a.m. the gradient gradually decrease and the cycle repeats itself.

Figures 21 through 28 shown the thermal gradient at 6 a.m. and 3 p.m. for the months of April, June, August, and September of 1987. Again the trends at Clare are similar to those observed at Rothsay, Minnesota and Tracy, California. Throughout the year, the 6 a.m. thermal gradient is typically negative, although two periods of positive gradient occur in June and August. The 3 p.m. gradient is positive with the exception of two periods of negative gradient in December. The overall results of these analysis are summarized below:

- The graph of the *6 a.m. and 3 p.m. gradients for April, 1987* are shown in figures 21 and 22. As expected, the 6 a.m. thermal gradient is negative throughout the month and the 3 p.m. thermal gradient is positive throughout the month. The gradient is low (at both times) for the first few days of the month and then increases rapidly, corresponding to a period of higher temperatures (both day and night), less extreme drops in temperature, and high levels of solar radiation. Due to these higher temperatures, the entire slab warms. The difference in temperature between the top and bottom of the slab is less pronounced during the morning hours because the nighttime temperature is warmer and the top of the slab does not cool as quickly. Whereas during the daytime hours, the top of the slab warms quickly and the bottom of the slab warms slower causes a larger difference in temperature. The gradient gradually decreases (becomes more negative at 6 a.m. and decreases at 3 p.m.) throughout the rest of the month.
- The graph of the *6 a.m. and 3 p.m. gradients for June, 1987* are shown in figures 23 and 24. The thermal gradient at 6 a.m. is positive for the first 7 days of the month, corresponding to a positive gradients at 3 p.m. This may be attributed to the intense solar radiation and relatively low changes temperature between the daytime and nighttime temperature during the first few days of the month. The gradient gradually decreases throughout the remainder of the month.
- The graph of the *6 a.m. and 3 p.m. gradients for August, 1987* are shown in figures 25 and 26. These graphs show the same trend as the graphs of the June gradients. The same temperature trends caused the similar behavior of the thermal gradients seen in these figures.
- The graph of the *6 a.m. and 3 p.m. gradients for December, 1987* are shown in figures 27 and 28. The 6 a.m. gradient is always negative as expected. The top of the slab is cooler than the bottom due to the cooling of the top of the slab at night. The 3 p.m. gradient is negative for a large portion of the month. This may be attributed to the cold temperatures and the prevailing cloud cover during the month. Because of the cloud cover, the top of the slab is not warmed by solar radiation and does not get warmer than the bottom of the slab. The daily temperature changes are not nearly as severe in the month of December as they were in April, June, and August and therefore, the thermal gradient is not as large during the daytime or small during the nighttime.

Figure 29 shows the depth of the frost line within the pavement structure at 6 a.m. and 3 p.m. for MI 1-10a. The program was executed for January 1987. The figure shows that the slab is frozen at 6 a.m. and 3 p.m. during the latter part

of the month. The temperature wavered just below freezing for the first part of the month where no frost lines are present. The temperatures toward the end of the month decreased to around an average 10 °F (-12.2 °C) during the day and below 0 °F (-18 °C) at night with very low temperatures occurring at the end of the month. The frost lines illustrate that the pavement is typically frozen deeper into the structure at 6 a.m. than it is at 3 p.m. This is expected due to the warming of the pavement surface from the sun.

The moisture model was attempted using the MI 1-10a during the month of April, 1987. The results provided by the program were somewhat confusing, in that, the moisture content of the soil did not change from the moisture content which was initially input into the program. A closer examination of the model provided an explanation of these results. The moisture analysis within the CMS program is based on five basic principles as follows:

1. The trend in pore water pressure, under certain conditions at a given level of the subgrade, is towards an equilibrium value depending solely on the height above the ground water level.
2. There is a relationship between the pore water pressure in the soil at a given level and the suction of the soil.
3. There is a relationship between the soil suction and the water content of the soil.
4. The temperature of the subgrade soil beneath the pavement structure is constant uniform, and above freezing.
5. The subgrade cannot receive moisture by infiltration through the surface of the pavement or by migration from adjacent soil masses with higher pore pressure, nor can it give up moisture by evaporation or migration to adjacent soil masses having a lower pore pressure.

The Clare sections were placed on a sandy soil (A-2-4) and the depth to the water table was greater than 6 ft (1.8 m). The combination of the soil type and the depth of the water table is not conducive to the movement of moisture and therefore, the moisture content of the soil did not change throughout the analysis period.

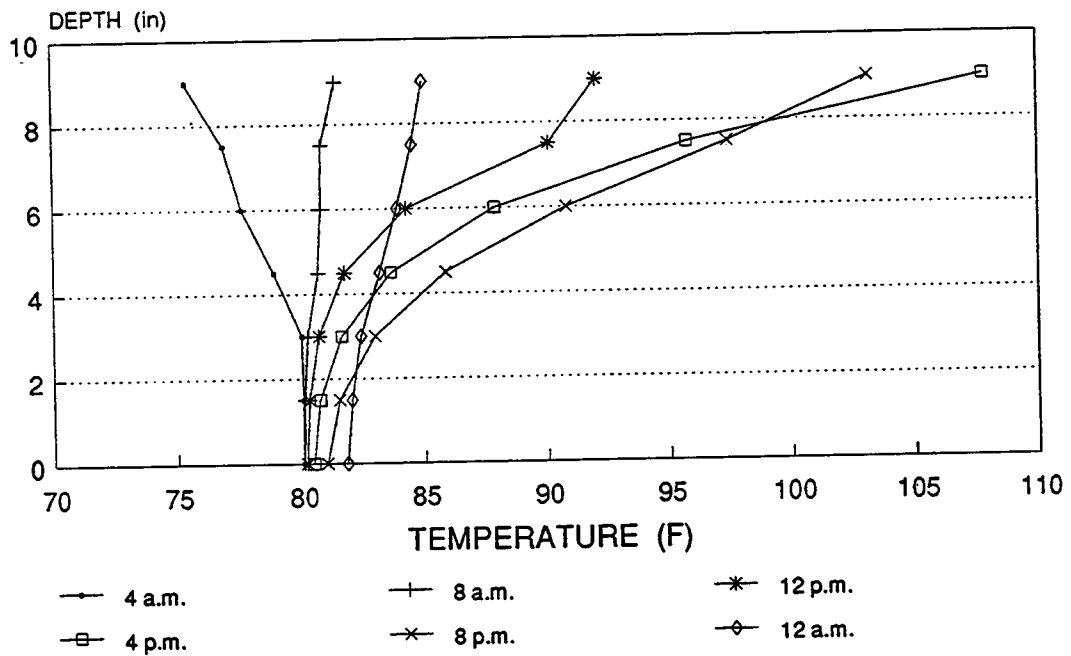
Rocky Mount, North Carolina

Figure 30 shows the graph of temperature versus depth for July 15, 1987 for the same times as specified for the MN 1-1, CA 1-1, and MI 1-10a. For July 15, 1987 the largest thermal gradient ($g = 2.97$ °F/in [1.65 °C/mm]) occurred at 4 p.m. and the smallest (most negative) thermal gradient ($g = -0.47$ °F/in [-0.26 °C/mm]) at 4 a.m. As expected, the maximum positive thermal gradient occurred during

ROCKY MOUNT, NORTH CAROLINA

TEMPERATURE VS. DEPTH

JULY 15, 1987



Temperature Drop = 39 F

Figure 30. Temperature profile versus depth through the slab on July 15, 1987, Rocky Mount, North Carolina.

the afternoon and the minimum thermal gradient occurred during the early morning. Table 19 presents a summary of the thermal gradients for all of the times under analysis.

Table 19. Summary of thermal gradients at specified times for NC 1-1 for July 15 through July 21, 1987.

T H E R M A L G R A D I E N T, °F / in						
Date	12 a.m.	4 a.m.	8 a.m.	12 p.m.	4 p.m.	8 p.m.
7/15/87	0.03	-0.47	0.01	1.41	2.97	2.06
7/16/87	0.10	-0.47	0.03	1.44	2.91	2.50
7/17/87	0.11	-0.53	0.13	1.53	3.02	2.30
7/18/87	0.12	-0.55	0.10	1.59	2.80	2.11
7/19/87	0.17	-0.49	0.09	1.58	2.91	2.22
7/20/87	0.03	-0.08	0.31	2.12	2.95	2.06
7/21/87	0.02	-0.09	0.33	2.29	3.03	2.02

The observed trends are very similar to those observed at Tracy and Clare. For the chosen analysis period, the maximum positive thermal gradient always occurs at 4 p.m. and the maximum negative gradient occurs at 4 a.m. Sometime between 12 a.m. and 4 a.m. the gradient changes from positive to negative and since the 12 a.m. gradient is very near zero the change probably occurs closer to 12 a.m. Between 4 a.m. and 8 a.m. the gradient shifts once again, this time from negative to positive. The time of the transition from negative to positive seems to occur very near 8 a.m. since the gradient is very near zero at 8 a.m. Due the high levels of solar radiation during the daytime hours, the gradient increases rapidly to its maximum sometime the late afternoon (near 4 p.m.). Between 4 p.m. and 12 a.m. the gradient gradually decrease and the cycle repeats itself.

Figures 31 and 32 show the thermal gradients at 6 a.m. and 3 p.m. for the month of July for NC 1-1. The 6 a.m. gradient is negative during the first portion of the month and then becomes positive toward the end of the month. This may be attributed to a very warm period. The temperature change between the daytime and nighttime were, on average, 12 °F (6.7 °C) for the period between the July 19 and July 31. This warm period also accounts for the high levels of positive gradient at 3 p.m.

Conclusion and Recommendations

CMS is a very comprehensive and theoretically rigorous analysis program which provides detailed outputs. The main usage of the program in the design of

ROCKY MOUNT, NORTH CAROLINA GRADIENT VS. DAY

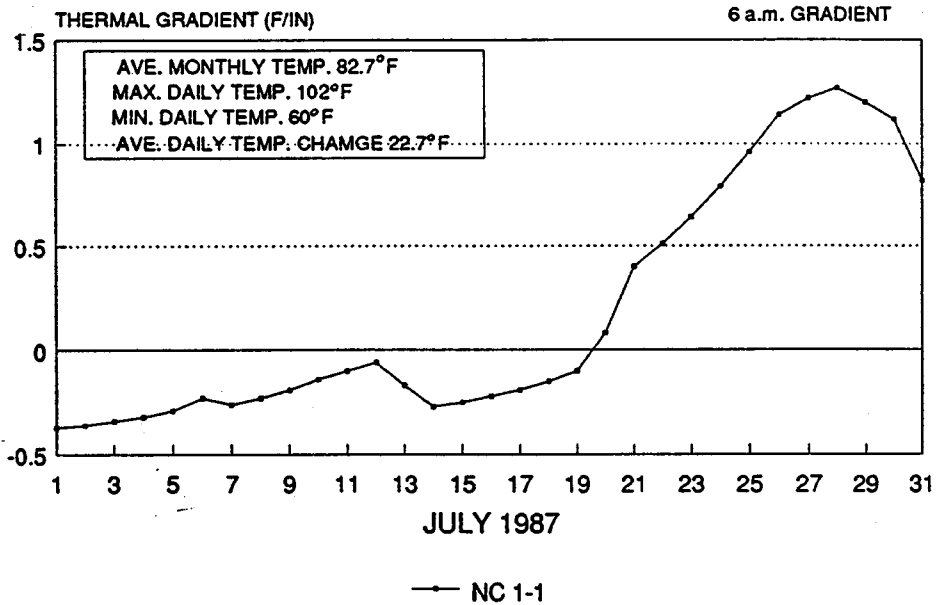


Figure 31. Change in 6 a.m. thermal gradient in July 1987, Rocky Mount, North Carolina.

ROCKY MOUNT, NORTH CAROLINA GRADIENT VS. DAY

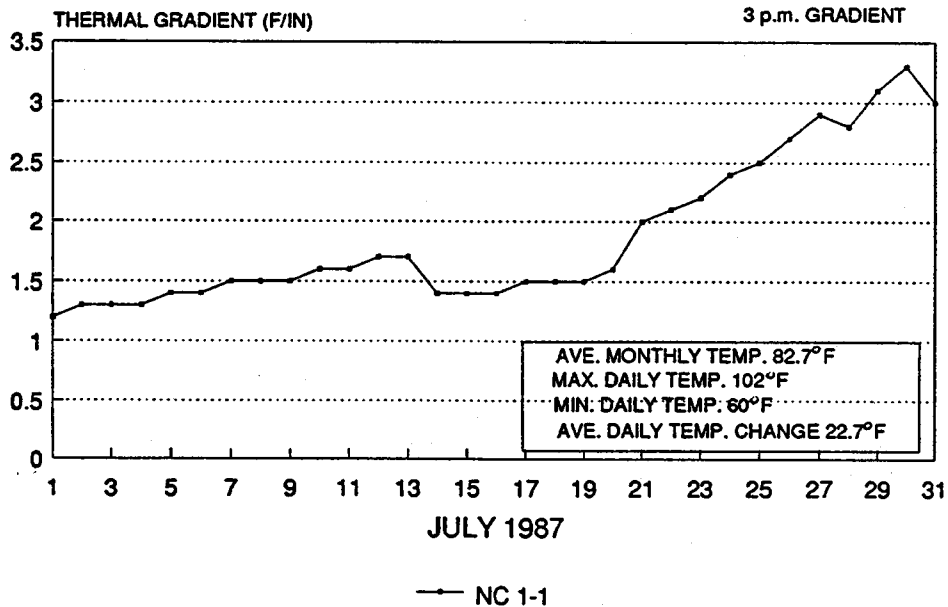


Figure 32. Change in 3 p.m. thermal gradient in April 1987, Clare, Michigan.

rigid pavements is the analysis of thermal gradients and the determination of the stiffness of the unbound paving layers during the thaw-recovery period.

The site-specific and accurate determination of thermal gradients, which could otherwise only be determined by long-term pavement instrumentation and monitoring, can aid the design engineer in the determination of thermal stresses. Additional work is in progress to modify, revise, and enhance the CMS program for ease of use and greater applicability. It is being combined with other climatic models to allow for the complete evaluation and analysis of environmental factors as they impact pavement design.

With the advent of resilient modulus testing, the properties of the subgrade under repeated loading behavior have been researched extensively. The results show that the resilient modulus decreases tremendously during the thaw-recovery period, especially for frost-susceptible soils. The CMS program incorporates this concept into the procedure. However, in order to use the CMS materials model with any degree of accuracy, the resilient modulus testing of the granular layers *must* be performed for the unfrozen condition.

The effects of thaw-weakening of the subgrade soil has largely been ignored in the design of rigid highway pavements, although it has been considered in the design of airfield rigid pavements. The weakened lower layers provide decreased support to the slab during the thaw-recovery period. Repeated traffic loading in combination with the weakened condition of the support layers may damage the slab. Incorporation of this into a design procedure would aid in reducing failures associated with loss of support.

Although the program provides a tremendous amount of useful information, the inputs required for the program are obscure, difficult to obtain, and quite numerous. A listing of the input variables required for an execution of the program is provided in appendix C of volume VI.

Several problems were encountered in running the analyses. These were:

1. The materials model did not execute. Input files which executed successfully when specifying the heat transfer model did not execute successfully when specifying the materials model. The *identical* input file was used to execute the materials model and an execution error resulted. The specification of the model for analysis is accomplished by a numeric flag in the first line of the input file (e.g., 1, if the model is specified; 0, if the model is not specified). The numeric flag was changed in an input file which executed successfully; however, when specifying the heat-transfer model, the same input file did not execute successfully.
2. The moisture model was specified for several analysis periods using MI 1-10a. The moisture content of the soil remained the same as the

moisture content input into the program. This result is expected due to the depth of the water table and the soil type at Clare (A-2-4). CMS calculates moisture changes in the subgrade soil due to isothermal movement from the water table *only*, meaning no moisture enters the pavement system through the surface of the pavement or through the edges of the pavement. Surface infiltration has been shown to contribute to moisture in the pavement system.^(30,31)

3. While each of the models are theoretically very rigorous and have been tested individually, the iteration between the models has never been tested or compared to instrumented pavements to determine its accuracy. This would require long-term monitoring of instrumented pavements, of which several such projects are underway.

4. EVALUATION OF THE LIU-LYTTON DRAINAGE MODELS

Introduction

The rate of deterioration of a pavement system is greatly increased by excess moisture in the system. Traffic loads in combination with moisture trapped in the lower paving materials can cause pumping and loss of support which can lead to faulting, corner breaks, and other distresses in rigid pavements. The Liu-Lytton drainage models provide a method of computing the amount of rain water that penetrates into a pavement through cracks and joints, and subsequently the rate of drainage out of the base course into the subgrade and into a lateral drainage system.

The accurate modeling of the effects of moisture on paving layers is important in the design of a pavement system. The program's outputs can be used in the design process to examine deterioration of the paving layers based on moisture infiltration into those layers. Using site-specific climatic data and detailed information about the paving materials, the program generates materials properties as a function of the free moisture available in the system. Based on the climatic inputs, the program generates the probability distribution for the saturated condition. This shows the user the percentage of the year the lower paving layers will be in the weakened state.

This output can be used as inputs to structural analysis models, fatigue analysis models, and predictive models which aid the engineer in the design of the pavement system. Through accurate modeling of effect of moisture on the paving system a more realistic pavement design is achieved.

Brief Technical Description

A detailed technical description of the program as well as a derivation of the models is presented in reference 13. A summary of the five parts of the procedure is given below:

1. An estimation of the amount of precipitation that falls on the pavement each day is calculated. A gamma distribution is employed for describing the probability density function for the quantity of rain that falls.
2. The program determines the infiltration of the water through the cracks and joints in the pavement surface. One of two methods are used to determine the infiltration of water through the joints and cracks. Ridgeway's infiltration rate is employed, if the user provides the length of cracks and joints.⁽³¹⁾ If the user does not provide the length of joints and cracks, the model developed by Dempsey and Robnett is employed.⁽³⁰⁾
3. The computation of the simultaneous drainage of water into the base and subgrade and into a lateral subdrainage system is performed by the program. A new method was developed by Liu and Lytton to compute the drainage of the pavement which overcomes the assumption of a straight line phreatic surface and an impermeable subgrade.
4. Through the use of a Markov chain model, the probabilities of the wet and dry conditions of the base course and subbase course are estimated.
5. The effect of moisture contents on the strength (modulus) of the lower paving layers is determined. The effect of saturation on the resilient modulus of the base course and the subgrade are calculated using linear relationships developed by various researchers.^(32,33)

As with the CMS model, the accuracy of this model is highly dependent on the input variables. In order to accurately characterize the pavement system in terms of the effectiveness of the drainage system, the probability of saturation, and determination of the structural properties of the paving layers, it is extremely important that accurate climatic data be used.

Analysis of Results

The Liu-Lytton program was executed for each of the large experimental projects in each of the four environmental zones. The results of the analyses will be presented individually for each project.

In order to execute the program using these experimental projects, several assumptions were made. These assumptions are presented below:

1. The program analyzes only sections with base course materials with permeabilities greater than 0.0001 ft/day (0.00003 m/day kPa). In order to analyze sections which included impermeable stabilized base

course materials, it was assumed that all of the cracks and joints in the surface course also existed in the stabilized base course and therefore, the water which infiltrated through the surface would also permeate through the base and into the subbase and subgrade. For sections with impermeable stabilized base courses, the subbase materials were modeled as the base material; hence, the program calculates the drainability of the subbase layer and subgrade. If the section had no subbase material beneath the stabilized base, the subgrade information was input as base information as well as subgrade information since the program *requires* base course information.

2. Those sections containing permeable asphalt-treated base materials were analyzed as if the base course were granular material. The *actual* permeability and the calculated porosity of the layer were used as inputs to the program.
3. Many of the sections were constructed on a granular subbase. The program only allows the user to model a single base layer over the subgrade. Sections which contained a granular base and a granular subbase were modeled as a single granular layer over subgrade. Sections with impermeable stabilized bases over granular subbases were modeled as explained in 1 above.
4. During the field surveys, the amount of cracking in the asphalt concrete shoulders was not recorded, although, it was recorded for the tied PCC shoulders. Therefore, the cracking in the shoulders was not considered in the analyses.
5. The program only analyzes fine-grained soils, as classified by AASHTO (A-4 through A-7-6). The MI 1, CA 1, and NC 1 sections were all placed on course-grained soils. An A-4 soil was chosen for these sections in order to perform the analyses.
6. The transverse slope chosen for the analysis was the *minimum* slope measured over the entire section. Typically three transverse slope measurements were taken within the project, the minimum of these three slopes was used in the analysis to render a worst case scenario.
7. The permeability of the subgrade material was determined from county soils maps based on soil type.
8. Since the program does not accept more than 99 consecutive dry days, 99 dry days were input for the CA 1 sections, which actually experienced over 140 consecutive dry days over the year.
9. The site-specific climatic data for 1987 was used for all sections.

Rothsay, Minnesota

The Liu-Lytton drainage model was executed for each of the experimental projects at Rothsay. The results of the analysis of the drainage time are summarized in table 20. The results are also presented graphically for MN 1-1, MN 1-5, and MN 1-9 in figure 33.

Table 20. Summary of the results of the Liu-Lytton percent drainage versus time analyses for MN 1.

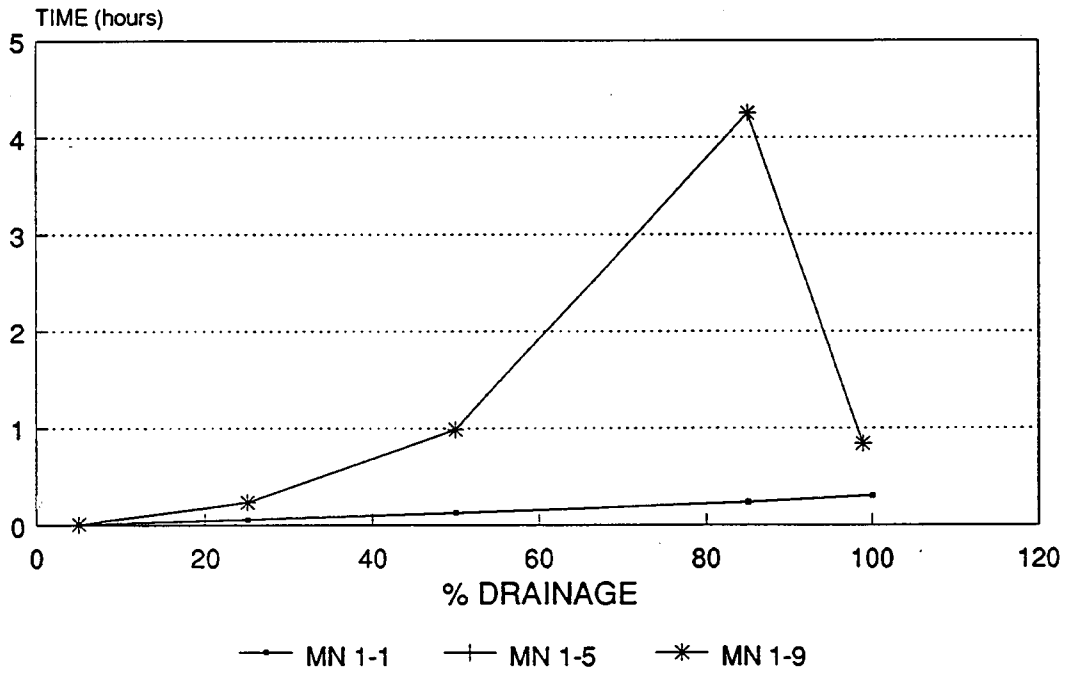
Percent Drainage Versus Time To Drain, hours					
Section ID	5 %	25 %	50 %	85 %	98.9 %
MN 1-1	0.0110	0.0593	0.128	0.239	0.309
MN 1-2	0.0363	0.1700	0.285	0.806	1.55
MN 1-3	0.0094	0.0516	0.115	0.226	0.295
MN 1-4	0.0083	0.0485	0.110	0.222	0.335
MN 1-5	0.0094	0.237	0.989	4.25	0.843
MN 1-6	0.0096	0.237	0.989	4.25	0.843
MN 1-7	0.0312	0.730	3.11	6.48	6.48
MN 1-8	0.0098	0.237	0.989	4.25	0.843
MN 1-9	0.0098	0.237	0.989	4.25	0.843
MN 1-10	0.0098	0.237	0.989	4.25	0.843
MN 1-11	0.0312	0.732	3.10	15.7	16.0
MN 1-12	0.0312	0.732	3.10	15.7	16.0

In examining the results of this analysis, several interesting trends are seen. MN 1-1 through MN 1-4 were placed on aggregate base courses. These are the only sections out of the experimental project which are within the assumptions of the program. The results for these aggregate base sections show that the aggregate material drains quite rapidly.

Sections MN 1-1, MN 1-3, and MN 1-4 exhibited high degrees of drainage in very short time periods. The degree or percent of drainage is defined as the area drained at a specified time divided by the total area of the analysis cross section (times 100). In fact, 98.9 percent of the cross sectional area drained within less than 0.34 hours. Section MN 1-2, however, drained *relatively* slower; this system reached 98.9 percent drainage within 1.55 hours. The drainage times differ due to the differences in permeabilities of the aggregate layers. The base course permeabilities of quick draining sections in the 0.7 range, whereas, the base course permeability of slower draining section was 0.17. The permeability of the base course plays a tremendous role in the drainage capabilities of the system.

ROTHSAY, MINNESOTA

% DRAINAGE VS. TIME



(MN 1-5 and MN 1-9 follow same curve)

Figure 33. Percent drainage versus time for MN 1-1, MN 1-5, and MN 1-9.

The remaining sections were constructed with either asphalt-treated bases (MN 1-5 through MN 1-8) or cement-treated bases (MN 1-9 through MN 1-12) which were placed directly on the subgrade. Sections MN 1-5, MN 1-6, MN 1-8, MN 1-9, and MN 1-10 illustrated a suspicious trend. These sections all displayed a negative -1.04 percent transverse slope. The transverse slope plays a large role in the calculation of the degree of drainage at a specified time. The models for the degree of drainage versus time were developed at TTI for the cases of flat (horizontal) and sloping bases. The equations of interest are shown below:

Case 1. - Less than or equal to 33 percent degree of drainage

$$T = (3/2)*S*U - (3/8)*S^2*\ln[(S + 4*U)/S] \quad (30)$$

Case 2. - Greater than 33 percent degree of drainage

$$T = S/2 - (3/8)*S^2*\ln[(3S + 4)/3S] + S*\ln[(9S - 9SU + 8)/(3*[1 - U]*[3S + 4])] \quad (31)$$

where:

- T = time factor
= $(t * k_1 * H) / (n_1 * L^2)$
- t = time
- k_1 = permeability coefficient of the base course
- H = thickness of the base course
- n_1 = effective porosity of the base course
- L = length of the drainage section (half-width of the pavement structure)
- S = slope factor
= $H / [L * \tan(\text{slope angle})]$
- U = degree of drainage
= drained area/total area

For the case of the Rothsay sections in question, the values of k_1 (0.500 ft/day [0.15 m/day]), H (99 ft [30.1 m]), n_1 (0.238), L (15 ft [4.6 m]), and S (slope = -1.04 percent) are all constant. If the user inputs a negative value for the slope, the program assigns the slope as 0.00001 percent. This was learned through an examination of the FORTRAN source code. It was not presented in the documentation of the program, the user's guide, or within the interactive input processor. The source code and program documentation revealed that the sign convention for the determination of the slope is not clearly presented. The slopes calculated under this study followed the typical convention as shown in the equation 32.

$$\text{Slope} = \frac{(\text{elevation of the lane/shoulder joint} - \text{elevation of the centerline}) * 100 \%}{\text{distance between the centerline and lane/shoulder joint}} \quad (32)$$

Therefore, for a typical crown section, which is sloping away from the centerline in both directions, the slopes are always negative. The only time that positive slopes occur is on a superelevated section. Within the program, a positive slope is assumed to be what has been defined as a negative slope under this study.

As shown above, if a negative slope of *any magnitude* is input, the program reassigns the slope as an extremely small slope. Furthermore, when the input variables are echoed in the output file, the user input slope is echoed and not the slope actually used in the calculation. The user is never aware that the slope is changed within the program. Therefore, input of a negative slope provides inaccurate results. A clear definition of the sign convention within the program documentation, user's guide, and interactive input processor must be provided.

For the particular inputs used for the sections with questionable results, the parabolic equation begins to decrease before the 100 percent degree of drainage is obtained. This phenomenon is more a function of the specific inputs than the accuracy of the equation. The equation was derived from basic principles of moisture movement and is theoretically correct.⁽¹³⁾

The remaining sections in which the drainage times appear reasonable, had larger drainage lengths (27 ft [8.2 m]) and much different slopes (+2 percent and -5 percent), however, k_1 , H , and n_1 are identical to the other sections. Section MN 1-7 had a +2 percent slope and achieved a 98.9 percent degree of drainage within 6.5 hours, whereas sections MN 1-11 and MN 1-12 had a -5 percent slope and achieved a 98.9 degree of drainage within 16 hours. Since the sections are identical with the exception of the slopes, it is expected that the section with the largest absolute value of the transverse slope would drain the quickest. This is not the case due to the assignment of a small positive slope (0.00001 percent) for the negative value of slope which was input. This results in a lesser degree of drainage for a given time period.

The program gives an overall rating of the degree of drainage as either satisfactory, marginal, or unsatisfactory based on the Moisture Accelerated Distress (MAD) index.⁽³⁴⁾ The MAD index is based on the time required to drain the pavement to an 85 percent saturation level. The time required to reach the critical level of saturation for all of the Rothsay granular base sections is calculated in the range of 0.02 hours to 0.04 hours for MN 1-1, MN 1-3, and MN 1-4. For MN 1-2, which exhibited a lower permeability, the time to reach the critical degree of drainage is calculated as 0.15 hours. All of the Rothsay sections were rated as a satisfactory drainage design.

Figure 34 shows the relationship between percent saturation of the base course material and the base course modulus for the MN 1 sections with the granular base materials. Similar figures for stabilized materials are meaningless because of the assumptions of the program. As can be seen in the figure, when the base course is saturated, the strength of the material is greatly reduced. A

ROTHSAY, MINNESOTA

% SATURATION VS. BASE MODULUS

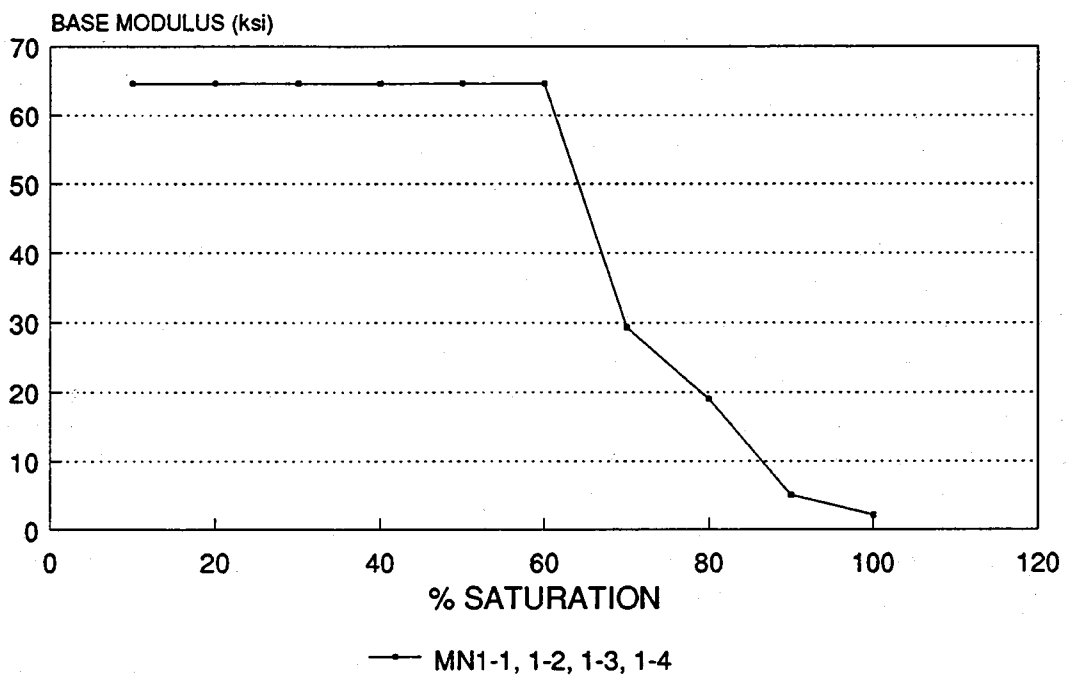


Figure 34. Percent saturation versus base course modulus for MN 1-1, MN 1-2, MN 1-3, and MN 1-4.

rapid decline in strength is seen as the levels of saturation increase from 60 to 100 percent. The relationships used in the determination of the base modulus are as shown in table 21. Because the base materials are well draining, the base is only in the weakened state for 0.04 to 0.05 hours (to a level of 85 percent saturation).

Table 21. Relationships used in the Liu-Lytton drainage program to determine the base strength based on the level of saturation.

Degree of Saturation	Rate of Modulus Change
0 % -- 60 %	Constant
60 % -- 85 %	0.24
> 85 %	3.5

The relationship between the level of saturation of the subgrade and the modulus of the subgrade is shown in figure 35. As the subgrade soil becomes more saturated, the modulus of the subgrade decreases. The fine-grained subgrade soils do not have a critical level of saturation as do the granular base materials. The decrease in modulus is determined by a set of relationships which were developed to determine the strength of the fine-grained soil as a function of the density and the degree of saturation. It is important to note that these relationships were developed *only* for fine-grained soils, which in this case is acceptable. However, in other cases, the subgrade soil is coarse-grained and no guidance is provided on how to input and/or analyze these cases.

The probability of wet base course was calculated to be 0.001 for all of the granular base sections. This probability is based on the rainfall distribution, the system's degree of drainage achieved within a 24-hour period, infiltration of moisture through the surface of the pavement, and the degree of saturation of the base course material. The overall base course modulus for all of the granular sections is calculated as 209.3 ksi (1443 MPa), which seems high for a base course material.¹ This value is computed by considering the wet condition of the base due to precipitation and infiltration, the material strength of the base course affected by the different saturation levels, and the dry and wet probabilities of the base course. The average wet modulus of 209.3 ksi (1443 MPa) is calculated by determining the average of a gamma distribution based on the wet and dry conditions.

¹ The elastic modulus is determined based on material testing performed on various types of materials. Crushed limestone material was determined to have a modulus of 209.3 ksi (1443 MPa) and gravel material was determined to have a modulus of 64.4 ksi (444 MPa). These defaults are built into the program.

ROTHSAY, MINNESOTA

% SATURATION VS. SUBGRADE MODULUS

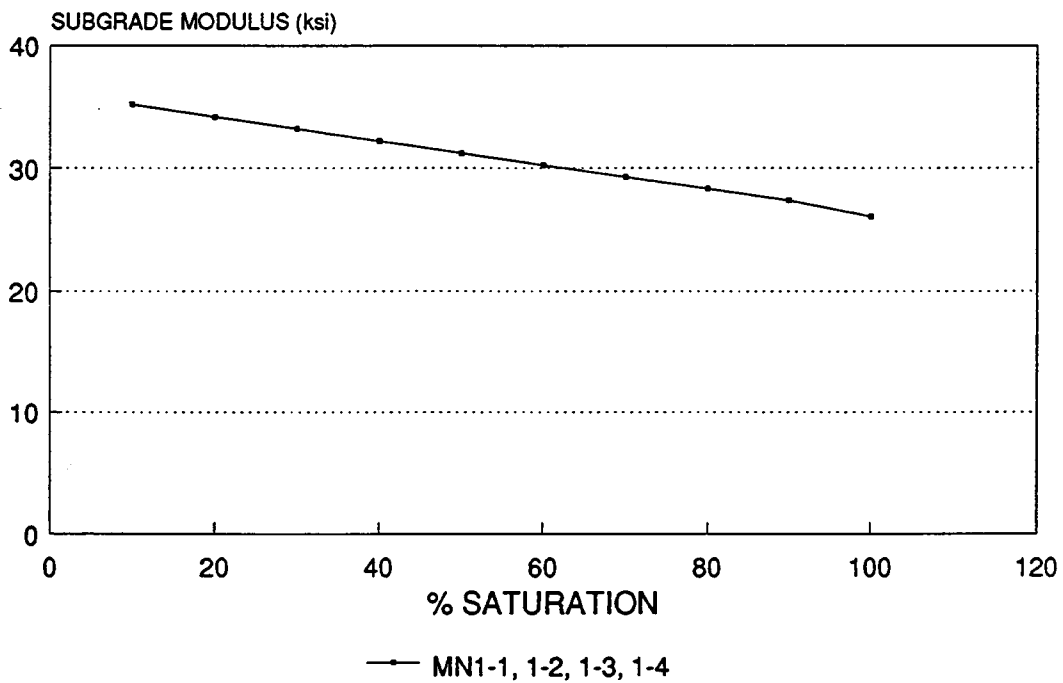


Figure 35. Percent saturation versus subgrade modulus for MN 1-1, MN 1-2, MN 1-3, and MN 1-4.

Tracy, California

The 5 experimental sections located on I-5 near Tracy were evaluated using the Liu-Lytton drainage model. Since the base course is either cement-treated or LCB, the drainability of the 24-in (610 mm) subbase material was evaluated. The results of the drainage time analysis are shown in table 22. Graphically, these results are illustrated in figure 36, for CA 1-1, CA 1-7, and CA 1-9.

Table 22. Summary of the results of the Liu-Lytton percent drainage versus time analyses for CA 1.

Percent Drainage Versus Time To Drain, hours					
Section ID	5 %	25 %	50 %	85 %	99.8 %
CA 1-1	0.0052	0.134	0.678	4.87	12.9
CA 1-3	0.0368	0.431	1.47	3.92	9.54
CA 1-5	0.0176	0.343	1.33	3.84	14.6
CA 1-7	0.0217	0.366	1.33	3.84	14.6
CA 1-9	0.0163	0.331	1.30	4.61	15.8

The slight differences seen in the drainage times between the sections can be attributed to the combination of the permeabilities and porosities of the subbase and subgrade layers. The permeability and porosity of the subbase layer is required as an input to the program; however, the program computes the porosity and permeability of the subgrade layer. The permeabilities and porosities of the subbase and subgrade are shown in table 23.

Table 23. Permeabilities and porosities of subbase and subgrade for CA 1.

Section ID	Subbase		Subgrade	
	k_1 , ft/day	n_1	k_2 , ft/day	n_2
CA 1-1	26.3	0.303	0.110	0.0596
CA 1-3	0.75	0.303	0.110	0.1783
CA 1-5	2.32	0.303	0.110	0.1274
CA 1-7	1.65	0.303	0.110	0.1412
CA 1-9	2.72	0.303	0.110	0.1214

TRACY, CALIFORNIA
% DRAINAGE VS. TIME

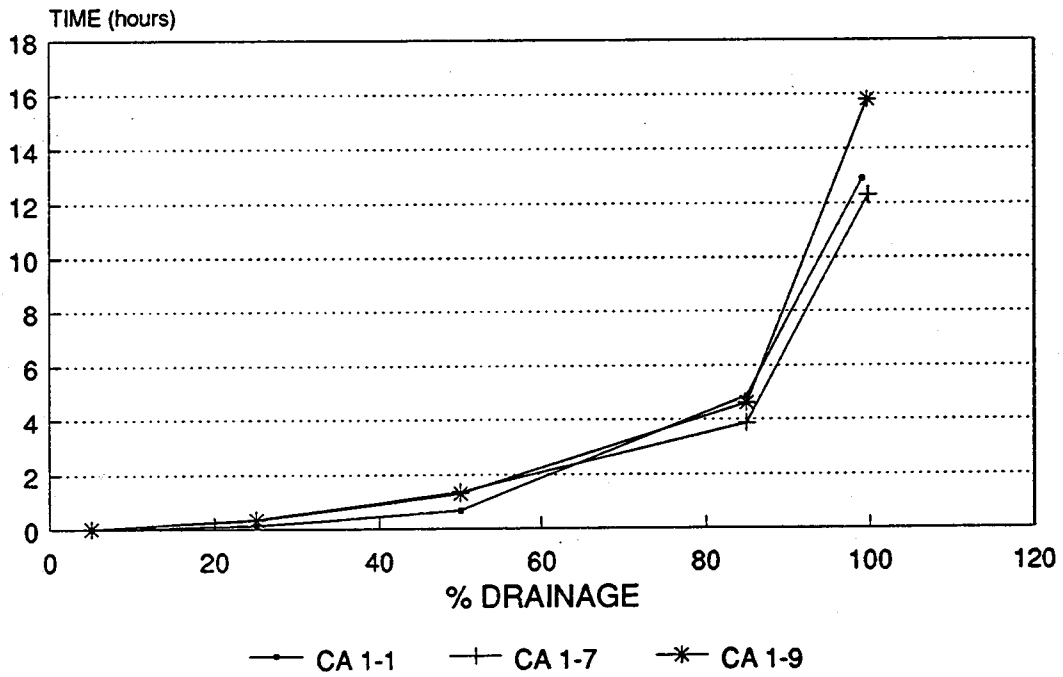


Figure 36. Percent drainage versus time for CA 1-1, CA 1-7, and CA 1-9.

The porosity of the subgrade is calculated by the program through a relationship between the permeability and porosity of the subbase material and the permeability and porosity of the subgrade material. The low calculated porosity of the subgrade material of section CA 1-1 accounts for its relatively low percent of drainage despite its high subbase permeability. The opposite is true for CA 1-3; the high subgrade porosity accounts for the high percent drainage despite its low subbase permeability. It is interesting to note that actually CA 1-3 (lower permeability) initially drains *slower*, which is when drainage is critical. Thus, the material remains at a higher level of saturation for a longer time period. However, once a 33 percent (see equation 30) degree of drainage is achieved, this section drains more rapidly.

Figure 37 shows the relationship between percent saturation of the subbase material and the subbase modulus for CA 1-1, 1-7, 1-9. As can be seen in the figure, when the base course is saturated, the strength of the material is greatly reduced. The reduction in strength is calculated using the relationships presented in table 21.

Table 24 shows the time required for the pavement to reach the 85 percent saturation level. Based on the time required to reach an 85 percent degree of saturation, all of the Tracy sections were rated to exhibit satisfactory drainage.

Table 24. Time required to reach an 85 percent saturation level for CA 1 sections.

Section ID	Time, hours
CA 1-1	0.17
CA 1-3	0.52
CA 1-5	0.40
CA 1-7	0.23
CA 1-9	0.21

The relationship between the saturation of the subgrade and the modulus of the subgrade for CA 1-1, CA 1-7, and CA 1-9 is shown in figure 38. As expected, the modulus of the subgrade decreases as the subgrade soil becomes more saturated. In this case, the subgrade soil is coarse-grained (A-1a and A-2-4). However, in using the model, the soil was modeled as an A-4 soil.

The probability of wet (weakened) subbase course is shown in table 25. The probability of a wet subbase is very small for these sections. Section CA 1-1, which has the highest subbase permeability shows the lowest probability. The average subbase modulus in the wet and the dry states for all of the sections is 64.4 ksi (444 kPA).

TRACY, CALIFORNIA

% SATURATION VS. SUBBASE MODULUS

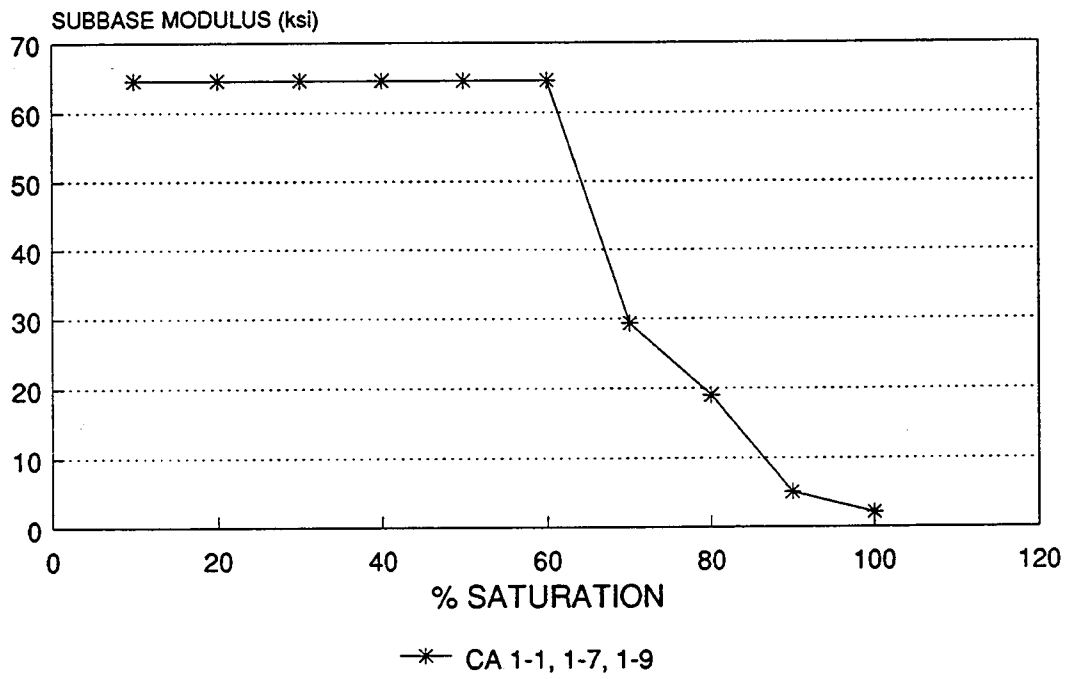


Figure 37. Percent saturation versus subbase modulus for CA 1-1, CA 1-7, and CA 1-9.

TRACY, CALIFORNIA

% SATURATION VS. SUBGRADE MODULUS

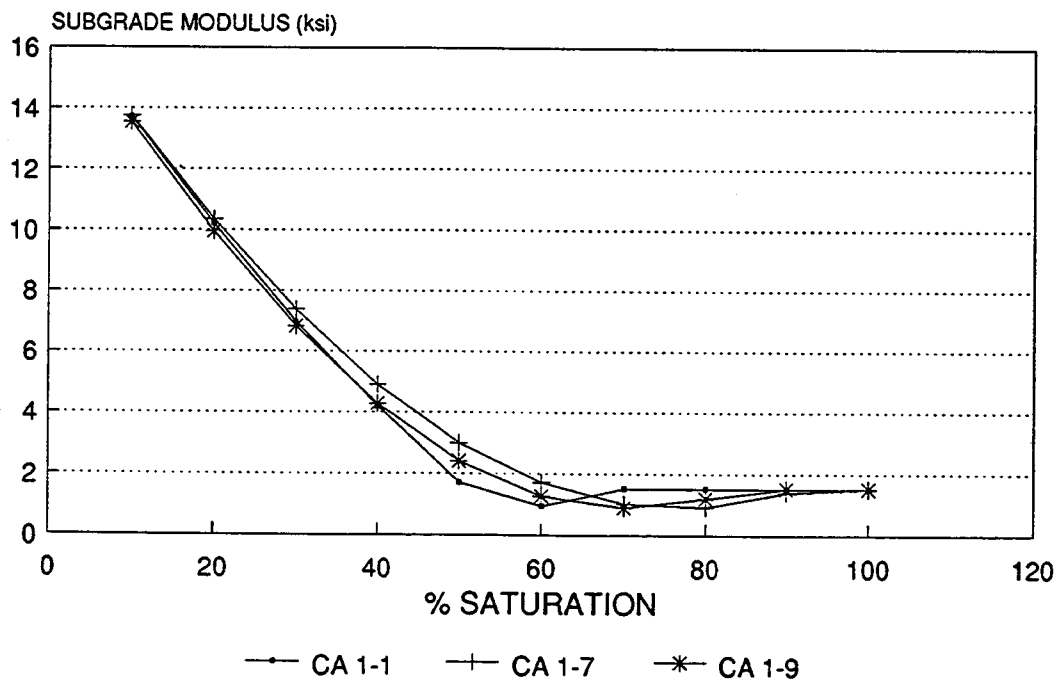


Figure 38. Percent saturation versus subgrade modulus for CA 1-1, CA 1-7, and CA 1-9.

Table 25. Probability of a wet subbase course for the CA 1 sections.

Section ID	Probability of Wet Subbase
CA 1-1	0.006
CA 1-3	0.013
CA 1-5	0.012
CA 1-7	0.012
CA 1-9	0.012

Clare, Michigan

The experimental sections located on US 10 near Clare were evaluated using the Liu-Lytton drainage model. A number of different base course materials were built within the Clare project. These include aggregate base material (MI 1-1a, MI 1-1b, MI 1-7a, and MI 1-7b), permeable asphalt-treated base material (MI 1-4a), and dense-graded, asphalt-treated base material (MI 1-10a, MI 1-10b, and MI 1-25). The permeable asphalt-treated material was analyzed as if it were an aggregate base. The actual permeability of the treated material was used for the analysis. The drainage capabilities of the subbase material was analyzed for sections with asphalt-treated bases and full-depth AC shoulders. The results of the drainage time analysis are shown in table 26. Graphically, these results for MI are illustrated in figure 39.

Table 26. Summary of the results of the Liu-Lytton percent drainage versus time analyses for MI 1.

Section ID	Percent Drainage Versus Time To Drain, hours				
	5 %	25 %	50 %	85 %	99.5 %
MI 1-1a	0.0627	0.260	0.402	4.45	5.32
MI 1-1b	0.264	1.11	1.74	18.1	20.3
MI 1-4a	0.0024	0.0476	0.174	0.444	0.705
MI 1-7a	0.262	1.14	1.94	18.1	23.2
MI 1-7b	0.132	0.584	0.981	8.64	11.7
MI 1-10a	0.0102	0.179	0.588	1.01	1.89
MI 1-10b	0.0174	0.0989	0.226	0.454	0.585
MI 1-25	0.0341	0.170	0.307	0.402	0.574

The differences seen in the drainage times (between the sections) can be attributed to the combination of the permeabilities and porosities of the subbase

CLARE, MICHIGAN

% DRAINAGE VS. TIME

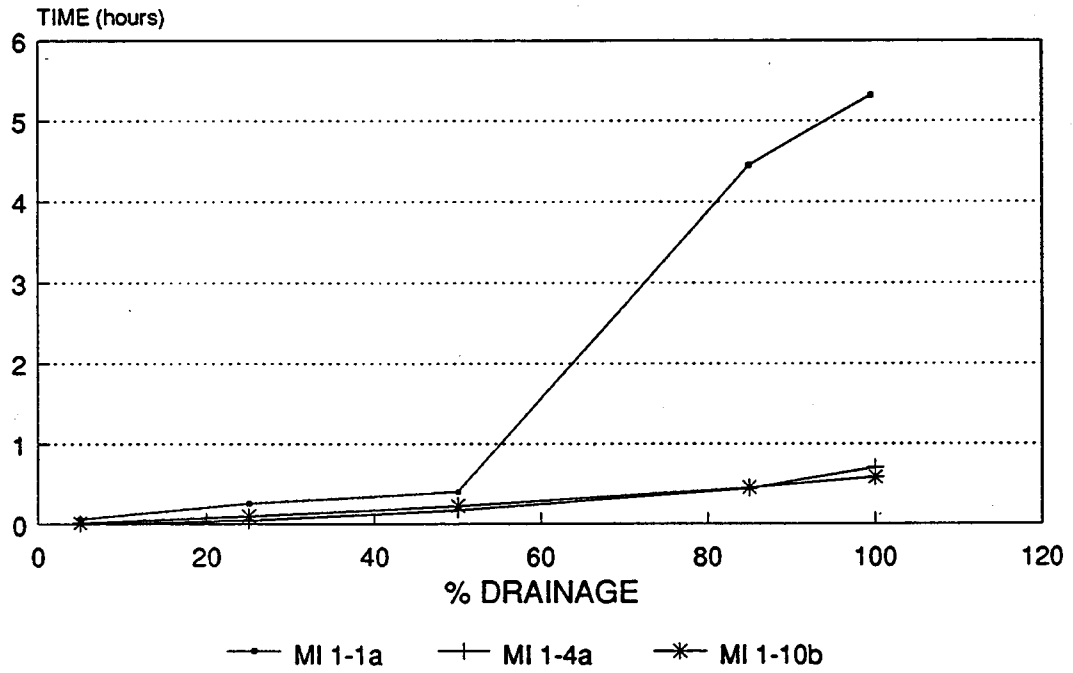


Figure 39. Percent drainage versus time for MI 1-1a, MI 1-4a, and MI 1-10b.

and subgrade layers. The permeabilities and porosities of the subbase and subgrade are shown in table 27.

Table 27. Permeabilities and porosities of subbase and subgrade for MI 1.

Section ID	Subbase		Subgrade	
	k_1 , ft/day	n_1	k_2 , ft/day	n_2
MI 1-1a	0.04	0.189	0.50	0.189
MI 1-1b	0.01	0.201	0.46	0.201
MI 1-4a	316.56	0.900	0.50	0.351
MI 1-7a	0.01	0.195	0.07	0.195
MI 1-7b	0.02	0.195	0.11	0.195
MI 1-10a	4.48	0.308	0.14	0.114
MI 1-10b	0.76	0.326	0.47	0.326
MI 1-25	0.32	0.326	0.62	0.326

Due to the low permeabilities of the dense-graded aggregate base, these sections showed the lowest degree of drainage for a given time. The sections with the asphalt treated material, in which the subbase material was analyzed, show much higher degrees of drainage for a given time period. The high permeability and porosity of the asphalt-treated permeable material (MI 1-4a) account for the high degree of drainage for a given time period.

Figure 40 shows the relationship between percent saturation of the base or subbase material and the base or subbase modulus for MI 1-1a, 1-4a, 1-10b. As can be seen in the figure, when the base course is saturated, the strength of the material is greatly reduced. The reduction in strength is calculated using the relationships presented in table 21. Table 28 shows the time required for the pavement to reach the 85 percent saturation level. Based on the time required to reach an 85 percent degree of saturation, all of the Clare sections appear to exhibit satisfactory drainage.

The relationship between the percent saturation of the subgrade and the modulus of the subgrade for MI 1-1a, MI 1-4a, and MI 1-10b is illustrated in figure 41. As expected, as the subgrade soil becomes more saturated, the modulus of the subgrade decreases. In this case, the subgrade soil is coarse-grained (A-2-4). However, in using the model, the soil was modeled as an A-4 soil. Therefore, the results of this analysis may be misleading.

CLARE, MICHIGAN

% SATURATION VS. BASE OR SUBBASE MODULUS

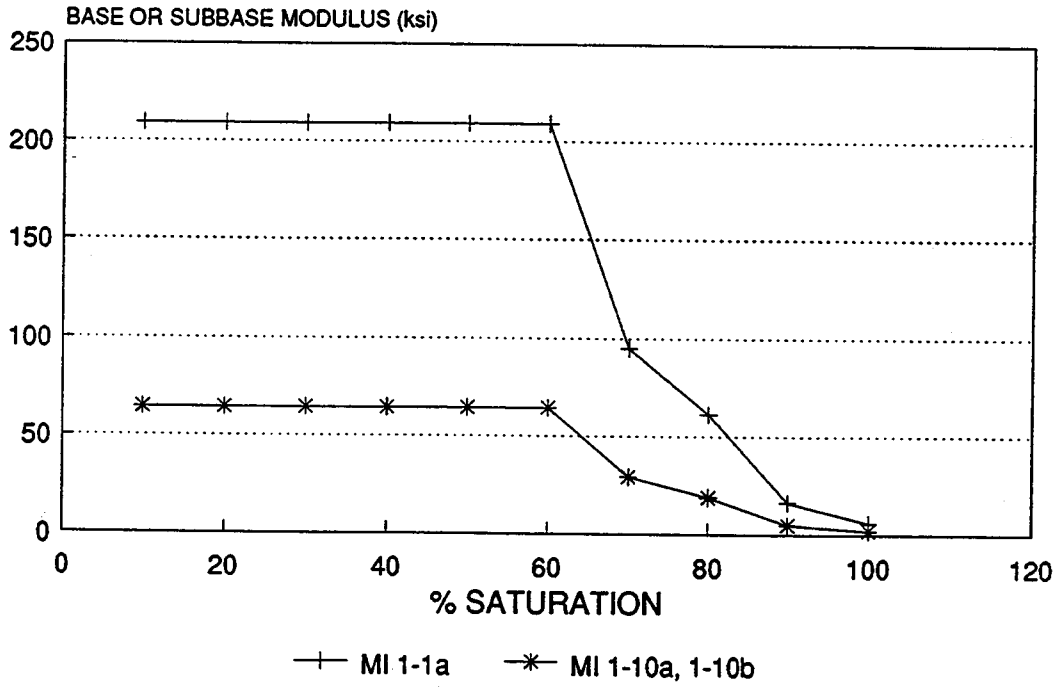


Figure 40 . Percent saturation versus base or subbase modulus for MI 1-1a, MI 1-10a, and MI 1-10b.

CLARE, MICHIGAN % SATURATION VS. SUBGRADE MODULUS

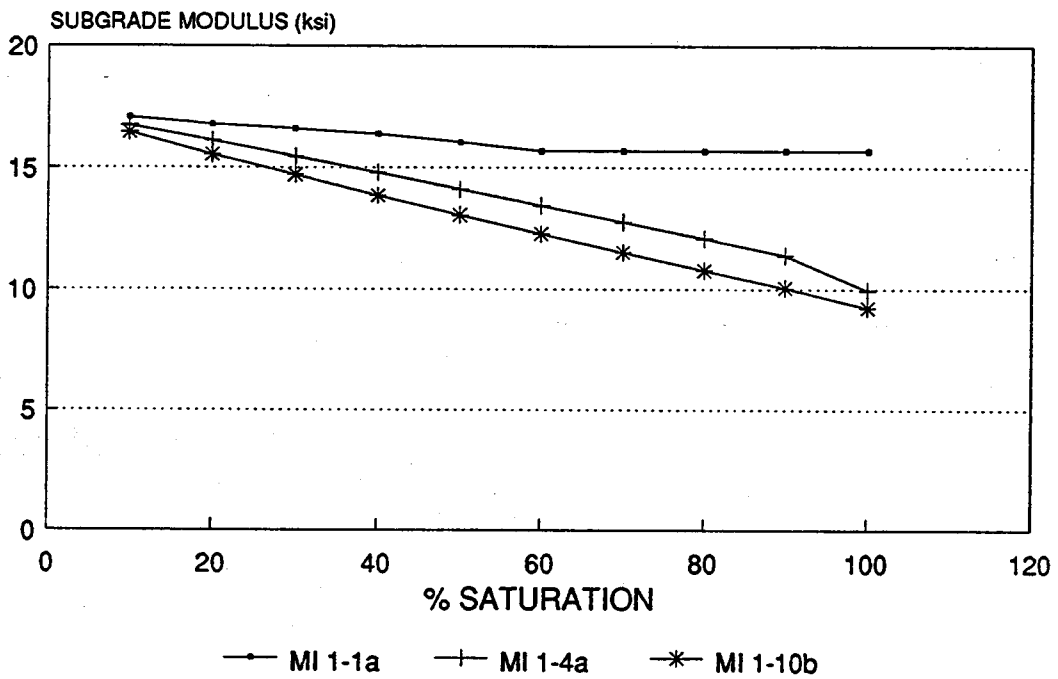


Figure 41. Percent saturation versus subgrade modulus for MI 1-1a, MI 1-4a, and MI 1-10b.

Table 28. Time required to reach an 85 percent saturation level for MI 1 sections.

Section ID	Time, hours
MI 1-1a	0.23
MI 1-1b	1.01
MI 1-4a	0.03
MI 1-7a	1.23
MI 1-7b	0.63
MI 1-10a	0.14
MI 1-10b	0.09
MI 1-25	0.15

The probability of wet (weakened) subbase course is shown in table 29. It is observed that the chances of finding the subbase in the wet state are very small. Again, these probabilities are based on a number of factors including the rainfall distribution, the system's degree of drainage achieved within a 24-hour period, infiltration of moisture through the surface of the pavement, and the degree of saturation of the base course (or subbase) material.

Table 29. Probability of a wet subbase course for the MI 1 sections.

Section ID	Probability of Wet Base or Subbase
MI 1-1a	0.006
MI 1-1b	0.025
MI 1-4a	0.003
MI 1-7a	0.028
MI 1-7b	0.014
MI 1-10a	0.008
MI 1-10b	0.003
MI 1-25	0.004

The average base course modulus in the wet and the dry states for all of the granular base sections is 209.3 ksi (1443 MPa). The average subbase modulus in the wet and dry states for all of the sections with stabilized base courses is 64.4 ksi (444 MPa).

Rocky Mount, North Carolina

A number of different base courses were constructed on this experimental project. These include aggregate bases (NC 1-1, NC 1-4, NC 1-7, and NC 1-8), soil-cement bases (NC 1-2 and NC 1-3), cement-treated bases (NC 1-5), and asphalt-treated bases (NC 1-6). The sections constructed with stabilized base courses were analyzed to evaluate the subgrade drainability by entering the subgrade information for both the base and subgrade inputs.

The results of the drainage time analysis are shown in table 30. Graphically, these results for NC 1-1, NC 1-2, and NC 1-7 are illustrated in figure 42.

Table 30. Summary of the results of the Liu-Lytton percent drainage versus time analyses for NC 1.

Percent Drainage Versus Time To Drain, hours					
Section ID	5 %	25 %	50 %	85 %	99.5 %
NC 1-1	0.0307	0.137	0.216	1.58	2.43
NC 1-2	0.0023	0.547	2.38	6.94	7.39
NC 1-3	0.0373	0.876	3.78	17.8	17.9
NC 1-4	0.0406	0.179	0.285	2.36	3.17
NC 1-5	0.108	2.55	1.11	32.6	34.6
NC 1-6	0.0246	0.579	2.50	11.8	11.8
NC 1-7	0.0284	0.127	0.201	1.38	2.14
NC 1-8	0.0265	0.119	0.188	1.18	1.92

The sections with the granular base materials drained far more rapidly than those with stabilized layers. Since the analysis of impermeable stabilized bases is not possible, the subgrade was evaluated in lieu of the stabilized layer. The subgrade was a course-grained A-2-4 material for all sections with the exception of NC 1-5 which was an A-4 material. The degree of drainage exhibited by this section relative to the others is much lower due to the lower permeability of the A-4 material (0.11 ft/day [0.03 m/day]) relative to the A-2-4 material (0.500 ft/day [0.15 m/day]) and A-2-6 material (0.33 ft/day [0.10 m/day]).

Figure 43 shows the relationship between percent saturation of the base or subbase material and the base or subbase modulus for the sections with a granular base course. As can be seen in the figure, when the base course is saturated, the strength of the material is greatly reduced. The reduction in strength is calculated using the relationships presented in table 21.

ROCKY MOUNT, NORTH CAROLINA

% DRAINAGE VS. TIME

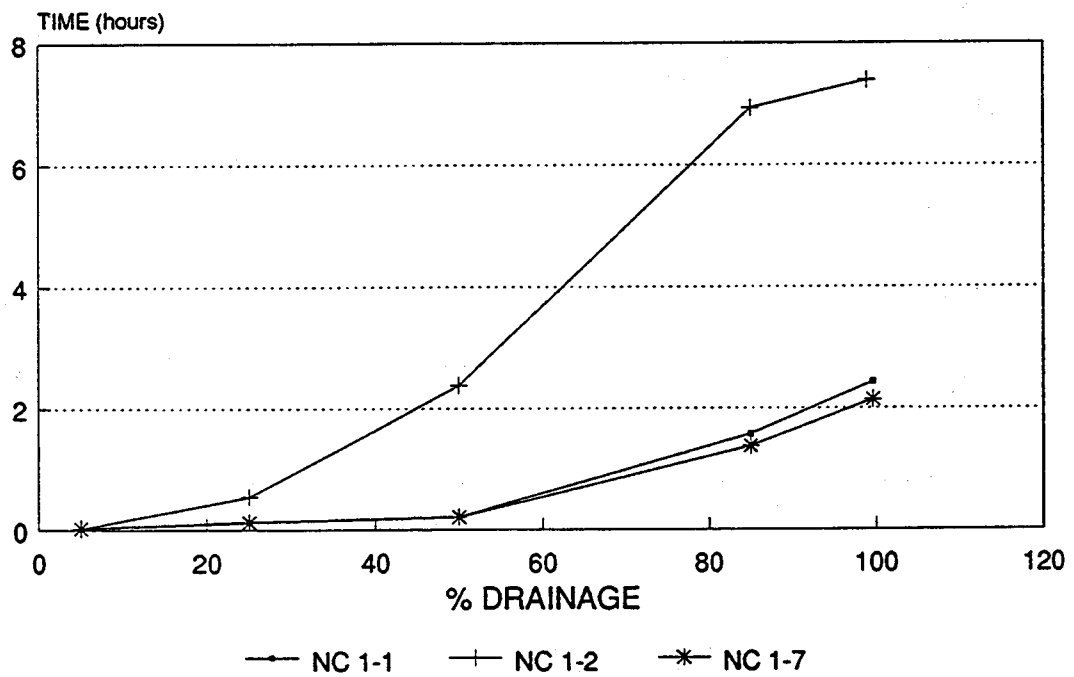


Figure 42. Percent drainage versus time for NC 1-1, NC 1-2, and NC 1-7.

ROCKY MOUNT, NORTH CAROLINA

% SATURATION VS. BASE MODULUS

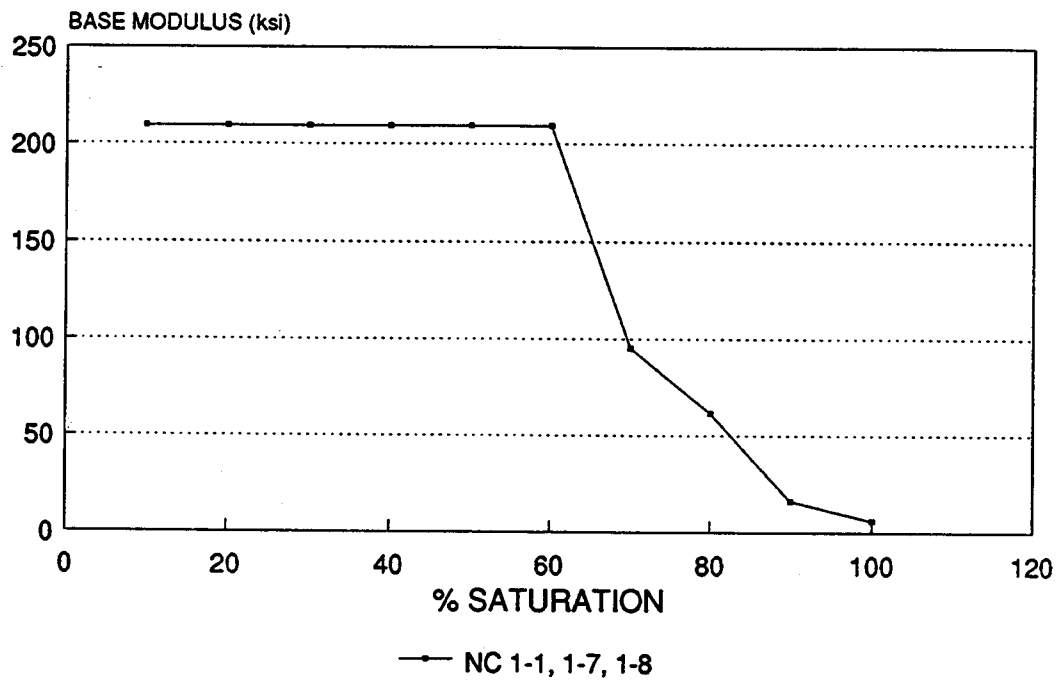


Figure 43. Percent saturation versus base modulus for NC 1-1, NC 1-7, and NC 1-8.

Table 31 shows the time required for the pavement to reach the 85 percent saturation level. Based on the time required to reach an 85 percent degree of saturation, all of the Rocky Mount sections appeared to exhibit satisfactory drainage.

Table 31. Time required to reach an 85 percent saturation level for NC 1 sections.

Section ID	Time, hours
NC 1-1	0.14
NC 1-2	0.61
NC 1-3	0.98
NC 1-4	0.19
NC 1-5	2.84
NC 1-6	0.65
NC 1-7	0.13
NC 1-8	0.13

The relationship between the degree of saturation of the subgrade and the modulus of the subgrade for the sections with granular base course material illustrated in figure 44. As the subgrade soil becomes more saturated, the modulus of the subgrade decreases. In this case, the subgrade soil is coarse-grained (A-2-4 or A-2-6). However, using the model, the soil was modeled as an A-4 soil.

The probability of wet (weakened) base course is calculated as 0.002 for all of the sections with granular base materials. The probability of a wet subbase is very small for all sections. The average base course modulus in the wet and the dry states for all of the sections is 209.3 (1443 MPA).

Conclusion and Recommendations

The Liu-Lytton drainage model provides useful information in the analysis of a pavements drainage capabilities as well as the effects of moisture on the strength of the pavement system. The model uses area-specific climatic data, surface infiltration potential, and material properties to determine the dry and wet strengths of the pavement layers. The overall drainage capacity of the pavement system is also determined through the analysis of the time required to drain the layers to a critical degree of saturation.

This program may prove very useful in the design process. The design of pavement drainage is critical to pavement design and performance. Since site-specific climatic data is used, the designer can determine the potential for moisture

ROCKY MOUNT, NORTH CAROLINA

% SATURATION VS. SUBGRADE MODULUS

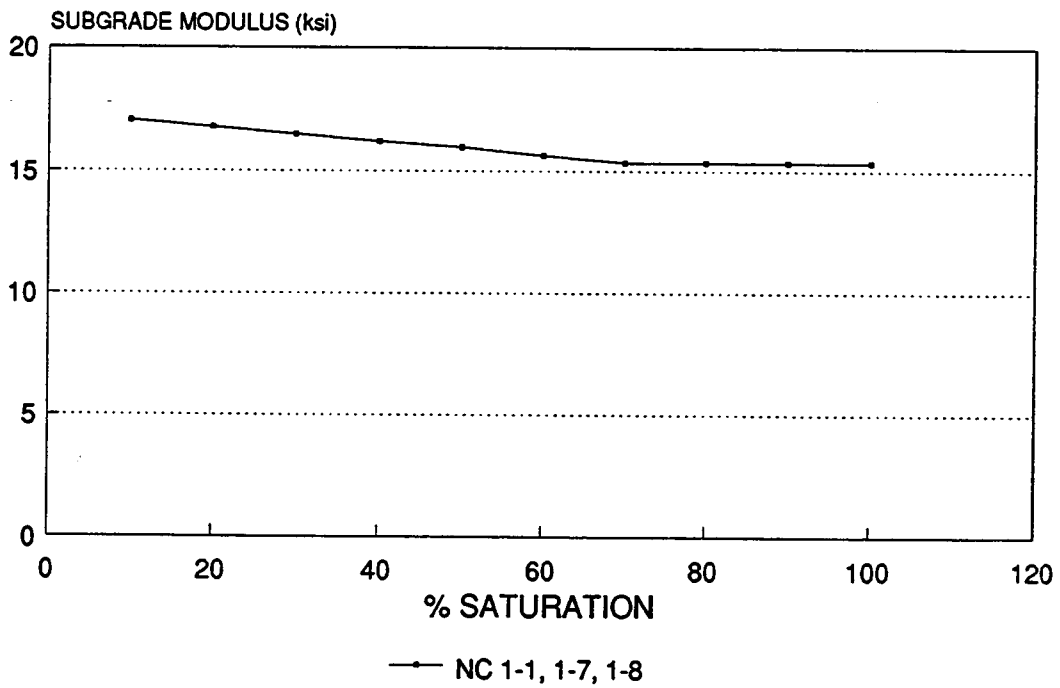


Figure 44. Percent saturation versus subgrade modulus for NC 1-1, NC 1-7, and NC 1-8.

problems within the locality of construction. The effect of changing the density and, therefore, the permeability of granular materials can be determined during the design process. The most probable strength of the materials within the paving system can be determined and used as inputs into a structural analysis program or a design procedure. This can greatly aid the design engineer to more accurately characterize the materials properties.

Several problems were encountered in the execution of the program. These problems are outlined below:

- The program will not accept impermeable base course layers. An option to choose a cement or lime stabilized layer exists, however, the permeability must be greater than or equal to 0.0001 ft/day (0.00003 m/day).
- The program only accepts a single base course layer beneath the slab. Very often, concrete pavements are constructed with a base layer and a subbase layer. These layers typically have different drainage properties. The program provides no provision for this condition.
- The material strengths are fixed based on testing for the types of materials which are allowable within the program. For example, a crushed limestone material is assumed to have a modulus of 209.3 ksi (1443 MPa) and a gravel material is assumed to have a modulus of 64.4 ksi (444 MPa). The user cannot input specific values for construction materials that will be used in a particular design. The default values are useful in some cases, although the option should be given to specify materials properties based on testing of the materials to be used in design.
- Only fine-grained (A-4 through A-7-6) subgrade materials are capable of being analyzed. The development of models to include coarse-grained soils should be developed and incorporated into the program.
- Only select input variables are echoed in the output file. It is valuable to the user to have a listing of the input variables used to calculate the program results. This prevents shuffling between a fixed-format input file and the output file.
- The format limits the number of consecutive dry-days to less than or equal to 99. For Tracy, California, there were more than 140 consecutive dry-days in 1987; the program should be expanded to consider more consecutive dry-days.
- The sign convention for the transverse slope is not defined within the program documentation, user's guide, or input processor. This should be clarified.

5. ANALYSIS OF JSLAB AND ILLISLAB

Introduction

A comparative evaluation of JSLAB and ILLISLAB was performed on the MI 1 sections located on U.S. 10 near Clare, Michigan. The relative technical merits and the ease of use of each program were evaluated to determine the program which allows the most flexibility for the in-depth analyses.

The capabilities and limitations of the two programs are provided in detail in volume VI, "*Synthesis of Concrete Pavement Design Methods and Analysis Models.*" In general, the two programs have similar features, with four very important differences:

1. ILLISLAB has the capability of modeling the subgrade with several different subgrade formulations. Although the Winkler foundation (dense liquid formulation) was used throughout this project and is the subgrade model used by JSLAB, it is believed that the response of the subgrade to repeated wheel loadings may be more accurately modeled using one of the other subgrade formulations. The program allows the user to choose between the Winkler formulation, elastic solid formulation, a stress dependent support model, the Vlasov formulation, and a spring constant model. These formulations may be used to more accurately model the pavement response to wheel loading. These subgrade models are explained in much greater detail in reference 16.
2. In the determination of thermal gradient stresses, the JSLAB program requires the user to perform two separate executions of the program and manually subtract the results to determine the thermal stresses. The user must also manually establish the loss of support conditions caused by the thermal stresses and modify the support conditions in subsequent executions. The program documentation states that three to four iterations are typically required to establish the appropriate support conditions.⁽¹⁸⁾ Therefore, in order to obtain *one* thermal stress the user must execute the program four to five times. This need to perform repetitive numerical operations is both time-consuming and an invitation to human error. On the other hand, the ILLISLAB program provides an iterative computation routine to model thermal gradient stresses within the program, both relieving the user of the tedious task of performing manual iterations and reducing the chance of human error. Also, since the ILLISLAB program requires the user to input the tolerance required for the loss of support conditions, no technical judgment concerning the convergence of a solution is required on the part of the user. The user simply inputs the number of iterations and, if the tolerances are not met, a message is given in the output file to increase the number of iterations.

3. The JSLAB model does not calculate subgrade stresses. Examination of the subgrade stress under a given load provides an indication of the stress levels that the subgrade will experience. The subgrade stress could be examined to study the repeated load behavior of the subgrade soil. This sort of analysis gives an indication of the stress sensitivity of the soil and thus the ability of the soil to withstand the expected loadings.
4. The JSLAB program does allow the user to model the dowel geometry as square or round. Although this feature was not used under this study, it may be useful to examine the effectiveness of different dowel bar geometries. The ILLISLAB program only allows the use of round dowel bars.

Several misconceptions that exist for both of these programs include:

- ILLISLAB has had the capability of modeling nonuniformly spaced dowels since the 1985 version of the program. JSLAB also has this capability. This option was not required under this study; however, it would be a useful tool in the examination of nonuniformly spaced dowels. Both programs also have the capability of modeling hollow dowel bars.
- JSLAB purports to be able to calculate moisture stresses. Actually, guidelines are given for the transformation of moisture gradients to equivalent thermal gradients. These transformation guidelines are pertinent for application of the moisture gradient under any circumstances.

Analysis of Results

The Clare, Michigan (MI 1) sections were chosen for the analysis of the two finite element programs. Each of the programs were run for the eight sections to determine the stresses and deflections for edge and corner loading conditions (no thermal curling). The programs were also executed to examine the independent effect of a temperature gradient through the slab. The results of these analyses are presented in tables 32 through 36. For a given section, exactly the same finite element mesh and load (or thermal gradient) was used for the execution of the programs. As an example of a typical mesh, the finite element mesh developed for the edge loading condition for MI 1-4a is shown in figure 45.

The maximum stresses and deflections were determined beneath a 14.4-kip (64 kN) dual wheel load having a tire pressure of 120 psi (83 kPa). The thermal gradients used for the analysis were determined for the environmental conditions at Clare through use of the CMS computer program. All of the required design inputs (e.g., thickness, slab length, dowel spacing and diameter, and others) used in this analysis are found in the summary tables in volume IV. The

Table 32. Summary of maximum surface deflection as calculated by ILLISLAB and JSLAB for a 14.4 kip (64 kN) dual wheel load with a tire pressure of 120 psi (83 kPa) placed at the slab's edge.

Section ID	Deflection, mils	
	ILLISLAB	JSLAB
MI 1-1a	24.0	25.6
MI 1-1b	25.4	28.2
MI 1-4a	17.3	22.0
MI 1-7a	24.3	30.1
MI 1-7b	25.7	31.6
MI 1-10a	20.8	23.1
MI 1-10b	19.0	22.0

Note: Effect of thermal gradient not included.

Table 33. Summary of maximum tensile stress as calculated by ILLISLAB and JSLAB for a 14.4 kip (64 kN) dual wheel load with a tire pressure of 120 psi (83 kPa) placed at the slab's edge.

Section ID	Maximum Tensile Stress, psi	
	ILLISLAB	JSLAB
MI 1-1a	431	397
MI 1-1b	440	412
MI 1-4a	372	381
MI 1-7a	434	404
MI 1-7b	429	408
MI 1-10a	432	393
MI 1-10b	411	373

Note: Effect of thermal gradient not included.

Table 34. Summary of maximum surface deflection as calculated by ILLISLAB and JSLAB for a 14.4 kip (64 kN) dual wheel load with a tire pressure of 120 psi (83 kPa) placed at the slab's corner.

Section ID	δ Under Load, mils	ILLISLAB		JSLAB		
		δ Across Joint, mils	δ Load Transfer, %	δ Under Load, mils	δ Across Joint, mils	δ Load Transfer, %
MI 1-1a	28.9	28.9	100	35.8	35.8	100
MI 1-1b	31.7	22.8	73	37.3	27.2	71
MI 1-4a	37.7	8.6	23	41.5	7.5	18
MI 1-7a	30.5	30.5	100	33.9	33.9	100
MI 1-7b	32.5	32.5	100	39.4	39.4	100
MI 1-10a	33.5	13.0	39	38.6	14.4	37
MI 1-10b	31.7	12.7	40	36.3	15.2	42

Note: Effect of thermal gradient not included.

Table 35. Summary of maximum tensile stress as calculated by ILLISLAB and JSLAB for a 14.4 kip (64 kN) dual wheel load with a tire pressure of 120 psi (83 kPa) placed at the slab's corner.

Section ID	σ Under Load, psi	ILLISLAB		JSLAB		
		σ Across Joint, psi	σ Load Transfer, %	σ Under Load, psi	σ Across Joint, psi	σ Load Transfer, %
MI 1-1a	104.7	104.7	100	99.9	99.9	100
MI 1-1b	157.5	52.0	33	149.8	52.8	35
MI 1-4a	206.0	12.4	6	203.7	14.3	7
MI 1-7a	108.0	108.0	100	100.9	100.9	100
MI 1-7b	106.0	106.0	100	98.3	98.3	100
MI 1-10a	160.2	33.9	17	154.9	26.3	17
MI 1-10b	167.8	31.9	19	164.9	29.7	18

Note: Effect of thermal gradient not included.

Table 36. Summary of maximum thermal stress as calculated by ILLISLAB and JSLAB.

M A X I M U M T H E R M A L S T R E S S , p s i

Section ID	Positive Gradient (+3.0 °F/in [1.67 °C/mm])		Negative Gradient (-1.0 °F/in [-0.56 °C/mm])	
	ILLISLAB	JSLAB	ILLISLAB	JSLAB
MI 1-1a	479	856	-173	-285
MI 1-1b	509	814	-182	-271
MI 1-4a	165	188	-114	-60.9
MI 1-7a	146	167	-107	-58.8
MI 1-7b	143	165	-103	-48.2
MI 1-10a	162	179	-116	-59.7
MI 1-10b	166	186	-111	-58.9

Note: MI 1-1 sections have long 71-ft slabs which are actually designed to crack. The actual thermal stresses will not be as high as indicated because of thermal cracks occurring in the pavement.

Sign Convention: (+) tension
 (-) compression

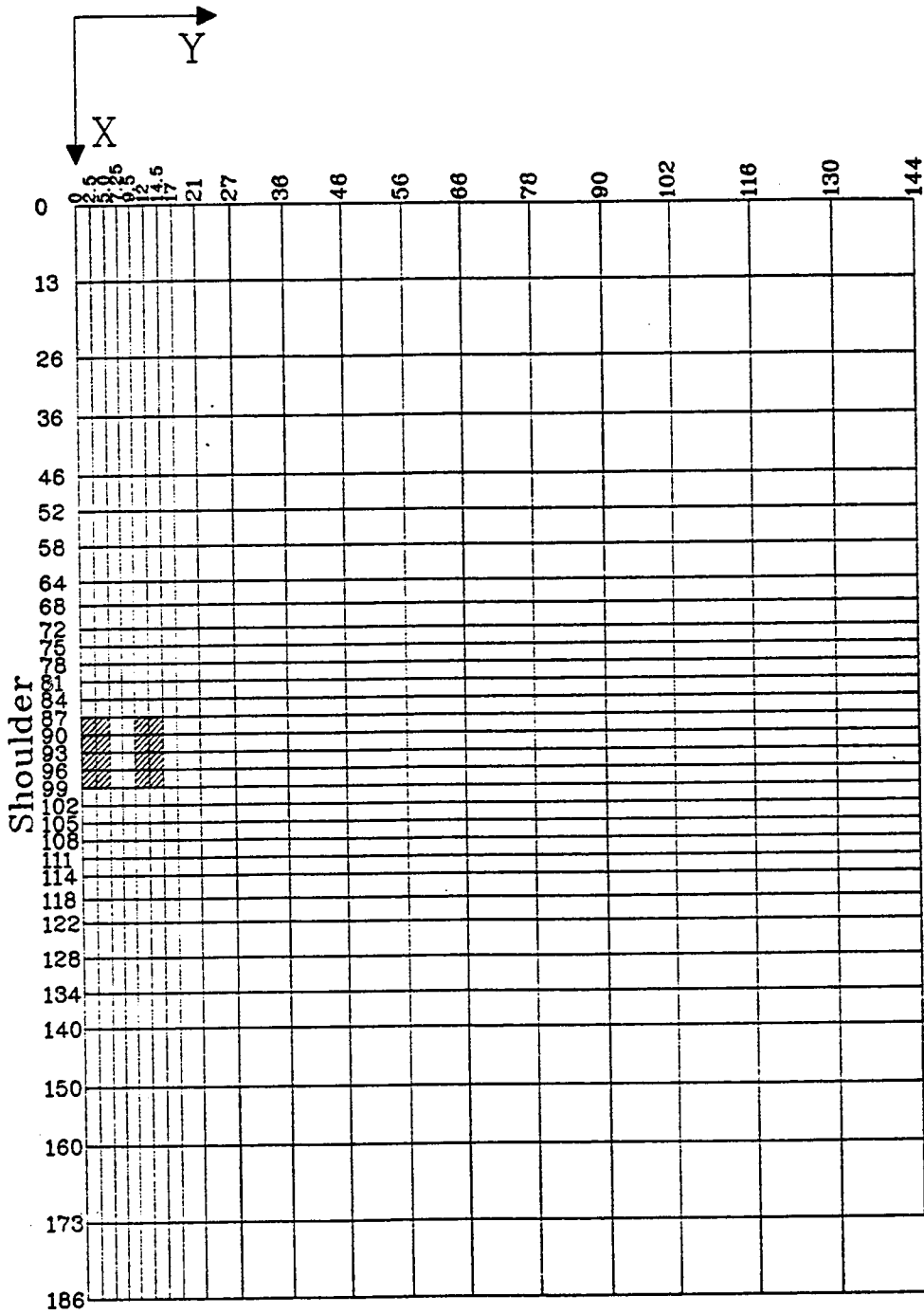


Figure 45. Example finite element mesh for the edge loading condition.

modulus of the surface (E_{pc}) and the *static* modulus of subgrade reaction (k_{stat})² were used to model the strength and support conditions of the pavement system. The slab lengths for sections which were constructed with random joint spacings were modeled using the average of the random joint spacing.

Analysis of the Edge Loading Condition

Since all of the MI 1 sections have full-depth asphalt concrete (AC) shoulders, the edge loading condition was modeled as a free edge. As expected, the point of maximum tensile stress and surface deflection was directly beneath the load at the outermost edge of the slab. The deflections as calculated by both ILLISLAB and JSLAB are shown in table 32. The deflections calculated by JSLAB are substantially higher than those calculated by ILLISLAB, over 20 percent higher in some cases. For the simple case of the single slab, edge loading condition, the two programs should produce *identical* deflections. The only explanation of this difference in deflections is the stiffness matrix defined within the finite element programs. JSLAB was based on a very early version of ILLISLAB, one in which the stiffness matrix was in error.⁽¹⁶⁾ The matrix was corrected in subsequent ILLISLAB versions in the early 1980's. It appears that the stiffness matrix in JSLAB is different than the stiffness matrix in ILLISLAB. ILLISLAB's stiffness matrix has been documented and shown to be correct by Ioannides.⁽¹⁶⁾

The edge stresses as calculated by ILLISLAB and JSLAB are shown in table 33. The stresses as calculated by the two programs differ by less than 10 percent. The difference in stresses can also be attributed to the error in JSLAB's stiffness matrix. The difference in stresses is less pronounced than the difference in deflections since the deflection calculation is directly resultant from the stiffness matrix, whereas the stresses are calculated through a series of calculations in which the effect of the error may be distorted through floating point calculations.

Analysis of the Corner Loading Condition

The results from each of the programs for the corner loading condition are shown in tables 34 and 35. In modeling the corner condition, the effect of load transfer was considered. In modeling the load transfer efficiency within the finite element models, every effort was made to match the deflection (δ) load transfer efficiency, as calculated from the Falling Weight Deflectometer (FWD) deflections,

² An estimate of the static k -value (k_{stat}) can be obtained by multiplying the backcalculated k -value by 0.5.

within 5 percent.³ The effect of voids beneath the slab were not considered for this analysis, however, their effects are considered in section 5 of this chapter.

Again, the errors in the JSLAB stiffness matrix yield deflections which are significantly higher than those calculated using ILLISLAB. The deflections on either side of the joint (both approach and leave sides of the joint) as calculated by JSLAB are 10 to 20 percent higher than those calculated by ILLISLAB. However, the modeling of load transfer efficiency was *not* affected by the difference in deflections between ILLISLAB and JSLAB. This is probably due to the fact that JSLAB consistently calculates higher deflections on *both* sides of the joint so the resulting load transfer efficiency, which is a ratio of the unloaded deflection to the loaded deflection, is relatively unaffected.

The corner stresses as calculated by ILLISLAB and JSLAB differ by approximately 10 percent. This is again due to JSLAB's stiffness matrix error. As with the case of the δ load transfer, the stress (σ) load transfer is unaffected by the error in the stiffness matrix.⁴ Again, this is probably due to the calculated σ load transfer being a ratio which evidently cancels out.

Analysis of a Temperature Gradient Through the Slab

The stresses due to a temperature gradient through the slab as calculated by the two programs are shown in table 36. The programs were executed for the case of a single, unconstrained slab without a wheel load. The thermal stresses as calculated by JSLAB are higher for the case of a positive thermal gradient and lower for the case of a negative thermal gradient. One explanation for this is that the JSLAB program ignores the effect of Poisson's ratio (ν). This can account for 10 to 15 percent of the difference in the stresses. As previously mentioned, the JSLAB program requires the user to execute the program a number of times and manually manipulate the data to determine the thermal gradient stresses.

Conclusions

The ILLISLAB program has been chosen for the remainder of the case studies for the following reasons:

1. The stiffness matrix in the ILLISLAB program has been shown to be correct.⁽¹⁶⁾ The JSLAB stiffness matrix appears to be in error because the

³ Deflection load transfer efficiency is defined as the δ of the unloaded slab (across the joint) divided by the δ of the loaded slab, multiplied by 100.

⁴ The stress load transfer efficiency is defined as the σ developing in the unloaded slab divided by the σ developing in the loaded slab and multiplied by 100. The σ load transfer efficiency is only equal to the δ load transfer efficiency at 0 percent and 100 percent load transfer efficiencies.

deflections are 10 to 20 percent higher than those calculated by ILLISLAB for identical inputs. In fact, JSLAB is based on an earlier version of ILLISLAB which was later shown to contain an error in the stiffness matrix.

2. In modeling the effect of a temperature thermal gradient through a slab, the ILLISLAB program correctly accounts for the effect of the concrete Poisson's ratio. The JSLAB program ignores the effect of Poisson's ratio altogether, which can account for a 10 to 15 percent difference in the stresses calculations between the two models. Also, in order to determine the thermal stress as calculated by JSLAB, the user must perform a number of executions of the program and manually manipulate the data. This approach is time-consuming and lends itself to human error.
3. ILLISLAB calculates the subgrade stresses, whereas JSLAB does not.
4. Like JSLAB, ILLISLAB has the ability to model nonuniform dowel spacings.
5. ILLISLAB allows the engineer to choose from a variety of subgrade formulations. This allows the engineer to select the most accurate subgrade formulation for the specific application.
6. The guidelines presented in the documentation on the JSLAB program concerning the development of moisture stresses are directly applicable to the ILLISLAB program.

6. EVALUATION OF THE ILLISLAB PROGRAM

Introduction

The performance of portland cement concrete is dependant on the stress induced in the material through repeated loading of various magnitudes. The accurate determination of the stress induced in a concrete pavement is critical in the determination of the number of repeated loadings possible before the slab begins to fail in fatigue. Nearly all design procedures are based on this concept. The procedures hinge on the accurate determination of the stresses which develop in slab. The ILLISLAB program is capable of determining the stresses induced by both axle loadings and temperature differences through the slab.

The ILLISLAB program is a finite element structural analysis program for the analysis of rigid pavements. Using design and material properties information, the stresses, deflections, and moments are calculated for the given slab configuration. The program is capable of modeling many design and analysis features, including, among others, various subgrade formulations, load transfer configurations, bonding conditions between layers, and axle load configurations. The program can examine any number of slabs in any arrangement and is also capable of calculating stress due to a temperature difference between the top and bottom of the slab.

Brief Technical Description

The ILLISLAB program is a finite element program which is based on medium-thick plate theory. It employs the four-noded, 12-degree of freedom plate bending (ACM or RPB 12) element.^(15,16) The mechanics of the finite element method is quite complicated and will not be discussed in detail herein, however, reference 39 presents the method in detail.

The ILLISLAB program was first developed in 1977 and has been under continuous revision, verification, and expansion at the University of Illinois. Through several research studies the program's accuracy and ease of application has been improved. Revisions have also been made to facilitate meaningful interpretation of its results and to incorporate new foundation models.

A short description of the basic assumptions regarding the concrete slab, stabilized base course, subgrade type, overlay, dowel bars, and aggregate interlock follows:

1. Small deformation theory of an elastic, homogeneous medium thick plate is employed for the concrete slab, stabilized base, and overlay. Such a plate is thick enough to carry a transverse load by flexure, yet it is not so thick that transverse shear forces become important.
2. The weight of the slab is neglected in the load stress calculations; however, it is considered in the calculation of temperature-induced stresses.
3. In the case of a bonded base or overlay, full strain compatibility exists at the interface. For the case of an unbonded base or overlay, shear stresses at the interface are neglected.
4. Dowel bars at joints are linearly elastic and are located at the neutral axis of the slab.
5. When aggregate interlock is specified for load transfer, load is transferred from one slab to another through shear. However, with dowel bars, some moment as well as shear is transferred across the joints. The *aggregate interlock factor* can range from 0.0 to more than $1 * 10^8$ for associated deflection load transfer efficiencies of 0 percent to 100 percent. This relationship is nonlinear and quite complex.
6. Several foundation support models have been incorporated into the ILLISLAB program, including the traditional Winkler foundation, elastic solid foundation, a spring model foundation, a "resilient" foundation model, and the Vlasov two-parameter foundation.

7. Loss of support beneath the slab may be modeled through the reduction of the support values at user specified areas.

Analysis of Results

The ILLISLAB program was executed for each pavement section evaluated in Minnesota, California, Michigan, and North Carolina to analyze the stress at the lane-shoulder joint midpoint between the transverse joints. The corner condition was also analyzed for several sections within each State. In this analysis the deflection load transfer efficiency, which was determined through the FWD testing, was modeled through the use of the aggregate interlock factor and dowel and tiebar configuration. An analysis was performed on MI 1-10a to model a specific corner which exhibited loss of support. The stresses induced by a thermal gradient were analyzed for the Rothsay, Minnesota (MN 1), Tracy, California (CA 1), Clare, Michigan (MI 1), and Rocky Mount, North Carolina (NC 1) sections.

The design information required to execute the program (slab thickness, joint spacing, PCC modulus of elasticity, k -value on top of the base, and others) are illustrated for each section in the summary tables in volume IV. Sections with random joint spacing were modeled using the average joint spacing.

Analysis of the Edge Loading Condition

In the analysis of the edge loading condition, the slab was loaded at the midpoint between the joints with a 14.4 kip (64 kN) dual wheel load and a tire pressure of 120 psi (83 kPa). A typical finite element mesh employing this load configuration is shown in figure 45. Sections with tied PCC shoulders were modeled using each sections individual tiebar configuration. The deflection load transfer efficiency, which was calculated from the results of the FWD testing, was matched in the ILLISLAB analysis through the use of the aggregate interlock factor. The sections with asphalt concrete shoulders were modeled as a free edge.

The result of the edge loading analysis are shown in table 37. As expected, the point of maximum tensile stress, subgrade stress and surface deflection was directly beneath the load at the outermost edge of the slab. The overall trends observed in the data are outlined below:

1. Sections with tied concrete shoulders and high and medium levels of deflection load transfer exhibited lower deflections, edge stresses, and subgrade stresses. The sections at Albert Lea, Minnesota (MN 2) are an excellent example of this trend. An average stress of 489 psi (3.4 MPa) was calculated for the 9-in (229 mm) thick sections with the asphalt shoulders, whereas the stress calculated for a 9-in (229 mm) thick section with tied concrete shoulders (100 percent deflection load transfer) was only 244 psi (1.7 MPa). This general trend can be seen throughout the data. For example, the California and Michigan sections with asphalt shoulders have much higher stresses and

Table 37. Summary of maximum surface deflection, maximum edge stress, and maximum subgrade stress as calculated by ILLISLAB for a 14.4 kip (64 kN) dual wheel load with a tire pressure of 120 psi (83 kPa) placed at the slab's edge.

Section ID	Maximum Surface Deflection, mils	Maximum Edge Stress, psi	Maximum Subgrade Stress, psi
MINNESOTA			
MN 1-1	13.0	235.6	2.48
MN 1-2	27.1	489.6	2.33
MN 1-3	15.0	283.2	3.26
MN 1-4	29.0	563.9	3.22
MN 1-5	22.1	568.3	3.36
MN 1-6	20.8	557.8	3.27
MN 1-7	19.9	464.3	3.85
MN 1-8	13.8	419.1	3.91
MN 1-9	10.8	224.6	3.14
MN 1-10	21.8	450.3	3.11
MN 1-11	12.7	282.3	3.10
MN 1-12	26.0	562.2	3.11
MN 5	29.2	486.6	2.37
MN 2-1	19.9	244.1	2.54
MN 2-2	21.7	293.4	2.75
MN 2-3	28.4	496.6	4.53
MN 2-4	32.5	480.9	4.54
MN 3	7.87	239.7	1.01
MN 4	12.1	310.7	1.35
MN 6	11.0	281.3	1.09
CALIFORNIA			
CA 1-1	41.9	397.6	4.86
CA 1-3	24.3	435.7	4.24
CA 1-5	17.0	263.5	2.84
CA 1-7	20.5	467.1	4.44
CA 1-9	24.6	491.5	3.67
CA 2-2	9.77	395.3	6.95
CA 2-3	15.5	330.6	4.43
CA 3-1	17.3	313.5	2.48
CA 3-2	13.7	219.5	2.13
CA 3-5	14.2	334.6	2.82
CA 6	24.6	438.9	3.61
CA 7	19.5	352.7	3.17
CA 8	7.34	183.5	1.24

Table 37. Summary of maximum surface deflection, maximum edge stress, and maximum subgrade stress as calculated by ILLISLAB for a 14.4 kip (64 kN) dual wheel load with a tire pressure of 120 psi (83 kPa) placed at the slab's edge (continued).

Section ID	Maximum Surface Deflection, mils	Maximum Edge Stress, psi	Maximum Subgrade Stress, psi
MICHIGAN			
MI 1-1a	24.0	431.4	4.23
MI 1-1b	25.4	440.5	3.81
MI 1-4a	17.3	371.8	4.05
MI 1-7a	24.3	434.3	3.55
MI 1-7b	25.7	429.0	3.46
MI 1-10a	20.8	432.2	4.54
MI 1-10b	19.0	411.0	4.77
MI 3	14.2	190.0	2.64
MI 4-1	16.9	375.6	2.40
MI 4-2	37.1	456.3	3.50
MI 5	15.2	290.0	1.78
NORTH CAROLINA			
NC 1-1	16.0	360.5	4.54
NC 1-2	20.1	385.7	3.49
NC 1-3	20.0	381.0	4.93
NC 1-4	18.4	385.1	5.26
NC 1-5	15.4	394.1	4.84
NC 1-6	14.3	355.9	4.82
NC 1-7	43.0	375.7	3.77
NC 1-8	19.8	396.7	5.07
NC 2	11.3	262.0	1.66

Note: Effect of thermal gradient not included.

deflections relative to the Minnesota sections with tied PCC shoulders. This trend is expected since the tied concrete shoulders (with some degree of load transfer) provide additional support to the mainline pavement slab.

2. Sections with widened lanes result in lower stresses and deflection. There are 4 sections with widened lanes, MN 3, MN 4, MN 6 and CA 8. These section exhibited lower stresses (approximated 50 percent less) due to the location of the load relative to the edge of the slab. These results may be confounded by slab thickness. The widened lane sections were built 9 in (229 mm), 7.5 in (191 mm), 8 in (203 mm), and 10.2 in (259 mm) thick, respectively.
3. Slab thickness has a large effect on the calculated stresses and deflections. The sections at Tracy, California (CA 1) illustrate this trend. Section CA 1-5 was constructed 11.4 in (290 mm) thick and the other sections at Tracy were constructed 8.4 in (213 mm) thick. Substantially lower stresses and deflection were calculated for CA 1-5. The overall trend can also be seen in the examination of the 10 in (254 mm) slabs constructed in Michigan (MI 3 and MI 5) relative to the 9 in (229 mm) slabs. Lower stresses and deflections are calculated for the sections which were constructed thicker. This is also expected, since the additional thickness of slab provides increased resistance to deflection and stress.
4. The effects of materials strength is difficult to determine due to the number of confounding variables (thickness, load transfer, slab length, and others).
5. The effect of joint spacing is indeterminable with the edge loading condition.

Analysis of the Corner Loading Condition

The MN 1, CA 1, MI 1, and NC 1 sections were analyzed for the corner loading condition. A 14.4-kip (64 kN) dual wheel with a tire pressure of 120 psi (83 kPa) was placed at the corner of the slab adjacent to the approach joint. The deflection load transfer calculated from FWD testing was matched to within 5 percent in the analysis of the corner loading condition. The results of the analysis are shown in table 38. Several interesting trends can be observed from the data.

1. A nonlinear relationship exists between the transfer of deflection and the transfer of stress. The deflection load transfer efficiency is much higher than the stress load transfer efficiency. The only time when deflection load transfer is equal to stress load transfer is at 0 and 100 percent. This trend is observed throughout all of the data.

Table 38. Summary of deflection and stress load transfer efficiencies as calculated by ILLISLAB for a 14.4 kip (64 kN) dual wheel load with a tire pressure of 120 psi (83 kPa) placed at the slab corner.

Section ID	δ Under Load, mils	δ Across Joint, mils	δ Load Transfer, %	σ Under Load, psi	σ Across Joint, psi	σ Load Transfer, %
MINNESOTA						
MN 1-1	60.2	14.1	23	168.9	13.4	8
MN 1-2	40.3	31.1	77	300.0	115.3	38
MN 1-3	54.2	26.8	49	212.5	44.8	21
MN 1-4	40.6	29.8	73	390.3	165.3	42
MN 1-5	38.1	20.0	53	213.9	44.6	21
MN 1-6	29.9	21.4	71	367.8	117.6	32
MN 1-7	39.0	16.4	42	166.0	30.0	18
MN 1-8	28.8	23.8	83	242.6	109.2	45
MN 1-9	40.6	16.9	42	163.0	30.8	19
MN 1-10	31.4	22.8	73	292.0	102.8	35
MN 1-11	42.3	24.7	59	215.3	55.3	26
MN 1-12	37.2	27.3	73	389.7	131.1	34
MN 5	43.2	33.9	78	286.0	114.1	40
CALIFORNIA						
CA 1-1	38.5	33.5	87	212.9	96.2	46
CA 1-3	32.3	27.5	85	210.9	93.3	44
CA 1-5	21.8	19.2	88	119.0	55.1	46
CA 1-7	25.8	21.9	85	209.0	94.3	45
CA 1-9	30.5	26.4	86	214.7	96.6	45
MICHIGAN						
MI 1-1a	28.9	28.9	100	104.7	104.7	100
MI 1-1b	31.7	22.8	73	157.5	52.0	33
MI 1-4a	37.7	8.6	23	206.0	12.4	6
MI 1-7a	30.5	30.5	100	108.0	108.0	100
MI 1-7b	32.5	32.5	100	108.0	108.0	100
MI 1-10a	33.5	13.0	39	106.0	106.0	100
MI 1-10b	31.7	12.7	40	160.2	33.9	17
NORTH CAROLINA						
NC 1-1	30.4	14.8	49	196.9	33.5	17
NC 1-2	30.0	30.1	100	103.5	101.4	98
NC 1-3	27.3	27.3	100	102.3	102.3	100
NC 1-4	25.8	16.5	64	282.7	83.2	29
NC 1-5	20.2	16.8	83	198.8	81.5	41
NC 1-6	24.0	13.6	57	189.1	39.7	21
NC 1-7	32.6	25.2	77	226.6	93.6	41
NC 1-8	43.3	6.89	16	197.6	8.56	4

Note: Effect of thermal gradient not included.

2. A reduction in stress and deflection is observed for sections with higher load transfer efficiency.
3. The corner stresses are lower than the edge stresses for the same pavement sections, even if the load transfer efficiency is low. For example, NC 1-8 has a free edge stress of 396.7 psi (2.7 MPa), whereas the corner stress is 197.6 psi (1.4 MPa). This is with a stress load transfer of only 4 percent and both the edge and the corner are fully supported.
4. The deflection is higher at the corner than at the edge for the same pavement sections. The corner loading condition is critical for deflection. For example, the deflection at the free edge for MI 1-4a is 17.3 mils (0.439 mm), whereas, the deflection at a corner with 23 percent load transfer is 37.7 mils (0.958 mm).
5. Sections with deteriorated load transfer will experience higher deflections and much higher levels of stress than sections with satisfactory load transfer efficiency. If a section exhibits poor load transfer, as the load passes from the approach slab to the leave slab, the approach and leave slabs will experience higher stresses and deflections. This can lead to pumping and loss of support beneath the slab.

Analysis of Voids Beneath the Slab

Voids beneath the slab are typically the result of a loss of material beneath the slab caused by pumping action and erosion at the joints. Loss of support is detrimental to the slab because in the areas where a void exists, the slab is totally unsupported. That is, the k -value is essentially reduced to 0 and the slab acts as a cantilever. Under repeated loading, the unsupported slab experiences higher stresses and rapid fatigue damage can occur.

The ILLISLAB program is capable of modeling voids of various sizes beneath the slab. This is accomplished through reducing the k -value to 0 under selected elements to represent a void.

An analysis was performed using the joint at STA 3+73 from MI 1-10a which exhibited voids at the approach and leave corners. The analysis approach and results are outlined below:

1. The deflection basin (represented by δ_o through δ_c) as measured by the FWD for the 13,000 lb (58 kN) load for the approach joint is as shown in table 39.

Table 39. Measured deflection basin under a 13,000 lb (58 mPa) load at STA 3+73 approach joint, MI 1-10a.

δ_0	δ_1	δ_2	δ_3	δ_4	δ_5	δ_6
14.1	3.5	3.1	2.6	2.1	1.6	11.9

Figure 46 illustrates the configuration of the FWD load plate and the sensor location. As illustrated in the figure, sensor number 6 is on the opposite side of the load plate from the joint.

2. A finite element mesh was developed to calculate the deflections at the sensor locations. The program was executed to determine the deflections at the sensor locations with full support using the backcalculated surface modulus value (6.23×10^6 psi [42,960 MPa]) and k -value (436 pci [118 kPa/mm]) for the section. The measured deflection load transfer efficiency was matched in the analysis through adjustment of the aggregate interlock factor. The adjusted deflection load transfer efficiency for the joint at STA 3+73 is 26.8 percent.⁵ The fully-supported, calculated deflection basin, which is shown in table 40, is very different from the measured basin.

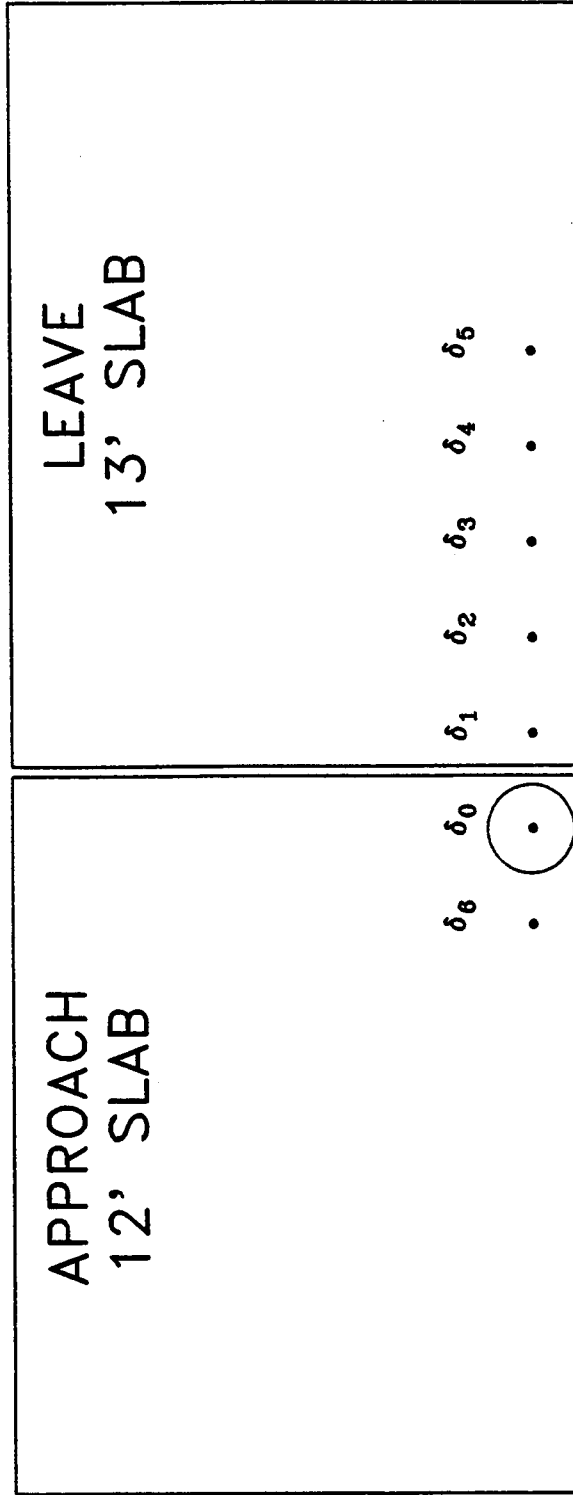
Table 40. Finite element analysis for the void analysis performed for STA 3+73, MI 1-10a.

Approach Slab Void Area, in ²	Leave Slab Void Area, in ²	Deflection Basin						
		δ_0	δ_1	δ_2	δ_3	δ_4	δ_5	δ_6
0	0	10.71	2.91	2.34	1.86	1.70	1.48	9.18
25	100	11.03	2.95	2.35	1.86	1.70	1.48	10.45
100	240	11.59	3.02	2.44	1.91	1.84	1.48	11.31
100	480	12.61	3.22	2.81	2.33	1.88	1.48	11.51
240	900	13.29	3.25	3.01	2.96	2.49	1.58	12.56
360	720	15.30	4.13	3.19	3.00	2.54	1.67	12.66

⁵ The deflection load transfer efficiency is adjusted using the center slab deflections to correct for the effects of slab bending.

MI 1-10a

STA. 3+73



All sensors are spaced 12" apart.

Figure 46. FWD sensor location at the approach joint.

3. The void area and location beneath the approach and leave sides of the joint was modified, holding the load transfer constant at approximately 27 percent until the calculated deflection basin matched the measured deflection basin.⁶ This required numerous executions of the program. Table 40 illustrates a summary of a fraction of the combination of void areas attempted.
4. The deflection basin which most accurately matches the measured basin is one in which a 240 in² (154,838 mm²) void was created at the approach joint and a 600 in² (387,096 mm²) void was created at the leave joint. The measured and calculated deflection basin is shown in figure 47. As figure 47 illustrates, the two basins closely match.
5. The determination of the measured deflection basin based on varying the size of the void is an extremely time-consuming process. Nearly 50 combinations of void sizes and void locations were executed to match the measured deflection basin. The final dimensions of the void beneath the approach slab are 10 in (254 mm) along the transverse joint and 24 in (610 mm) along the longitudinal joint. The dimensions of the void beneath the leave slab are 15 in (381 mm) along the transverse joint and 60 in (1524 mm) along the longitudinal joint.

This analysis shows that voids can be modeled beneath slabs using the ILLISLAB program. The deflection basin as calculated by the program resembles the measured deflection basin for the void sizes and locations stated above. Since the determination of the voids is a time-consuming process, it was only performed on a single joint. In order to draw conclusions regarding the accuracy of the program or the void detection procedure, additional joints should be analyzed.

Analysis of a Temperature Gradient Through a Slab

A temperature gradient through a slab causes stresses to develop. A positive thermal gradient, which indicates that the top of the slab is warmer than the bottom, results in the development of a tensile stress at the bottom of the slab, whereas a negative thermal gradient results in a compressive stress at the bottom of the slab. During the times when the gradient is positive, typically during the daytime, the total combined stress (combination of thermal stress and load-induced stress) at the bottom of the slab edge is much greater than when the gradient is negative.

⁶ Initially a 5 in by 5 in (127 mm by 127 mm) void was created at the corner of the joint at the approach and leave slabs. As the void area was increased, the support was removed along the lane-shoulder and transverse joints until the measured basin was matched.

Void Analysis

MI 1-10a STA 3+73

Approach Void Area = 240 in²

Leave Void Area = 600 in²

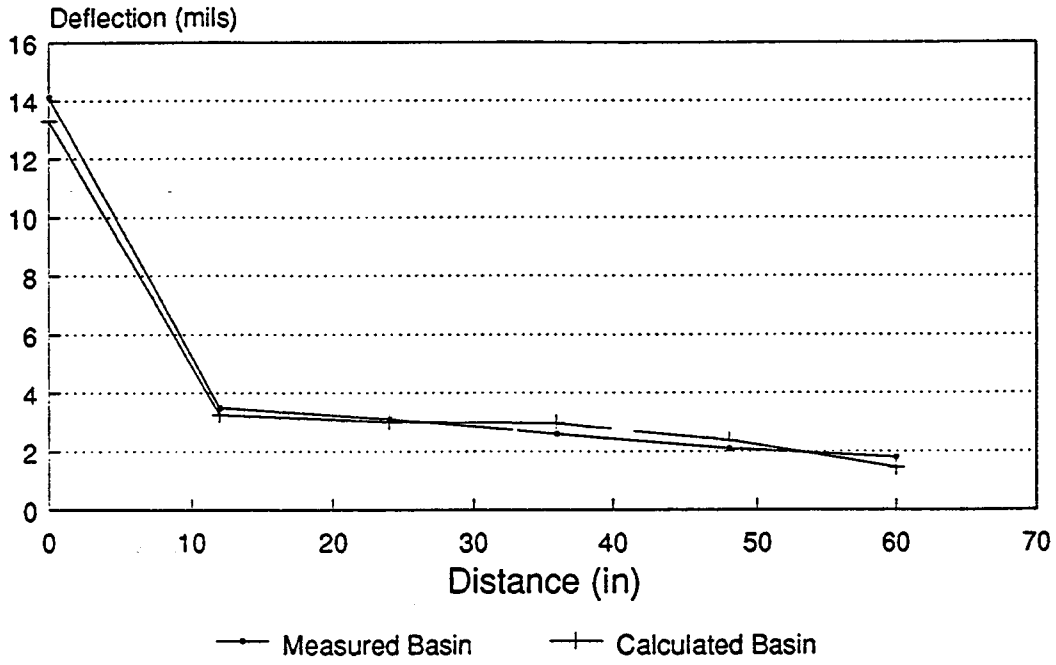


Figure 47. Measured deflection basin and calculated deflection basin from void analysis.

The ILLISLAB program was executed to examine the thermal stresses which develop in the slab. The gradients used in the analysis were calculated using the CMS program and are illustrated in table 41. The results of the thermal stress analysis for the MN 1, CA 1, MI 1, and NC 1 projects are presented in table 42.

Table 41. Maximum positive and minimum negative thermal gradient calculated by the CMS program for MN 1, CA 1, MI 1, and NC 1.

Location	Positive Gradient, °F/in	Negative Gradient, °F/in
Rothsay, MN	2.44	-0.54
Tracy, CA	2.10	-1.30
Clare, MI	2.96	-0.97
Rocky Mount, NC	3.30	-0.32

The results of this analysis are presented below:

1. Sections with stiffer bases result in higher thermal stresses. The Rothsay sections provide an example of this phenomenon. MN 1-6 exhibits a higher thermal stress than does MN 1-3. MN 1-6 is an 8 in (203 mm) JRCP over a stabilized base material having a k -value of 314 pci (85 kPa/mm). MN 1-3 is an 8 in (203 mm) JRCP over a granular base having a k -value of 217 pci (59 kPa/mm). The differences in thermal stresses are due to the differences in the stiffness of the base materials. The stiffer the base material, the less the base will conform to the curling of the slab under a temperature gradient. Very soft bases allow the slab to curl and conform more to the shape of the curling slab, thus resulting in less stress.
2. Larger positive thermal gradients result in higher thermal stresses. The maximum thermal gradient at Tracy is lower than the maximum thermal gradient at Rocky Mount as are the resulting stresses. However, this factor is confounded by many of the design variables within the study.
3. Positive thermal gradients result in tensile stresses at the bottom of the slab along the longitudinal joint.
4. Negative thermal gradients result in compressive stresses at the bottom of the slab along the longitudinal joint and a tensile stress (of lower magnitude) at the corner of the slab.

Table 42.- Stresses developing due to thermal gradients through the slab.

Section ID	Tensile Stress Due to Positive Gradient, psi	Compressive Stress Due to Negative Gradient, psi
MN 1-1	433	120
MN 1-2	444	129
MN 1-3	415	102
MN 1-4	427	106
MN 1-5	518	140
MN 1-6	526	144
MN 1-7	483	142
MN 1-8	471	135
MN 1-9	435	115
MN 1-10	437	116
MN 1-11	473	123
MN 1-12	463	119
CA 1-1	101	99.4
CA 1-3	190	153
CA 1-5	144	138
CA 1-7	213	177
CA 1-9	195	172
MI 1-1a	472	168
MI 1-1b	502	175
MI 1-4a	164	113
MI 1-7a	145	105
MI 1-7b	142	101
MI 1-10a	162	114
MI 1-10b	166	109
NC 1-1	460	47.8
NC 1-2	500	52.5
NC 1-3	399	41.1
NC 1-4	422	43.7
NC 1-5	537	56.8
NC 1-6	508	53.3
NC 1-7	437	44.2
NC 1-8	423	43.7

5. Thicker slabs exhibit less thermal stress than thinner slabs. This can be seen in the Tracy, CA sections. Less thermal stress develops in the 11.4 in (290 mm) slab (CA 1-5), than in the 8.4 in (213 mm) slabs (all with the same joint spacing). The weight of the slab acts to prevent thermal curling.
6. Shorter jointed pavements exhibit less thermal stress than longer jointed pavements. The Tracy, CA sections provide an example of this phenomenon as well. CA 1-1, which was constructed with a much shorter joint spacing than the other sections, exhibits much less thermal stress than the other sections.

Conclusions and Recommendations

The ILLISLAB program is a comprehensive finite element program which was specifically developed to analyze rigid pavement structures. The inputs required for execution of the program are readily obtainable. However, the user must carefully observe the recommendations on the development of the finite element mesh as this can have a large impact on the accuracy of the program's outputs.

The calculation of stresses due to thermal gradients is an important addition to the ILLISLAB program. The determination of the thermal stress is based on an *internal* iterative routine which eliminates the need for the user to manually determine the stress through successive executions of the program. Thermal stresses, which can have a large impact on the performance of rigid pavements, have largely been ignored in the traditional pavement design process. Thermal stresses, in combination with traffic loading, act to increase the stresses developing in the slab. Thermal stresses are responsible for the transverse cracking that is exhibited by long-jointed pavements on stiff bases.

This program is directly applicable to the design of rigid pavements. The accurate calculation of the stresses which develop in rigid pavements under loading (due to temperature or traffic) is critical for the determination of the life of a given pavement cross section. Several design procedures have been developed which rely on the calculation of stresses induced by given axle loads and configurations. Relationships have been developed which relate the number of repeated loadings at a given stress level (relative to the strength of the material) to the life of a concrete pavement.

7. EVALUATION OF THE PMARP PROGRAM

Introduction

The PMARP program is a finite element program developed at Purdue University which accounts for the effects of fatigue on the performance of rigid pavements.^(20,21) The PMARP program is based on an early version of the

ILLISLAB program.⁽¹⁵⁾ As stated previously, several errors have been found in the stiffness matrix in that early version ILLISLAB program and, therefore, are presumably repeated within the PMARP program. The program is introduced as a "nonlinear finite element method in which the pavement components are assumed to have stress or strain dependent behavior."^(20,21)

Brief Technical Description

The basic concept leading to the development of PMARP was that the structural integrity of a pavement system is continuously undergoing deterioration at various rates. Ordinarily, the assumption in design has been that the structural integrity of the pavement slabs before failure is constant and is defined by the flexural stiffness of the PCC material at the beginning of its design life. Structural deterioration is a response to the applied load repetitions and fatigue consumption. Because of this deterioration, the structural characteristics of the pavement must be periodically updated and new estimates of its remaining life obtained. This would reflect the actual (as opposed to the anticipated) traffic that the system experiences between construction and any given instant in time. The deterioration suffered by the pavement may be quantified in terms of several items, including a reduction in the stiffness of the concrete slab, the amount of cracking developed, the decay in load transfer efficiency, as well as the damage caused by the onset of pumping and the loss of support between the pavement layers and the foundation. The PMARP method for calculating the response of a rigid pavement subjected to fatigue damage was intended for both design as well as rehabilitation applications. Accordingly, the desired solution is obtained through an iterative scheme, which accommodates the stress- or strain-dependent behavior of each pavement system component. The assumptions of the finite element portion of the program are the same as those presented in section 6 on the ILLISLAB program.

In addition to the stiffness matrix problem, several other technical problems exist within the program and are outlined below:

1. The characterization of the subgrade in PMARP is one of the major weaknesses of the program. The developers state that the Winkler subgrade, which is considered in conventional finite element analysis and consists of concentrated nodal spring elements whose stiffness is proportional to the modulus of subgrade reaction (k -value), was modified in PMARP by the incorporation of the resilient modulus of subgrade reaction, K_R .⁽⁴⁰⁾ In incorporating the K_R foundation in PMARP, four of the five broad soil categories (very soft, soft, medium, hard, and very hard) were eliminated, retaining only the "medium" subgrade option. The "medium" subgrade option is extended to all soil types within the PMARP program. The developers of the theoretically-derived "resilient response" concept demonstrate that the response of the different soil types is very different.⁽⁴⁰⁾ Therefore, the extension of the medium subgrade option to all soil types is questionable. Also, the derivation of this concept

was based purely on a theoretical analysis and is intended for "research purposes only."⁽⁴⁰⁾ However, the PMARP program is intended to be used for the design and rehabilitation of rigid pavements.

2. Fatigue damage effects are accommodated in PMARP through the adjustment of the slab modulus value, E_c . To accomplish this, a plot of the applied stress to modulus of rupture ratio versus the logarithm of the number of load applications to failure, N_f was developed. In addition, two more assumptions are made:
 - (a) The curve is used in a reverse application. Conventionally, and in accordance to the experimental procedure employed in developing such curves, an estimate of the number of load repetitions before failure occurs is determined in a specimen with a given initial strength. In PMARP, however, the curve is used to determine the reduced modulus of rupture at any time, based on the previous load history of the specimen. The use of the fatigue curve in this manner has not been validated through research.
 - (b) Statistical correlations between the modulus of rupture and unconfined compressive strength of the concrete and between unconfined compressive strength and the concrete elastic modulus are used to determine an "updated" value of the modulus of elasticity. For example, the compressive strength is determined based on the modulus of rupture and, in turn, using this compressive strength, the elastic modulus is determined. This is used in subsequent PMARP iterations, presumably to reflect the influence of fatigue on the elastic modulus. The use of the correlations in this manner may not yield accurate estimates of the modulus of elasticity.
3. The approach employed in PMARP to account for deterioration of load transfer efficiency as a function of the number of load repetitions has not been validated theoretically or practically. The researchers qualify that the method can only result in "a trend of behavior" rather than a quantitative estimate of the effect of fatigue on load transfer efficiency. The deterioration of load transfer is based on a reduction of the dowel-concrete interaction (DCI) factor. A regression equation for a DCI reduction factor, RF, was obtained from data reported in reference 41. A fundamental characteristic of regression equations is that they lack general applicability. Thus, employing this expression indiscriminately to cases beyond the range for which it was developed can only lead to inaccurate, perhaps misleading, conclusions.

4. In developing the pumping model, a concept involving energy principles was employed.⁽⁴²⁾ The particular strengths and weaknesses of this concept are still the subject of substantial research efforts. A number of weaknesses in its implementation in PMARP can, nevertheless, be identified. These include:
 - (a) The normalized pumping index, NPI, is determined using a regression equation of limited applicability, and does not take into account important subbase and subgrade properties, such as gradation, permeability, and erodibility, among others.
 - (b) Determination of the void area hinges on an assumption regarding the "average void depth," which is *estimated* by the user.

Analysis of Results

The PMARP program (PC version) was run for each of the MN 1, CA 1, MI 1, and NC 1 sections. The program was executed to examine the edge condition at all sites and the corner condition at selected sites. The analysis of the corner condition was used to evaluate the pumping potential of the design.

The mesh capabilities of the PMARP PC program are severely limiting. The maximum mesh size allowed must satisfy the requirements of equation 33 presented below.

$$26*x*y^2 < 26,500 \quad (33)$$

where:

x = number of node lines in the x-direction
y = number of node lines in the y-direction

Figure 48 shows an example finite element mesh used for the corner loading condition for a 15 ft (4.6 m) slab. The mesh violates the general guidelines for the development of a finite element mesh. Typically, the aspect ratio, which is defined as the ratio of the length to width of a given element (or width to length depending on the orientation of the mesh), should not exceed 8 anywhere on the slab, except at the joint elements which are elements with length but no width. Also, the aspect ratio should be less than 3 near loaded elements.

Obviously, the mesh illustrated in figure 48 does not abide by the general guidelines for the development of finite element meshes. Aspect ratios as large as 19 occur. The violation of the aspect ratio principles was necessary in order to stay within the memory requirements of the program. It is interesting to note that the program allows the user to use as many as six slabs. With the memory

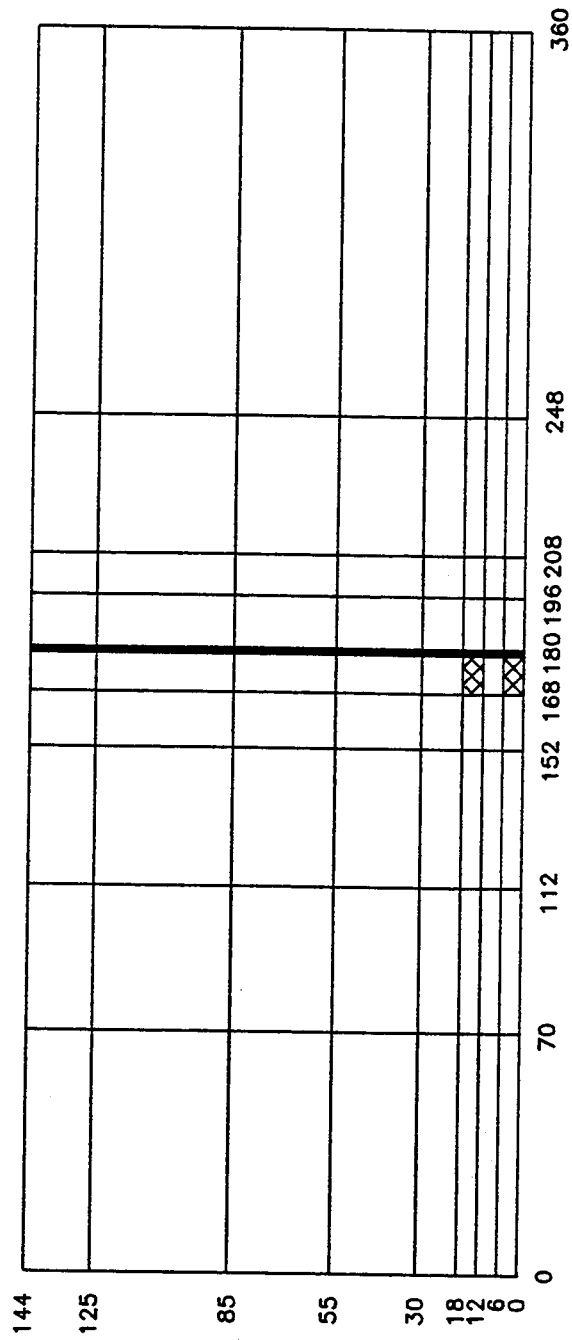


Figure 48. Finite element mesh for a 15-ft (4.6 m) slab used in the PMARP evaluation of the corner loading condition.

limitations of the program, a mesh for a two slab system, much less a six slab system, is questionable.

Analysis of the Edge Loading Condition

Table 43 illustrates the results obtained from the PMARP program. In addition to the stresses and deflections due to loading, a fatigue damage number, a pumping index, damage area, and type of damage is determined.

The results of the stress and deflection analysis reveal the same trends regarding the effects of slab thickness and tied shoulders as was observed with the ILLISLAB program. A reduction in stress is observed for thicker slabs and sections with tied concrete shoulders. However, the maximum stresses and deflections do not always occur directly beneath the loaded elements. In fact, in some cases the maximum stresses and deflections occur no where near the loaded elements. Also, the point of maximum stress and deflection do not always occur at the same node. The mesh fineness can account for some of the error involved in the calculation of the results, but the maximum stress and deflection should always occur directly beneath the load. The fact that the maximum stress and deflection do not occur directly beneath the load indicates a serious problem with the calculation routine.

The observations regarding the additional analyses performed by the PMARP program are presented below:

1. The fatigue damage is calculated based on the ratio of the number of allowable loads to failure and the number of loads that the pavement has sustained. The fatigue damage number is calculated based on Miner's damage. It is the summation of the number of actual applied loads (18 kip [80 kN] ESAL's) to the number of allowable loads (based on the decay in the PCC material's strength properties). As the fatigue damage number approaches 1, cracking is expected to occur.

Examination of the fatigue damage numbers reveal some interesting trends. Several of the sections have a negative fatigue damage. The pertinent equations within research documentation appear correct and indicate that calculation of a negative fatigue damage number is not possible. The method by which the *program* calculates the fatigue damage is unclear.

The program indicates that all of the NC 1 sections, and many of the MN 1, CA 1, and MI 1 sections should have failed due to decay in the strength of the PCC modulus. The failure occurs at the longitudinal edge of the slab. An examination of the summary tables presented in volume IV shows that the majority of these sections are performing quite well.

Table 43. Summary of PMARP results for the edge loading condition employing a 9-kip (40 kN) dual wheel load with a tire pressure of 80 psi (55 kPa).

Section ID	Maximum Surface δ , mils	Maximum Tensile σ , psi	Fatigue Damage	Pumping Index	Damage Area, in ²	Type of Decay
MN 1-1	4.5	141	-8.3	0	42	E _c
MN 1-2	11.1	285	-5.0	0	0	--
MN 1-3	5.5	183	-5.5	1.5	36	E _c
MN 1-4	9.3	370	94	1.3	336	E _c
MN 1-5	9.2	350	-0.54	0.10	42	E _c
MN 1-6	8.3	351	-0.50	0.05	42	E _c
MN 1-7	8.5	286	0	0	0	--
MN 1-8	8.4	284	-1.6	0	0	--
MN 1-9	4.6	141	3.8	0.05	126	E _c
MN 1-10	9.1	281	2.7	0.04	126	E _c
MN 1-11	5.0	183	0.8	0.47	8	E _c
MN 1-12	10.2	363	37	0.58	168	E _c
CA 1-1	13.4	250	3.2	53	53	E _c
CA 1-3	13.8	325	130	17	576	E _c
CA 1-5	9.2	189	-1.2	0.08	0	--
CA 1-7	12.7	343	111	9.9	468	E _c
CA 1-9	12.3	346	91	8.5	360	E _c
MI 1-1a	5.6	239	1.3	0.38	216	E _c
MI 1-1b	10.3	241	0.75	0.27	216	E _c
MI 1-4a	10.0	258	2.1	0.23	216	E _c
MI 1-7a	9.9	245	0.03	0.15	0	--
MI 1-7b	10.1	243	-0.25	0.20	0	--
MI 1-10a	10.7	257	1.3	0.16	216	E _c
MI 1-10b	10.7	238	2.3	0.43	216	E _c
NC 1-1	11.2	232	176	2.3	630	E _c
NC 1-2	10.6	237	145	1.3	630	E _c
NC 1-3	12.0	225	267	4.1	1008	E _c
NC 1-4	10.6	228	274	0	809	E _c
NC 1-5	10.3	237	124	0.72	378	E _c
NC 1-6	10.6	233	118	1.4	378	E _c
NC 1-7	10.3	244	45	0.71	240	E _c
NC 1-8	11.7	228	166	3.2	819	E _c

2. The damaged area is the nodal area affected by the decay in the PCC material. It is determined through a fatigue damage analysis for each individual node. The results indicate a large damaged area for many of the sections. The nodes affected by the fatigue damage are typically at the edge of the slab midway between the transverse joints. As the affected area increases, the damaged area propagates inward from the edge toward the middle of the slab and also toward the transverse joints.
3. The pumping index is calculated as shown in chapter 3. It is an indication of the pumping potential of the material. It is defined as the volume of the material pumped out from under the slab, per unit length of the pavement. The pumping index is more pertinent to the corner loading condition and will be discussed in that section.

Analysis of the Corner Loading Condition

The PMARP program was executed for several sections within each of the four large experimental projects in order to examine the pumping potential as well as the decay in load transfer potential of the various designs. The results are presented in table 44.

Table 44. Summary of PMARP results for the corner loading condition employing a 9-kip (40 kN) dual wheel load with a tire pressure of 80 psi (55 kPa).

Section ID	Maximum Surface δ , mils	Maximum Tensile σ , psi	Deflection Load Transfer, %	Pumping Index	Damage Area, in ²	Type of Decay
MN 1-1	12.6	134	100	8.2	0	--
MN 1-6	14.3	199	100	67.5	0	--
MN 1-11	11.6	138	100	5.2	0	--
CA 1-1	8.9	96	100	0	0	--
CA 1-7	8.6	110	100	0	0	--
MI 1-1a	13.6	112	100	2.7	0	--
MI 1-7a	12.6	114	100	1.8	0	--
MI 1-10b	20.6	98	100	9.6	0	--
NC 1-2	13.7	95	100	12.0	0	--
NC 1-4	14.9	98	100	18.6	0	--

As with the edge condition, the maximum deflection and stress did not occur beneath the loaded element. The problem was even more frequent with the corner loading condition than with the edge loading condition. Also, for the exact same finite element mesh, the maximum stress and deflection do not occur at the same node. For example, a finite element mesh for the corner loading condition was developed for a 15 ft (4.6 m) slab and the same mesh was used for the analysis of both of the CA 1 sections under study. The design parameters (thickness, modulus of rupture, k -value, and others) were changed to reflect the specific section (CA 1-1 or CA 1-7). For section CA 1-1, the maximum deflection occurred at node 58 and the maximum stress occurred at node 114. For section CA 1-7 (using the exact same mesh), the maximum deflection occurred at node 46 and the maximum stress occurred at node 19. The dual wheels were placed between nodes 37, 38, 46, and 47 (outer edge of slab along the transverse joint) and between nodes 39, 40, 48, and 49 (12 in [305 mm] from the outer edge along the transverse joint). Figure 48 illustrates the mesh and the location of the loaded area. Again, this indicates a serious problem with the calculation routine.

As with the ILLISLAB program, attempts were made for the sections with tied PCC shoulders to match the load transfer across the transverse and longitudinal joints as calculated from the FWD deflections. This could not be accomplished using the PMARP program; no matter what aggregate interlock factor or dowel configuration was used, the deflection load transfer efficiency was always 100 percent.

Since the load transfer efficiency was always 100 percent, the results of the pumping analysis are questionable. The program indicates that the Minnesota designs and the North Carolina designs have the highest pumping potential given their levels of traffic and climate. In actuality, a small amount of pumping was observed for these sections, but significant faulting was observed for the nondoweled sections.

The damaged area was 0 for all of the sections under analysis. The measured load transfer efficiency for the MN 1-1, MN 1-6, MN 1-11, and MI 1-10b is less than 50 percent. If the load transfer of these sections could be modeled, it is expected that decay in load transfer would be calculated by the program.

Conclusions and Recommendations

Several technical problems with the PMARP program were presented in this section. Additional problems were encountered in the input processor and in the execution of the program which were not discussed; these are presented below.

1. The PMINT input processor misassigns several variables. For example, the reinforcement ratio in the x -direction is assigned to the reinforcement ratio in the y -direction. The same is true for the dowel bar diameter inputs.

2. The largest aggregate interlock factor that the input processor allows the user to input $10 * 10^8$; however, the input screen indicates values of $10 * 10^{10}$ are to be used for keyed joints.
3. The input processor changes the users values for the plate deflection versus resilient modulus inputs. The first two entries are accepted while the third entry for both the deflection and modulus is changed to 0.0.

In general, PMARP constitutes a compendium of individual concepts and solutions suggested over the last several decades to address some of the most difficult issues in rigid pavement analysis and design. While each one of these concepts reflected the state-of-the-art at the time of publication, the individual researchers involved in their development generally recognized their limitations, as well as their limited scope of applicability and their predominantly qualitative nature. The incorporation of the research in a continuous analysis program, such as PMARP, tends to compound the individual weaknesses of the various research approaches and may be expected to lead to incorrect conclusions.

8. EVALUATION OF THE ZERO-MAINTENANCE DESIGN PROCEDURE

Introduction

The Zero-Maintenance design procedure was developed in 1976 for use in the structural design of jointed plain concrete pavements for heavily trafficked highways.⁽²⁾ The procedure was computerized at that time for use on a mainframe computer and was entitled JCP-1 (Jointed Concrete Pavements - 1). This program was converted for use on a microcomputer in 1986.⁽²⁴⁾ The program consists of two different design approaches: serviceability and fatigue cracking. The serviceability prediction model was based on a very limited sample of data, and is not under evaluation in this study. The fatigue cracking model is based upon fundamental mechanistic-empirical concepts and uses a finite element model described in reference 43.

Brief Technical Description

The JCP-1 model requires a number of inputs, including slab dimensions, subgrade and base material data, PCC strength, traffic weight and volume data based on the axle load distribution, thermal gradient data, and other design information. Miner's fatigue damage is computed over the specified design period with the user provided inputs. The mechanistically-generated fatigue model was calibrated with a limited amount of JPCP field performance data. A reasonable correlation between transverse slab cracking and the fatigue damage number was found.

The procedure was derived through the development of a large database of mechanistically-calculated and field-measured values. A matrix for load and

thermal curling stresses was obtained through the use of a finite element program to assure that the factors and interactions of factors were determinable. The field-measured cracking data were included in the database, as well. The database was used to develop the fatigue damage model, eliminating the need for the user to perform complicated finite element analyses.

The fatigue damage model is based upon the following concepts and assumptions:

1. Through mechanistic analysis, the location of critical fatigue damage was shown to be at the longitudinal edge of the slab midway between the joints (for slab shorter than, say, 20 ft [6.1 m]). Evaluation of field data showed that transverse cracks were found to initiate at this point and progress toward the center of the slab, supporting the mechanistic theory.
2. Determination of critical stresses in the slab was performed using a finite element program. Truck axles were modeled and placed at various positions on slab to determine the location of critical stress. As Westergaard had shown earlier, the critical stress occurs midslab at the outermost edge of the slab. In order to more realistically model a field-observed phenomenon, a normal distribution of truck loads was assumed so that only a proportion of the trucks are loading the outer edge. Miner's fatigue damage was shown to be highest at the edge of the slab.
3. The effects of thermal stresses is considered within the procedure. Stresses were computed for both daytime and nighttime thermal gradient conditions for each month of the year. The finite element program realistically combined load and thermal gradient stresses to produce a total stress at the slab edge. Nonlinear regression equations were developed to model the effects of the combination stresses.
4. Since the strength of the concrete increases over time, the fatigue analysis is time-dependent. Field strength data was used to develop a regression equation which models the concrete pavement's gain in strength over time.
5. The erosion of the subbase material is considered in the design procedure in terms of the loss of support to the rigid slab.
6. Total fatigue damage is computed by summing the Miner's damage over each month of the year, daytime and nighttime condition for thermal gradient, and axle load distribution as shown below:

$$\sum_{k=1}^{k=p} \sum_{j=1}^{j=2} \sum_{i=1}^{i=m} [n_{ijk} / N_{ijk}] \quad (34)$$

where:

- i = counter for magnitude of single and tandem axle load
- j = counter for day and night
- k = counter for months over the design period
- m = total number of single and tandem axle load groups
- p = total number of months in the design period
- n_{ijk} = number of applied axle load applications of i^{th} magnitude over day or night for the k^{th} month
 $= ADT_m * T * DD * LD * A * 30 * P * C * DN * TF * CON$
- ADT_m = average daily traffic at the end of the month under consideration
- T = percent trucks
- DD = directional distribution
- LD = lane distribution
- A = mean number of axles per truck
- P = percent axles in the i^{th} group
- C = percent of total axles in the lane that are within 6 in of the slab edge
- DN = percent of trucks during the day or night
- TF = factor to adjust the truck volume for a given month
- CON = 1, for single axles
 = 2, for tandem axles
- N_{ijk} = number of allowable axle load applications of i^{th} magnitude over day or night for the k^{th} month determined from PCC fatigue cracking curve which is based on the stress induced by a given load and thermal gradient

The stress induced by the combination of load (from a variety of axle configurations) and thermal curling (thermal gradients based on the time of the year and location) was calculated by the finite element program for each section in the experimental matrix. Regression equations were developed and incorporated into the program to determine the combination stresses without the use of a finite element program.

The flexural fatigue life of the pavement is determined based on the following equation which was developed through laboratory testing of PCC beams:

$$\log_{10}(N) = 16.61 - 17.61 * (\text{STRESS}/M_r) \quad (35)$$

where:

N = number of load applications to flexural failure of a PCC beam

STRESS = tensile stress at the bottom of the slab

M_r = modulus of rupture of the PCC adjusted for time dependence

Analysis of Results

The JCP-1 computer program was executed for the JPCP sections of the large experimental projects within the four climatic zones. The JPCP sections from Albert Lea, Minnesota (MN 2), Tracy, California (CA 1), Clare, Michigan (MI 1), and Rocky Mount, North Carolina (NC 1) were used for the analysis. The JRCP sections at Rothsay, Minnesota could not be used since the design procedure is for JPCP only or *uncracked* JRCP (the JRCP slabs at Minnesota were cracked).

The required design inputs for the program were obtained from the summary tables which are provided in volume IV. The axle load distribution was obtained from the Weigh-In-Motion studies performed for this project. Various input variables which were not available for several of the sections (such as the time between pavement construction and opening to traffic, 28-day modulus of rupture, etc.) were estimated.

Upon execution of the program, the total Miner's fatigue damage is computed over time. The timeframe used for the analysis is the time from opening of the pavement to traffic through the 1987 survey.

The cracking index is calculated using the transverse cracking measured from the 1987 field surveys. It is summarized in table 45 for each pavement section under analysis. The original Zero-Maintenance plot of cracking index versus fatigue damage is shown in figure 49. The new data points generated for MN 2, CA 1, MI 1, and NC 1 are plotted on the original Zero-Maintenance graph.

The data indicates that, excluding North Carolina and CA 1-9, a general trend exists between calculated fatigue damage and transverse cracking. There is also a general agreement between the original Zero-Maintenance data and the data collected under this study. However, the data collected under this study exhibits less cracking for the same fatigue damage. This may be explained by the use of WIM axle load distributions for the analysis. These were considerably higher than the original data which used mainly W-4 table axle load distributions.

Section CA 1-9 exhibits an extremely large cracking index relative to its fatigue damage. From those familiar with the section, this cracking occurred very soon after construction and may have been due to shrinkage. Since the Zero-Maintenance model was developed to analyze structural cracking, this data point may not be representative.

Table 45. Summary of Miner's fatigue damage and transverse cracking for MN 2, CA 1, MI 1, and NC 1.

Section ID	Thickness, in	Cracking Index, in ft/1000 ft ²	n_{ijk}/N_{ijk}
MN 2-1	9.0	0.0	0.194
MN 2-2	8.0	0.0	0.234
CA 1-1	8.4	0.947	0.05
CA 1-3	8.4	5.687	0.728
CA 1-5	11.4	0.0	0.269
CA 1-7	8.4	14.19	0.370
CA 1-9	8.4	35.88	0.370
MI 1-4a	9.0	0.0	3.299×10^{-5}
MI 1-7a	9.0	0.0	3.874×10^{-5}
MI 1-7b	9.0	0.0	3.500×10^{-5}
MI 1-10a	9.0	0.0	4.501×10^{-5}
MI 1-10b	9.0	3.322	4.635×10^{-5}
MI 1-25	9.0	5.571	4.910×10^{-5}
NC 1-1	9.0	0.948	746.6
NC 1-2	9.0	1.896	746.8
NC 1-3	9.0	0.943	746.7
NC 1-4	9.0	0.0	746.7
NC 1-5	9.0	0.0	746.7
NC 1-6	9.0	0.0	761.7
NC 1-8	9.0	12.17	746.7

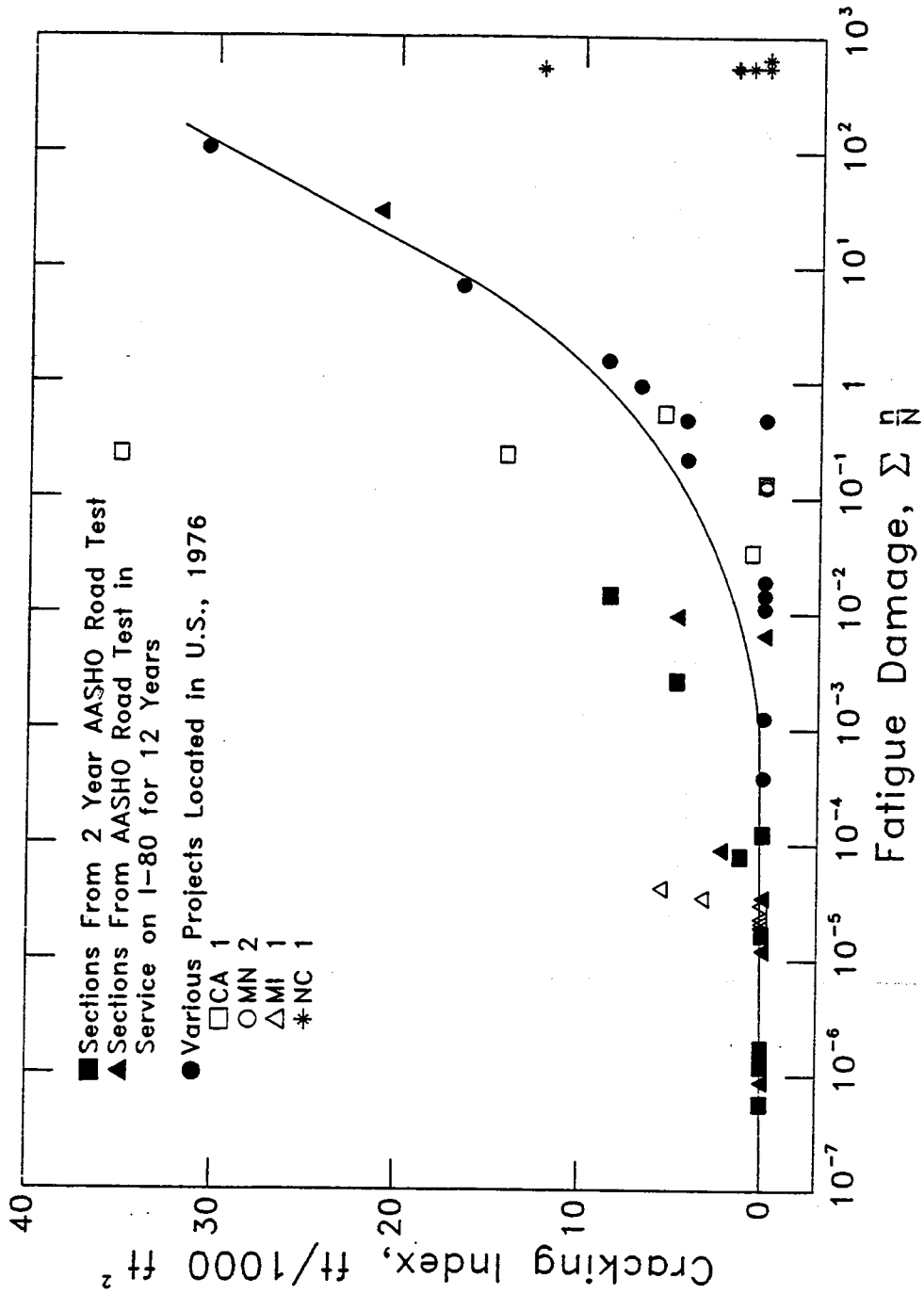


Figure 49. Original zero-maintenance fatigue damage curve supplemented with projects from current study.

The results from the 30 ft (9.1 m) JPCP North Carolina sections are generally far different than the rest of the data collected from this study or from the original Zero-Maintenance data. These pavements appear to be able to withstand a large amount of fatigue damage without exhibiting cracking. The transverse cracking is very low for the long-joint spacing and large amount of traffic carried by these 20-year-old pavements. One possible explanation is that the aggregate may exhibit a low thermal coefficient of expansion which would reduce the thermal curling stresses greatly, and, therefore, decrease the amount of transverse cracking in these long-jointed plain pavements.

Conclusions and Recommendations

The JCP-1 program can directly and mechanistically consider several key design factors, including the stiffness of the base/subgrade, climatic area, axle load distributions and slab thicknesses. The JCP-1 program may be used to examine the effects of joint spacing on a given design. Using the relationship between fatigue damage and cracking, presented in figure 49, the proposed joint spacing can be analyzed to determine the likelihood of significant transverse cracking. If the total fatigue damage is greater than approximately 1.0, a significant amount of transverse cracking may be expected to develop over the serviceable life of the pavement.

At this time, the increased support provided by tied PCC shoulder cannot be evaluated using the existing program. However, widened lanes can be evaluated by increasing the lateral distance of truck wheels. The incorporation of tied PCC shoulders as a design option would require the additional analysis of the effects of tied shoulders on stresses induced by traffic loading and thermal curling.

9. EVALUATION OF JCS-1

The JCS-1 (Jointed Concrete Shoulder) program was developed to provide a method of designing jointed concrete shoulders based on a fatigue damage approach.⁽²⁵⁾ Field and laboratory data were collected and finite element analyses were performed to aid in the development of a relationship between slab cracking and fatigue damage in jointed concrete shoulders.

The JCS-1 program can be an integral part of the design process. The engineer can examine the *actual* structural thickness requirements of a tied concrete shoulder which will be much less than that of the mainline pavement. A thinner concrete shoulder section could result in a substantial savings especially on large construction projects in areas where differential frost heave is not a problem.

Brief Technical Description

The inputs required for this program are quite similar to the JCP-1 program since the two procedures are based on a fatigue damage approach. The required inputs include the thickness of the mainline pavement, the expected load transfer

efficiency across the tied shoulder, concrete strength properties, shoulder width, estimated shoulder thickness, axle load distribution, current and future year ADT and a foundation support (*k*-value) value.

The fatigue damage analysis was based on the following set of concepts and assumptions:

1. The two critical fatigue damage locations on the shoulder are at the lane-shoulder longitudinal joint and outer edge of the shoulder. These locations were determined through finite element analysis and confirmed through field observation of shoulder fatigue cracking.
2. Reduction in critical edge stresses caused by traffic loading will diminish transverse cracking in the tied PCC shoulder.
3. The stresses induced by traffic loading were computed using a finite element program over a range of design values. Two individual stress prediction models were developed for the locations of critical stress (inner and outer edge of the shoulder).
4. A fatigue curve relating the ratio of repeated flexural stress to modulus of rupture and the number of stress applications to failure was developed. The reliability of the relationship is 76 percent.
5. The shoulder traffic is determined as a proportion of the mainline pavement traffic for encroaching traffic (lane/shoulder joint) and parked traffic (outer shoulder edge). These percentages were determined through field studies and the examination of previous research on the subject.
6. Fatigue damage is calculated in terms of Miner's damage analysis.
7. A relationship between computed fatigue damage and measured shoulder cracking was developed.

Analysis of Results

The JCS-1 program was executed for all of the sections on SR 360 in Phoenix, Arizona (AZ 1) and for a section on I-69 near Charlotte, Michigan (MI 4-1). The axle load distribution for MI 4-1 was based on the Weigh-In-Motion distribution collected under this study. The axle load distribution for the AZ 1 sections was obtained from W-4 tables representing statewide averages. The use of the W-4 tables may not be an accurate evaluation of the axle distribution for AZ 1 since these sections are located in a highly urban area where no loadometer stations are in place. The remainder of the input variables required for the analysis are shown in the summary tables presented in volume IV. The results of the analysis are shown in table 46.

Table 46. Shoulder fatigue damage analysis for AZ 1 and MI 4-1 using the JCS-1 program.

Section ID	Design Thickness, in	Fatigue Damage Parking	Fatigue Damage Encroachment
AZ 1-2	9.5	5.11×10^{-6}	2.77×10^{-8}
AZ 1-4	13.0	7.49×10^{-9}	2.08×10^{-8}
AZ 1-5	11.0	3.00×10^{-8}	3.91×10^{-8}
AZ 1-6	9.0	8.41×10^{-8}	1.98×10^{-8}
AZ 1-7	9.0	6.87×10^{-7}	1.66×10^{-8}
MI 4-1	7.5	4.23×10^3	2.13×10^{-4}

As the fatigue damage resulting from parked traffic approaches a value of 1.0, cracking is expected to initiate at the outer edge of the shoulder. As the fatigue damage due to encroaching traffic approaches 1.0 then cracking is expected to initiate at the lane shoulder joint.

The AZ 1 sections are relatively new (less than 10 years old) and have exhibited no cracking. The fatigue damage computed by the JCS-1 program indicates similar results since the shoulders are very thick and have experienced relatively little traffic. The effect of shoulder thickness on the calculated fatigue damage is evident in the results shown above. Less accumulated fatigue damage is computed for sections with thick shoulders (AZ 1-4 and AZ 1-5).

The fatigue damage due to parked traffic calculated for MI 4-1 is very large, indicating that cracks should have developed at the outer edge of the shoulder slabs. Examination of the field survey and photographic records indicate that the tied PCC shoulders have performed very well and showed no signs of structural deterioration (1 percent of the slabs cracked). It appears, for MI 4-1, that the program does not indicate the condition of the shoulder. A likely explanation is that the traffic calculations within the program are over-conservative, estimating too many parked vehicles. Estimation of shoulder traffic is even more difficult due to the variability of encroaching traffic and parked traffic.

Conclusions and Recommendations

The JCS-1 program provides a method to design the thickness required for a tied PCC shoulder. Traditionally, tied concrete shoulders have not been designed; standard thicknesses instead have been used. However, similar to pavement design, shoulders can be designed for a certain amount of traffic. Based on previous research, the amount of traffic that the shoulder must support is far less than the mainline pavement.^(35,36)

The program provides an estimate of the fatigue damage of a shoulder. An iterative approach is required to determine the minimum thickness to achieve a fatigue damage of approximately 1.0 over the life of the pavement.

10. EVALUATION OF BERM

The BERM program was developed as part of a research project which focused on the structural design of shoulders.⁽²⁶⁾ The program is capable of designing both flexible and rigid shoulders; however, only the flexible shoulder design portion will be evaluated under this study.

Many problems exist with the construction of an asphalt shoulder next to a concrete pavement. The resulting joint between the shoulder and pavement is difficult to seal due to the different bonding properties of the two materials. Further, the difference in stiffness of the materials causes different responses to loading and environment, and the difference in expansion properties of the two materials also cause problems. Due to these factors and others, asphalt shoulders have quite frequently been under-designed resulting the structural deterioration of the shoulder. Therefore, a design procedure to aid the engineer in the selection of a structural thickness which will support the traffic would be a useful tool.

Brief Technical Description

The BERM program was developed using the RISC finite element program and a cracking model that was based on results from the AASHO Road Test.^(37,38) Regression equations were developed to determine the critical stresses and strains within the shoulder. The stresses and strains are then related to the number of 18-kip (80 kN) equivalent axle loads (ESAL) that the shoulder could sustain before cracking. As with the JCS-1 program, the critical locations were determined as the shoulder area adjacent to the lane-shoulder joint for encroaching traffic and the outer edge of the shoulder for parked traffic.

The fatigue damage analysis was based on the following set of concepts and assumptions:

1. The two critical fatigue damage locations on the shoulder are at the lane-shoulder longitudinal joint and outer edge of the shoulder.
2. Reduction in critical stresses and strains caused by traffic loading will diminish fatigue cracking in the asphalt concrete shoulder.
3. The stresses induced by traffic loading were computed using the RISC program over a range of design values. Two individual stress/strain prediction models were developed for the critical locations (inner and outer edge of the shoulder).

4. A fatigue curve relating the critical stresses and strains to the allowable number of 18-kip (80 kN) ESAL's was developed based on cracking observed at the AASHO Road Test.
5. The user is responsible for determining the number of 18-kip (80 kN) ESAL's *expected* on the shoulder over the life of the pavement. As stated previously, this is a very difficult quantity to estimate. An iterative approach adjusting thickness is required until the expected ESAL's are roughly equal to the ESAL's computed by the program.

Analysis of Results

The BERM program was executed for all of the sections on I-95 near Rocky Mount, North Carolina (NC 1). The input variables required for the analysis are provided in the summary tables presented in volume IV. The user must determine the number of ESAL's that the shoulder must sustain during its life. Several studies have been performed to examine the traffic sustained by the shoulder relative to the mainline.^(35,36) The studies indicate that the encroaching traffic and parked traffic is 1 to 8 percent and 0.005 percent to 0.0005 percent, respectively, of the mainline traffic. For this analysis, it is assumed that 4 percent of the mainline traffic encroaches onto the shoulder and 0.003 percent of the mainline pavement parks on the shoulder. For NC 1, the total number of ESAL's sustained by the mainline pavement was estimated to be 9.137 million ESAL's. Therefore, 0.366 ESAL's encroach onto the shoulder and 2.74×10^3 million ESAL's park on the shoulder. The fatigue damage is manually determined as the ratio of the number of estimated ESAL's (percentage of the mainline traffic) and the number of allowable ESAL's (as calculated by the program). The results of the analysis are shown in table 47.

Table 47. Shoulder fatigue analysis for NC 1 using the BERM program.

Section ID	Design Thickness, in	Fatigue Damage Parking	Fatigue Damage Encroachment
NC 1-1	3.0	6.93	2.27×10^{-2}
NC 1-2	3.0	6.93	2.27×10^{-2}
NC 1-3	3.0	3.28	3.97×10^{-2}
NC 1-4	3.0	3.28	3.97×10^{-2}
NC 1-5	3.0	6.93	2.27×10^{-2}
NC 1-6	3.0	13.76	1.41×10^{-2}
NC 1-7	3.0	13.76	1.41×10^{-2}
NC 1-8	3.0	13.76	1.41×10^{-2}

If the fatigue damage for either location approaches 1.0, then the asphalt shoulder is expected to crack. The results of the analyses indicate that the fatigue damage due to encroachment for the design thickness of 3 in (76 mm) is relatively

small and little damage has accumulated at the lane-shoulder interface due to encroaching traffic. Parked traffic has caused more accumulation of fatigue damage at the outer edge of the shoulder. These results would indicate that the shoulder is in relatively poor condition because of cracking due to parked traffic. Upon examination of the field surveys and photographic records, the shoulders appear to be performing fairly well. Although they show signs of weathering and raveling and sympathetic cracking at locations collinear with the joints in the mainline pavement, they show little sign of structural deterioration. The program indicates that the shoulders should exhibit signs of fatigue cracking at the outer edge of the shoulder. This discrepancy may be due to the estimate of the amount of parked traffic on the shoulder which is very difficult to estimate.

Conclusions and Recommendations

The BERM program provides a method of determining asphalt shoulder thickness based on the materials' properties and estimated traffic. This program would be very useful in design, since many asphalt concrete shoulders appear to be under-designed.

The fatigue model used in the program was developed from AASHO Road Test data which consists of interior loading of asphalt concrete pavements. The lane-shoulder joint represents an edge condition where the strain under load would be much higher. Since the road test was conducted in a single location with very controlled materials, the applicability of the data for use throughout the country is questionable.

11. SUMMARY AND CONCLUSIONS

This chapter has presented case studies, employing various analysis programs and design methods, for several of the large experimental projects included in this study. The programs evaluated in this study include CMS, the Liu-Lytton drainage models, ILLISLAB, PMARP, the Zero-Maintenance design procedure, and the JCS-1 and BERM shoulder design methods. The case studies provide insight into the usefulness of these procedures in the rigid pavement design process.

The response of the pavement system to the environment has long been ignored in the design of rigid pavements. The CMS model uses site-specific climatic data to determine the material's response to daily, seasonal, and yearly changes in the environmental conditions. The Liu-Lytton drainage model was developed to analyze the drainage capabilities of a given cross-section subjected to specific environmental conditions. These models provide not only valuable insight into the response of the pavement to the environment but they also are potentially valuable tools for the design of rigid pavements.

The outputs of the CMS and Liu-Lytton models provide the design engineer the ability to analyze the drainage capabilities of a rigid pavement system and to

determine the effects of the environment on that pavement. These models may be used in conjunction with a structural model, such as ILLISLAB, to determine the stresses and deflections resulting from the environment and the combination of load and environment. These stresses and deflections can, with the use of a fatigue equation or transfer function, be translated into the number of repetitions that a pavement slab before failing in fatigue. This is the basis of a mechanistic-empirical design procedure. However, the Liu-Lytton and CMS programs require numerous and obscure inputs. Also, the interpretation of the results requires that the user be familiar with the theoretical concepts analyzed in order to fully use the programs' capabilities. Work is underway to chain these models together and to simplify the procedure.

The ILLISLAB and PMARP programs can be used in the structural analysis of a specific pavement cross section. Each program has specific capabilities and applications to design. For example, the PMARP program can be used to examine the pumping potential of the pavement system or the accumulated fatigue damage for a given level of traffic. However, it should be noted that several technical problems were discovered with this program while performing the case studies. The ILLISLAB program was shown to have broad application to rigid pavement analysis by examining the stresses induced in a slab due to a temperature differential between the top and bottom of the slab, traffic loading, and the combination of these factors. Future enhancements to ILLISLAB should include a generation of the finite element mesh using program limitations and other graphical outputs to facilitate data interpretation.

The structural analysis models also require some degree of expertise in that the user must develop a finite element mesh. The accuracy of the results is highly dependent on the mesh.

The Zero-Maintenance design procedure was developed based on mechanistic-empirical principles. The procedure accounts for the effect of thermal gradients and load stresses on the fatigue of rigid pavements. The procedure provides a useful tool in the design and analysis of rigid pavements.

In the past, design of pavement shoulders has been based on engineering judgment or policy decisions. Two design procedures have been developed which aid the engineer in determining the thickness required to support the estimated shoulder traffic. The JCS-1 program may be used to design the thickness and load transfer required for a tied PCC shoulder. The BERM program may be used to design the required thickness for an asphalt shoulder. With these programs, adequate shoulder designs can be achieved.

The potential benefits obtained through the use of design and analysis programs such as these can contribute to the improvement of rigid pavement design. However, it must be realized that the procedures are only tools to assist in pavement design and analysis; they are intended to supplement, not replace, engineering judgment and knowledge.

CHAPTER 5 DEVELOPMENT OF NEW PREDICTION MODELS

1. INTRODUCTION

With the acceptance that the existing prediction models for concrete pavements have some deficiencies, it is desirable to try to develop new models which more accurately predict the performance of inservice concrete pavements. Realizing that the 95 pavement sections from this study would not be of sufficient number to allow the development of accurate models, the 95 sections from the RIPPER database were combined with the over 400 concrete pavement sections from the COPES database to allow for a large number of sections and a variety of different pavement designs and design features. While there are certainly limitations with the new models, they are nevertheless believed to be more accurate than any other prediction models currently available.

2. NEW PREDICTION MODELS

Present Serviceability Rating (PSR)

The combined RIPPER and COPES database was utilized to develop predictive models for the mean panel present serviceability ratings (PSR). The models were of the form where PSR is the dependent (y) variable and pavement distress types are the independent (x) variables.

The prediction of panel PSR ratings has been modeled several ways in the past. The original PSR equation from the AASHO Road Test was based upon both roughness and distress.⁽⁴⁴⁾ Many other models have been developed based solely on roughness (reference 45), or solely on visual distress (reference 46).

The best way to predict PSR is using roughness. However, a PSR model based on only key distress types is useful in mechanistic-empirical design of pavements to approximately relate physical deterioration (that can be estimated using other models) to serviceability, or user response.

PSR prediction models were developed for both JPCP and JRCP. Whereas all measured types of distress were initially considered, only three key distress types proved significant: joint faulting, joint deterioration (spalling), and transverse cracking. The presence of full-depth patching also displayed some significance and hence is included in the equations.

The models for each pavement type are shown below.

Jointed Plain Concrete Pavements

$$\begin{aligned} \text{PSR} = & 4.356 - 0.0182 \text{ TFAULT} - 0.00313 \text{ SPALL} - 0.00162 \text{ TCRKS} \\ & - 0.00317 \text{ FDR} \end{aligned} \quad (36)$$

Where:

- PSR = Mean panel rating of pavement (0 to 5 AASHTO Scale)
- TFAULT = Cumulative transverse joint faulting, in/mi
- SPALL = Number of deteriorated (medium- and high-severity) transverse joints per mile
- TCRKS = Number of transverse cracks (all severities) per mile
- FDR = Number of full-depth repairs per mile

Statistics:

$$\begin{aligned} R^2 &= 0.58 \\ SEE &= 0.31 \text{ (units of PSR)} \\ n &= 282 \end{aligned}$$

Jointed Reinforced Concrete Pavements

$$\begin{aligned} \text{PSR} &= 4.333 - 0.0539 \text{ TFAULT} - 0.00372 \text{ SPALL} \\ &\quad - 0.00425 \text{ MHTCRKS} - 0.000531 \text{ FDR} \end{aligned} \tag{37}$$

Where:

- PSR = Mean panel rating of pavement (0 to 5 AASHTO Scale)
- TFAULT = Cumulative transverse joint faulting, in/mi
- SPALL = Number of deteriorated (medium- and high-severity) transverse joints per mile
- MHTCRKS = Number of medium- and high-severity cracks per mile
- FDR = Number of full-depth repairs per mile

Statistics:

$$\begin{aligned} R^2 &= 0.64 \\ SEE &= 0.37 \text{ (units of PSR)} \\ n &= 434 \end{aligned}$$

The values for R^2 and SEE are similar to those of the original PSR models developed at the AASHO Road Test.⁽⁴⁴⁾

Examination of the PSR models shows that transverse joint faulting has the greatest effect on reducing the PSR. Spalling, transverse cracking and full-depth repairs have a much lesser effect on reducing PSR.

The primary limitation of these models is that they do not include all distress types nor "long wavelength" roughness, such as would be caused by settlements or heaves. In fact, the relatively low R^2 and high standard errors clearly indicate that there exists other sources of variation in PSR.

These models are not intended to be used to predict PSR (or PSI) in place of roughness, since it can be shown that measured roughness is the best way to predict serviceability. These models are intended only for use in predicting serviceability when only key distress types are available. Even then, the models should be used with caution, recognizing their limitations.

Longitudinal Cracking

Longitudinal cracks run parallel to the centerline of the pavement, in either lane. Longitudinal cracking included in this analysis is for all severity levels. Longitudinal cracking existed on 17 percent of the sections in the RIPPER database. However, a significant amount of longitudinal cracking (e.g., over 500 ft/mi, or about 10 percent of the section length) only occurred on only 3 percent of the sections.

Longitudinal cracking is a major concern if it occurs in the wheelpaths. This has occurred due to inadequate centerline sawing practices, which includes depth of sawing and timing of sawing and must also consider the type of base (friction, bond). However, major foundation movements from swelling or expansive soils can also cause random slab cracking.

An analysis was conducted to determine if a model could be developed that would predict the occurrence of longitudinal cracking. The entire COPES and RIPPER databases were used in the analysis, although some of the sections from the AASHO Road Test were excluded since they were so short. The resulting database included 658 sections of JPCP and JRCP. The sections represent a wide range of pavement designs and climates.

The major deficiency of the database was that no construction-specific data exists on the construction of the longitudinal joint, such as measured saw depths and time between slab placement and sawing operations. A large majority of pavements were two-lane, one-directional Interstate highways having deformed rebar ties across the longitudinal joint. Only those pavement in California did not have tie bars across the lanes.

A number of factors were identified in the database that might have an effect on the development of longitudinal cracking. These included yearly mean temperature range, mean annual precipitation, mean freezing index, traffic

loadings, pavement type (JPCP or JRCP), age, slab thickness, base type and type of joint forming technique (plastic tape insert or saw cutting).

All attempts to develop a prediction model were unsuccessful. One reason was the low proportion of sections to exhibit longitudinal cracking (17 percent), but it is believed that the major reason was that some of the key factors influencing longitudinal cracking are construction-related. Therefore, it was only possible to identify a few design factors that affected the occurrence of longitudinal cracking.

After numerous correlation and regression analyses that considered all variables in the database, only two factors appeared to have a significant effect on longitudinal cracking. These factors were base type and joint forming method (sawcut or plastic tape insert). The database was averaged over these factors and the results are shown in table 48. There appears to be a significant difference in longitudinal cracking between the plastic tape insert method and the saw cut method. The plastic tape insert method results in far more longitudinal cracks than the saw cut method (215 ft/mi vs. 38 ft/mi).

Table 48 also shows the effect of base type on the occurrence of longitudinal cracking. Aggregate bases or no base type (slab on grade) appears to have fewer longitudinal cracks than those with stabilized bases, either with inserts or sawcut joints. Cement-treated, asphalt-treated, and lean concrete bases all have much higher amounts of longitudinal cracking than aggregate or subgrade. Due to the limited number of certain base types, further differentiation is not possible.

Concrete slabs placed on an asphalt-treated base with plastic inserts used to form the longitudinal joints seem to be the worst case, although there are only four such cases in this study. However, the plastic insert method appears to be acceptable with aggregate bases.

The base type is believed to be critical because of the friction produced between the slab and base course. Friction testing results generally show that slabs on grade or slabs on an aggregate base have much less sliding friction than a slab on a stabilized base. This data indicates that concrete pavements placed on any type of stabilized base are particularly susceptible to longitudinal crack development. The use of proper saw cutting is the most important factor in reducing the crack potential. While the depth of saw cut was not measured on any of the projects, the depth of the longitudinal joint from plans indicated that depths between 25 and 33 percent of the slab depth were generally adequate.

Transverse Joint Faulting

Transverse joint faulting is a major distress type that causes loss of serviceability in a jointed concrete pavement. Many jointed concrete pavements have shown serious faulting which has contributed to the need for expending funds for their rehabilitation.

Table 48. Mean longitudinal cracking for all sections included in COPEs and RIPPER databases.

LONG. JT. FORM TYPE	BASE TYPE	N CASES	LCRKS (FT/MILE)	LCRKS (FT/MILE)
INSERT	AGG	41	27	
INSERT	ATB	4	2051	215
INSERT	CTB	12	224	
INSERT	LCB	2	346	
SAW	None	17	17	
SAW	AGG	353	19	
SAW	ATB	65	58	38
SAW	CTB	136	73	
SAW	LCB	8	170	

Notes:

1. Longitudinal cracks (LCRKS) include all severities—low, medium, and high—occurring in two adjacent traffic lanes.
2. Base types:
 - None - slab on grade
 - AGG - aggregate base
 - ATB - asphalt-treated base
 - CTB - cement-treated base
 - LCB - lean concrete base
3. Joint forming type:
 - INSERT - plastic tape insert
 - SAW - saw cut in hardened concrete

Design engineers have attempted to reduce faulting through many different ways, including the use of dowels, nonerodible bases, permeable bases, and shorter joint spacing. Many of these attempts have been unsuccessful or only partially successful. Procedures are urgently needed to assist designers in developing joint designs that will experience limited faulting over their service life, yet not result in large initial construction costs due to overdesign.

Several attempts have been made to predict the faulting of transverse joints.^(5,6,10) All of these attempts have been partially successful in that prediction models were obtained that showed reasonable results. The major limitation of these models was in the limited database of designs that was used to generate them.

The combined RIPPER and COPES databases provides for a greatly expanded database that includes pavement sections with new design features, such as permeable bases, thick slabs, and dowels in dry climates. Table 49 provides a matrix of data illustrating the distribution of types of pavement designs and climates in the combined database. There is fairly good dispersion of pavement sections with only a few "holes" such as the lack of dowels in dry-nonfreeze areas (e.g., southwestern U.S.). There are also too few pavements with open-graded bases in certain areas like the southeastern U.S.

Table 49. Distribution of pavement sections and designs used in development of faulting models.

Climatic Region	B A S E T Y P E							
	None/AGG		CTB/ATB		LCB		PERM	
	ND	D	ND	D	ND	D	ND	D
Wet-freeze (IL,MI,OH,PA,ONT,NJ,NY)	5	257	5	44	2	--	2	5
Wet-nonfreeze (CA,FL,NC,GA,LA)	14	11	82	35	--	4	--	--
Dry-freeze (MN,NE,UT)	2	141	86	10	--	--	--	1
Dry-nonfreeze (CA,AZ)	3	--	127	--	14	1	--	--

ND = Nondoweled
D = Doweled

Two predictive models were developed using the combined databases; one for nondoweled pavements and one for doweled pavements. Because of the mechanisms involved in faulting, it was not possible to combine these two design

types into one model. The models were developed using a combination of mechanistic and empirical approaches. The form of the model was based upon observations of the development of faulting from field pavements. Key variables were identified that affect faulting from the RIPPER and COPES data analysis. Both linear and nonlinear regression techniques were utilized. Linear regression was used to help identify significant factors in the database, and nonlinear regression was used to establish the final coefficients on the factors in the form of the model established.

Doweled Concrete Pavements

The mechanistic-empirical faulting model for doweled concrete pavement is as follows:

$$\begin{aligned} \text{FAULT} = & \text{ESAL}^{0.5280} * [0.1204 + 0.04048 * (\text{BSTRESS1} / 1000)^{0.3388} + \\ & 0.007353 * (\text{AVJSPACE} / 10)^{0.6725}) - 0.1492 \\ & * (\text{KSTAT} / 100)^{0.05911} - 0.01868 * \text{DRAIN} - 0.00879 \\ & * \text{EDGESUP} - 0.00959 * \text{STYPE}] \end{aligned} \quad (38)$$

Where:

FAULT = Mean transverse joint faulting, in;

ESAL = Cumulative equivalent 18-kip (80 kN) single-axle loads in lane, millions;

BSTRESS = Maximum concrete bearing stress using closed-form equation, psi;
 $= f_d * P * T * [K_d * (2 + \text{BETA} * \text{OPENING}) / (4 * E_s * I * \text{BETA}^3)]$

BETA = $[K_d * \text{DOWEL} / (4 * E_s * I)]^{0.25}$

f_d = Distribution factor;
 $= 2 * 12 / (l + 12)$

l = Radius of relative stiffness, in;
 $= [E_c * \text{THICK}^3 / (12 * (1 - u^2) * \text{KSTAT})]^{0.25}$

E_c = Concrete modulus of elasticity, psi;
 $= 14.4 * 150^{1.5} * \text{MR}_{28}^{0.77}$

- I = Moment of inertia of dowel bar cross section, in⁴;
= $0.25 * 3.1416 * (\text{DOWEL} / 2)^4$
- THICK = Slab thickness, in;
- MR₂₈ = Concrete modulus of rupture at 28 days, psi;
- u = Poisson's Ratio, set to 0.15;
- P = Applied wheel load, set to 9000 lb;
- T = Percent transferred load, set to 0.45;
- K_d = Modulus of dowel support, set to 1,500,000 pci;
- BETA = Relative stiffness of the dowel-concrete system;
- DOWEL = Dowel diameter, in;
- E_s = Modulus of elasticity of the dowel bar, set to
29,000,000 psi;
- KSTAT = Effective modulus of subgrade reaction, on the top of base, psi/in;
- OPENING = Average transverse joint opening, in
= $\text{CON} * \text{AVJSPACE} * 12 * (\text{ALPHA} * \text{TRANGE} / 2 + e)$
- AVJSPACE = Average transverse joint spacing, ft;
- CON = Adjustment factor due to base/slab frictional restraint,
= 0.65 if stabilized base,
= 0.80 if aggregate base or lean concrete base with bond breaker
- ALPHA = Thermal coefficient of contraction of PCC, set to 0.000006 /°F;
- TRANGE = Annual temperature range, °F;
- e = Drying shrinkage coefficient of PCC, set to 0.00015 strain;
- DRAIN = Index for drainage condition,
= 0, if no edge subdrain exists,
= 1, if edge subdrain exists;
- EDGESUP = Index for edge support,
= 0, if no edge support exists,
= 1, if edge support exists;

SType = Index for AASHTO subgrade soil classification,
 = 0, if A-4 to A-7,
 = 1, if A-1 to A-3;

Statistics:

R² = 0.67
 SEE = 0.0571 in
 n = 559

This prediction model includes many variables that have been shown by field investigations to affect faulting. These include repeated heavy traffic loadings, dowel bearing stress (which is greatly affected by dowel diameter), joint spacing, effective *k*-value, longitudinal drains, edge support from tied PCC shoulders or widened traffic lanes, and type of subgrade (probably because granular soils exhibit better drainage characteristics).

A plot showing predicted versus actual faulting is given in figure 50. A sensitivity of the doweled faulting model is shown in figures 51 and 52. Dowel diameter (for a constant dowel spacing of 12 in [305 mm]) and provision for subdrainage are observed to be the most critical design factors affecting transverse joint faulting.

Nondoweled Concrete Pavements

The faulting model for nondoweled concrete pavement slabs is as follows:

$$\begin{aligned} \text{FAULT} = & \text{ESAL}^{0.2500} * [0.000038 + 0.01830 * (100 * \text{OPENING})^{0.5585} \\ & + 0.000619 * (100 * \text{DEFLAMI})^{1.7229} + 0.0400 * (\text{FI} / 1000)^{1.9840} \\ & + 0.00565 * \text{BTERM} - 0.00770 * \text{EDGESUP} - 0.00263 * \text{SType} \\ & - 0.00891 * \text{DRAIN}] \end{aligned} \quad (39)$$

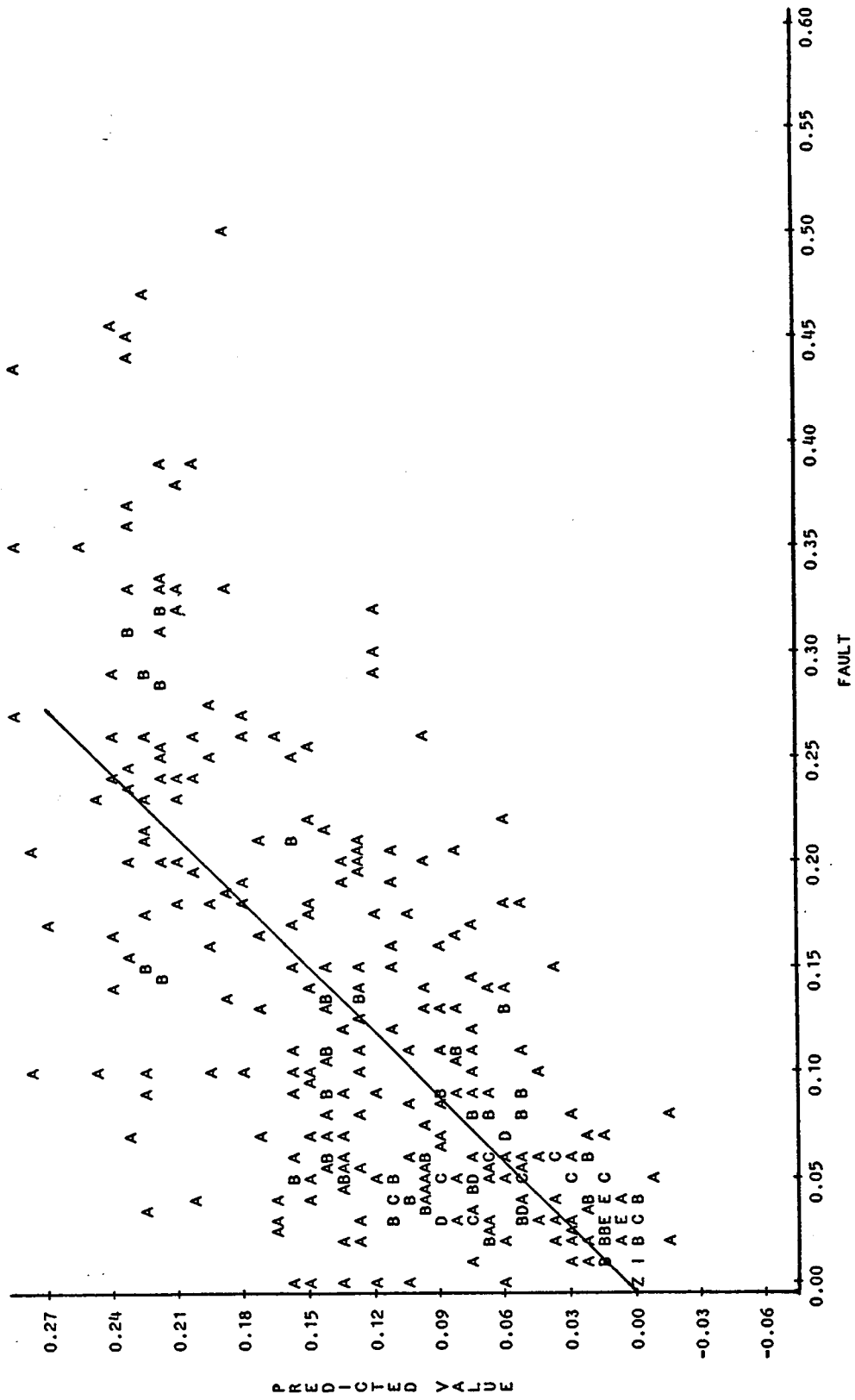
Where:

FAULT = Mean faulting across the transverse joints, in;

ESAL = Cumulative 18-kip (80 kN) equivalent single-axle loads in traffic lane, millions;

OPENING = Average transverse joint opening, in;
 = CON * AVJSPACE * 12 * (ALPHA * TRANGE / 2 + e)

LEGEND: A = 1 OBS, B = 2 OBS, ETC.



NOTE: 160 OBS HIDDEN

Figure 50. Predicted versus actual faulting for doweled joint faulting model.

JOINT FAULTING

JRCP: Dowel Diameter

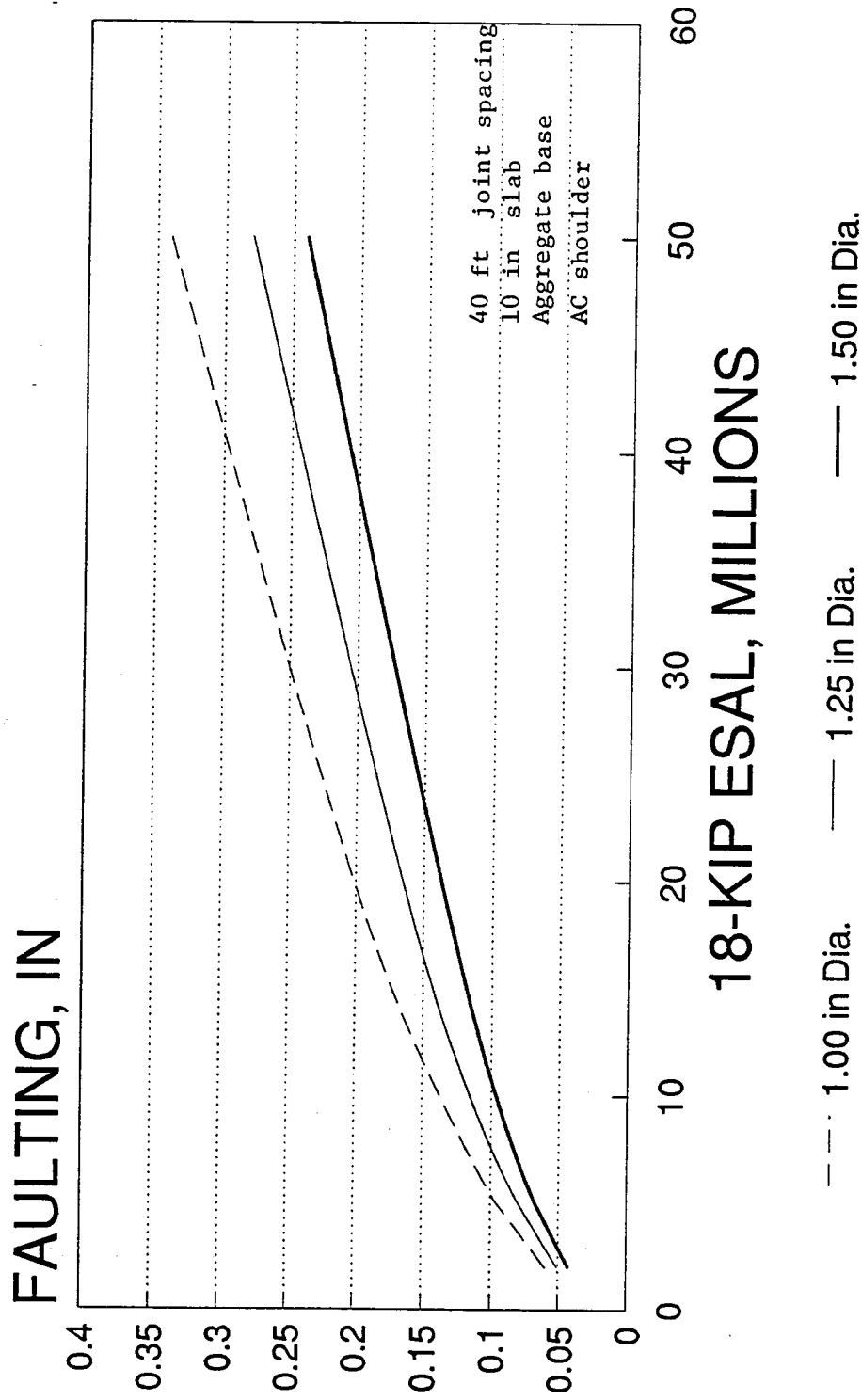


Figure 51. Sensitivity of doweled joint faulting model to dowel diameter.

JOINT FAULTING

JRCP: Drainage/PCC Sh.

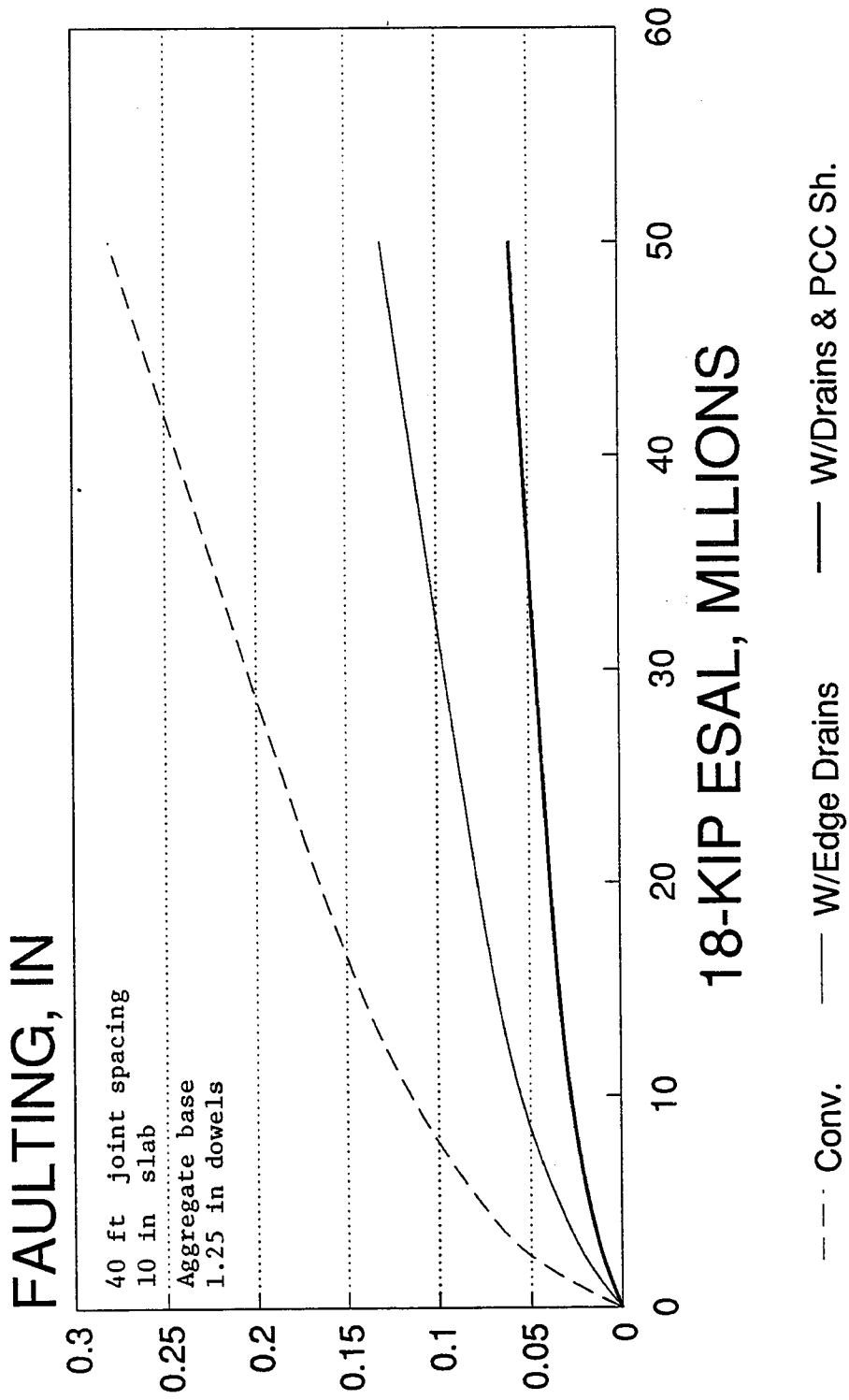


Figure 52. Sensitivity of doweled joint faulting model to drainage and shoulder type.

- CON = Adjustment factor due to base/slab frictional restraint,
 = 0.65 if stabilized base,
 = 0.80 if aggregate base;
- AVJSPACE = Average transverse joint spacing, ft;
- ALPHA = Thermal coefficient of contraction of PCC, set to 0.000006 /°F;
- TRANGE = Annual temperature range, °F; (Minimum average January temperature - Maximum average July temperature)
- e = Drying shrinkage coefficient of PCC, set to 0.00015 strain;
- DEFLAMI = Ioannides' corner deflection, in;⁽⁴⁷⁾
 = $P * (1.2 - 0.88 * 1.4142 * a / l) / (KSTAT * \beta)$
- l = Radius of relative stiffness, in;
 = $[E_c * THICK^3 / (12 * (1 - u^2) * KSTAT)]^{0.25}$
- E_c = Concrete modulus of elasticity, psi;
 = $14.4 * 150^{1.5} * MR_{28}^{0.77}$
- P = Applied wheel load, set to 9000 lb;
- a = Radius of the applied load, set to 5.64 in, assuming tire pressure = 90 psi;
- KSTAT = Modulus of subgrade reaction, on the top of base, psi/in;
- THICK = Slab thickness, in;
- u = Poisson's Ratio, set to 0.15;
- MR₂₈ = Concrete modulus of rupture at 28 days, psi;
- BTERM = Base type factor;
 = $10 * [ESAL^{0.2076} * (0.04546 + 0.05115 * GB + 0.007279 * CTB + 0.003183 * ATB - 0.003714 * OGB - 0.006441 * LCB)]$
- GB = Dummy variable for dense-graded aggregate base,
 = 1 if aggregate base,
 = 0 otherwise;
- CTB = Dummy variable for dense-graded, cement-treated base,
 = 1 if cement-treated base,
 = 0 otherwise;

- ATB = Dummy variable for dense-graded, asphalt-treated base,
 = 1 if asphalt-treated base,
 = 0 otherwise;
- OGB = Dummy variable for open-graded aggregate base
 or open-graded asphalt-treated base,
 = 1 if open-graded base,
 = 0 otherwise; and
- LCB = Dummy variable for lean concrete base,
 = 1 if lean concrete base,
 = 0 otherwise.
- FI = Freezing index, Degree-Days;
- DRAIN = Index for drainage condition,
 = 0, if no edge subdrain exists,
 = 1, if edge subdrain exists;
- EDGESUP = Index for edge support,
 = 0, if no edge support exists,
 = 1, if edge support exists;
- STYPE = Index for AASHTO subgrade soil classification,
 = 0, if A-4 to A-7,
 = 1, if A-1 to A-3;

Statistics:

R^2 = 0.81
 SEE = 0.028 in
 n = 398

This prediction model includes many variables that have been shown by field investigations to affect faulting of nondoweled joints. These include repeated heavy traffic loadings, base type, free corner deflection (which is a function of slab thickness and effective k-values), joint opening (which is a function of temperature, joint spacing and slab/base friction), climate, longitudinal drains, edge support from tied PCC shoulders or widened traffic lanes and type of subgrade (probably because granular soils exhibit better drainage characteristics).

A plot showing predicted versus actual joint faulting is given in figure 53. A sensitivity of the doweled and nondoweled faulting model is shown in figure 54. Base type, drainage, joint spacing and ESAL are observed to be the most critical design factors affecting transverse joint faulting.

LEGEND: A = 1 OBS, B = 2 OBS, ETC.

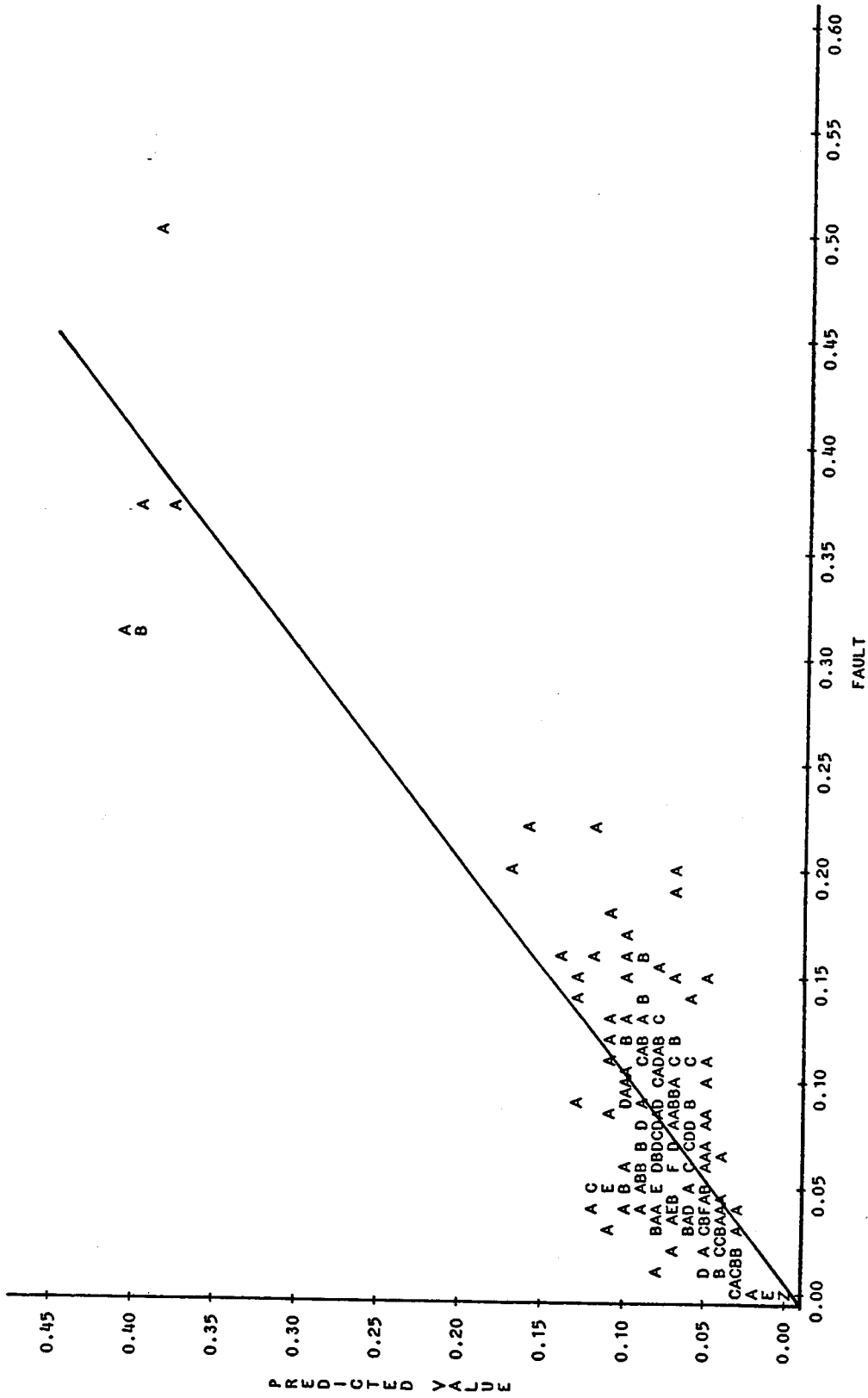


Figure 53. Predicted versus actual faulting for nondoweled joint faulting model.

JOINT FAULTING

JPCP: Dowels, Drains, Sh.

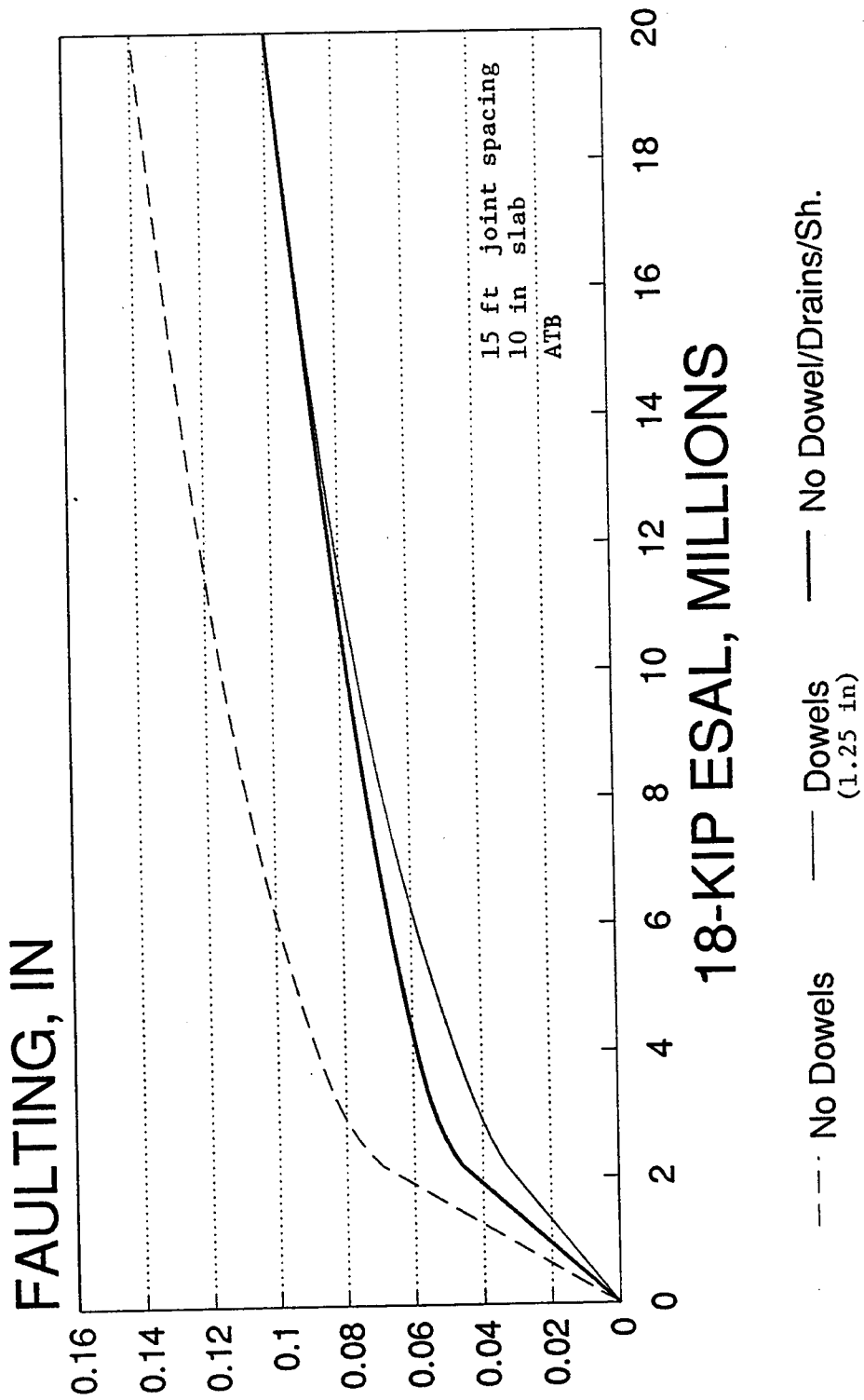


Figure 54. Sensitivity of doweled and nondoweled faulting models to drainage and shoulder type.

These mechanistic-empirical models for joint faulting can be utilized for checking joint designs to determine if the design will prevent significant faulting for the given design traffic, climate, and subgrade soils. Examples of applying this type of model for checking joint designs is given in reference 7.

Transverse Cracking

Transverse cracking in concrete slabs may occur for a number of reasons. Large temperature gradients through the slab, heavy truck loadings, and shrinkage of the concrete immediately after placement can all produce stresses in the slab which can result in transverse cracking. Once initiated, transverse cracks are entry points for water and incompressibles and can deteriorate further under traffic loadings. The presence of excessive transverse cracking can significantly detract from the overall serviceability of a concrete pavement.

Transverse cracks can occur in both jointed plain and jointed reinforced pavements. However, the mechanism influencing its occurrence in each pavement type is different. For example, transverse cracks occurring in JPCP are usually due to either thermal curling or truck loading (fatigue) whereas transverse cracks occurring in JRCP are generally due to thermal curling and shrinkage. This can be attributed to the fact that JRCP is actually designed to crack. That is, the long joint spacing for JRCP (generally on the order of 40 ft [12.2 m] or longer) produce excessive thermal stresses which result in transverse cracking. However, the slabs contain reinforcing steel which is expected to hold the cracks tight. Thus, for the reason that JRCP are expected to crack, no model was developed for JRCP. Instead, efforts concentrated on developing a model for transverse cracking in jointed plain concrete pavements.

The model developed was based on a fatigue-consumption approach similar to the one used in reference 2. This concept theorizes that a concrete pavement has a finite life and can withstand a maximum allowable number of repetitions, N , of a given traffic loading. Every individual traffic loading applied, n , decreases the life of the pavement by an infinitesimal amount. Theoretically, when $\sum n/N = 1$, fracture of the concrete material would occur. However, because of the range in variability of materials, traffic loading, and other properties, fracture of the slab (due to fatigue) can occur at values less than 1.

The following sections outline the procedure followed in the development of the JPCP cracking model. Only the 52 JPCP sections from the RIPPER database were considered in this evaluation.

Applied n

Based on historical traffic data, W-4 tables, and WIM data, the number of 18-kip (80 kN) equivalent single-axle load (ESAL) applications was estimated for each JPCP section. However, not all of these loadings would have been located at the slab edge. Studies have shown that trucks encroach into an edge loading

condition (say, within 12 in [305 mm] of the slab edge) between 3 and 7 percent of the time.⁽⁴⁸⁾ Thus, it was assumed that an average of 5 percent of the trucks loaded the slab at the critical edge location. However, if a pavement section had a widened outside traffic lane, it was assumed that only 0.1 percent of the truck loadings produced an edge loading condition.⁽⁴⁸⁾ The edge loading condition is considered critical for JPCP pavements as this is the location of the maximum stress in the slab under temperature and traffic loading and will be the point of crack initiation.

For example, if a pavement has endured an estimated 10 million 18-kip (80 kN) ESAL applications, it is assumed that only 5 percent or 0.5 million ESAL applications occur at the critical edge location; therefore $n = 0.5$ million. Similarly, if the pavement has a widened outside traffic lane, only 0.1 percent or 0.01 million 18-kip (80 kN) ESAL applications ($n = 0.01$ million) are assumed to occur at the critical edge location.

As the indicator for applied loadings, 18-kip (80 kN) ESAL applications were selected because it is an easier quantity to compute than detailed axle load data. Detailed axle load information would provide more accurate results, but it can often be a tedious and difficult computation and, furthermore, reliable axle load data is not always readily available. Additionally, as will be illustrated, a fairly good relation was obtained for the 18-kip (80 kN) ESAL applications.

It should be noted that the load equivalency factors used in estimating ESAL applications are from the AASHO Road Test and are based on serviceability, *not* on cracking. Therefore, there is some error associated with using ESAL applications as the loading factor in the fatigue analysis. Distress-based load equivalency factors would undoubtedly provide a better estimate of 18-kip (80 kN) ESAL applications.

Allowable N

The maximum number of allowable number of repetitions, N , is computed using concrete fatigue damage considerations. First, stresses at the concrete slab edge were computed for a combination of traffic loading and thermal curling. These stresses were calculated using equations developed in reference 2. A 9000 lb (40 kN) wheel load was assumed for the load calculation and the yearly average thermal gradients depicted in table 50 were assumed for the thermal curling calculation. These thermal gradients are daytime gradients, which represents the critical thermal curling condition when thermal stresses and load stresses are additive. By considering the gradients, the total stress at the slab edge due to loading and thermal curling was determined.

The stress at the slab edge was reduced, however, if tied concrete shoulders were present. Tied concrete shoulders are expected to provide support to the mainline pavement and thereby reduce the magnitude of the critical edge stress. Since the deflection load transfer between the mainline pavement and tied concrete

Table 50. Yearly average daytime thermal gradients used in curling computations.(2)

Slab Thickness, in	AVERAGE DAYTIME THERMAL GRADIENT, °F/in		
	Wet-Nonfreeze Climatic Zone	Dry/Wet-Freeze Climatic Zones	Dry-Nonfreeze Climatic Zone
8	1.40	1.13	1.41
9	1.30	1.05	1.31
10	1.21	0.96	1.21
11	1.11	0.87	1.10
12	1.01	0.79	1.00

shoulder had been obtained during the field testing, the amount of support, or edge stress reduction, could be estimated from figure 55. This figure provides the equivalent stress load transfer for a given deflection load transfer and this stress load transfer was used to determine the amount of support (and hence the reduction in the number of 18-kip (80 kN) ESAL applications) provided by the concrete shoulders. For example, if the deflection load transfer efficiency (LTE) for a concrete shoulder is 43 percent, the equivalent stress LTE is approximately 14 percent (only 14 percent of the stress is being transferred). Therefore, since

$$\text{Total Stress} = \text{Stress}_{\text{loaded}} + \text{Stress}_{\text{unloaded}} \quad \text{and}$$

$$\text{Stress LTE} = \text{Stress}_{\text{unloaded}} / \text{Stress}_{\text{loaded}}$$

Then

$$\text{Total Stress} = \text{Stress}_{\text{loaded}} + (\text{Stress}_{\text{loaded}}) * \text{Stress LTE}$$

or

$$\text{Stress}_{\text{loaded}} = \text{Total Stress} / (1 + \text{Stress LTE})$$

Thus, for the above example, the computed (total) edge stress would be multiplied by a factor of $[1/(1 + 0.14)]$ or 0.88.

The stress equations in reference 2 require several section-specific design inputs, including slab thickness, composite k -value, and slab length. It should be noted that, for sections with random slab lengths (e.g., 12-13-19-18 ft [3.7-4.0-5.8-5.5 m]), each slab length was considered individually as the stresses produced on each slab would be different. This also required that the percentage of slabs cracked be broken down according to slab length. In this way, there were actually 184 cases representing the 52 JPCP sections.

With the critical stress value calculated for the slab edge, the stress ratio was computed. The stress ratio is defined as the ratio of the edge stress to the 28-day modulus of rupture (third point). This value was then directly entered into the following fatigue equation:

$$\text{Log}_{10} N = 2.13 * [1 / \text{SR}]^{1.2} \quad (40)$$

where:

- N = Allowable 18-kip (80 kN) applications
- SR = Stress Ratio, ratio of computed edge stress to 28-day modulus of rupture

The above equation was originally developed for airport work and has shown good results in various applications.⁽⁴⁹⁾

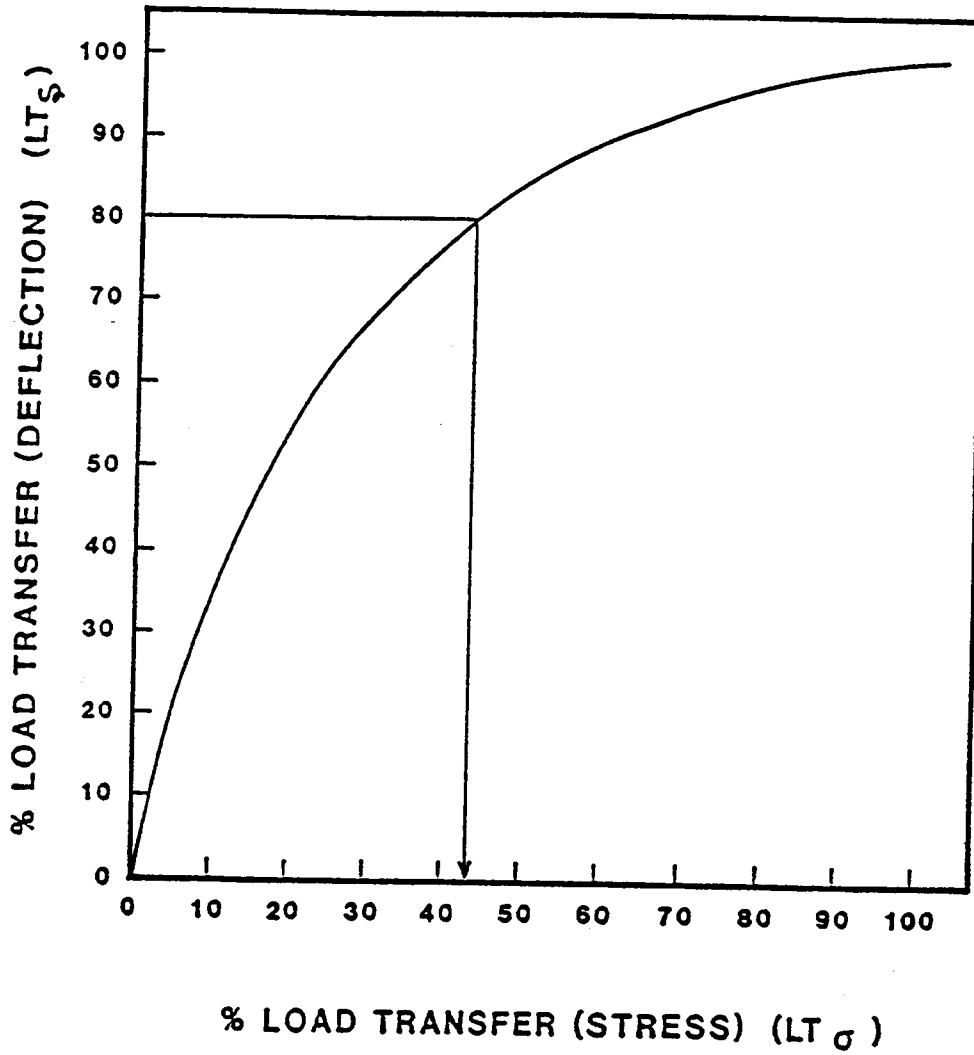


Figure 55. Relation between deflection load transfer efficiency and stress load transfer efficiency.

JPCP Cracking Model

With the determination of n and N , cumulative fatigue damage (n / N) was calculated for each JPCP section (or for each individual slab length for JPCP sections with random joint spacing). The base ten logarithm was taken of each fatigue damage value and plotted against the corresponding percent slabs cracked. This is illustrated by the individual data points shown in figure 56. This figure indicates that most transverse slab cracking occurs in a vertical band between -2 and +2. Thus, as fatigue damage approaches 1 ($\log_{10} [n/N]$ approaches 0), the likelihood of transverse slab cracking increases. The reason for the range of values is because of variations in material properties, traffic estimations, and other factors.

Linear and nonlinear regression procedures were used to try to fit a model through the data. However, the large scatter of data prevented the development of a reasonable model. Therefore, a model was fit through the data for the sections exhibiting cracking. As such, this model would provide a conservative estimate of the development of transverse cracking since many of the sections that had fatigue damage near 1 and no slab cracking were excluded. The model, which is plotted in figure 56, is given below.

$$P = \frac{1}{0.01 + 0.03 * [20^{-\log (n/N)}]} \quad (41)$$

where:

- P = Percent of Slabs Cracked
- n = Actual number of 18-kip (80 kN) ESAL applications at slab edge
- N = Allowable 18-kip (80 kN) ESAL applications (from Eq. 40)

This equation fits the data fairly well and is in the classical S-shaped curve, which is thought of as representing actual distress development. As such, the curve meets the required boundary conditions (i.e., zero slab cracking for zero fatigue damage and 100 percent slab cracking for infinite fatigue damage).

A sensitivity analysis was performed on the equation for several key pavement design inputs. Figure 57 provides slab cracking as a function of 18-kip (80 kN) lane (not edge) ESAL applications for different shoulder types. It is observed that the section with a tied PCC shoulder (20 percent stress load transfer efficiency assumed) and the section with a widened outside traffic lane and AC shoulder exhibit very little, if any, transverse cracking. However, the section with the AC shoulder displays a significant amount of transverse cracking.

Figure 58 provides a similar sensitivity analysis for joint spacing. The positive influence of shorter slabs on reducing transverse cracking is clearly evident. The reduction in slab cracking between 20 ft (6.1 m) and 15 ft (4.6 m) slabs is quite significant, but additional benefit is also seen in reducing the joint spacing to 10 ft (3.0 m).

ACCUMULATED FATIGUE DAMAGE

$$\text{Log } N = 2.13 * (1 / \text{SR})^{**1.2}$$

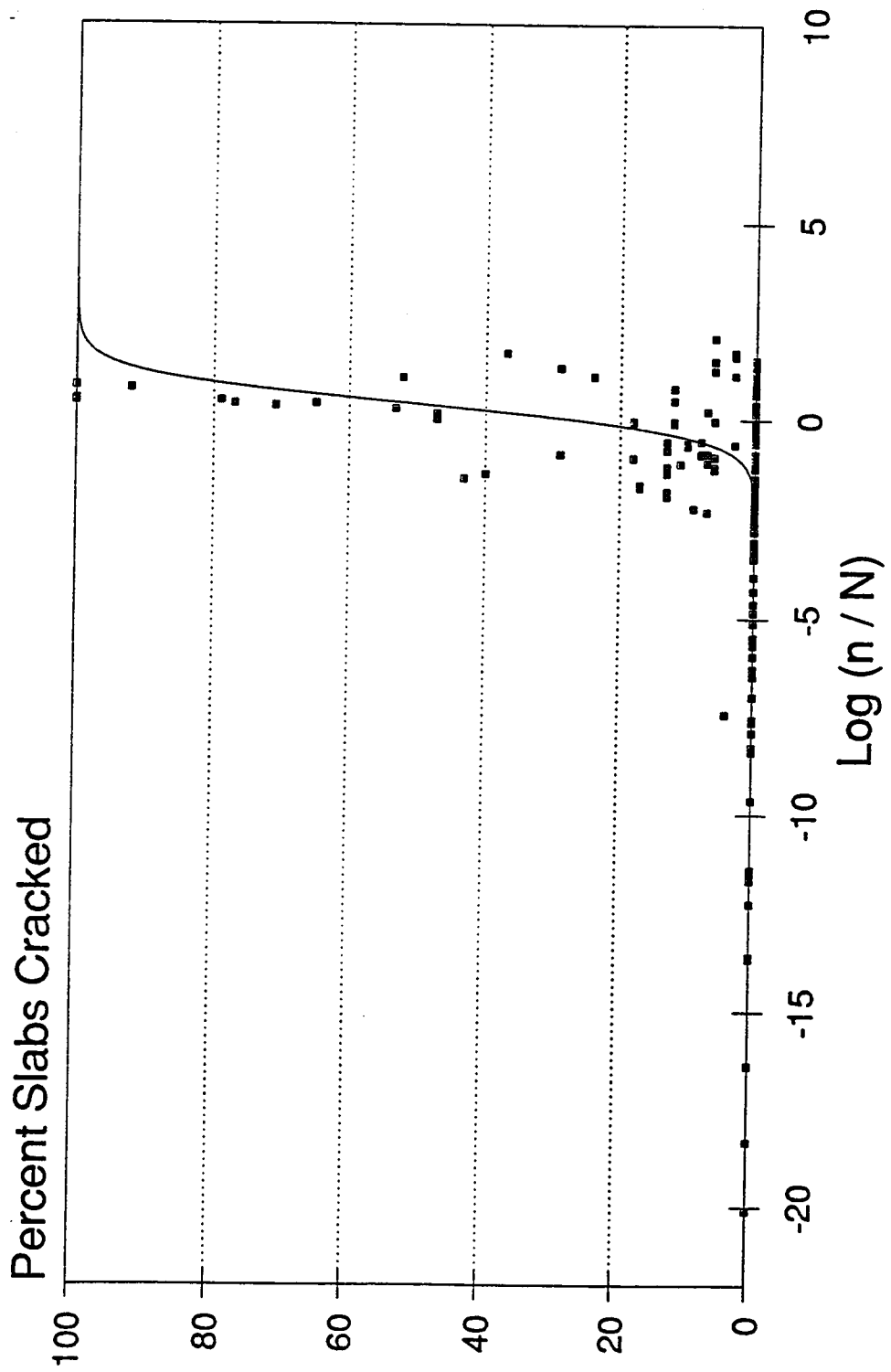


Figure 56. Percent slabs cracked versus accumulated fatigue damage.

TRANSVERSE CRACKING

Shoulder Type

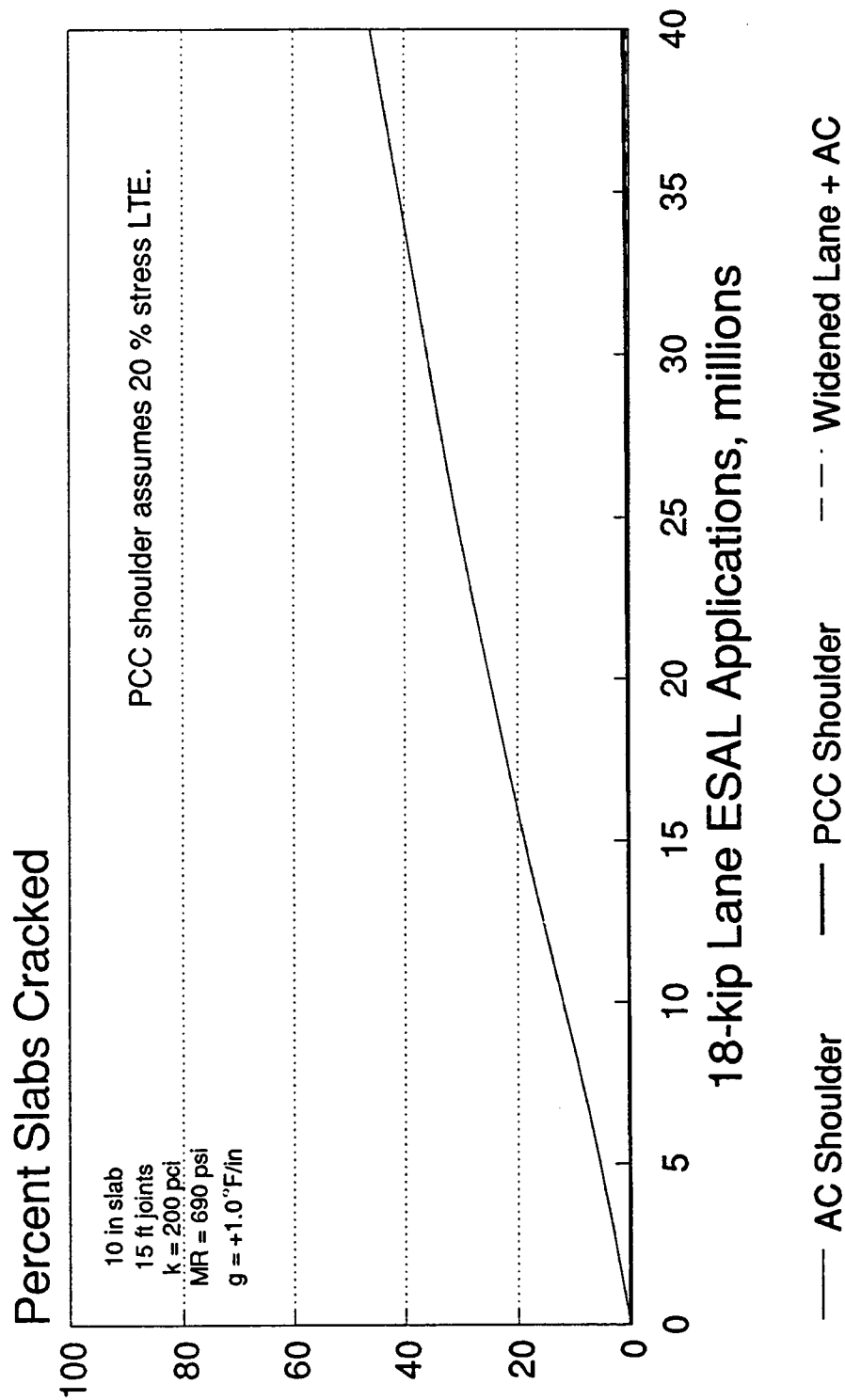


Figure 57. Sensitivity of cracking model to shoulder type.

TRANSVERSE CRACKING

Joint Spacing

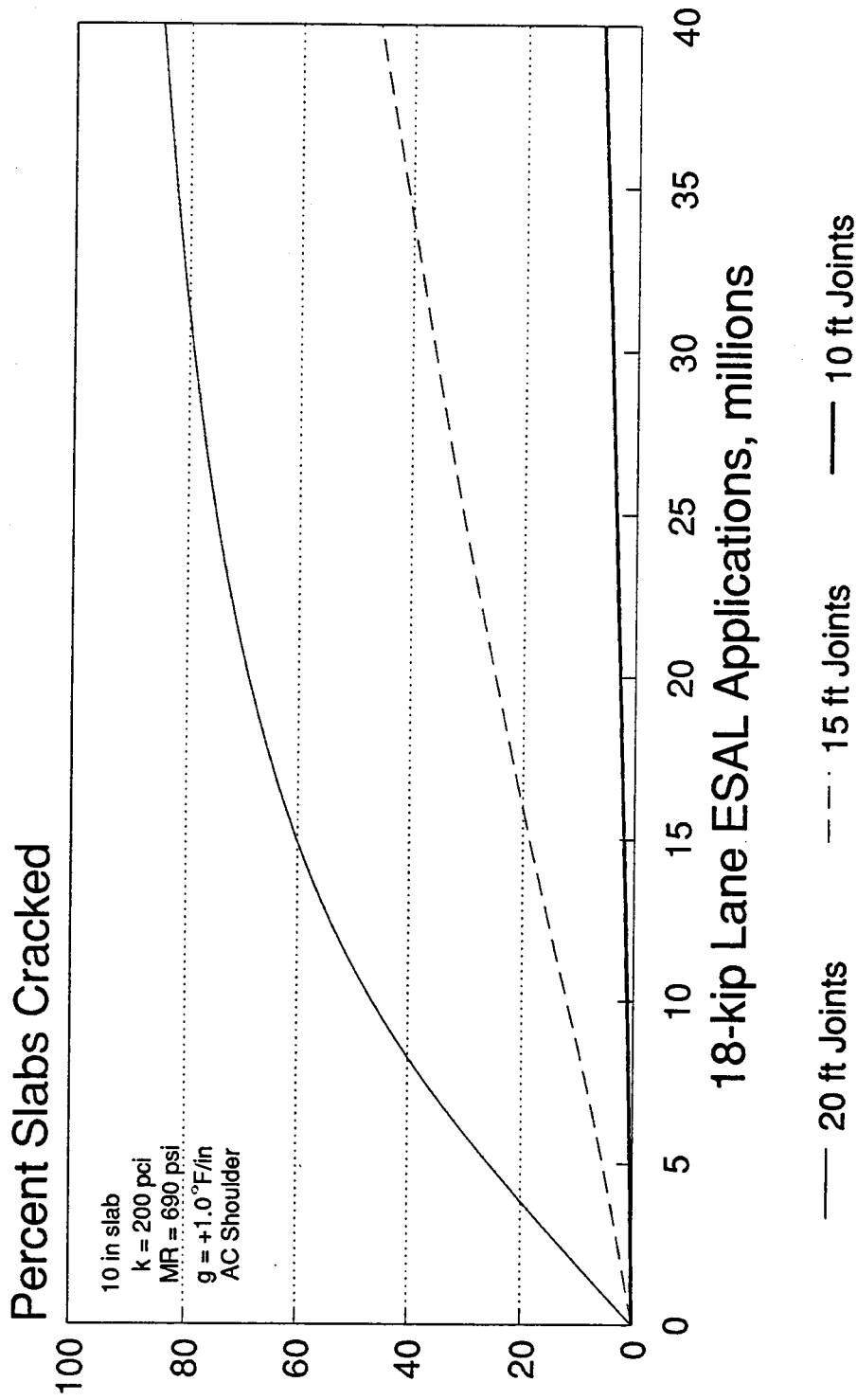


Figure 58. Sensitivity of cracking model to joint spacing.

Figure 59 provides a sensitivity analysis of the transverse cracking model with respect to slab thickness. The 8-in (203 mm) slab is observed to exhibit extensive slab cracking very early in its life. Increasing the slab thickness from 8 in (203 mm) to 10 in (254 mm) has an enormous effect on reducing the development of fatigue cracking. Likewise, an increase in slab thickness from 10 in (254 mm) to 12 in (305 mm) reduces the amount of transverse slab cracking to essentially zero.

While the cracking model employs a mechanistic approach to the development of transverse cracking, there are other factors currently not incorporated (e.g., thermal coefficient of expansion, friction from the base) that also are believed to contribute to cracking.

Transverse Joint Spalling

Using the definition provided in reference 50, joint and corner spalling is defined as any type of fracture or deterioration of the transverse joints, excluding corner breaks. Only medium- and high-severity joint spalling is included in the prediction models.

A wide range of designs are included in this evaluation. The COPES database and the RIPPER database were combined to produce a larger database for development of the joint spalling models: 262 data points for JPCP and 280 data points for JRCP. The data was cleaned to remove any sections that had unusual load transfer mechanisms (e.g., ACME devices) or that were constructed using ineffective joint forming methods (e.g., Unitube joint inserts). This was done since these devices may actually contribute to joint spalling, and most new construction does not use these devices.

The data represents a wide range of climates across the U.S. from the major climatic zones, wet-freeze, wet-nonfreeze, dry-freeze and dry-nonfreeze. The only exception was that there were no JRCP sections located in dry-nonfreeze areas.

Prediction models were developed separately for JPCP and JRCP. Extensive efforts to develop a single model for joint spalling was not successful. One reason may be that most of the joint spalling for JPCP was of medium-severity, with very few joints with high-severity spalling. JRCP sections, however, had a much greater proportion of joints exhibiting high-severity joint spalling.

JPCP Joint Spalling Model

The final joint spalling model for JPCP is given as follows:

$$\text{JTSPALL} = \text{AGE}^{2.178} * [0.0221 + 0.5494 \text{DCRACK} \\ - 0.0135 \text{LIQSEAL} - 0.0419 \text{PREFSEAL} + 0.0000362 \text{FI}] \quad (42)$$

TRANSVERSE CRACKING

Slab Thickness

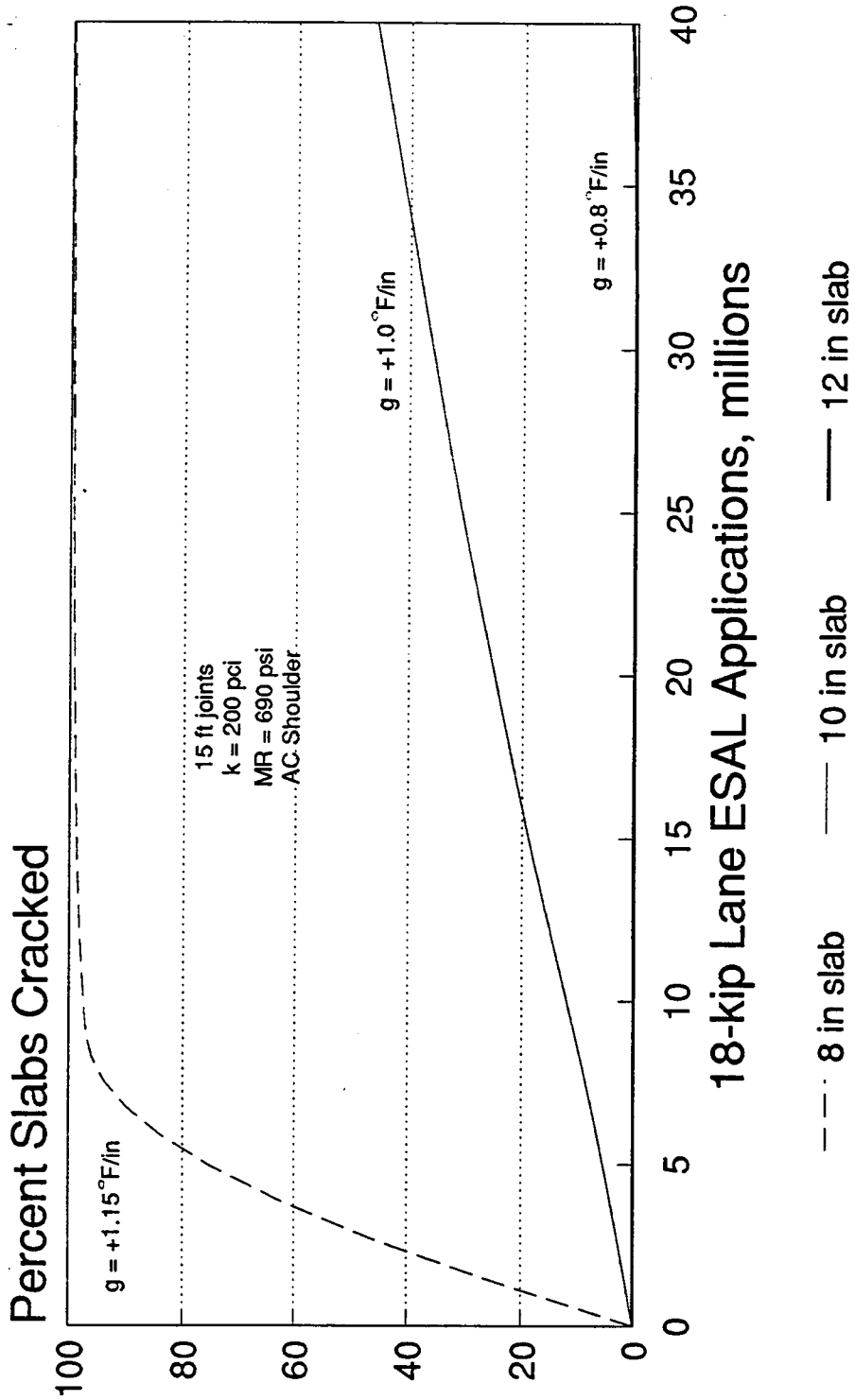


Figure 59. Sensitivity of cracking model to slab thickness.

Where:

JTSPALL = Number of medium-high joint spalls/mile

AGE = Age since original construction, years

DCRACK = 0, if no D-cracking exists
= 1, if D-cracking exists

LIQSEAL = 0, if no liquid sealant exists in joint
= 1, if liquid sealant exists in joint

PREFSEAL = 0, if no preformed compression seal exists
= 1, if preformed compression seal exists

FI = Freezing Index, degree days below freezing

Statistics:

R ²	=	0.59
SEE	=	15 joints/mi
n	=	262

A sensitivity of the model is shown in figures 60 and 61. Figure 60 shows the average effect that joint sealants have on a JPCP in a cold climate (FI = 400, no D-cracking). Having a liquid joint sealant reduces the amount of spalling by nearly 50 percent over a 30-year-period. A preformed sealant reduces the amount of joint spalling to essentially zero over a 30-year-period. One such example of this was the ONT 2 section. This pavement section contained a preformed joint sealant and did not exhibit any joint spalling over a period of 15 years. Since it is believed that incompressibles are the major cause of joint spalling, it appears that preformed sealants are capable of keeping incompressibles from infiltrating the joints for a significant period of time.

Figure 61 shows the dramatic effect of D-cracking on joint spalling. It also shows the effect of a warm climate (FI = 0) and a freezing climate (FI = 400) on the development of joint spalling.

JRCP Joint Spalling Model

The final joint spalling model for JRCP is given as follows:

$$\begin{aligned} \text{JTSPALL} = & \text{AGE}^{4.1232} * [0.00024 + 0.0000269 \text{ DCRACK} \\ & + 0.000307 \text{ REACTAGG} - 0.000033 \text{ LIQSEAL} \\ & - 0.0003 \text{ PREFSEAL} + 0.00000014 \text{ FI}] \end{aligned} \quad (43)$$

JOINT SPALLING -- JPCP

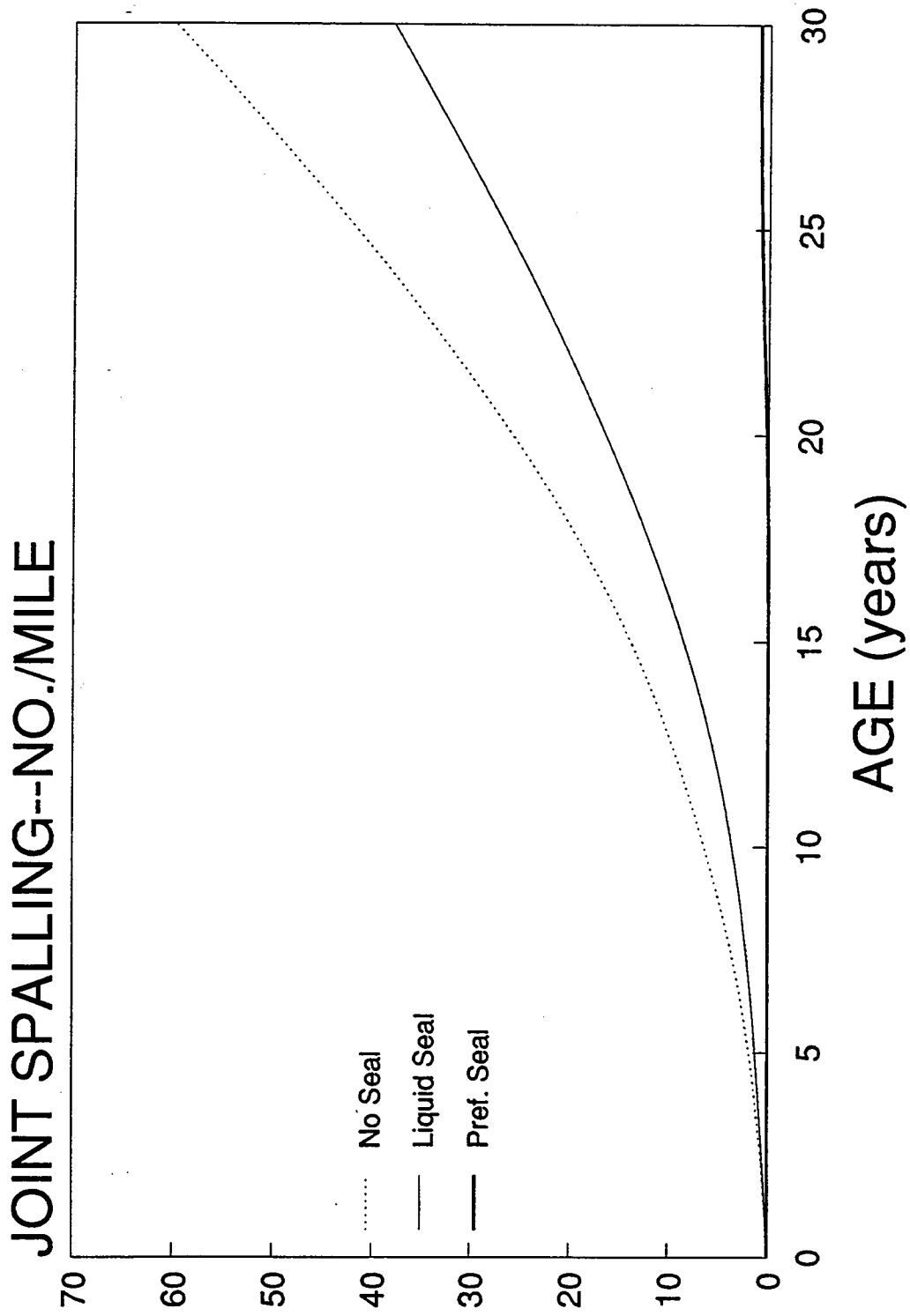


Figure 60. Sensitivity of JPCP joint spalling model to sealant type.

JOINT SPALLING -- JPCP

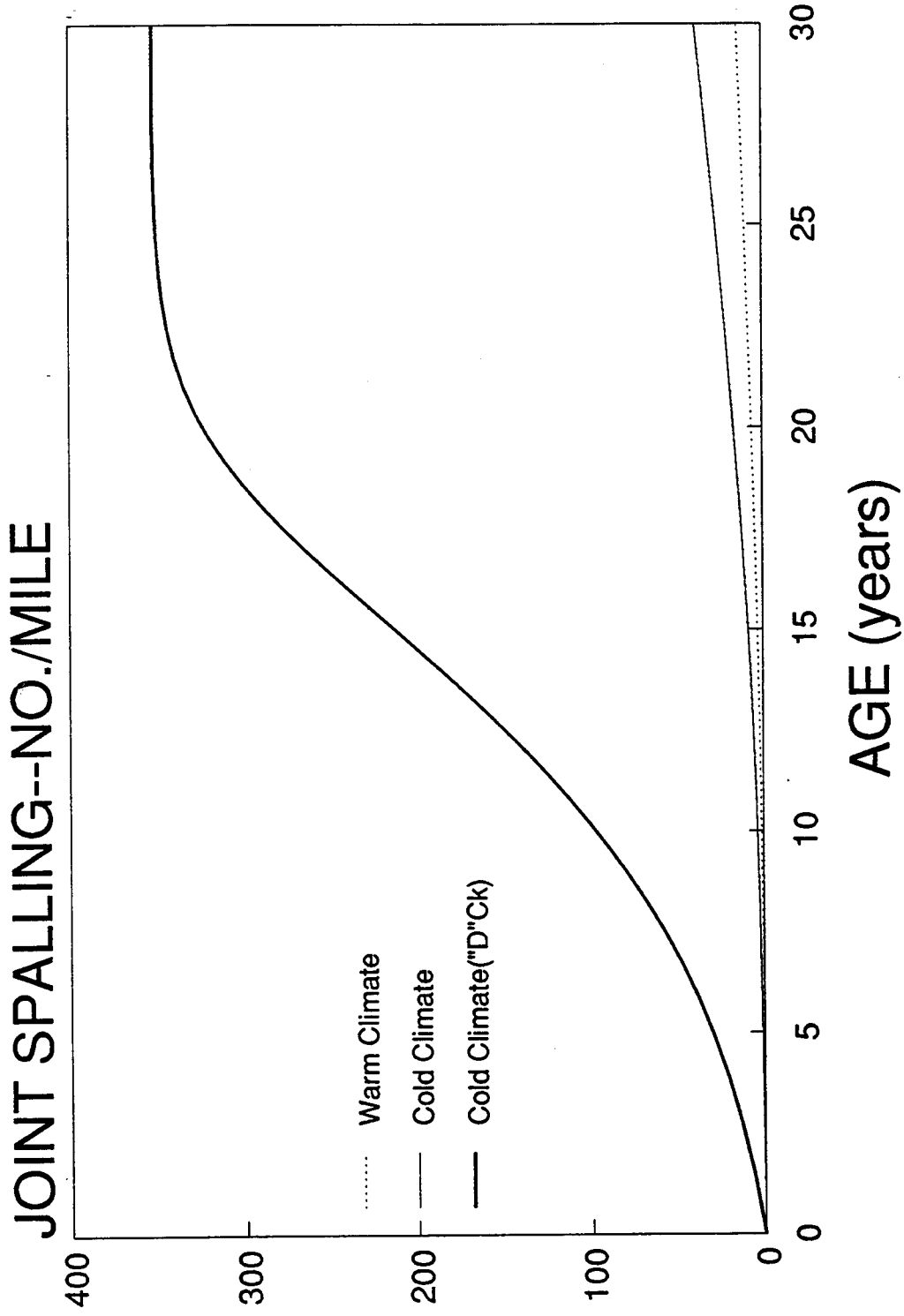


Figure 61. Sensitivity of JPCP joint spalling model to climate.

Where the terms are all as defined previously except:

REACTAGG = 0, if no reactive aggregate exists
= 1, if no reactive aggregate exists

Statistics:

R ²	=	0.47
SEE	=	13 joints/mi
n	=	280

A sensitivity of the model is shown in figure 62. This figure shows the average effect that joint sealants have on a JRCP in a cold climate (FI = 400, no D-cracking). Having a liquid joint sealant reduces the amount of spalling by about 11 percent over a 30-year-period. However, a preformed sealant reduces the amount of joint spalling to essentially zero over the same 30-year-period.

One such example of this performance was MI 4-1 near Charlotte, Michigan. This pavement, which had a preformed sealant, did not exhibit any joint spalling over a period of 15 years. Again, the preformed sealants are apparently keeping out incompressibles, which are believed to be the major cause of joint spalling.

JOINT SPALLING -- JRCP

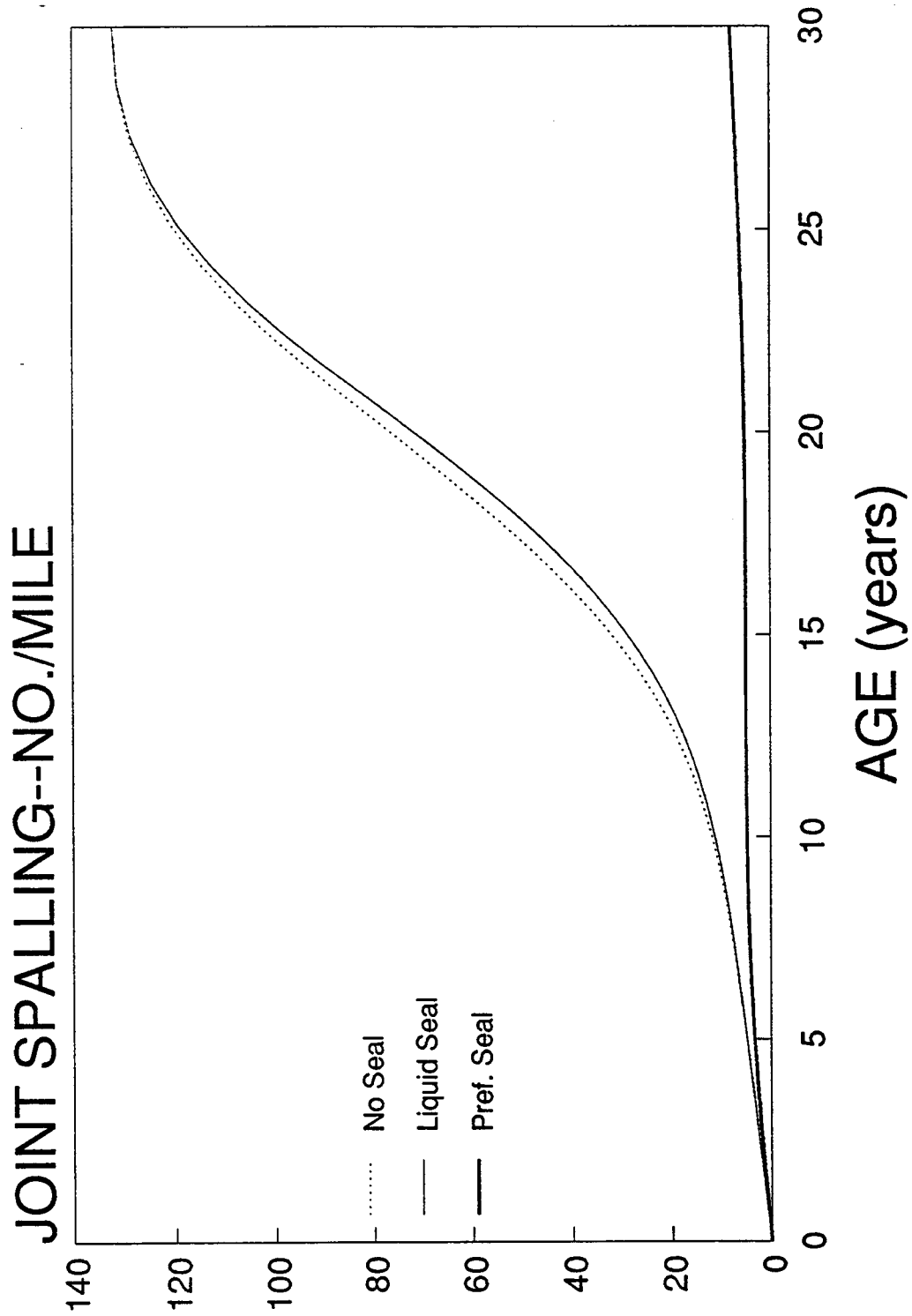


Figure 62. Sensitivity of JRCP joint spalling model to sealant type.

CHAPTER 6 EVALUATION OF THE COST-EFFECTIVENESS OF SELECTED PAVEMENT DESIGN FEATURES

1. INTRODUCTION

There are a number of design features that can be included as options in a given pavement design. This study has examined the performance of many of these features, such as base type, the use of load transfer devices, and construction of tied concrete shoulders. Performance data has supported findings such as the beneficial effect of dowel bars on reducing faulting and of short joint spacing in reducing transverse cracking. However, the inclusion of any of these design features as an option invariably increases the construction cost of the pavement.

In order to fully evaluate the effectiveness of these design features, it is necessary to know the improved performance from their use and also to quantify the costs of these features. This can be accomplished by estimating the increased costs and the additional life that is gained from the use of the design feature and comparing those to the costs and life of a similar pavement which did not contain the design feature. The design features that are being evaluated for their cost-effectiveness follow:

- Dowel bars.
- Base types.
- Joint spacing.
- Widened lanes.
- Thick slabs.
- Joint sealants.
- Edge drains.
- Pavement type.
- Tied shoulders.
- Joint orientation.

These features were evaluated based on data collected at one or more locations on project sections in Minnesota, Michigan, North Carolina, Arizona, and California.

2. ANALYSIS PROCEDURE

The evaluation of the design features is possible because each feature is included in a project where an adjacent section exists without the feature. The performance of each of the features was estimated using the new distress models for faulting, transverse cracking, and spalling presented in chapter 5. The traffic that the pavement would carry before reaching critical levels was calculated and compared to the pavement without that feature. The critical levels that were utilized are shown in table 51.

Table 51. Critical distress levels, by pavement type.⁽⁴⁶⁾

Pavement Distress	JPCP	JRCP
Transverse joint spalling, %	15-20	20-30
Transverse joint faulting, in	0.10	0.20
Transverse cracks/mi	67	70

NOTES:

Transverse joint spalling is defined as only medium- and high-severity levels for both pavement types.

All transverse cracks are counted for JPCP; only deteriorated (medium- and high-severity) cracks are counted for JRCP.

Cost Information

Actual construction costs were requested and received from each of the States participating in this part of the study. A summary of those costs is found in appendix A to this report. Current (1989) costs were requested on a two-lane-mile basis, including shoulders. The respondents were asked to assume that all of the pavements were Rural Interstate highways, with two lanes in each direction. The pavements were assumed to be constructed at grade, with a 6 ft (1.8 m) inner shoulder and a 10 ft (3.0 m) outer shoulder.

It is worth mentioning that only the initial construction costs were considered. Costs were not included for bridges, other structures, or other pavement appurtenances. Maintenance costs, user costs, or any other costs were also not considered. This approach was used for the sake of simplicity; it is not a life-cycle cost analysis, but a comparative initial cost analysis only.

Life Prediction

Each of the prediction models presented in chapter 5 relates key distress types with appropriate contributory factors, including traffic. Thus, given the critical level of each distress and the other inputs for the models, it was possible to predict the traffic carried by the pavement to reach the critical distress level. The traffic to reach the critical distress level is calculated for each of the three distresses shown in table 51. The lowest traffic calculated for each design identifies which distress will control "failure" of the pavement and is the traffic level used in the cost-effectiveness calculation. For the case of transverse cracking on JRCP, the COPES prediction model was used since no new models were developed for JRCP transverse cracking.

Although some of the models account for the detrimental effect of materials durability distress (which some of the sections did exhibit), it was not considered in the cost-effectiveness evaluation since it is not a factor that would be deliberately included into a pavement design.

Cost-Effectiveness

The cost-effectiveness of each design feature (or combination of design features in some cases) was evaluated in a direct comparison between the design without the feature (conventional design) and the design with the feature (new design). The calculations used in the procedure are shown below:

	<u>New Design</u>	<u>Conventional Design</u>
Costs	New costs	Conventional costs
Life	X ESAL's	Y ESAL's

The percent cost increase of the new design over the conventional design can be calculated as:

$$\Delta P = [(New\ costs/Conventional\ costs) - 1] * 100$$

The percent life increase of the new design over the conventional design can be calculated as:

$$\Delta L = [(X\ ESAL's/Y\ ESAL's) - 1] * 100$$

If the percent life increase of the new design over the conventional design is greater than the percent cost increase, the new design (incorporation of the design feature) is considered to be more cost-effective, or worth the additional costs. This assumes that all other costs will be the same, which most likely will not always be the case.

3. RESULTS

Arizona

Three different concrete pavement design features were evaluated using pavements in the Phoenix area. The specific design features evaluated were slab thickness, base type, and the combination of dowels and PCC shoulders. Table 52 presents the results of the analysis of these different design features. Table 57 of appendix A provides design information for the Arizona sections evaluated.

Comparative Design 1

The first design compares a thickened, 13-in (330 mm) JPCP slab constructed directly on the subgrade to the conventional 9-in (229 mm) slab constructed on a cement-treated base. These sections were constructed on S.R. 360 in the Phoenix Urban Corridor. In this case, both the initial construction costs of the new design were lower than the conventional design and the estimated performance life was longer. Thus, the new design is considered cost-effective. The critical distress for the new design was faulting, compared to transverse cracking for the thinner slabs of the conventional design. The actual performance of the corresponding pavements shows that the new design is performing very well after 3.1 million ESAL applications, while the conventional design is exhibiting significant joint faulting and joint spalling after 3.4 million ESAL applications.

Comparative Design 2

The cost-effectiveness of base types was also compared on S.R. 360. The conventional design consisted of the standard cross section with a CTB; the new design had the same cross section, with a lean concrete base replacing the CTB. Again, in this case the construction costs of the lean concrete base were actually less than those of the conventional CTB. However, the estimated performance of

Table 52. Cost-effectiveness evaluation for Arizona.

	DESIGN 1		DESIGN 2		DESIGN 3	
	New Design 13 in PCC No Base	Conventional Design 9 in PCC CTB	New Design 9 in PCC LCB	Conventional Design 9 in PCC CTB	New Design Dowels PCC Shld	Conventional Design No Dowels AC Shoulders
FAULTING (ESAL's, millions)	12	15	17	15	55	18
TRANSVERSE CRACKING (ESAL's, millions)	14000000	5.3	3.1	5.3	7000	47
TRANSVERSE SPALLING (ESAL's, millions)	23.1	23.1	23.1	23.1	43.5	43.5
COSTS	\$425,340	\$478,140	\$460,540	\$478,140	\$538,636	\$495,740
LIFE (critical ESAL's)	12	5.3	3.1	5.3	43.5	18
Percent Increase in Costs	-11%		-4%		9%	
Percent Increase in Life	126%		-42%		142%	
COST-EFFECTIVE (Yes/No)	Yes		No		Yes	

the new design was 42 percent less, with the critical distress level in both designs occurring due to transverse cracking. The actual field data indicates that the new design is performing very well after 2 million ESAL applications, and the conventional is exhibiting significant joint faulting and joint spalling after 3.4 million ESAL applications.

Comparative Design 3

The third design, on I-10 in Phoenix, evaluated the cost-effectiveness of the combination of dowels and concrete shoulders. The conventional design consisted of 10 in (254 mm) JPCP with asphalt shoulders and no dowels. This was compared to the same design with PCC shoulders and 1.25-in (32 mm) diameter dowel bars. The new design was almost 10 percent more expensive than the conventional design, but provided a much longer service life (150 percent increase). The critical distress for the conventional design was transverse cracking and the critical distress for the new design was transverse joint faulting. The actual inservice performance of each of these sections is excellent after about 1.6 million ESAL applications.

California

There were a total of six different conventional and newer designs studied in California pavements. The design features included thickened slabs, different base types, shorter joint spacing, lane width, joint sealing, and edge drains. The results from these comparisons are presented in table 53 while table 58 of appendix A provides design information for the California sections evaluated.

Comparative Design 1

The first design compares a conventional California design with an 8.4-in (213 mm) JPCP slab to an 11.4 in (285 mm) JPCP slab, holding all other design features held constant. These pavements are located on I-5 near Tracy. The new design, with the thicker slab, cost approximately 20 percent more to construct than the conventional design. However, the new design provided a much longer service life, carrying 35 times as much traffic as the conventional design. The failure mode for the new design was by faulting; the conventional design reached a critical level of transverse cracking. After 7.6 million ESAL applications, the actual performance of the new and conventional designs is roughly equivalent; the new section has no cracking, but does display significant faulting. The conventional section shows extensive longitudinal and transverse cracking.

Comparative Design 2

The next design compares the cost-effectiveness of the conventional design with a CTB to the same design with a lean concrete base. These sections are also located on I-5 in Tracy. These two different designs were constructed at approximately the same cost. The critical distress for both designs was transverse

Table 53. Cost-effectiveness evaluation for California.

	DESIGN 1		DESIGN 2		DESIGN 3	
	New Design	Conventional Design	New Design	Conventional Design	New Design	Conventional Design
	11.4 in PCC	8.4 in PCC	LCB	CTB	7.75 ft Jts	15.5 ft Jts.
FAULTING (ESAL's, millions)	22	18	21	18	54	18
TRANSVERSE CRACKING (ESAL's, millions)	1500	0.315	0.345	0.315	1.07	0.315
TRANSVERSE SPALLING (ESAL's, millions)	24.3	24.3	24.3	24.3	24.3	24.3
COSTS	\$491,000	\$414,800	\$419,400	\$414,800	\$419,700	\$414,800
LIFE (critical ESAL's)	22	0.315	0.345	0.315	1.07	0.315
Percent Increase in Costs	18%		1%		1%	
Percent Increase in Life	6884%		10%		240%	
COST-EFFECTIVE (Yes/No)	Yes		Yes		Yes	

Table 53. Cost-effectiveness evaluation for California (continued).

	DESIGN 4		DESIGN 5		DESIGN 6	
	New Design AC	Conventional Design CTB	New Design Jt. Seal	Conventional Design No Seal	New Design Drains	Conventional Design No Drains
FAULTING (ESAL's, millions)	111	73	31	31	46	21
TRANSVERSE CRACKING (ESAL's, millions)	61	67	57	57	26	26
TRANSVERSE SPALLING (ESAL's, millions)	36.5	36.5	21.5	13.9	45.2	45.2
COSTS	\$538,000	\$487,000	\$431,200	\$414,800	\$513,400	\$487,000
LIFE (critical ESAL's)	36.5	36.5	21.5	13.9	26	21
Percent Increase in Costs		10%		4%		5%
Percent Increase in Life		0%		55%		24%
COST-EFFECTIVE (Yes/No)		No		Yes		Yes

cracking, and while the new design was more cost-effective, neither design was able to sustain any significant volume of traffic before a critical level of transverse cracking occurred. This is in contrast to the actual field performance which indicates that, after 7.6 million ESAL applications, the new design is showing about twice as much transverse cracking as the conventional design.

Comparative Design 3

The third design compares the conventional joint spacing of 12-13-19-18 ft (3.7-4-5.8-5.5 m) with a shorter joint spacing pattern of 8-11-7-5 ft (2.5-3.4-2.1-1.5 m). Like the previous designs, these designs were also constructed at about the same cost. While the new design was more cost-effective than the conventional design, both reached critical levels of transverse cracking at an unacceptably low level of traffic. These results seem to agree with the actual field results, which show the new design performing better (less cracking, faulting) than the conventional design after 7.6 million ESAL applications.

Comparative Design 4

The fourth California design evaluated was located on U.S. 101, near Thousand Oaks. The conventional design was compared to a similar pavement with two exceptions: the outer lane was 15 ft (4.6 m) wide instead of 12 ft (3.7 m) and the base was a dense-graded hot mix asphalt concrete instead of a CTB. The new design cost 10 percent more to construct than the conventional design but did not result in an increase in life. However, both designs reached a critical level of spalling after 36.5 million ESAL applications, representing an acceptable performance period. The actual field performance results show that the conventional design has significant faulting and a few transverse cracks while the new design is performing well and displaying little distress.

Comparative Design 5

A comparison of the cost-effectiveness of sealing the transverse joints was made with two sections on U.S. 101 near Geyserville. The conventional design did not contain sealed transverse joints, while those of the new design were sealed with rubberized asphalt. Sealing the joints added about 4 percent to the construction costs of the new design and resulted in a 55 percent increase to the pavement life. Both designs reached a critical level of spalling, with the new design failing at 21.5 million ESAL applications and the conventional design failing at 13.9 million ESAL applications. The actual field data indicates that both sections are exhibiting significant faulting and cracking after 3.6 million ESAL applications, but the new section does have slightly less spalling.

Comparative Design 6

The final design comparison in California is located on I-5, near Sacramento. The conventional design was constructed without any drainage and the new

design was constructed with edge drains. The addition of drainage resulted in a 5 percent increase in construction costs over the conventional design. However, the conventional design reached a critical level of faulting after carrying 90 percent less traffic than the new design was able to carry to reach a critical level of transverse cracking. Thus the addition of edge drains to this pavement was cost-effective.

Michigan

There were six different conventional and newer pavement designs evaluated in Michigan. Two of the comparisons were made with a combination of factors: both new designs included load transfer and different base types. The other four design features compared were different pavement types, edge drains, PCC shoulders, and permeable bases. The results of these comparisons and the cost-effectiveness of the new designs is shown in table 54. The design features that were evaluated on the Michigan sections included thickened slabs, different base types, shorter joint spacing, lane width and base types, joint sealing, and edge drains; these are summarized in table 59 of appendix A.

Comparative Design 1

The first sections were selected to evaluate the cost-effectiveness of the combination of load transfer and base type on U.S. 10 near Clare. The conventional design had 1.25-in (32 mm) diameter dowels and an aggregate base. The new design, which had an asphalt-treated base and did not contain dowels, cost approximately 6 percent more to construct than the conventional design, and, according to the models, was able to provide 38 percent more life. The new design reached a critical level of faulting after 2.2 million ESAL applications while the conventional design reached a critical level of cracking after 1.6 million ESAL applications. However, in terms of reducing joint faulting, the new design was inadequate as failure in that mode occurred after only 2.2 million ESAL applications. The conventional design, which contained dowel bars, was able to sustain 35 million ESAL applications before failing in transverse joint faulting.

Comparative Design 2

The second set of designs, also on U.S. 10 near Clare, evaluate the cost-effectiveness of load transfer and base type. The difference with this set of designs is that the conventional design had dowels and an aggregate base while the new design did not contain dowels and had an asphalt-treated permeable base. This design cost 7 percent more to construct than the conventional design and showed an increase in life of 56 percent. The critical distresses were transverse cracking and joint faulting for the conventional design and new design, respectively. Again, however, the new design failed in terms of faulting after only 2.2 million ESAL applications, which is unacceptable for this type of highway. The doweled conventional design was projected to sustain 35 million ESAL applications before failing in transverse joint faulting.

Table 54. Cost-effectiveness evaluation for Michigan.

	DESIGN 1		DESIGN 2		DESIGN 3	
	New Design	Conventional Design	New Design	Conventional Design	New Design	Conventional Design
	ATB No Dowels	AGG Dowels	PATB No Dowels	AGG Dowels	14.5 ft Jts. JPCP	71 ft Jts. JRCP
FAULTING (ESAL's, millions)	2.2	35	2.5	35	35	28
TRANSVERSE CRACKING (ESAL's, millions)	4.7	1.6	4.6	1.6	1.6	10
TRANSVERSE SPALLING (ESAL's, millions)	3.2	3.2	3.2	3.2	3.2	*
COSTS	\$369,600	\$349,600	\$373,800	\$349,600	\$349,600	\$323,800
LIFE (critical ESAL's)	2.2	1.6	2.5	1.6	1.6	10
Percent Increase in Costs	6%		7%		8%	
Percent Increase in Life	38%		56%		-84%	
COST-EFFECTIVE (Yes/No)	Yes		Yes		No	

* Model reached capacity before critical failure level was reached.

Table 54. Cost-effectiveness evaluation for Michigan (continued).

	DESIGN 4		DESIGN 5		DESIGN 6	
	New Design	Conventional Design	New Design	Conventional Design	New Design	Conventional Design
	Drains	No Drains	PCC Shldr	AC Shoulders	PAGG	AGG
FAULTING (ESAL's, millions)	127	28	27	18	106	28
TRANSVERSE CRACKING (ESAL's, millions)	11	10	9.4	9.4	13.4	8.7
TRANSVERSE SPALLING (ESAL's, millions)	*	*	*	*	*	*
COSTS	\$332,100	\$323,800	\$285,400	\$284,000	\$331,300	\$323,800
LIFE (critical ESAL's)	11	10	9.4	9.4	13.4	8.7
Percent Increase in Costs		3%		0%		2%
Percent Increase in Life		10%		-100%		54%
COST-EFFECTIVE (Yes/No)		Yes		No		Yes

* Model reached capacity before critical failure level was reached.

Comparative Design 3

The next sections compare the cost-effectiveness of long-jointed JRCP (the conventional design) to short-jointed JPCP. These sections are also located on U.S. 10 near Clare. The new short-jointed JPCP was approximately 8 percent more expensive to construct than the conventional design, but was predicted to reach a critical distress level (cracking) much sooner than the conventional design. Thus, the construction of the short-jointed JPCP was not cost-effective in this case. The actual field performance data indicates that both designs are performing about the same after 0.9 million ESAL applications.

Comparative Design 4

The fourth set of designs evaluate the cost-effectiveness of edge drains, using two sections on U.S. 10, near Clare. The new design, which had edge drains, had 3 percent higher construction costs than the conventional design. The model for transverse cracking showed that this was the critical distress for both designs, and predicted that the conventional design would fail after carrying 10 percent less traffic than the new design. In addition, the faulting of the drained design was far less than that of the nondrained design. Because the added life of the new design was greater than its additional costs, the construction of edge drains on this project was cost-effective. The actual performance data of these designs discloses that the drained section has slightly less cracking and faulting than the nondrained design after nearly 0.9 million ESAL applications.

Comparative Design 5

A pair of designs on I-69 near Charlotte, Michigan was used to evaluate the cost-effectiveness of PCC shoulders. The conventional design had an AC shoulder, while the new design had PCC shoulders, although the construction costs were about the same. The model for transverse cracking showed that this was the critical distress for both designs, and predicted that both designs would fail at the same time. However, because a new model for JRCP transverse slab cracking was not developed, the COPES JRCP transverse cracking model had to be used which does not consider the influence of tied concrete shoulders. Therefore, the indication that the concrete shoulders are not cost-effective is not a valid conclusion. The actual field data indicates that the section with AC shoulders is performing better than the section with concrete shoulders after 4.4 million ESAL applications.

Comparative Design 6

The final set of designs in Michigan evaluate the cost-effectiveness of a permeable base, constructed on I-94 near Marshall. The conventional design had a aggregate base while the new design had a permeable aggregate base. The new design cost only 2 percent more to construct than the conventional design, and had a predicted life 56 percent greater than the conventional design. These results

showed the construction of the permeable base was a cost-effective design. However, the field performance results indicate fair-poor performance of the permeable base section due to the use of a 1 in (25 mm) maximum size coarse aggregate used in the concrete.

Minnesota

The cost-effectiveness of five different design features was evaluated using paired pavement designs in Minnesota. The design features that were studied were dowels, base type, joint spacing, widened lanes, and the combination of widened lanes with a permeable base. The results of these comparisons are shown in table 55. Table 60 of appendix A provides design information for the Minnesota sections evaluated.

Comparative Design 1

The first set of designs was selected to evaluate the cost-effectiveness of dowels. The designs, located on I-94 near Rothsay, were identical, except that the new design had dowel bars for load transfer and the conventional design had no load transfer devices. The additions of dowels made this design 8 percent more expensive than the conventional design. However, the conventional design was predicted to develop a critical level of faulting fairly rapidly and failed long before the new design. Thus the inclusion of dowels on this section was cost-effective. This information agrees with the field performance data, which shows that the doweled section had 0.06 in (1.5 mm) of faulting and the nondoweled section 0.31 in (8 mm) of faulting after 4.7 million ESAL applications.

Comparative Design 2

The second set of designs compares the cost-effectiveness of a design with a dense asphalt-treated base to a conventional design with an aggregate base. These sections were located on I-94 near Rothsay. The new design was approximately 6 percent more expensive than the conventional design. The new design was predicted to perform better in terms of faulting and cracking, but spalling was determined to be the critical distress for each design. Therefore, the construction of the asphalt-treated base was not cost-effective. From the field performance data, the section with the asphalt-treated base displayed much more spalling and cracking after 5.5 million ESAL applications than the conventional section.

Comparative Design 3

The next set of designs, also located on I-94 near Rothsay, were selected to evaluate the cost-effectiveness of different joint spacings. The designs were identical, except that the new design had a 27-ft (8.2 m) transverse joint spacing compared to the conventional spacing of 40 ft (12.2 m). The cost of the two designs was approximately the same and no increase in pavement life was achieved by the new design as both designs reached a critical level of spalling.

Table 55. Cost-effectiveness evaluation for Minnesota.

	DESIGN 1		DESIGN 2		DESIGN 3	
	New Design	Conventional Design	New Design	Conventional Design	New Design	Conventional Design
FAULTING (ESAL's, millions)	31	No Dowels 0.28	ATB 37	AGG 31	27 ft Jts. JRCP 31	40 ft Jts. JRCP 24
TRANSVERSE CRACKING (ESAL's, millions)	11.3	11.3	12.8	11.3	11.3	7.3
TRANSVERSE SPALLING (ESAL's, millions)	5.7	5.7	5.7	5.7	5.7	6
COSTS	\$500,000	\$462,660	\$531,900	\$500,000	\$500,000	\$493,300
LIFE (critical ESAL's)	5.7	0.28	5.7	5.7	5.7	6
Percent Increase in Costs		8%		6%		1%
Percent Increase in Life		1936%		0%		-5%
COST-EFFECTIVE (Yes/No)		Yes		No		No

Table 55. Cost-effectiveness evaluation for Minnesota (continued).

	DESIGN 4			DESIGN 5	
	New Design Widened Outer Lane	Conventional Design Standard Lane	New Design	Conventional Design	
			PATB	AGG	
FAULTING (ESAL's, millions)	34	21	63	33	
TRANSVERSE CRACKING (ESAL's, millions)	9.4	8.8	5.7	5.5	
TRANSVERSE SPALLING (ESAL's, millions)	8.3	8.3	3.1	3.1	
COSTS	\$524,500	\$493,700	\$539,900	\$479,400	
LIFE (critical ESAL's)	8.3	8.3	3.1	3.1	
Percent Increase in Costs		6%		13%	
Percent Increase in Life		0%		0%	
COST-EFFECTIVE (Yes/No)		No		No	

However, the new design was effective in reducing the amount of transverse cracking and transverse joint faulting. This agrees with the field data which shows that the conventional design had more spalling and faulting after 5.5 million ESAL applications.

Comparative Design 4

The fourth set of designs, on I-90 near Austin, are used to evaluate the cost-effectiveness of widened lanes. The new design differed from the conventional design in that the outer lane was 14 ft (4.2 m) rather than 12 ft (3.7 m). This resulted in an increase in the construction costs over the conventional design of 6 percent. The widened lane did increase life in terms of faulting but did not affect transverse joint spalling, however, which was the critical distress for both designs. No difference in cracking was observed because the JRCP cracking model does not account for the effect of a widened outside traffic lane. Because they both reached a critical level of spalling at the same time, the widened lanes was not cost-effective on these pavements. The actual performance of the widened lane was excellent after 1.5 million ESAL applications, slightly better than the actual performance of the conventional pavement after 2.8 million ESAL applications.

Comparative Design 5

The final set of designs in Minnesota evaluates the cost-effectiveness of the combination of widened lanes and a permeable base. The conventional design had an outer lane of standard width and a granular base. The new design had a widened outer lane of 14 ft (4.2 m) and a permeable asphalt base. This resulted in a pavement that was 13 percent more expensive, but was predicted to fail at the same time as the conventional design due to spalling. For this reason, this combination of features was not cost-effective for this pavement. However, the new design did increase predicted life in terms of faulting and cracking.

North Carolina

Pavement sections on I-95 near Rocky Mount were used to evaluate the cost-effectiveness of three different design features, load transfer, base type, and transverse joint orientation. The results of these evaluations are summarized in table 56. Table 61 of appendix A provides design information for the North Carolina sections evaluated.

Comparative Design 1

The cost-effectiveness of dowel bars was evaluated by comparing a new design, with 1.25-in (32 mm) dowel bars to the identical design without dowels. The use of dowels resulted in an increase in construction costs of 5 percent but no increase in life since a critical level of transverse cracking was reached for both designs. However, in terms of faulting, the new section was able to sustain over 7 times the amount of ESAL applications before failure. The actual field

Table 56. Cost-effectiveness evaluation for North Carolina.

	DESIGN 1		DESIGN 2		DESIGN 3	
	New Design	Conventional Design	New Design	Conventional Design	New Design	Conventional Design
	Dowels	No Dowels	ATB	AGG	Skewed Joints	Nonskewed Joints
FAULTING (ESAL's, millions)	23	3.1	5.2	3.1	3.2	3.2
TRANSVERSE CRACKING (ESAL's, millions)	0.08	0.08	0.36	0.08	0.08	0.08
TRANSVERSE SPALLING (ESAL's, millions)	31.1	31.1	31.1	31.1	31.1	31.1
COSTS	\$486,000	\$465,000	\$541,000	\$465,000	\$476,000	\$465,000
LIFE (critical ESAL's)	0.08	0.08	0.36	0.08	0.08	0.08
Percent Increase in Costs		5%		16%		2%
Percent Increase in Life		0%		350%		0%
COST-EFFECTIVE (Yes/No)		No		Yes		No*

* Joint orientation, the design feature being evaluated, did not enter into the models.

performance of these sections was very similar with the exception that the nondoweled section had slightly more cracking. This evaluation reveals the inability of the models to predict the performance of the long-jointed JPCP in North Carolina and Georgia which have historically displayed good performance.

Comparative Design 2

The second set of designs were used to evaluate the cost-effectiveness of a design with an asphalt-treated base to the conventional design with a aggregate base. The section with the asphalt-treated base cost 16 percent more to construct than the section with the aggregate base. As above, the critical distress for both designs was transverse cracking, and while the asphalt-treated base was cost-effective, the number of loads required to reach the critical levels was low for both designs. The actual performance of the section with asphalt-treated base was better than the actual performance of the conventional aggregate base section.

Comparative Design 3

The only evaluation of the cost effectiveness of skewed transverse joints was performed on the third set of designs in North Carolina. The conventional design had perpendicular transverse joints while the new design had skewed transverse joints. The new design was 2 percent more expensive than the conventional design to construct, but was not shown to provide longer performance than the conventional design. However, it must be noted that the models that were used to predict performance did not include a factor for joint orientation and thus it was impossible to differentiate performance with those models. Actual field performance indicates slightly better performance for a section with skewed joints than for a section with perpendicular joints after 9 million ESAL applications.

4. SUMMARY

The cost-effectiveness of new design features was evaluated by comparing the predicted performance of the pavements with these features to the predicted performance of similar pavements at the same location without the features. The models presented in chapter 5 were used to predict performance. This approach was used because the pavements with the new design features have not, in most cases, carried enough traffic. Therefore it was not possible to evaluate the cost-effectiveness of the design features with actual data.

It is clear, however, that this approach has several drawbacks. The models that were used may not be good predictors for the specific designs that were selected. An example would be the evaluation of the cost-effectiveness of skewed joints where the available models do not differentiate in performance by joint orientation. Additionally, pavement failure may also occur through some distress for which a model was not developed and applied. This is especially possible with materials problems or construction problems, which were not covered by the models.

Another problem is that the models are being applied to predict the performance of pavements that are actually constructed and carrying traffic. The models have, in some cases, predicted failure by a given distress when the actual pavement has carried more traffic and has still not failed. An example of this is North Carolina Comparative Design 1, which had carried approximately 9 million ESAL's at the time of its evaluation. The models show both the new design and the conventional design failing by reaching a critical level of transverse cracks (67/mile) at 0.4 and 0.2 million ESAL's respectively. However, the conventional design actually has 5 cracks/mile while the new design actually has no cracking.

Finally, while reaching the critical level of any distress was used as a trigger to identify failure, failure of the different distresses is probably not equal. Rehabilitation of a faulted pavement would probably be much less expensive than rehabilitation of a cracked or spalled pavement. For the sake of simplicity, however, these failure modes were all considered to be equal.

While there are problems with the methodology selected for this analysis, the approach is useful for comparing the performance of these design features at specific locations although the pavements have not carried sufficient loads to allow an analysis of cost-effectiveness with actual data. It would be desirable to look at these designs in the future when they have carried a significantly large volume of traffic.

Only a few comparisons could be carried across several of the different sections. However, those that could showed some interesting results. They are discussed below.

The inclusion of dowels was cost-effective on Minnesota Comparative Design 1, but not on North Carolina Comparative Design 1 (due to transverse cracking). The dowels were shown to be effective in reducing faulting, however. In conjunction with a change of base type, the inclusion of dowels was cost-effective on Michigan Comparative Designs 1 and 2.

The construction of thicker slabs was cost-effective on the two projects where this was the only variable (California Comparative Design 1 and Arizona Comparative Design 1). Shorter joint spacing was cost-effective on both JPCP (California Comparative Design 3) and JRCP (Minnesota Comparative Design 3).

The use of a lean concrete base instead of a cement-treated base was cost-effective on California's Comparative Design 2 but not on Arizona's Comparative Design 2. The selection of a permeable aggregate base instead of a regular aggregate base was cost-effective on Michigan's Comparative Design 6, but the use of an asphalt-treated base rather than an aggregate base was not cost-effective on Minnesota's Comparative Design 2.

In general, the addition of drainage was cost-effective. This was shown at both California Comparative Design 6 and Michigan Comparative Design 4. Furthermore, the addition of the permeable base discussed above was cost-effective. In addition, the use of an asphalt-treated permeable base without dowel bars was a cost-effective alternative as observed from Michigan Comparative Design 2, although the models showed that the design would fail prematurely in terms of joint faulting.

The rest of the design features were not replicated at more than one site and thus no general conclusions can be made.

CHAPTER 7 SUMMARY AND CONCLUSIONS

An evaluation of pavement design and prediction models has been presented. Actual field performance distresses for 95 concrete pavement sections were compared with the distress predictions from several prediction models. It was found that none of the available prediction models (AASTHO, PEARDARP, PREDICT, and PFAULT) adequately predict the performance of the inservice concrete pavements included in this study.

In addition to the evaluation of the prediction models, detailed case studies utilizing various design and analysis methods were conducted at four locations (representing the four main climatic regions): I-94, Rothsay, Minnesota; I-5, Tracy, California; U.S. 10, Clare, Michigan; and I-95, Rocky Mount, North Carolina. The detailed case studies included an investigation of the CMS climatic model, the Liu-Lytton drainage model, the ILLISLAB and JSLAB structural analysis models, the JCP-1 plain jointed concrete design method, and the BERM and JCS-1 shoulder design methods.

The CMS model was found to be a very comprehensive and rigorous analysis program which provides information on the thermal gradients that are acting on the slab. The thermal stresses, combined with stresses due to wheel loadings, allow for the determination of critical stresses to be used in a mechanistic design procedure. However, while the program provided useful information, it required some very obscure inputs.

The Liu-Lytton drainage model considers the effect of moisture on the structural capacity of the individual paving layers. It examines the drainage capabilities of the pavement structure and also the effects of moisture on the strength of the pavement structure. The program was determined to be very useful in the design process to assess a pavement's potential for moisture problems and also to provide the most probable strengths of the materials within the paving system. It is worth noting that the CMS climatic model and the Liu-Lytton drainage model are currently being combined into a comprehensive analysis program.

The comparison between the ILLISLAB and JSLAB finite element programs revealed that JSLAB has several limitations, including an error in its stiffness matrix, neglect of the Poisson's ratio in thermal curling calculations, and requiring two runs to determine thermal stresses. As part of the finite element analyses, PMARP was also evaluated and shown to contain numerous errors and limitations. ILLISLAB has undergone countless revisions and enhancements to expand its capabilities and is a useful tool for the determination of stresses in the slab due to both wheel loading and thermal curling conditions.

The JCP-1 program mechanistically considers several key design factors in its analysis, including the stiffness of the base/subgrade, axle load distributions,

climatic influences, joint spacing, and slab thicknesses. However, at this time, the influence of tied concrete shoulders can not be evaluated with the existing program.

The JCS-1 and BERM programs provide methods to determine the structural thicknesses required for concrete and asphalt shoulders, respectively. The JCS-1 program estimates the fatigue damage of the concrete shoulder so that adequate shoulder thicknesses can be determined. The BERM program also utilizes a fatigue damage approach to determine the thickness of asphalt concrete shoulders. Both programs require inputs of parked and encroaching traffic which can be very difficult parameters to estimate.

New prediction models were developed for Present Serviceability Rating (PSR), transverse joint faulting, transverse slab cracking (JPCP only), and transverse joint spalling. These models were developed using the combined RIPPER and COPES databases (approximately 500 pavement sections). Using many of these newly-developed models, an analysis of the cost-effectiveness of the addition of various design procedures was conducted.

APPENDIX A—PAVEMENT DESIGNS FOR COST-EFFECTIVENESS EVALUATION

In this appendix, pavement design data is provided for the cost-effectiveness evaluation performed in chapter 6; costs are also given for each design. All pavements were assumed to be rural Interstate highways with two lanes in each direction. It was also assumed that the pavements were located at grade with 6-ft (1.8 m) inner and 10-ft (3.0 m) outer shoulders.

All costs are current (1989) costs for a two-lane roadway (including shoulders) in the general area indicated. The costs of bridges or other structures are not included.

Tables 57 through 61 provide design information for pavement sections from Arizona, California, Michigan, Minnesota, and North Carolina.

Table 57. Arizona designs for cost-effectiveness evaluation.

DESIGN 1 - COST-EFFECTIVENESS OF THICKER SLAB ON ROUTE 360

<u>DESIGN FEATURE</u>	<u>CONVENTIONAL DESIGN</u>	<u>NEWER DESIGN</u>
Slab Design	9 in JPCP	13 in JPCP
Joint spacing	13-15-17-15 ft	13-15-17-15 ft
Sealant	standard	standard
Base type	CTB	None
Outer shoulder	AC	AC
Cost/2-lane mi	\$478,140	\$425,340

New Design Cost Effective: Yes

DESIGN 2 - COST-EFFECTIVENESS OF BASE TYPES ON ROUTE 360

<u>DESIGN FEATURE</u>	<u>CONVENTIONAL DESIGN</u>	<u>NEWER DESIGN</u>
Slab Design	9 in JPCP	9 in JPCP
Joint spacing	13-15-17-15 ft	13-15-17-15 ft
Sealant	standard	standard
Base type	CTB	Lean concrete
Outer shoulder	AC	AC
Cost/2-lane mi	\$478,140	\$460,540

New Design Cost Effective: No

DESIGN 3 - COST-EFFECTIVENESS OF DOWELS & PCC SHOULDERS ON I-10

<u>DESIGN FEATURE</u>	<u>CONVENTIONAL DESIGN</u>	<u>NEWER DESIGN</u>
Slab Design	10 in JPCP	10 in JPCP
Joint spacing	13-15-17-15 ft	13-15-17-15 ft
Sealant	standard	standard
Base type	LCB	LCB
Dowels	None	1.25 in
Outer shoulder	AC	PCC
Cost/2-lane mi	\$495,740	\$538,636

New Design Cost Effective: Yes

Table 58. California designs for cost-effectiveness evaluation.

DESIGN 1 - COST-EFFECTIVENESS OF THICKER SLAB AT TRACY

<u>DESIGN FEATURE</u>	<u>CONVENTIONAL DESIGN</u>	<u>NEWER DESIGN</u>
Slab Design	8.4 in JPCP	11.4 in JPCP
Joint spacing	12-13-19-18 ft	12-13-19-18 ft
Sealant	none	none
Base type	CTB	CTB
Outer lane width	12 ft	12 ft
Outer shoulder	AC	AC
Cost/2-lane mi	\$414,800	\$491,400
New Design Cost Effective:		Yes

DESIGN 2 - COST-EFFECTIVENESS OF BASE TYPES AT TRACY

<u>DESIGN FEATURE</u>	<u>CONVENTIONAL DESIGN</u>	<u>NEWER DESIGN</u>
Slab Design	8.4 in JPCP	8.4 in JPCP
Joint spacing	12-13-19-18 ft	12-13-19-18 ft
Sealant	none	none
Base type	CTB	Lean concrete
Outer lane width	12 ft	12 ft
Outer shoulder	AC	AC
Cost/2-lane mi	\$414,800	\$419,400
New Design Cost Effective:		Yes

DESIGN 3 - COST-EFFECTIVENESS OF JOINT SPACING AT TRACY

<u>DESIGN FEATURE</u>	<u>CONVENTIONAL DESIGN</u>	<u>NEWER DESIGN</u>
Slab Design	8.4 in JPCP	8.4 in JPCP
Joint spacing	12-13-19-18 ft	8-11-7-5 ft
Sealant	none	none
Base type	CTB	CTB
Outer lane width	12 ft	12 ft
Outer shoulder	AC	AC
Cost/2-lane mi	\$414,800	\$419,700
New Design Cost Effective:		Yes

Table 58. California designs for cost-effectiveness evaluation (continued).

DESIGN 4 - COST-EFFECTIVENESS OF LANE WIDTH & BASE TYPE ON US 101, THOUSAND OAKS

<u>DESIGN FEATURE</u>	<u>CONVENTIONAL DESIGN</u>	<u>NEWER DESIGN</u>
Slab Design	10.2 in JPCP	10.2 in JPCP
Joint spacing	12-13-15-14 ft	12-13-15-14 ft
Sealant	none	none
Base type	CTB	HMAC
Outer lane width	12 ft	15 ft
Edge drains	yes	yes
Outer shoulder	AC	AC
Cost/2-lane mi	\$487,000	\$538,000

New Design Cost Effective: **No**

DESIGN 5 - COST-EFFECTIVENESS OF JOINT SEALANTS ON US 101, GEYSERVILLE

<u>DESIGN FEATURE</u>	<u>CONVENTIONAL DESIGN</u>	<u>NEWER DESIGN</u>
Slab Design	9 in JPCP	9 in JPCP
Joint spacing	12-13-19-18 ft	12-13-19-18 ft
Sealant	none	rubberized asphalt
Base type	CTB	CTB
Outer shoulder	PCC	PCC
Outer lane width	12 ft	12 ft
Cost/2-lane mi	\$414,800	\$431,200

New Design Cost Effective: **Yes**

DESIGN 6 - COST-EFFECTIVENESS OF EDGE DRAINS ON I-5, SACRAMENTO

<u>DESIGN FEATURE</u>	<u>CONVENTIONAL DESIGN</u>	<u>NEWER DESIGN</u>
Slab Design	10.2 in JPCP	10.2 in JPCP
Joint spacing	12-13-19-18 ft	12-13-19-18 ft
Sealant	none	none
Base type	CTB	CTB
Outer shoulder	AC	AC
Outer lane width	12 ft	12 ft
Edge drains	None	Yes
Cost/2-lane mi	\$487,000	\$513,400

New Design Cost Effective: **Yes**

Table 59. Michigan designs for cost-effectiveness evaluation.

DESIGN 1 - COST-EFFECTIVENESS OF LOAD TRANSFER & BASE TYPE AT CLARE

<u>DESIGN FEATURE</u>	<u>CONVENTIONAL DESIGN</u>	<u>NEWER DESIGN</u>
Slab Design	9 in JPCP	9 in JPCP
Joint spacing	13-17-16-12 ft	13-19-18-12 ft
Dowels	1.25 in	none
Sealant	standard	standard
Base type	granular	asphalt-treated
Outer lane width	12 ft	12 ft
Outer Shoulder	AC	AC
Cost/2-lane mi	\$349,600	\$369,600

New Design Cost Effective: Yes

DESIGN 2 - COST-EFFECTIVENESS OF LOAD TRANSFER & BASE TYPE AT CLARE

<u>DESIGN FEATURE</u>	<u>CONVENTIONAL DESIGN</u>	<u>NEWER DESIGN</u>
Slab Design	9 in JPCP	9 in JPCP
Joint spacing	13-17-16-12 ft	13-19-18-12 ft
Dowels	1.25 in	none
Sealant	standard	standard
Base type	granular	asphalt-treated permeable
Outer lane width	12 ft	12 ft
Outer Shoulder	AC	AC
Cost/2-lane mi	\$349,600	\$373,810

New Design Cost Effective: Yes

DESIGN 3 - COST-EFFECTIVENESS OF PAVEMENT TYPES AT CLARE

<u>DESIGN FEATURE</u>	<u>CONVENTIONAL DESIGN</u>	<u>NEWER DESIGN</u>
Slab Design	9 in JPCP	9 in JPCP
Joint spacing	71 ft	13-17-16-12 ft
Dowels	1.25 in	1.25 in
Sealant	standard	standard
Base type	granular	granular
Outer lane width	12 ft	12 ft
Outer Shoulder	AC	AC
Cost/2-lane mi	\$323,810	\$349,600

New Design Cost Effective: No

Table 59. Michigan designs for cost-effectiveness evaluation (continued).

DESIGN 4 - COST-EFFECTIVENESS OF EDGE DRAINS AT CLARE

<u>DESIGN FEATURE</u>	<u>CONVENTIONAL DESIGN</u>	<u>NEWER DESIGN</u>
Slab Design	9 in JRCP	9 in JRCP
Joint spacing	71 ft	71 ft
Dowels	1.25 in	1.25 in
Sealant	standard	standard
Base type	granular	granular
Edge Drains	none	yes
Outer lane width	12 ft	12 ft
Outer Shoulder	AC	AC
Cost/2-lane mi	\$323,810	\$332,100

New Design Cost Effective: Yes

DESIGN 5 - COST-EFFECTIVENESS OF PCC SHOULDERS AT CHARLOTTE

<u>DESIGN FEATURE</u>	<u>CONVENTIONAL DESIGN</u>	<u>NEWER DESIGN</u>
Slab Design	9 in JRCP	9 in JRCP
Joint spacing	71 ft	71 ft
Dowels	1.25 in	1.25 in
Sealant	standard	standard
Base type	granular	granular
Outer lane width	12 ft	12 ft
Outer Shoulder	AC	PCC
Cost/2-lane mi	\$284,020	\$285,400

New Design Cost Effective: No

DESIGN 6 - COST-EFFECTIVENESS OF PERMEABLE BASE AT MARSHALL

<u>DESIGN FEATURE</u>	<u>CONVENTIONAL DESIGN</u>	<u>NEWER DESIGN</u>
Slab Design	9 in	10 in JRCP
Joint spacing	71 ft	41 ft
Dowels	1.25 in	1.25 in
Sealant	standard	standard
Base type	granular	granular (permeable)
Outer lane width	12 ft	12 ft
Outer Shoulder	AC	PCC
Cost/2-lane mi	\$323,810	\$331,300

New Design Cost Effective: Yes

Table 60. Minnesota designs for cost-effectiveness evaluation.

DESIGN 1 - COST-EFFECTIVENESS OF DOWELS AT ROTHSA Y

<u>DESIGN FEATURE</u>	<u>CONVENTIONAL DESIGN</u>	<u>NEWER DESIGN</u>
Slab Design	9 in JRCP	9 in JRCP
Joint spacing	27 ft	27 ft
Dowels	none	1.25 in
Sealant	standard	standard
Base type	granular	granular
Outer lane width	12 ft	12 ft
Outer Shoulder	AC	AC
Cost/2-lane mi	\$462,660	\$500,000

New Design Cost Effective: Yes

DESIGN 2 - COST-EFFECTIVENESS OF BASE TYPES AT ROTHSA Y

<u>DESIGN FEATURE</u>	<u>CONVENTIONAL DESIGN</u>	<u>NEWER DESIGN</u>
Slab Design	9 in JRCP	9 in JRCP
Joint spacing	27 ft	27 ft
Dowels	1.25 in	1.25 in
Sealant	standard	standard
Base type	granular	asphalt treated
Outer lane width	12 ft	12 ft
Outer Shoulder	AC	AC
Cost/2-lane mi	\$500,000	\$531,920

New Design Cost Effective: No

DESIGN 3 - COST-EFFECTIVENESS OF JOINT SPACING AT ROTHSA Y

<u>DESIGN FEATURE</u>	<u>CONVENTIONAL DESIGN</u>	<u>NEWER DESIGN</u>
Slab Design	9 in JRCP	9 in JRCP
Joint spacing	40 ft	27 ft
Dowels	1.25 in	1.25 in
Sealant	standard	standard
Base type	granular	granular
Outer lane width	12 ft	12 ft
Outer Shoulder	AC	AC
Cost/2-lane mi	\$493,300	\$500,000

New Design Cost Effective: No

Table 60. Minnesota designs for cost-effectiveness evaluation (continued).

DESIGN 4 - COST-EFFECTIVENESS OF LANE WIDTH AT AUSTIN

<u>DESIGN FEATURE</u>	<u>CONVENTIONAL DESIGN</u>	<u>NEWER DESIGN</u>
Slab Design	9 in JRCP	9 in JRCP
Joint spacing	27 ft	27 ft
Dowels	1.00 in	1.00 in
Sealant	standard	standard
Base type	granular	granular
Outer lane width	12 ft	14 ft
Outer Shoulder	AC	AC
Cost/2-lane mi	\$493,650	\$524,500

New Design Cost Effective: No

DESIGN 5 - COST-EFFECTIVENESS OF LANE WIDTH & PERMEABLE BASE AT TRUMAN

<u>DESIGN FEATURE</u>	<u>CONVENTIONAL DESIGN</u>	<u>NEWER DESIGN</u>
Slab Design	8 in JRCP	8 in JRCP
Joint spacing	27 ft	27 ft
Dowels	1.00 in	1.00 in
Sealant	standard	standard
Base type	granular	Perm. asphalt
Outer lane width	12 ft	14 ft
Outer Shoulder	AC	AC
Cost/2-lane mi	\$479,390	\$539,880

New Design Cost Effective: No

Table 61. North Carolina designs for cost-effectiveness evaluation.

DESIGN 1 - COST-EFFECTIVENESS OF LOAD TRANSFER AT ROCKY MOUNT

<u>DESIGN FEATURE</u>	<u>CONVENTIONAL DESIGN</u>	<u>NEWER DESIGN</u>
Slab Design	9 in JPCP	9 in JPCP
Joint spacing	30 ft	30 ft
Dowels	none	1.25 in
Sealant	standard	standard
Base type	granular	granular
Outer lane width	12 ft	12 ft
Outer Shoulder	AC	AC
Cost/2-lane mi	\$465,000	\$486,000

New Design Cost Effective:

No

DESIGN 2 - COST-EFFECTIVENESS OF BASE TYPE AT ROCKY MOUNT

<u>DESIGN FEATURE</u>	<u>CONVENTIONAL DESIGN</u>	<u>NEWER DESIGN</u>
Slab Design	9 in JPCP	9 in JPCP
Joint spacing	30 ft	30 ft
Dowels	none	none
Sealant	standard	standard
Base type	granular	asphalt-treated
Outer lane width	12 ft	12 ft
Outer Shoulder	AC	AC
Cost/2-lane mi	\$465,000	\$541,000

New Design Cost Effective:

Yes

DESIGN 3 - COST-EFFECTIVENESS OF TRANSVERSE JOINT ORIENTATION AT ROCKY MOUNT

<u>DESIGN FEATURE</u>	<u>CONVENTIONAL DESIGN</u>	<u>NEWER DESIGN</u>
Slab Design	9 in JPCP	9 in JPCP
Joint spacing	30 ft	30 ft
Dowels	none	none
Joint orientation	perpendicular	skewed
Sealant	standard	standard
Base type	granular	granular
Outer lane width	12 ft	12 ft
Outer Shoulder	AC	AC
Cost/2-lane mi	\$465,000	\$476,000

New Design Cost Effective:

No

REFERENCES

1. "AASHTO Guide for Design of Pavement Structures, 1986," American Association of Highway and Transportation Officials, 1986.
2. Darter, M. I. and E. J. Barenberg, "Design of Zero-Maintenance Plain Jointed Pavement, Vol. I - Development of Design Procedures," Federal Highway Administration, Report No. FHWA-RD-77-111, April 1977.
3. van Wijk, A. J., "Rigid Pavement Pumping: 1. Subbase Erosion, 2. Economic Modeling," Federal Highway Administration, FHWA Contract Number DTFH61-82-C-00035, Final Report, September 1985.
4. van Wijk, A. J., J. Larralde, C. W. Lovell, and W. F. Chen, "Pumping Prediction Model for Highway Concrete Pavements," ASCE, Journal of Transportation Engineering, Volume 115, Number 2, March 1989.
5. van Wijk, A. J., "Purdue Economic Analysis of Rehabilitation and Design Alternatives for Rigid Pavements: A User's Manual for PEARDARP," Federal Highway Administration, FHWA Contract Number DTFH61-82-C-00035, Final Report, September 1985.
6. Darter, M. I., J. M. Becker and M. B. Snyder, "Development of a Concrete Pavement Evaluation System (COPES), Volume I -Research Report," NCHRP Report No. 277, 1984.
7. Heinrichs, K. W., M. J. Liu, M. I. Darter, S. H. Carpenter, A. M. Ioannides, "Rigid Pavement Analysis and Design," Federal Highway Administration, FHWA-RD-88-068, July 1989.
8. Statistical Analysis System (SAS), Version 6.03, SAS Institute Inc., Cary, North Carolina, 1987.
9. Rauhut, J. B., R. L. Lytton, and M. I. Darter, "Pavement Damage Functions for Cost Allocation, Volume I - Damage Functions and Load Equivalency Factors," Federal Highway Administration, Report No. FHWA/RD-82/126, July 1982.
10. Packard, R. J., "Design Considerations for Control of Joint Faulting of Undoweled Pavements," Proceedings, First International Conference on Concrete Pavement Design, Purdue University, 1977.
11. Dempsey, B. J., W. A. Herlache, and A. J. Patel, "The Climatic-Materials-Structural Pavement Analysis Program User's Manual," FHWA/RD-86/085, 1986.

12. Dempsey, B. J., W. A. Herlache, and A. J. Patel, "Environmental Effect on Pavements - Vol. III, Theory Manual," Federal Highway Administration, FHWA/RD-84/115, 1986.
13. Liu, S. J., and R. L. Lytton, "Environmental Effects on Pavements - Vol. IV, Drainage Manual," Federal Highway Administration, FHWA/RD-84/116, 1986.
14. Kopperman, S., G. Tiller, and M. Tseng, "TTI Pavement Drainage Model: TTIDRN and TTIINF Interactive Microcomputer Version, User's Manual: IBM-PC and Compatible Version," Federal Highway Administration, FHWA Contract No. DTFH61-85-C-0051, Final Report, January 1986.
15. Tabatabaie, A. M., E. J. Barenberg, and R. E. Smith, "Longitudinal Joint Systems in Slip-Formed Rigid Pavements, Volume II Analysis of Load Transfer Systems for Concrete Pavements," U.S. Department of Transportation, Report No. FAA-RD-79-4, II, November 1979.
16. Ioannides, A. M., "Analysis of Slab-on-Grade for a Variety of Loading and Support Conditions," Ph.D. Thesis, 1984.
17. Ioannides, A. M., E. J. Barenberg, and M. R. Thompson, "Finite Element Model with Stress Dependent Support," TRB, Transportation Research Record 954, 1984.
18. Tayabji, S. D., and B. E. Colley, "Analysis of Jointed Concrete Pavements," Federal Highway Administration, FHWA Report FHWA/RD-86/041, February 1986.
19. Tayabji, S. D., and B. E. Colley, "Improved Rigid Pavement Joints," Federal Highway Administration, FHWA Report No. FHWA/RD-86/040, February 1986.
20. Larralde, J., "Structural Analysis of Rigid Pavements with Pumping," Federal Highway Administration, FHWA Contract No. DTFH61-82-C-00035, Final Report, September 1985.
21. Larralde, J., "PMARP User's Manual," Federal Highway Administration, FHWA Contract No. DTFH61-82-C-00035, Final Report, September 1985.
22. Abbo, E., "The Influence of Heavy Vehicle Dynamics on Rigid Pavement Response," Final Report, 1985.
23. Kopperman, S., G. Tiller, and M. Tseng, "Purdue Pumping Model: PMARP and PEARDARP: Interactive Microcomputer Version, User's Manual: IBM-PC and Compatible Version," Federal Highway Administration, FHWA Contract No. DTFH61-85-C-00051, January 1986.

24. Kopperman, S., G. Tiller, and M. Tseng, "JCP-1: Interactive Microcomputer Version, User's Manual: IBM-PC and Compatible Version," Federal Highway Administration, FHWA-TS-87-205, January 1986.
25. Sawan, J. S, M. I. Darter, and B. J. Dempsey, "Structural Analysis and Design of Portland Cement Concrete Highway Shoulders," Federal Highway Administration, FHWA/RD-81/122, April 1982.
26. Majidzadeh, K., and G. J. Ilves, "Structural Design of Roadway Shoulders - Final Report," Federal Highway Administration, FHWA/RD-86/089, May 1986.
27. Thompson, M. R. and Q. L. Robnett, "Final Report: Resilient Properties of Subgrade Soils," Civil Engineering Studies, Transportation Engineering Series No. 14, Illinois Cooperative Highway and Transportation Series No. 160, June 1976.
28. Johnson, T. C., D. M. Cole, and E. J. Chamberlain, "Influence of Freezing and Thawing on the Resilient Properties of a Silt Soil Beneath an Asphalt Concrete Pavement," CRREL Report 78-23, September 1978.
29. Bergan, A. T. and C. L. Monismith, "Characterization of Subgrade Soils in Cold Regions for Pavement Design Purposes," Highway Research Record 431, 1973.
30. Dempsey, B. J. and Q. L. Robnett, "Influence of Precipitation, Joints, and Sealing on Pavement Drainage," TRB, Transportation Research Record 705, 1979.
31. Ridgeway, H. H., "Infiltration of Water Through the Pavement Surface," TRB, 1976.
32. Haynes, J. A. and E. J. Yoder, "Effects of Repeated Loadings on Gravel and Crushed Stone Base Materials in the AASHO Road Test," Highway Research Record 19, 1963.
33. Thompson, M. R. and Q. L. Robnett, "Resilient Properties of Subgrade Soils," ASCE, Transportation Engineering Journal, 1979.
34. Carpenter, S. H., M. I. Darter, B. J. Dempsey, and S. M. Herrin, "A Pavement Moisture Accelerated Distress (MAD) Identification System - Volume I," FHWA Report FHWA/RD-81/079, 1981.
35. Barksdale, R. D., and R. G. Hicks, "Improved Pavement Shoulder Joint Design," NCHRP Report 202, June 1979.

36. Emery, D. K., "A Preliminary Report on the Paved Shoulder Encroachment and Transverse Lane Displacement for Design Trucks on Rural Freeways," Proceedings, Specialty Conference on Pavement Design for Predicting Engineers, Atlanta, Georgia, June 1975.
37. Majidzadeh, K., G. J. Ilves, and H. Sklyut, "Mechanistic Design of Rigid Pavements, Volume I: Development of the Design Procedure," Federal Highway Administration, FHWA Contract DTFH 11-9568, June 1984.
38. Majidzadeh, K., G. J. Ilves, and H. Sklyut, "Mechanistic Design of Rigid Pavements, Volume II: Design and Implementation Manual," Federal Highway Administration, FHWA Contract DTFH 11-9568, June 1984.
39. Dowe, D. S., "A Finite Element Approach to Plate Vibration Problems," Journal of Mechanical Engineering Science, Volume 7, Number 1, 1965.
40. Fischer, J. A., M. R. Thompson, A. M. Ioannides, and E. J. Barenberg, "K_R: The Resilient Modulus of Subgrade Reaction," Transportation Research Record 954, Transportation Research Board, Washington, D.C., 1984.
41. Teller, L. W., and H. D. Cashell, "Performance of Dowels Under Repetitive Loading," Public Roads, Volume 3, Number 1, April 1958.
42. Packard, R. G. and S. D. Tayabji, "Mechanistic Design of Concrete Pavements to Control Joint Faulting and Subbase Erosion," International Seminar on Drainage and Erodability at the Concrete Slab - Subbase - Shoulder Interfaces, Paris, France, March 1983.
43. Huang, Y. H. and S. T. Wang, "Finite Element Analysis of Concrete Slabs and its Implications for Rigid Pavement Design," Highway Research Board, Highway Research Record No. 466, 1973.
44. "The AASHO Road Test, Report 5—Pavement Research," Highway Research Board, Special Report 61E, Publication No. 954, 1962.
45. Darter, M. I. and E. J. Barenberg, "Zero-Maintenance Pavements: Results of Field Studies on the Performance Requirements and Capabilities of Conventional Pavement Systems," Federal Highway Administration, FHWA-RD-76-105, 1976.
46. Hall, K. T., J. M. Connor, M. I. Darter, and S. H. Carpenter, "Rehabilitation of Concrete Pavements, Volume III—Concrete Pavement Evaluation and Rehabilitation System," Federal Highway Administration, FHWA-RD-88-073, July 1989.

47. Ioannides, A. M., M. R. Thompson, and E. J. Barenberg, "Westergaard Solutions Reconsidered," Transportation Research Record 1043, Transportation Research Board, 1985.
48. Benekohal, R. F. and K. T. Hall, "Effect of Lane Widening on Lateral Distribution of Truck Wheels," Draft Paper prepared for presentation at the 69th Annual Meeting of the Transportation Research Board, August 1989.
49. Darter, M. I., "A Comparison Between Corps of Engineers and ERES Consultants, Inc. Rigid Pavement Design Procedures," Technical Report Prepared for the United States Air Force SAC Command, August 1988.
50. Darter, M. I. and K. T. Hall, "Structural Overlay Strategies for Jointed Concrete Pavements, Volume IV - Guidelines for the Selection of Rehabilitation Alternatives," Federal Highway Administration, FHWA-RD-89-145, January 1990.

